

Role of Penicillin-Binding Proteins in Synthesis and modification of *Bacillus subtilis* cell envelope

Yousef Nifaj Alanazi

A thesis submitted for the degree of **Doctor of Philosophy**.

Newcastle University
Faculty of Medical Science
Bioscience Institute

August 2024

Acknowledgments

Firstly, I would like to express my sincere gratitude to my supervisor, Dr. Richard Daniel, for his continuous support, patience, motivation, enthusiasm, and immense knowledge. I really appreciated your guidance, valuable suggestions and always opened door of your office over the course of the research as well as writing of the thesis. Literally, I was a lucky PhD student for having you as a supervisor.

A big thank to Dr. Ling Juan Wu, which generously answered my questions and helped me during my PhD journey.

I would also like to thank my mother, my siblings and my wife, Tahani, for her great and precious social support and encouragement abroad. I also thank my friend Ali Alahmari for his support.

Finally, I must acknowledge the Saudi Arabian government and Northern Borders University, for funding my PhD study and offering me this golden opportunity in my academic life.

Abstract

The bacterial cell wall is a critical structure that maintains cell integrity by preventing lysis due to internal osmotic pressure and defining cell shape. In *Bacillus subtilis*, the major components of the cell wall are peptidoglycan (PG) and teichoic acids (TAs). PG forms a net-like structure around the cytoplasmic membrane, with penicillin-binding proteins (PBPs) playing a central role in its synthesis by utilizing lipid II as a precursor. Most bacteria encode multiple PBPs, many of which are functionally redundant, allowing survival despite the loss of certain PBPs.

PBPs have been key antibiotic targets for decades, particularly following the discovery of penicillin, leading to extensive research on their redundancy and functional roles. Understanding PBP redundancy in *B. subtilis* is essential for designing novel antibiotics that specifically target essential PBPs to combat antibiotic resistance.

This thesis investigates PBP redundancy and functional specialization in *B. subtilis* by systematically deleting PBPs to determine which are essential for growth during the exponential phase. The findings reveal that PBP2a (PBPH) and PBP2b are the only essential PBPs required for maintaining bacterial viability. Further, structural manipulation of PBP2a and its redundant partner PBPH identified the transmembrane domain of PBPH as a key regulator of PBP2a transcription and functional redundancy.

Additionally, this research characterizes the previously unstudied PBPX in *B. subtilis*. A bioinformatics-based structural analysis predicted its D-alanine transferase activity, which was subsequently confirmed experimentally. These findings expand our understanding of PBP functional diversity and may contribute to the development of new antibacterial strategies targeting cell wall biosynthesis in *B. subtilis* and related bacteria

Contents

Chapter 1 Introduction	12
1.1 Bacterial Cell Structure	12
1.1.1 Peptidoglycan precursor biosynthesis	14
1.1.2 Peptidoglycan Biosynthesis	17
1.2 Cell shape determination and elongation	19
1.3 Cell Division	21
1.4 PBPs	25
1.4.1 PBP Structure	26
1.4.2 PBP Classification and Functional Roles	28
1.4.3 Characterisation of PBPs involved in <i>B. subtilis</i> division	29
1.5 Teichoic Acid	36
1.5.1 Lipoteichoic Acid (LTA)	37
1.5.2 Wall Teichoic Acid (WTA)	39
1.6 Function and Modification of Teichoic Acid	41
1.6.1 TA involvement in Cell Elongation and Division	42
1.6.2 Control of Autolytic Activity	42
1.6.3 Cation-Binding Activities	43
1.7 Modifications of TA	43
1.7.1 Glycosylation of Teichoic Acid	43
1.7.2 D-alanylation of Teichoic Acid	
1.8 Specific Aims of this Project	46
Chapter 2 Materials and methods	47
2.1 Bacterial Strains collection	47
2.2 Plasmids	50
2.3 Media supplements	52
2.4 Plasmid DNA extraction	52
2.5 Agarose gel electrophoresis	53
2.6 Genomic DNA extraction	53
2.7 Transformation of <i>B. subtilis</i>	53
2.8 Bacterial transformation of E. coli	54
2.9 Purification of DNA bands from agarose gels	55
2.10 Western blotting	56
2.11 Polymerase chain reaction	57
2.12 Restriction digestion of DNA	58
2.13 Bocillin staining	59
2.14 DNA ligation	60

2.15 Beta-galactosidase activity assay	60
2.16 DNA purification	63
2.17 Fluorescent Labeling of Bacterial Cells Using Poly-L-Lysine-FITC Dextran-Rhodamine	
2.18 Microscopy	64
2.19 Transmission electron microscopy	64
2.20 Cloning using the NEBuilder® HiFi DNA assembly	65
2.21 Zetasizer for cell surface charge	66
2.22 Cell-Tak application for AFM (Atomic Force Microscopy)	67
2.23 Atomic force microscopy for cell rigidity	68
2.24 Cell wall analysis methods	68
2.25 Muropeptide analysis	70
2.26 Reverse transcription-quantitative PCR	70
2.27 Site-directed mutagenesis	71
2.28 Protein band intensity by ImageJ	74
2.29 gDNA sequencing analysis	74
2.30 D-Alanine assay	75
2.30.1 WTA isolation for D-Alanine assay	75
2.30.2 LTA isolation for the D-Ala assay	77
2.31 Measuring D-Ala in WTA and LTA by the D-Ala assay	78
2.31.1 Assay preparation and execution	78
2.31.2 Incubation and measurement.	78
2.31.3 Data analysis	79
Chapter 3 Creation and characterisation of a <i>B. subtilis</i> strain with a minimal spBPs	
3.1 Introduction	80
3.2 Results	82
3.2.1 Construction of a B. subtilis strain with a minimal set of PBPs	82
3.2.2 Deletion of ponA in strain PBPs GG136	85
3.2.3 Deletion of pbpH or pbpA from a strain with multiple deletions (YA-X) 88
3.2.4 Growth and morphology of the strain with minimal PBPs	90
3.2.5 HPLC analysis of muropeptides from 168, YA-X and YA-XI cells	92
3.2.6 Peptidoglycan composition and cross-linking of the strain with a minim of PBPs	
3.2.7 Deleting multiple PBPs reduces the cell rigidity of <i>B. subtilis</i>	99
3.2.8 Deletion of multiple PBPs impacts the motI, spo0F and spo0B genes	102
3.2.9 Analyses of the <i>B. subtilis</i> YA-XI ultrastructure by TEM	104
3.3 Discussion	106

Chapter 4 Analysis of the functional redundancy of PBP2a and PBPH	112
4.1 Introduction	112
4.2 Results.	114
4.2.1 Deletion of <i>pbpH</i> changes the abundance of PBP2a	114
4.2.2 Overexpression and purification of PBP2A and PBPH	120
4.2.3 Effect of PBPH deletion on PBP2A quantity	125
4.2.4 Determining if <i>pbpH</i> expression results in reduced <i>pbp2a</i> transcription	on129
4.2.5 Effect of <i>pbpH</i> deletion on <i>pbpA</i> expression measured by RT-qPCR	131
4.2.6 Effects of PBP2a or PBPH cytosolic tail deletions on bacterial growt	h134
4.2.7 A chimeric PBPH with the transmembrane domain of PBP2a	141
4.2.8 Site-directed mutagenesis of the PBPH transmembrane domain	144
4.3 Discussion	148
Chapter 5 D-Ala transfer from LTA to WTA is mediated by PBPX	153
5.1 Introduction	153
5.2 Results	155
5.2.1 Comparative Analysis of PBPX and Related Proteins Across M Bacterial Species	_
5.2.2 Minimal inhibitory concentration of the AMP CAMA against <i>B. subt</i> and <i>S. aureus</i> Je2	
5.2.3 Deletion of <i>pbpX</i> or <i>dltAB</i> increases <i>B. subtilis</i> sensitivity to the AMP CAMA	
5.2.4 Deletion of <i>fmtA</i> and <i>flp, in S. aureus,</i> have opposite effects in relativity to cationic AMPs	
5.2.5 Deleting <i>pbpX</i> or <i>dltAB</i> increases the cell capacity to bind a fluorescent label but decreases binding to an anionic fluorescent label	
5.2.6 Deleting <i>pbpX</i> or <i>dltAB</i> shifts the cell surface charge towards negative subtilis	
5.2.7 Deleting <i>fmtA</i> decreases cell surface charge negativity but deletincreases it in <i>S. aureus</i>	
5.2.8 Determination of the distribution of D-ala on the teichoic acids in envelope	
5.2.9 The effect of <i>fmtA</i> or <i>flp</i> deletion on D-Ala associated with LTA an in <i>S. aureus</i>	
5.2.10 Deleting <i>pbpX</i> , <i>dltAB</i> or <i>LTA</i> decreases cell envelope rigidity compthe wild type	-
5.3 Discussion	179
Chapter 6 General discussion and future directions	186
Chapter 7 References	189
Appendices	210

Figure List

Figure 1.1: Structure of a Peptidoglycan (PG) Precursor and Lipid II Synthesis in Cytoplasm of Bacterial Cells	
Figure 1.2: Elongasome Complexes Responsible for Peptidoglycan (PG) Synthes During Lateral Cell Wall Growth.	
Figure 1.3: The Peptidoglycan (PG) Synthesis Complex at the Division Site	24
Figure 1.4: Biosynthesis of Lipoteichoic Acid (LTA) in of B. subtilis	39
Figure 1.5: Wall teichoic acid biosynthesis in B. subtilis.	41
Figure 1.6: D-alanylation of teichoic acid.	45
Figure 2.1: Membrane labelling	64
Figure 2.2: Schematic of the Zetasizer machine.	67
Figure 2.3: Site-directed mutagenesis.	73
Figure 3.1: Bocillin-FL-based detection of penicillin-binding proteins in the 168 GG136 strains.	
Figure 3.2: Bocillin-FL-based detection of penicillin-binding proteins in the 168 YA-X strains.	
Figure 3.3: Deletion of PBPH from strain YA-X and detection using Bocillin FL.	89
Figure 3.4: Growth and morphology of strains lacking multiple PBPs	91
Figure 3.5: Reverse-phase high-performance liquid chromatography analysis of cellular muropeptides.	95
Figure 3.6: Structural composition of identified muropeptides	96
Figure 3.7: High-performance liquid chromatography analysis of peptidoglycan f strains with penicillin-binding protein deletions.	
Figure 3.8: Cell envelope rigidity of 168 and YA-XI strains by AFM	101
Figure 3.9: Genomic DNA sequencing of YA-XI reveals mutations in <i>motI</i> , <i>spo0</i> and <i>spo0B</i> .	
Figure 3.10: Transmission electron microscopy images for strain 168 and a strain multiple penicillin-binding protein deletions (YA-X)	
Figure 4.1: Deleting PBPH increases the activity of PBP2a.	117
Figure 4.2: Deleting pbpH increases pbp2a detection.	118
Figure 4.3: Production and purification of PBP2a.	122
Figure 4.4: Production and purification of PBPH	124
Figure 4.5: Effect of <i>pbpH</i> deletion on PBP2A abundance	127
Figure 4.6: Expression of <i>pbpA</i> in the absence and presence of <i>pbpH</i>	130
Figure 4.7: Expression of <i>pbpA</i> in the absence and presence of <i>pbpH</i>	133

Figure 4.8: Cytosolic domains of PBP2a and PBPH.	35
Figure 4.9: Effect of the deletion of the PBP2a cytosolic domain on <i>B. subtilis</i> grown 1	
Figure 4.10: Effect of deletion of the PBPH cytosolic domain on <i>B. subtilis</i> growth.	
Figure 4.11: Creation of a chimeric PBPH and evaluation of its effect on PBP2a quantity by western blotting.	43
Figure 4.12: Expression of a mutated <i>pbpH</i> gene where the transmembrane domain was altered and the impact on PBP2a abundance	47
Figure 5.1: The function of the FmtA protein	54
Figure 5.2: Proteins homologous to PBPX from <i>B. subtilis</i> in various bacterial specie and their sequence alignments	
Figure 5.3: Determinig MIC of CAMA in B. subtilis 168 and S. aureus Je21	60
Figure 5.4: Sensitivity of 168, ΔpbpX and ΔdltAB to the cationic antimicrobial peptide CAMA.	62
Figure 5.5: Sensitivity of Je2, Δ Fmta and Δ Flp to the cationic antimicrobial peptide CAMA.	
Figure 5.6: Labelling of 168, ΔpbpX and Δdlt with cationic and anionic fluorescent-tagged chemicals	
Figure 5.7: Cell surface charge of strains 168, $\Delta pbpX$, $\Delta dltAB$, Δlta and $\Delta tagO1$	71
Figure 5.8:. Cell surface charge of Je2, ΔfmtA and Δflp analysed using the Zetasizer machine	
Figure 5.9: D-alanine assay for 168, $\Delta pbpX$, Δdlt , Δlta and $\Delta tagO$	78
Figure 5.10:. D-alanine assay for Je2, Δ fmtA and Δ flp	74
Figure 5.11:. Cell wall rigidity of 168, ΔpbpX, Δlta and Δdlt measured by atomic force microscopy	76
Figure 5.12: Surface charge modulation in <i>B. subtilis</i> and <i>S. aureus</i>	81

Tables

Table 1.1: Characteristics of identified PBPs in B. subtilis	.35
Table 2.1: Strains Collection	.47
Table 2.2: Plasmid counstucts	.50
Table 2.3: Antibiotic, substrate and inducer final concentrations used in liquid and	
solid media	52

Abbreviations

MW - molecular weight

 $\mu l - microlitre(s)$ μm – micrometre(s) $\mu M - micromolar$ Amp – ampicillin ATP – Adenosine triphosphate bp – base pair(s) BSA – bovine serum albumin CAA – casamino acids Cam – chloramphenicol DNA - deoxyribonucleic acid dsDNA - double stranded DNA EDTA - Ethylenediaminetetraacetic acid Erm – erythromycin FtsZ – filamentous temperature-sensitive mutant Z g-gramsgDNA - genomic DNA GFP – green fluorescent protein HEPES - 2-[4-(2-hydroxyethyl)piperazin-1-yl]ethanesulfonic acid IPTG - Isopropyl β-D-1-thiogalactopyranoside Kan - kanamycin Kb - kilobase(s) KDa - kilodaltons L-litreLB - Luria-Bertani broth M - molarmg – milligrams mg/ml - milligrams per millilitre mM – millimolar

NA – nutrient agar

°C – degrees centigrade

OD600 – optical density at a wavelength of 600 nm

ONPG - 2-Nitrophenyl β-D-galactopyranoside

ori – origin of replication

PBP - penicillin binding protein

PBS – phosphate buffered saline

PCR – polymerase chain reaction

PG - peptidoglycan

PGol-phosphatidylglycerol

RNA - Ribonucleic acid

rpm - Revolutions per minute

SDS-PAGE - Sodium dodecyl sulphate-polyacrylamide gel electrophoresis

SMM – Spizizens minimal media

Spec – spectinomycin

SSC - saline sodium citrate

ssDNA – single stranded DNA

TAE - Tris-Acetate-EDTA

TEM – transmission electron microscopy

X-Gal - 5-bromo-4-chloro-3-indoly1-beta-D-galactopyranoside

ATP - adenosine triphosphate

Chapter 1 Introduction

1.1 Bacterial Cell Structure

The cell structure of bacteria was first classified by Hans Christian Gram, who differentiated bacteria based on their ability to retain a precipitated dye. This classification led to the terms Gram-positive (G+) for bacteria that retain dye, and Gram-negative (G-) for those that do not (Bartholomew & Mittwer, 1952). However, the underlying mechanism explaining why some bacteria retained the dye while others did not become apparent until much later. For instance, G- bacteria, such as *Escherichia coli* (*E. coli*), do not retain dye because they possess an outer membrane with a thin, mesh-like layer of polymers 3-6 nm thick, composed of carbohydrates and peptides (peptidoglycan; PG) that enclose the cytoplasmic membrane (Gan *et al.*, 2008). This PG layer is a crucial component of the cell, akin to the cell wall in plants.

In contrast, G+ bacteria, such as Bacillus subtilis (B. subtilis), have a thicker PG layer, consisting of between 10-20 layers, but they lack an outer membrane (Foster et al., 2008). The chemical composition of G+ and G- cell walls share some similarities, as both contain cell wall PGs, a polymer composed of disaccharide-peptide repeats. The structural integrity of the PG cell wall is provided by glycosidic linkages that connect the disaccharide-peptide repeats, forming linear glycan strands of varying lengths. The peptide stems attached to the disaccharide repeats interlink glycan strands together to form a mesh-like structure that is essentially a single molecule enclosing the cell. Furthermore, the form of the mesh-like structure of bacterial cell wall also gives bacterial cells their distinctive shapes, such as spheres, rods, and spirals. Historically, in addition to Gram classification, the shape of a bacterium, which is generally a fixed property, has been used to identify individual species. This shape is largely determined by the cell envelope and, specifically, by the way the PG is assembled (Zhang et al., 2021). However, G+ bacterial wall also contains large amounts, often up to 60% of the dry weight, of long anionic polymers referred to as wall teichoic acid (WTA), which are distributed through the PG meshwork. These WTAs are generally take the form of linear polymers of a modified carbohydrate resulting in a net negative charge and are covalently attached to the PG meshwork. In addition, a variant of this polymer, denoted lipoteichoic acid (LTA) is anchored to the head groups of membrane lipids (Silhavy et al., 2010). The high concentration of TAs in G+ bacteria is a major contributor to the envelope structure and function of the cells and has been suggested to share similarities with the outer membrane in G-bacteria (Swoboda et al., 2010).

Bacterial proliferation involves two processes cell growth and then division to result in two cells that may then repeat the process depending on the environmental conditions. For growth, the biomass of the cell increases through replication of key cytosolic components, the most important of which being the chromosomal DNA This is accompanied by some degree of enlargement of the cell, generally by elongation for rod shaped cells. This is then followed by cell division where the cell coordinates the segregation of the replicated material and the division of the enlarged cell to form two daughter cells with identical genomes (Silhavy *et al.*, 2010). TAs play a vital role in the growth, division, and morphogenesis of bacterial cells. Inhibition of TA synthesis has been shown to result in round and defective progeny (Schirner *et al.*, 2009). In contrast, G- bacteria rely on their outer membrane for viability, which not only filters toxic molecules but also contains extra cytoplasmic enzymes essential for cell wall growth and degradation (Lugtenberg & Van Alphen, 1983).

Focusing on *B. subtilis*, a Gram-positive, rod-shaped (bacillus) bacterium characterized by a thick peptidoglycan (PG) layer in its cell wall, which retains the crystal violet stain by binding to the PG during the Gram staining process (Shugar & Baranowska, 1954). Species of the genus *Bacillus* are notable for their ability to form endospores, which permits viability for long periods under unfavorable conditions. These endospores also serve as an important virulence factor, contributing to the bacteria's resilience against medical treatments and enabling them to cause diseases under certain conditions (Oggioni *et al.*, 1998; Tam *et al.*, 2006).

In addition to providing structural shape, the peptidoglycans (PGs) in the bacterial cell wall play a crucial role in protecting bacteria from environmental stressors, preventing lysis due to internal osmotic pressure, and maintaining cell wall stiffness, tension, and integrity. The cell wall must be dynamically remodeled to permit bacterial growth and division. It is generally presumed that two distinct PG-synthesizing complexes, the divisome and the elongasome, are responsible for PG synthesis during cell division and elongation, respectively.

The divisome, a highly conserved complex in bacteria, orchestrates cell division by constricting both the inner and outer membranes, synthesizing new PGs, and building the septum. Central to its function is the tubulin-like protein FtsZ, which forms a contractile Z-ring at the division site, serving as a scaffold for recruiting other

division-related proteins. Septum formation by the divisome is critical for generating new polar caps in the daughter cells after division (Vollmer et al., 2008).

In contrast, the elongasome, typically found in non-spherical bacteria, drives lateral PG synthesis along the cell's long axis, enabling cylindrical growth and cell enlargement. This process relies on the actin-like protein MreB, which localizes along regions of cell wall expansion to guide PG insertion. While the elongasome is essential for rod-shaped bacteria like *E. coli* and *B. subtilis*, variations in these processes have been observed in coccoid or polymorphic bacteria, which lack the elongasome and achieve growth and division through alternative mechanisms.

Murein, more commonly referred to PG, are an essential and distinct component of almost all bacterial cell walls (except Chlamydia), located on the outside of the cytoplasmic membrane. While PGs have a variety of functions, their most critical role is likely maintaining cell integrity by resisting turgor pressure (Egan *et al.*, 2020). The importance of PG is evident when their synthesis is inhibited, either by mutations or antibiotics, leading to cell lysis. Additionally, PGs provide a scaffold for the attachment of proteins, teichoic acids, and other components within the cell envelope, while also playing a crucial role in maintaining cell shape, growth, and the division (Dramsi *et al.*, 2008).

1.1.1 Peptidoglycan precursor biosynthesis

Lipid II is a crucial precursor for the synthesis of PGs in bacterial cell walls, including those of G+ bacteria like *B. subtilis* because the lipid II synthesis is the step where the peptidoglycan synthesis is translocated from cytoplasm to outer membrane (Ruiz, 2008). The synthesis of Lipid II is mediated by a series of enzymes and regulatory proteins that function in a coordinated manner to produce the final product. The first step in lipid II synthesis involves the formation of uridine phosphate (UDP)-GlcNAc, a reaction catalysed by the enzyme GlmS. GlmS is a glutamine-fructose-6-phosphate aminotransferase that catalyses the conversion of fructose-6-phosphate and glutamine into glucosamine-6-phosphate and glutamate (Mengin-Lecreulx and van Heijenoort., 1993). The glucosamine-6-phosphate is then converted into UDP-GlcNAc through a series of enzymatic reactions involving GlmM and GlmU (Figure 1.1) (Galinier *et al.*, 2023).

The conversion of UDP-GlcNAc to Lipid II involves a sequence of enzymatic reactions. Initially, the biochemical mechanism described by Benson *et al.* (1993) and Wanke and Amrhein (1993) involves the transfer and modification of molecular groups. Specifically, enol pyruvate moieties are transferred to the 3'-hydroxyl group of UDP-N-acetylglucosamine (UDP-GlcNAc) from phosphoenol pyruvate (PEP) by the enzyme UDP-GlcNAc enol pyruvate transferase, also referred to as MurA. This process results in the synthesis of UDP-GlcNAc-enol pyruvate (Kock *et al.*, 2004).

Subsequently, enolisation and reduction occur in a series of processes; UDP-GlcNAc is converted to UDP-N-acetylmuramic acid (UDP-MurNAc) following enolisation, facilitated by the enzyme UDP-N-acetyl allylacetone glucosamine reductase, or MurB (Megrian *et al.*, 2022). Next, a pentapeptide is added to UDP-MurNAc, catalysed by a series of ligases. This process is initiated by the enzyme MurC, which attaches L-alanine (L-Ala) to the nucleotide precursor UDP-N-acetylmuramic acid (UDP-MurNAc). Following this, the ATP-dependent enzyme MurD adds D-glutamic acid to the UDP-MurNAc-L-Ala complex, playing a crucial role in the creation of acylphosphate and tetrahedral intermediates during the construction of PGs (Bouhss *et al.* 2002). MurE further contributes by attaching meso-diaminopimelate (mDAP) or L-lysine to the UDP-MurNAc-L-Ala-D-Glu complex. This step is important because the amino acid must be positioned in the third position of growing peptides chain (van Heijenoort, 2007).

The enzyme D-alanine D-alanine ligase (Ddl) dimerises D-alanine into D-Ala-D-Ala (Walsh, 1989), which is subsequently added to the developing nucleotide precursor. This addition results in the formation of UDP-MurNAc-L-Ala-D-Glu-meso-diaminopimelate D-Ala-D-Ala, facilitated by the enzyme MurF (Green, 2002). The formation of UDP-MurNAc-pentapeptide phosphotransferase (MraY) is essential for using undecraprenyl-phosphate to anchor UDP-MurNAc-pentapeptide to the cell membrane, thus creating Lipid I (Bouhss *et al.*, 2004).

The final stage of Lipid II synthesis involves the process of linking Lipid I to a GlcNAc molecule. This step is facilitated by decadecenyl diphosphate-MurNAc-pentapeptide-UDP-N-acetylglucosamine (GlcNAc) transferase (MurG), resulting in the formation of UDP-N-acetylmuramoyl-L-alanyl-D-glutamyl-meso-diaminopimelate-D-Ala (UDP-MurNAc-pentapeptide) (Lipid II), the primary building block of PG

(Anderson et al., 1967; Scheffers, 2005; Garde, 2021. Vollmer et al., 2008; Oluwole, 2022).

The regulation of Lipid II synthesis in bacteria, including B. subtilis is tightly regulated by several factors (Zhao, 2017). One of these factors is the WalRK twocomponent system, a histidine kinase/response regulator system that senses changes in the cell wall and regulates the expression of genes involved in cell wall biosynthesis (Devine, 2012). Specifically, the WalRK system regulates cell wall growth by balancing PG synthesis and autolysins (YocH, CwlO, LytE). Inhibition or attenuation of WalRK in B. subtilis cultures has been shown to induce cell lysis, detected upon the attenuation of growing exponentially on a Luria-Bertani (LB) medium, defined by a doubling period of roughly 20 minutes. The cell lysis detected is likely to have occurred due to an imbalance between the Lipid II synthesis and autolysins, particularly YocH, CwlO, and LytE (Domínguez-Cueva 2011). Interestingly, previous research has also observed that deletion of WalRK in B. subtilis significantly reduces autolysin production (Fabret and Hoch, 1998). These findings highlight the importance of Lipid I and II synthesis and PG formation in bacterial cell walls. However, further research is needed to determine whether the observed imbalance between PG synthesis and autolysins is unidirectional or bidirectional (Bisicchia, 2007; Fabret, C 1998).

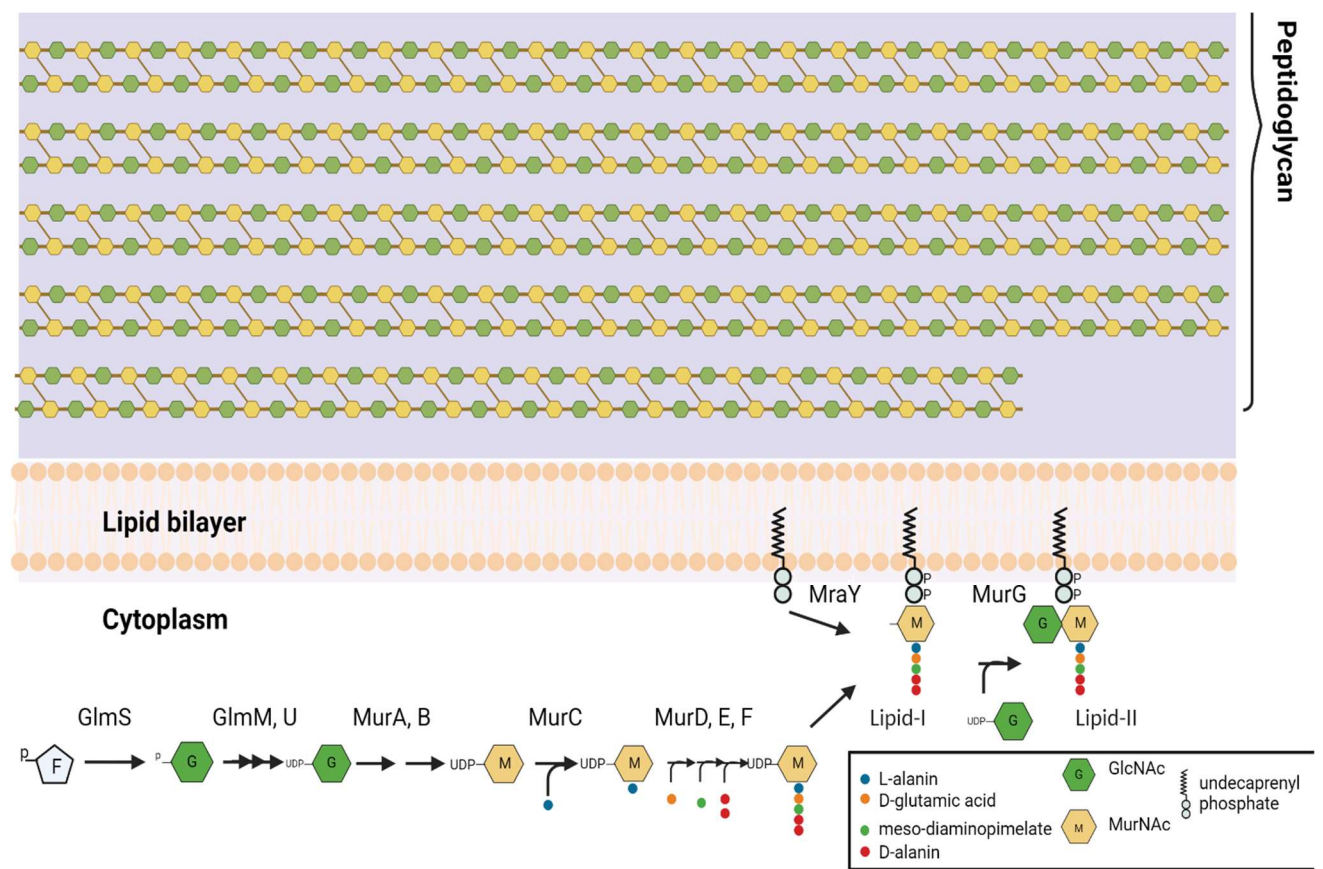


Figure 1.1: Structure of a Peptidoglycan (PG) Precursor and Lipid II Synthesis in the Cytoplasm of Bacterial Cells. Lipid II serves as a precursor for the construction of PGs. Lipid II's are synthesised in the cytoplasm through a series of enzymatic processes, including the GlmS, GlmM&U, MurA, MurB, MurC, MurD, MurE, MurF, MraY, MnaA and MurG. Subsequently, Lipid II are linked to C_55-P in the inner membrane.

1.1.2 Peptidoglycan Biosynthesis

The biosynthesis of PG in *B. subtilis* is a complex, multistep process involving the sequential assembly and polymerisation of disaccharide-peptide units, as well as the crosslinking of peptide bridges between adjacent glycan strands. The process begins with the synthesis of the PG precursor, lipid II, which is synthesised in the cytoplasm. This precursor is then transported to the cell surface by a family of lipid-linked carriers known as the bactoprenol family (Typas *et al.*, 2010; Barreteau *et al.*, 2008). These bactoprenol-carrier lipid intermediates are flipped across the cytoplasmic membrane to the periplasmic side by flippases, such as MurJ and FtsW, where they are subsequently polymerised to form the PG layer of the bacterial cell wall (Scheffers and Pinho, 2005; Meeske *et al.*, 2015).

PG production, which is essential for bacterial cell wall integrity, occurs in two main stages. Initially, glycan chains are polymerised by assembling glycan monomers. This is followed by the second stage, where these strands are cross-linked. Glycosyltransferases facilitate the translocation of mature PG monomers, integrating them into the growing glycan strands at their reducing ends (Ward and Perkins, 1973). The mature PGs form when glycan strands cross-link via their stem peptides, a process driven by transpeptidases (Sauvage *et al.*, 2008). This cross-linking occurswhen the carboxyl group on the fourth D-alanine residue of a stem peptide bonds with the amino group of m-A2pm on another stem peptide (Vollmer *et al.*, 2008).

Previous studies have shown that only pentapeptide stems can function as donor side chains during transpeptidation, which is followed by cross-linking and the loss of their terminal D-alanine residues (the fifth residue) (Vollmer *et al.*, 2008). However, acceptor peptide side chains may originate from stem peptides containing tri-, tetra-, or pentapeptides, though not all stem peptides participate in cross-linking (Egan and Vollmer, 2013). For example, in vegetative *B. subtilis* cells, only 30–40% of stem peptides participate in cross-linking (Atrih *et al.*, 1999; Sekiguchi and Yamamoto, 2012). Moreover, Atrih *et al.* (1999) observed an increase in cross-bridges during the stationary phase of *B. subtilis* growth. The final product of this process is the formation of a PG layer which is polymerised and crosslinked predominantly by the action of penicillin-binding proteins (PBPs) (PBPs will be discussed in detail in section 1.4) (Sauvage *et al.*, 2008; Zapun *et al.*, 2008).

The key structural features of PGs include short peptide sequences that join linear glycan chains. These glycan chains consist of alternating N-acetylglucosamine (GlcNAc) and N-acetylmuramic acid (MurNAc) residues connected by β -1 \rightarrow 4 linkages (Work., 1961), through transglycosylation processes. These glycan chains can undergo various modifications, such as N-deacetylation, O-acetylation, and N-glycosylation. These modifications are employed as strategies to evade detection and neutralization by the immune system (Brott and Clarke., 2019).

Mur enzymes catalyse PG synthesis and contribute to variations in the peptide stems of PGs, particularly in the composition of the interpeptide bridges and the mechanism of cross-linking. There are two predominant types of cross-linkages, with the most common being the 3–4 linkages, which run from the carboxyl group of d-Ala

at position 4 of one peptide unit to the amino group of a side-chain residue at position 3 of another peptide. The second, less common form of cross-linkages is the 2–4 linkage, found in a small number of bacterial species, connecting the d-Ala carboxyl group at position 4 of one peptide unit to the α -carboxyl group of d-Glu at position 2 of another (Egan *et al.*, 2020).

1.2 Cell shape determination and elongation

Bacterial cells exhibit distinctive shapes that are crucial for their survival, motility, and nutrient acquisition (van Teeseling *et al.*, 2017). *B. subtilis* cells are characterised by their unique morphology, appearing as elongated, consistently cylindrical tubes capped with hemispherical poles (Young, 2010). *B. subtilis* growth primarily occurs through elongation along the longitudinal axis, with cell division taking place once the cell's length has approximately doubled, while maintaining a diameter of approximately 850 nanometres (Sharpe, 1998; Young, 2010).

The enzymes responsible for the synthesis and hydrolysis of the PG matrix do not function in isolation but work in collaboration with synthases and hydrolases. This collaboration ensures that their activity is targeted to specific cellular compartments as required, and their activation is properly timed during the cell cycle (Errington and Wu, 2017). This complex coordination is mediated by intricate multiprotein complexes, with the elongation systems in rod-shaped bacteria commonly referred to as the Rod system or elongasome (Rohs, *et al* 2021). The key components of the Rod System include MreB, MreC, MreD, RodA, RodZ, and PBP2 (PBP2a and PBPH in *B. subtilis*), as evidenced by multiple inhibition studies showing that the absence of these proteins results in the loss of the rod-like structure. Alterations to the rod-like structure of *B. subtilis* have been shown to cause developmental abnormalities and, in extreme cases, can be fatal to the cells (Leaver and Errington, 2005; Figge *et al*, 2004; Jones *et al*, 2011).

MreB, a key protein of the Rod system, is an actin-like protein that forms antiparallel filaments along the inner cell membrane, guiding PG insertion during elongation. Genomic studies have revealed that *B. subtilis* contains three genes, located in distinct regions of the chromosome, that encode proteins similar to MreB, specifically *mbl* (MreB like) and *mreBH* (MreB homologue). The significance of these genes in cell growth and morphology has been documented in mutation studies, where mutations in any of these genes have been shown to cause distinct morphological

changes (Errington and Wu, 2017). For example, deletion of the *mreB* gene has been shown to increase cell width, while mutations in *mbl* induce highly twisted and swollen cells. In contrast, mutations in *mreBH* produce a less dramatic phenotype, such as reduced cell thickness and width compared to wild type cells (Jones *et al*, 2001; Carballido-López *et al*, 2006; Defeu Soufo *et al*, 2006). Although all three genes are important for maintaining cell morphology, some may have more redundancy than others.

Early research attempting to localise the three MreB family proteins in *B. subtilis* suggestedthe presence of helical filaments near the cell's periphery, likely close to the inner surface of the cytoplasmic membrane (Jones *et al.*, 2001). These structures correlate with new PG insertion, as identified through labelling methods for nascent cell wall synthesis, and are proposed to serve as trackers for PG synthesis enzymes. (Daniel *et al.* 2003). However, advances in microscopic imaging with higher spatiotemporal resolution have since revealed that MreB does not form continuous filaments. Instead, MreB assembles into small arcs on the membrane, perpendicular to the long axis (Garner *et al.*, 2011). Recent in vivo imaging studies employing various super-resolution techniques in *B. subtilis* have shown that MreB preferentially targets areas of negative curvature and "corrects" this curvature by depositing new PG. These findings demonstrate that *B. subtilis* possess a self-regulating feedback mechanism that ensures cells maintain their rod shape, which is vital for cell viability and survival (Billings *et al.*, 2014; Ursell *et al.*, 2014; Morgenstein *et al.*, 2015).

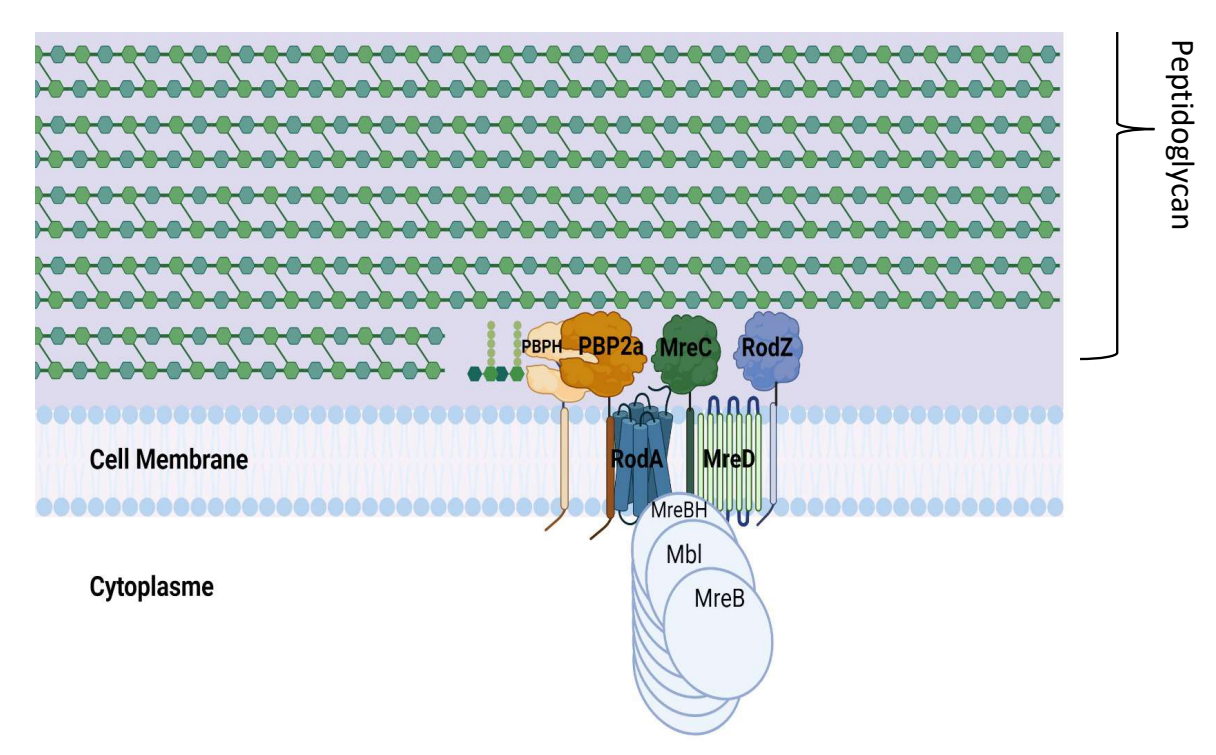


Figure 1.2: Elongasome Complexes Responsible for Peptidoglycan (PG) Synthesis During Lateral Cell Wall Growth. The proteins involved in cell wall elongation include MreB (Mbl and MreBH), which regulate the movement of the cell wall elongation enzyme complexes by forming filaments. MreD and MreC link cytosolic MreB and MreB-like proteins to the extracellular PG-synthesising machinery. RodA, a member of the shape, elongation, division, and sporulation (SEDS) family of PG glycosyltransferases, plays a crucial role in the elongasome complex responsible for synthesising the lateral cell wall. RodZ is essential for proper septum positioning during vegetative growth. PBP2a and PBPH are transpeptidases that belong to the elongation complex.

1.3 Cell Division

In most bacteria, cell division begins when a division apparatus known as the divisome assembles at the midpoint of the cell, following a period of elongation. This process involves invagination of the membrane, the synthesis of new cell wall material, and the formation of a cross wall, or septum, dividingthe cell into two compartments (Harry *et al.*, 2006). The junction between the two newly formed cells is completed by the action of various autolytic enzymes, which produce hemispherical poles and facilitate the separation of the resulting daughter cells. A key cytoskeletal protein for determining the site of cell division and coordinating the process of division is FtsZ (Rohs & Bernhardt, 2021). FtsZ shares structural and biochemical similarities with tubulin, a protein superfamily involved in the construction of microtubules, and is widely conserved among bacteria, though some exceptions exist (Rohs & Bernhardt, 2021). Given its essential role in cell division, FtsZ has been explored as a target for

antibacterial compounds, including the benzamide derivative PC190723 (Anderson et al., 2012), which specifically inhibits FtsZ polymerization and disrupts bacterial cytokinesis (Haydon et al., 2008).

The formation of the mature divisome is facilitated by FtsZ. Early research suggested that a continuous filament of FtsZ coiling around the mid-cell was essential for promoting cell division (Michie and Löwe, 2006). However, further studies have shown that the Z-ring, composed of multiple individual filaments or bundles of filaments, exhibits rotational movement, ensuring dynamic assembly and disassembly around the mid-cell (Bisson-Filho *et al.*, 2017; Loose and Mitchison, 2014; Yang *et al.*, 2017).

Cell division in *Bacillus subtilis* presents an interesting paradigm due to its two distinct methods of division: the "conventional mode," which occurs in cells undergoing vegetative growth, and a modified, highly asymmetric division in sporulating cells (Errington & Wu, 2017).

FtsZ relies heavily on GTPase activity for the coordination of its dynamic treadmilling movement, which coincides with the comparable movement of cell division-associated bPBPs around the septum. This movement differs significantly from MreB-directed motion. While FtsZ filaments treadmill independently of peptidoglycan (PG) synthesis, guiding the circumferential motion of cell wall enzymes at the septum, MreB movement is directly coupled to PG synthesis. MreB does not treadmill but rather associates with the elongation machinery and moves circumferentially as a result of localized PG synthesis and expansion (Bisson-Filho et al., 2017; Loose & Mitchison, 2014; Yang et al., 2017; Domínguez-Escobar et al., 2011).

Advances in microscopy, imaging techniques, and biochemical pull-down experiments for early divisome proteins have revealed that the divisome assembles in at least two distinct, temporally separated stages (Gamba et al., 2009; Ishikawa et al., 2006). Initially, the FtsZ protein forms the "Z-ring," which primarily interacts with cytosolic factors, often referred to as "early divisome proteins," including FtsA, SepF, ZapA, and EzrA. These factors help assemble FtsZ into a dynamic complex. Following a brief pause, the second stage of divisome assembly occurs, involving the recruitment

of "late" proteins, which generally consist of integral membrane proteins or proteins with substantial extracellular domains (Errington & Wu, 2017).

Additionally, several regulatory proteins—including MinC, MinD, MinJ, GpsB, and DivIVA—become involved in divisome assembly. These proteins likely participate in the second stage of assembly or during PG ingrowth. The recruitment of late-assembling proteins such as DivIVA may be signaled by PG ingrowth (Eswaramoorthy et al., 2011).

For a long time, the primary synthases involved in the divisome were believed to be PBPs. However, the discovery of SEDS proteins revealed that they can also function as PG polymerases, challenging the previous understanding (Meeske *et al.*, 2016). PBPs are commonly located at sites of cell division in various bacteria, indicating their role in septal PG synthesis. For instance, in *E. coli*, both PBP1a and PBP1b have been shown to interact with several proteins critical for cell division, including ZipA, with these interactions altering their enzymatic activities *in vitro* (Müller *et al.*, 2007; Gray *et al.*, 2015). Importantly, at least one of these PBPs—either PBP1a or PBP1b—is necessary for cell division in *E. coli*, as the simultaneous deletion of both is lethal, highlighting their essential role in maintaining cell viability (Pazos *et al.*, 2018). Additionally, in *B. subtilis*, PBP1a/b, encoded by the *ponA* gene, has been implicated in PG synthesis during both division and elongation.

Interestingly, the role of PBPs in cell division appears to differ significantly between *E. coli* and *B. subtilis*. In contrast to the situation in *E. coli*, where at least one class A PBP (either PBP1a or PBP1b) is required for cell division, septal PG synthesis in *B. subtilis* can occur independently of all class A PBPs (aPBPs) (Rohs and Bernhardt, 2021). Recent findings by Rohs and Bernhardt (2021) have challenged the previously held belief in the indispensability of aPBPs for divisome functionality. Their research demonstrated that a strain of *B. subtilis* remained viable despite genetic deletions of all four known aPBPs (PBP1, PBP2c, PBP4, and PBP4d) (McPherson and Popham, 2003). Additionally, McPherson and Popham (2003) found that PBP2c and PBP2d were more active during cell sporulation, making them less critical for vegetative growth compared to spore formation. Conversely, Scheffers *et al.* (2004) suggested that although PBP1 and PBP4 are not essential, they still contribute to septal and lateral cell wall PG

synthesis. These findings indicate that *B. subtilis* can maintain viability and cell division even in the absence of all class A PBPs, likely through the action of alternative enzymes or pathways that compensate for their loss. However, penicillin can still kill bacteria because it primarily inhibits class B PBPs, such as PBP2b and PBP2a, which are essential for septal PG synthesis and cell division. Without functional class B PBPs, cell wall synthesis is disrupted, leading to cell lysis and death (Typas et al., 2012; Morales Angeles et al., 2017)..

However, a significant research gap remains in understanding the redundancy and functional interplay among PBPs, particularly in organisms like *B. subtilis*. While the deletion of up to four PBPs has provided insights into their dispensability, further studies are necessary to explore the effects of deleting additional PBPs, especially considering that no more than four PBPs have been deleted simultaneously in previous research. Investigating these additional deletions could provide a deeper understanding of the compensatory mechanisms in *B. subtilis* and reveal whether there are limits to the redundancy within the PBP family, thereby contributing to a more comprehensive understanding of bacterial cell wall synthesis and its regulation.

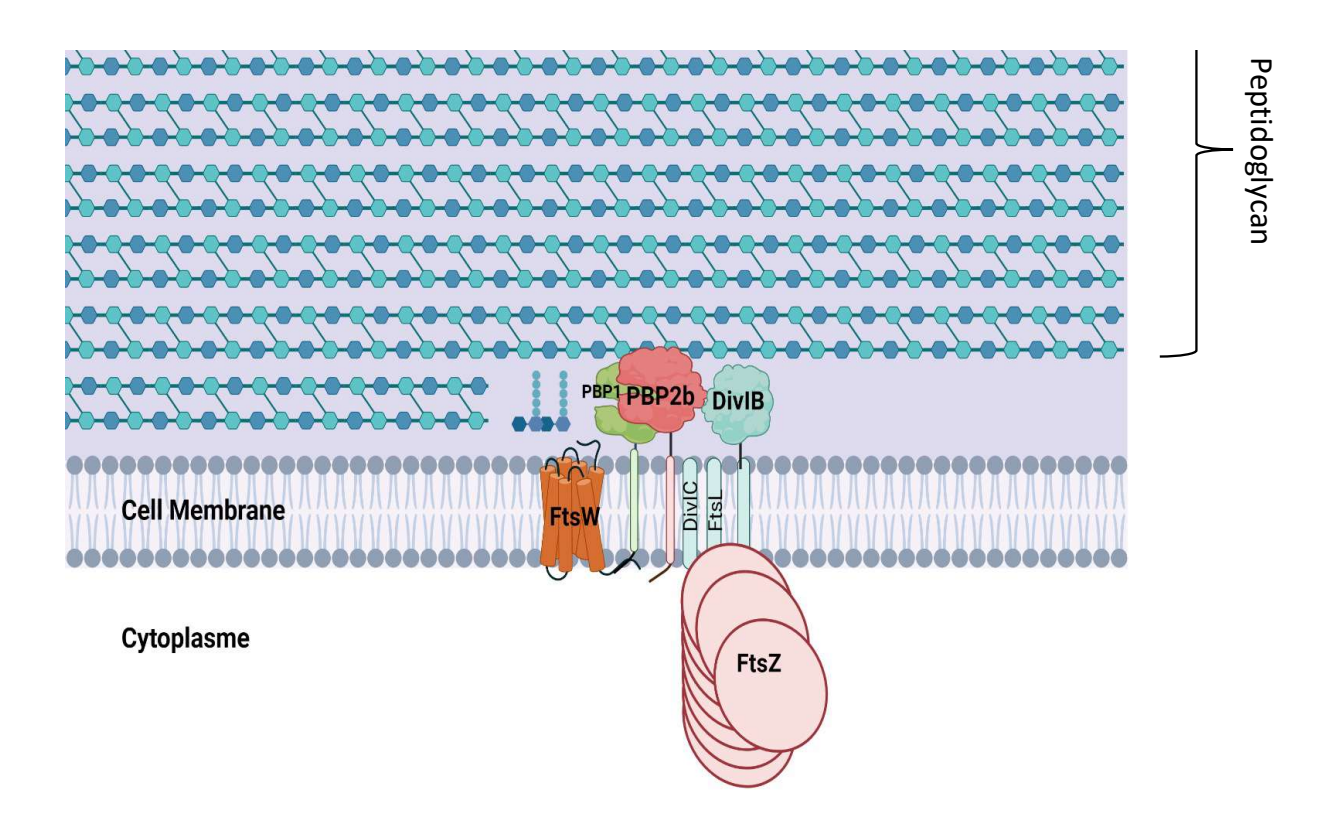


Figure 1.3: The Peptidoglycan (PG) Synthesis Complex at the Division Site.

Proteins involved in septum formation and PG synthesis at the cell division site in *Bacillus subtilis* (*B. subtilis*). The light red complex denotes the polymerised FtsZ ring. FtsL and DivIC proteins, illustrated in light blue, are embedded in the cell membrane. DivIB, also denoted in light blue, has two domains, one located in the cytoplasmic membrane and the second extending into the periplasmic space and outer cell wall layer. PBP2b and PBP1 denoted in red and green, respectively, are transpeptidase and transglucosylase, respectively. FtsW denoted in orange is a membrane protein with transglucosylase activity.

1.4 PBPs

The groundbreaking work of Sir Alexander Fleming in 1928 led to the discovery of penicillin, a substance produced by the fungus *Penicillium notatum*, which exhibited significant antibacterial effects. However, the mechanism of action of penicillin remained unknown for over 30 years (Fleming, 1929). It wasn't until the work of Tipper and Strominger (1965) that the antibacterial effect of penicillin was understood. The authors revealed that penicillin functions by inhibiting enzymes responsible for crosslinking PGs, resulting in bacterial cell wall instability and subsequently cell lysis. The authors also discovered that penicillin forms a covalent bond with the enzymes, which were later termed PBPs due to their ability to bind not only penicillin but also other β -lactam antibiotics (Tipper and Strominger, 1965). Identifying the presence and function of PBPs led to intense research into PBPs and significant advancements in the development of early antimicrobial therapies.

PBPs are a diverse group of membrane-associated proteins that vary in molecular weight, catalytic activity, structure, function, and roles in PG synthesis (Spratt, 1975). Since the initial studies on PBPs, many classes of these proteins have been identified, and our understanding of their activity, their role in bacterial cell wall production, and their importance in maintaining cell viability has greatly expanded (Sauvage *et al.*, 2008). Additionally, insights into β -lactam antibiotic resistance have emerged, particularly through the discovery that different bacterial species and strains possess varying complements of PBPs (Waxman and Strominger, 1983).

Antibiotics targeting PBPs primarily belong to the β -lactam class, including penicillin, cephalosporins, monobactams, and carbapenems. These antibiotics share a common β -lactam ring structure, enabling them to bind and inhibit PBPs, thereby disrupting PG synthesis, leading to cell lysis and eventual bacterial cell death (Sauvage *et al.*, 2008). β -lactam antibiotics have been invaluable in treating infections and

reducing mortality rates. However, the rising prevalence of antibiotic resistance has prompted the development of novel antibiotics targeting PBPs, as well as the use of adjuvants such as β-lactamase inhibitors that enhance the efficacy of existing antibiotics and help combat antibiotic resistance (Bush and Bradford, 2020). For these reasons, PBPs continue to be a crucial focus of research in the quest to develop novel antibiotics and address the growing challenge of antibiotic resistance. A thorough understanding of the structure, classification, function, and interaction of PBPs with lactam antibiotics is essential for designing effective antimicrobial treatments.

1.4.1 PBP Structure

PBPs are crucial in bacterial cell construction, replication, and determining cell shape, relying on their unique structure. It is the specific structure of PBPs that makes PBPs effective targets for β-lactam antibiotics, rendering these drugs bactericidal. PBPs consist of three domains, including the N-terminal transmembrane domain, the non-penicillin-binding (nPBP) domain, and the penicillin-binding (PB) domain. Each of these domains contributes to the overall function and regulation of PBPs in bacterial cell wall synthesis (Waxman and Strominger, 1983).

The N-terminal transmembrane domain of PBPs consists of predominantly hydrophobic amino acid residues that form alpha-helical structures embedded within the lipid bilayer of the bacterial cell membrane. This domain ensures the anchoring of PBPs to the bacterial cell membrane, facilitating access to PG precursors and other proteins in cell wall biosynthesis. The N-terminal transmembrane domain also plays a critical role in maintaining the spatial organisation of PBPs, which is essential for efficient catalytic activity (Goffin *et al.* 1996; Ghuysen, 1991; Waxman and Strominger, 1983).

The nPBP domain, also known as the regulatory domain, has been identified as having a potential role in modulating PBP activity. Unlike class A PBPs, which polymerise glycan chains via transglycosylase activity, the nPBP domain does not exhibit glycan chain polymerisation activity (Adam *et al.* 1997). The nPBP domain is composed of a conserved core structure, including β -sheets and α -helices, with variations in loops and connecting regions. This conformational flexibility allows the nPBP domain to adapt to the binding of different substrates and modulate the folding and activity of the enzyme (PBPs) (Goffin and Ghuysen, 1998). Additionally, there is evidence suggesting

that the nPBP domain may interact with other proteins or cellular factors, facilitating communication and regulation in the complex process of PG biosynthesis (Ghuysen *et al.*, 1996; Anderson *et al.*, 1967).

The PB domain of PBPs is the primary site where β -lactam antibiotics interact with these proteins, playing a crucial role in their catalytic activity (Bertonha *et al.* 2023). This domain contains a conserved motif known as the *Ser-X-X-Lys* (SXXK) sequence, where 'Ser' and 'Lys' represent serine and lysine residues, respectively, and 'X' denotes any amino acid (Smith et al., 2013). While this motif is a key feature of penicillin-binding proteins (PBPs), the ability to interact with penicillin depends not only on the presence of SXXK but also on the overall three-dimensional structure of the protein, including the active site conformation and additional conserved domains required for β -lactam recognition and binding (Goffin & Ghuysen, 1998). The serine residue in this motif is essential for forming a covalent bond with the β -lactam ring of penicillin and other β -lactam antibiotics (Bertonha *et al.* 2023). Additionally, the PB domain is vital for catalysing various enzymatic reactions involved in cell wall synthesis, including transpeptidation, and carboxypeptidation, depending on the specific PBP (Goffin and Ghuysen, 1998).

The catalytically active PB domains can vary in size and orientation, potentially reflecting their distinct functions and specificities (Sauvage et al., 2008). For example, the crystal structure of PBP3 isolated from *Pseudomonas aeruginosa* (*P. aeruginosa*) revealed a unique loop region in the transpeptidase domain, which may play a role in substrate recognition and binding (Sainsbury et al., 2011). In E. coli, the crystal structure of PBP5 in complex with a PG mimetic peptide demonstrated specific interactions between the enzyme and substrate, offering insights into the catalytic mechanism of PBPs (Silvaggi and Pratt, 2004). Beyond their role in cell wall synthesis, PBPs exhibit unique biochemical properties that contribute to their functionality. For example, a well-characterised D-alanine carboxypeptidase PBP5 from E. coli serves as a prototypical enzyme, providing deeper insights into the structure, function and catalytic mechanism of PBPs (Waxman and Strominger, 1983). This enzyme, a subclass of PBPs, remove the terminal D-Ala residue from the PG peptide chain, modulating the degree of cross-linking in the cell wall and affecting the mechanical properties of the bacterial cell. This understanding further elucidates the important roles and variations observed in PBPs (Vollmer et al., 2008).

The structural properties of PBPs are essential for their interaction with penicillin and other β-lactam antibiotics. The β-lactam ring of penicillin is designed to mimic the D-Ala-D-Ala peptide bond of the PG substrate, enabling the antibiotic to bind to the active site of PBPs and inhibit their enzymatic activity (Waxman and Strominger, 1983). It is important to be consider various factors that can influence the binding and catalytic activity of PBPs to ensure that potential therapies effectively utilise or address these factors, such as pH, temperature, and the presence of specific ions (Egan and Vollmer, 2013). Furthermore, alterations to the active site or overall protein structure of PBPs can impact their susceptibility to antibiotic inhibition, which has significant implications for antibiotic resistance (Schneider and Sahl, 2010).

Although β-lactam antibiotics revolutionised the treatment of bacterial infections, ongoing research into PBPs is providing new insights into why some PBPs display varying affinities for penicillin and other β-lactam antibiotics. These differences are often related to the structural and chemical properties of PBPs (Grebe and Hakenbeck, 1996). For example, in *Neisseria gonorrhoeae*, PBPs have shown variations in penicillin susceptibility among clinical isolates (Barbour, 1981). Furthermore, studies examining PBPs across different species of *Enterococcus* species revealed that the *genus* could be divided into at least nine distinct species based on PBP variations and the results of physiological and fermentation tests (Williamson *et al.*, 1986). These findings highlight that variations in penicillin susceptibility are common, and that understanding the reasons behind these differences could help reduce the incidence of antibiotic resistance.

1.4.2 PBP Classification and Functional Roles

PBPs can be divided into two main groups based on their molecular weights: high-molecular-weight (HMW) and low-molecular-weight (LMW) PBPs (Macheboeuf *et al.*, 2006). Additionally, PBPs are categorized according to their enzymatic activities and roles in peptidoglycan (PG) synthesis and remodeling into Classes A, B, or C (Sauvage *et al.*, 2008).

HMW PBPs are described as large, bifunctional proteins with both glycosyltransferase (GT) and transpeptidase (TP) activities, responsible for polymerizing glycan chains and cross-linking peptide chains during PG synthesis (Goffin and Ghuysen, 1998). These HMW PBPs can be further divided into Class A, which includes enzymes active in both GT and TP, and Class B, which consists of

monofunctional TP enzymes that exclusively cross-link peptide chains in PG (Sauvage et al., 2008).

In contrast, LMW PBPs are smaller, lack a GT domain, and belong to Class C (Macheboeuf *et al.*, 2006). These LMW PBPs are primarily involved in the maturation and remodeling of PG, functioning mainly as carboxypeptidases and endopeptidases, which cleave peptide bonds within the peptide chain (Sauvage *et al.*, 2008).

The presence of PBPs is crucial for bacterial cell viability; however, the number and type of PBPs present can vary significantly depending on the bacterial species, reflecting specific physiological requirements (Sauvage *et al.*, 2008). For example, PBPs are integral to various cellular processes, including cell wall biosynthesis, cell division, and morphogenesis. The effectiveness of PBPs as targets for β-lactam antibiotics also varies depending on the bacterial species. *E. coli*, a gram-negative bacterium, contains at least 12 different PBPs involved in various cell wall biosynthesis processes (Sauvage *et al.*, 2008). In contrast, *Staphylococcus aureus* has four (PBP1, PBP2, PBP3, and PBP4), *Streptococcus pneumoniae* has six (PBP1a, PBP1b, PBP2a, PBP2b, PBP2x, and PBP3), and *Pseudomonas aeruginosa* possesses five HMW PBPs (PBP1a, PBP1b, PBP2, PBP3, and PBP3a) and three LMW PBPs (PBP4, PBP5, and PBP7) (Fuda *et al.*, 2005; Gordon *et al.*, 2000; Zapun, Contreras-Martel, and Vernet, 2008).

These PBPs are all critical for bacterial cell viability, contributing to cell shape maintenance and peptidoglycan biosynthesis, yet many have also developed antibiotic resistance (Aguilera Rossi *et al.*, 2016). While the importance of PBPs for cell viability is well established, further research is needed to understand why certain bacteria develop antibiotic resistance and whether any PBPs possess functional redundancies. Bacteria require multiple PBPs because different PBPs specialize in distinct aspects of peptidoglycan synthesis—some are involved in cell elongation, others in septum formation during division, and some in repair and remodeling of the cell wall. This diversity allows bacteria to survive under various conditions, compensate for the loss of certain PBPs, and develop resistance by altering PBP binding affinity to β-lactam antibiotics (Goffin & Ghuysen, 1998; Sauvage *et al.*, 2008).

1.4.3 Characterisation of PBPs involved in B. subtilis division

In *B. subtilis*, PG synthesis necessitates the involvement of PBPs at distinct locations, including the division septum for cellular division, the lateral cell wall for

cellular elongation, and the pre-spore septum for spore development (Errington *et al.*, 2003). *B. subtilis* harbors a total of 16 PBPs, which are categorized into different functional classes based on their roles in PG synthesis and remodeling. While all class A PBPs are distributed across the membrane, PBP1a/b is specifically localised at the division septum (Gamba *et al.*, 2009). PBP 2c and 2d, which belong to class A, have been identified to play a role in spore formation and shown to localise at the pre-spore septum during this process (Gutelius *et al.*, 2014).

Although PBP1a/b is not distributed along the membrane of *B. subtilis*, it plays a crucial but redundant role in cell division, growth, and cell wall synthesis (Scheffers *et al.*, 2004). The naming of PBP1 is based on the Sodium dodecyl-sulfate polyacrylamide gel electrophoresis (SDS-PAGE) migration, where what initially appears as one protein is later identified as two distinct proteins, leading to their naming them as PBP1a and PBP1b instead of only PBP1. Due to its significance in the physiology and metabolism of this gram-positive model bacterium, PBP1a/b has been the subject of numerous studies (Pedersen *et al.*,1999; Claessen *et al.*, 2008). It has been shown to localise at the cell's midpoint during cell division, suggesting its involvement in catalysing PG synthesis at the division septum (Gamba *et al.*, 2009). Furthermore, PBP1a/b expression remains consistent during cell growth but declines during sporulation which suggest that it's involved in cell growth during exponential phase but not in sporulation (Gutelius *et al.*, 2014).

While Class A PBPs are typically regarded as non-essential for bacterial viability, Gutelius *et al.* (2014) observed that a *B. subtilis* strain lacking PBP1a/b exhibited a slightly reduced growth rate, which was attributed to the impact of the PBP1a/b mutation on the formation and function of the FtsZ ring. Additionally, inhibitors of PBP1, such as aztreonam, faropenem, piperacillin, cefuroxime, and cefsulodin, have been identified, alongside various co-selective inhibitors targeting other PBPs in *B. subtilis* (Macheboeuf *et al.*, 2006). These findings suggest that, despite being classified as non-essential, PBP1 plays a significant role in bacterial growth and division. This role highlights the potential for PBP1-targeted therapies to disrupt these critical processes, thereby providing a promising avenue for combating bacterial infections

The importance of PBP1 in cell division is further emphasised by the consequences of PBP1 knockout in *B. subtilis*. Early work of Popham and Setlow (1995) on PBP1 knockout strains using the peptide chain release factor 1 showed reduced growth rates in a variety of growth media. The authors also suggested that the PBP1 knockout strains may have impaired asymmetrical sporulation septum formation and altered localisation of the septum (Popham and Setlow, 1995). These findings further supported the hypothesis that PBP1 plays a significant role in the cell division machinery. Moreover, evidence suggests that *B. subtilis* strains lacking PBP1, encoded by the *ponA* gene, require higher levels of Mg²⁺ and/or Ca²⁺ for vegetative growth or spore outgrowth compared to wild-type strains and strains lacking other HMW PBPs (Murray *et al.*, 1998; Scheffers *et al.*, 2004). These findings suggest that PBP1 not only contributes to the cell division during vegetative growth but also play a role in division during spore outgrowth.

Another notable class A PBP in B. subtilis is PBP4, encoded by the bifunctional pbpD gene, which was previously thought to have no discernible role in normal cellular processes, including cell division, growth, spore heat resistance, spore formation, or spore germination initiation (Popham and Setlow, 1994). Despite the apparent redundancy of PBP4, surprisingly, the expression of the pbpD gene increases during vegetative growth and decrease during sporulation. However, the implications of these findings remain unknown (Popham & Setlow, 1994). In addition to PBP4, B. subtilis also expresses other Class A PBPs, such as those encoded by the *pbpG* and *pbpF* genes. The pbpG gene encodes PBP2d, while the pbpF gene encodes PBP2c. Interestingly, the expression of these genes is low during exponential growth but increases during sporulation, suggesting a potential redundancy in their functions (McPherson, Driks, & Popham, 2001). Sporulation in B. subtilis is typically triggered by nutrient limitation or other environmental stresses, such as starvation or high cell density. These conditions activate the master regulator Spo0A, which orchestrates the sporulation process through a complex regulatory cascade (Fawcett et al., 2000). It has been shown that the increase in pbpG and pbpF expression during sporulation is controlled by sporulation-specific sigma factors (e.g., σ^F or σ^G) in that case of pbpG and σ^G for pbpF) that activate genes necessary for spore cortex synthesis and assembly. Although deletion of the pbpG gene does not appear to affect spore formation, electron microscopy has revealed incomplete cortex formation and round spores, indicating that pbpG may have some functional importance. Moreover, when both pbpG and pbpF genes are mutated, a consistent defect in spore morphology is observed across all spores, further highlighting their potential roles in maintaining proper spore structure (McPherson $et\ al.$, 2001).

Despite their involvement in various stages of growth and development, including vegetative growth and sporulation, class A PBPs, including PBP1, PBP4, PBP2d, and PBP2c, are ultimately dispensable, as *B. subtilis* can grow and divide without them, particularly during vegetative growth

As previously mentioned, B. subtilis possesses six distinct LMW (class C) PBPs, most of which have hydrolase activity (Vollmer et al., 2008). The most abundant LMW PBP in vegetative B. subtilis is PBP5, encoded by the dacA gene. PBP5 functions as a D-alanyl-D-alanine carboxypeptidase, catalysing the removal of terminal D-Ala residues from muropeptide subunit pentapeptide side. Despite its high abundance, the absence of PBP5 in B. subtilis has been shown to have no impact on growth and survival (Atrih et al., 1999). Additionally, two other carboxypeptidases, PBP5* and DacF, encoded by the dacB and dacF genes respectively, have been shown to modulate PG cross-linking during sporulation, although they are non-essential for bacterial growth (Vollmer et al., 2008). Another interesting class C PBP in B. subtilis is PBP4a, a DDcarboxypeptidase encoded by the dacC gene. PBP4a is primarily expressed during the stationary phase of growth and is not essential for survival. Similarly, PBP4*, an endopeptidase encoded by the pbpE gene, has been shown to cleave various LD- and DD-bonds in stem peptides. Despite increased expression during the stationary phase of growth, PBP4* is also nonessential for growth (Huang et al., 1999; Vollmer et al., 2008). Finally, the product of the *pbpX* gene, which will be discussed in further detail in Chapter 5, plays a significant role in the context of *B. subtilis* LMW PBPs.

Unlike class A PBPs, class B PBPs are only capable of catalysing TP reactions at various loci (Pereira *et al.*, 2007). One class B PBP, considered an essential TP, is PBP2b, which plays a critical role at the division site during cell division, as evidenced by its peak expression during vegetative growth and spore formation (Daniel and Errington, 2003). Intriguingly, Sassine *et al.* (2017) discovered that *B. subtilis* strains with inactive PBP2b can still divide and replicate, which the authors attributed to the naturally dispensable PBP3 becoming indispensable. Further studies have provided insights into the localisation patterns of PBP2b, demonstrating that it assembles at sites

of cell elongation along the lateral cell wall (Daniel and Errington, 2003; Tiyanont *et al.*, 2006). Furthermore, Eichenberger et al. (2004) observed that PBP2b is subject to tight regulation, with the transcription of its encoding gene, pbpB, being controlled by the sigma factor σ^A M, which is specifically activated under cell envelope stress conditions. These include exposure to cell wall-targeting antibiotics (e.g., vancomycin and bacitracin), high salt concentrations, and other envelope perturbations that compromise peptidoglycan integrity (Cao et al., 2002; Eiamphungporn & Helmann, 2009). This regulatory control is essential for coordinating cell wall synthesis with other cellular processes (Eichenberger *et al.*, 2004). In addition to its importance in cell morphology and growth, PBP2b has also been implicated in the development of antibiotic resistance in *B. subtilis*, where mutations in the pbpB gene have been linked to reduced susceptibility to β -lactam antibiotics (Macheboeuf *et al.*, 2006).

There is no doubt that PBP2b in B. subtilis is a vital protein that plays a critical role in cell division and peptidoglycan (PG) biosynthesis (Daniel et al., 2000). This protein is essential for proper cell division and interacts with other components of the division machinery, such as DivIB, performing a transpeptidase (TP) function responsible for cross-linking PG. The Penicillin-binding protein and Serine/Threonine kinase Associated (PASTA) domains of PBP2b are particularly important in strengthening interactions with DivIB and have been associated with impaired cell division and heat-sensitive phenotypes when removed (Morales Angeles et al., 2020). PBP2b is also involved in the mraZ operon, which encodes essential cell division factors such as FtsL and PBP2b itself (White et al., 2022). Another important group of Class B PBPs includes PBP4b (PBP I) and SpoVD, which, like PBP2b, play a role in PG synthesis at the division septum during sporulation (Popham & Setlow, 1995). Specifically, B. subtilis PBP4b is crucial for cortex formation during spore development, while SpoVD is indispensable for assembling the cortex. There is also evidence demonstrating that spoVD mutations impair sporulation and spore resistance (Zheng and Losick, 1990). However, despite increased PBP4b expression during spore formation, null-mutated PBP4b does not impact sporulation (Ruzin et al., 1991).

Finally, the last group of Class B PBPs, PBP2a and PBPH, have been found to localize along the cell during vegetative growth and at the cell's center (Kawai *et al.*, 2009). PBPs in bacteria are critical for cell growth, but as we learn more about PBPs, it is becoming increasingly clear that not all PBPs are essential for cell viability. PBP2a

and PBPH, identified as functionally redundant Class B PBPs, seem to play a role in directing cylindrical cell wall synthesis (Wei *et al.*, 2003). Despite this redundancy, these PBPs localize along the cylinder part of cells during vegetative growth as well as at the cell's center (Kawai *et al.*, 2009). This dual localization raises questions about whether PBP2a and PBPH have roles in both cell division and elongation. However, genetic studies suggest that these PBPs predominantly contribute to side-wall synthesis. A double mutant for PBP2a and PBPH can be constructed that remains conditionally viable, requiring osmoprotection and increased Mg2+ in the growth medium. Interestingly, this mutant exhibits a round phenotype but is still capable of dividing and propagating (Wei*et al.*, 2003).

Table 1.1: Characteristics of identified Penicillin Binding Proteins (PBPs) in the Wild Type Bacillus subtilis (B. subtilis) strain 168

Class	Encoding Gene	Protein Name (PBP)	Molecu	lar weight (kDa)	Expression	Essentiality	Predicted Activity	
A	ponA	PBP1	99		V and Spo	No	D:C .: 1	
	pbpD	PBP4	70		V	No	Bifunctional, Transpeptidase and	
	pbpF	PBP2c	79		Spo	No	Hlycosyltransferase	
	pbpG	PBP2d	71		Spo	No	, , , , , , , , , , , , , , , , , , ,	
	pbpA	PBP2a	80	HMW	V and Spo	Partially redundant		
	pbpB	PBP2b	79	79 74 77 71	V	Yes		
В	pbpC	PBP3	74		V	No	Monofunctional, Transpeptidase	
Б	pbpH	PBPH	77		V and Spo	Partially redundant		
	spoVD	SpoVD	71		Spo	No		
	yrrR (pbpI)	PBP4b	65		Spo	No		
	dacA	PBP5	48	LMW	V	No		
	dacB	PBP5*	42		Spo	No	Carbovynontidoso	
С	dacC	PBP4a	52		S	No	Carboxypeptidase	
	dacF	DacF	43		Spo	No		
		pbpE	PBP4*	51	_	V	No	Endomontidoss
	pbpX	PBPX	43		V	No	Endopeptidase	

Classification, encoding genes, protein name, molecular weight, corresponding development stage, essentiality, and proposed function is presented. Proteins are categorised into groups A, B, and C according to their projected characteristics and molecular weight. V, stage of vegetative development; S, stationary phase of growth; Spo, sporulation stage; kDa, kilodalton; HMW, high molecular weight; LMW, low molecular weight; Table adapted from Sauvage *et al.* (2008).

1.5 Teichoic Acid

Teichoic acids are anionic glycopolymers present in the cell walls of G+bacteria, first identified by Armstrong *et al.*, (1958) during their investigation into the roles of cytidine diphosphate (CDP)-glycerol and CDP-ribitol in various bacteria, including *B. subtilis* and *S. aureus*. The discovery of the first teichoic acid led to the identification of other cell surface glycopolymers, collectively known as teichoic acids, which are typically characterised by their phosphodiester-linked polyol repeat units. The term "teichoic acid" is derived from the Greek word "teichos," meaning "wall," and refers to all bacterial cell wall, membrane, and capsular polymers containing glycerol phosphate (GroP) or ribitol phosphate (RboP) residues (Vollmer *et al.*, 2008). This early research provided valuable insights into identifying different cell surface glycopolymers, collectively referred to as teichoic acids, characterized by their phosphodiester-linked polyol repeat units (Vollmer *et al.*, 2008).

Teichoic acids can be categorised into LTAs and WTAs. LTAs are anchored in the bacterial membrane through a glycolipid and extend into the PG layer, while WTAs are covalently connected to PG and extend through and beyond the cell wall (Kojima *et al*, 1985). Both LTAs and WTAs are types of zwitterionic cell wall polymers, meaning they possess both positively and negatively charged functional groups. However, they are synthesised via distinct pathways. WTAs typically consist of RboP, GroP, or more complex sugar-containing polymers that are polymerised on a C_55-P precursor within the cytoplasm and then transported across the membrane to be linked to PGs. In contrast, lipoteichoic acids (LTAs) have a simpler structure than wall teichoic acids (WTAs), consisting of a polyglycerol phosphate chain attached to the bacterial membrane via a glycolipid anchor (Rahman *et al.*, 2009). LTAs and WTAs work together to form a 'continuum of negative charge,' extending from the bacterial surface through the outermost layers of the peptidoglycan (PG) (Neuhaus & Baddiley, 2003). Despite their overall negative charge, these molecules remain associated with the cell wall due to several stabilizing mechanisms.

Divalent cations such as Mg²⁺ and Ca²⁺ help neutralize electrostatic repulsion, ensuring stability within the PG matrix (Peschel *et al.*, 2000; Reichmann & Grundling, 2011). Additionally, the incorporation of *D-alanine* modifications into WTAs and LTAs provides regions of positive charge, reducing electrostatic repulsion and further stabilizing their interactions with the PG and surrounding cell envelope.

The role of *D-alanylation* in teichoic acid function and bacterial physiology will be discussed in detail later in this chapter.

1.5.1 Lipoteichoic Acid (LTA)

LTA is a vital component of the cell walls of many G+ bacteria, including *B. subtilis* and *S. aureus* (Brown and Santa Maria, 2013). LTA plays crucial roles in bacterial physiology, cell division, autolysis, host-pathogen interactions, and also acts as an immunomodulatory agent during infections (Gründling and Schneewind, 2007; Reichmann and Gründling, 2011). Although LTA is membrane-anchored, it can be shed into the extracellular environment or recognized at the bacterial surface by host pattern recognition receptors (PRRs), particularly Toll-like receptor 2 (TLR2) and CD14. This interaction activates downstream immune responses, including cytokine production, inflammation, and recruitment of immune cells (Morath *et al.*, 2002; Schroder *et al.*, 2003). The biosynthesis of LTA in both *B. subtilis* and *S. aureus* has been extensively studied, offering valuable insights into the molecular mechanisms underlying this process and identifying potential therapeutic targets.

LTA synthesis begins in the cytoplasm with the formation of a glycolipid anchor, catalysed by the enzymes GtaP and processive diacylglycerol βglucosyltransferase (UgtP). This leads to the creation of a diglucosyl-diacylglycerol linkage unit (Price et al, 1997) (Figure 1.4). Subsequently, this anchor is translocated to the outer membrane via a flippase, setting the stage for subsequent phases of biosynthesis (Jorasch et al., 1998). One such phase is the polymerisation of the LTA backbone, a process mediated by three distinct LTA synthases: lipoteichoic acid synthase (LtaS), which functions under normal conditions, and its orthologues YfnI, which is active during stress responses, and YqgS, which is involved in sporulation (Schirner et al., 2009). These synthases facilitate the polymerisation of glycerol phosphate, with the crucial step being the transfer of the glycerol phosphate moiety from phosphatidylglycerol (PGol) mediated by an active-site threonine residue (Wörmann et al., 2011). This reaction begins with the covalent attachment of the glycerol phosphate component of PGol to the threonine residue, causing the liberation of diacylglycerol and the incorporation of the glycerol phosphate unit into the growing LTA chain (Percy and Gründling, 2014).

In *S. aureus*, Kiriukhin *et al.* (2001) revealed that LTA biosynthesis follows a similar pathway to *B. subtilis*, involving the formation of a glycolipid anchor and polymerisation of the glycerol-phosphate backbone. However, the authors revealed that enzymes involved are distinct from those in *B. subtilis*. In *S. aureus*, LTA biosynthesis begins with the synthesis of the anchor in the bacterial cytoplasm, mediated by the GT enzyme processive 1,2-diacylglycerol β-glucosyltransferase (YpfP). The anchor is then presumed to be flipped to the outer membrane by the flippase protein LtaA (Kiriukhin *et al.*, 2001). LtaS then catalyses the capture of glycerol phosphate from the membrane lipid diacyl-PGol and incorporates it into the elongating LTA chain. In contrast to *B. subtilis*, *S. aureus* has only a single LTA synthase LtaS (Percy, 2014), and this gene is a conditionally essential enzyme proposed as a potential target for anti-bacterial therapies due to its crucial role in cell viability (Schirner *et al.*, 2009; Pogliano *et al.*, 2012).

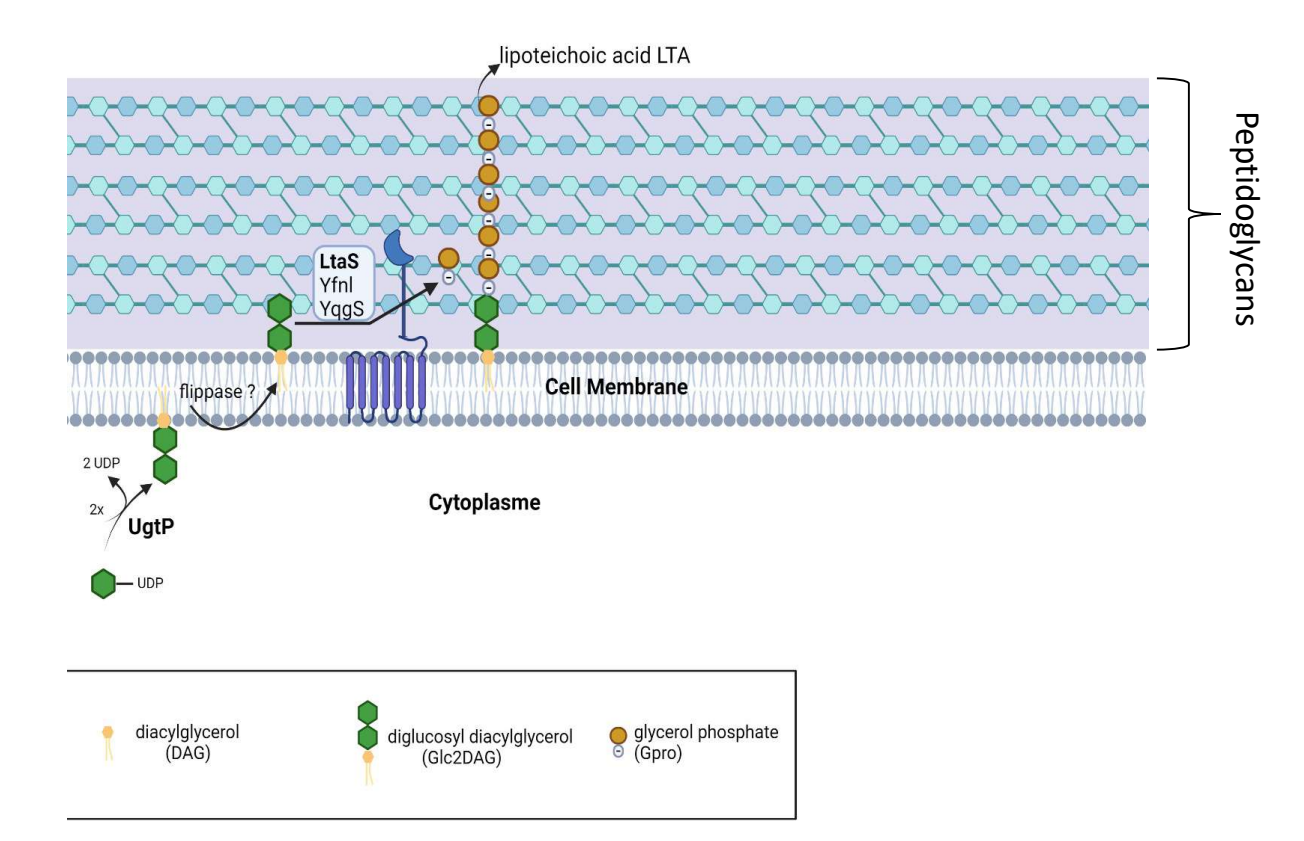


Figure 1.4: Biosynthesis of Lipoteichoic Acid (LTA) in B. subtilis.

Green hexagons illustrate diglucosyl attached to diacylcerol (DAG) illustrated by yellow circles in the cytoplasm forming Glc2DAG. Glc2DAG flips to the outer side of the cell membrane via the action of a flippase. LtaS and its homologues, Yfnl and YqgS then begin building the LTA chain by attaching glycerol phosphate, illustrated in gold from phosphatidylglycerol.

1.5.2 Wall Teichoic Acid (WTA)

WTA are anionic, phosphate-rich polymers crucial for bacterial physiology, playing key roles in cell division, cell shape maintenance, autolysis, and host interactions during infection (Brown *et al.*, 2013; Swoboda *et al.*, 2010). Research on WTA biosynthesis in *B. subtilis* and *S. aureus* has elucidated the pathways and genes involved. These pathways are common to many bacteria, though significant variations exist in the polymer subunits. In *Bacillus* species, two primary variations involve the use of either glycerol or ribitol in a phosphorylated form to generate the polymer. Under phosphate-limiting conditions, an alternate pathway is used employed, generating uronic acid polymers to minimise phosphate use. Additionally, a small proportion of the teichoic acid can be composed of poly (glucopyranosyl N-acetylgalactosamine 1-phosphate) (Bhavsar *et al*, 2004). In contrast, *S. aureus* only produces the ribitol phosphate polymer.

The biosynthesis of WTA in the wild type strain B. subtilis (168) begins with the formation of the lipid carrier undecaprenyl phosphate (C 55-P), which serves as a substrate for the successive addition of ribitol-phosphate or glycerol-phosphate subunits (Swoboda 2010). The enzyme TagO initiates WTA biosynthesis by transferring a GlcNAc moiety from UDP-GlcNAc to C 55-P, which is then attached to the undecaprenyl-phosphate carrier lipid (Soldo, B 2002). The enzyme TagA then transfers a ManNAc from UDP-ManNAc to the C4 hydroxyl of GlcNAc, forming the ManNAc-β1,4-GlcNAc disaccharide. This disaccharide serves as a primer for the subsequent polymerisation of the ribitol (glycerol)-phosphate subunits (Zhang, Y. H. 2006). A glycerol-phosphate unit is then transferred from CDP-glycerol to the C4 position of ManNAc by the glycerophosphotransferase TagB. TagF and TagD subsequently catalyse the repeated polymerisation of glycerol-phosphate with TagD synthesising CDP-glycerol and providing the necessary pyrophosphate moiety to ManNAc-β1,4-GlcNAc disaccharide. Finally, TagF adds approximately 45 – 60 glycerol-phosphate units (Lovering, A. L. 2010, Pereira, M. P. 2008, Kojima, N. 1985) (Figure 1.5).

In *S. aureus*, WTAs consist of a poly(ribitol-phosphate) backbone, which is similarly assembled on a C_55-P lipid carrier (Brown *et al.*, 2013). The process begins with the enzyme TarO catalysing the transfer of GlcNAc from UDP-GlcNAc to the C_55-P, forming lipid I (Swoboda *et al.*, 2010; Brown, 2010). The enzyme TarA then transfer a ManNAc from UDP-ManNAc to the C4 hydroxyl of a GlcNAc to form the ManNAc-β1,4-GlcNAc disaccharide (Brown S. 2010). TarD functions similarly to TagD in *B. subtilis* (Badurina. 2003). The polymerisation of the glycerol-phosphate subunits onto lipid II is facilitated by the integral membrane protein TarF, and the ribitol-phosphate is added by the TarL enzyme. (Meredith, T. C 2008; Brown *et al.*, 2012). Finally, the lipid-linked wall teichoic acid (WTA) polymer is subsequently transported to the outer surface of the bacterial membrane by a two-component ATP binding cassette (ABC) transporter called TagGH (or TarGH) (Lazarevic and Karamata, 1995). The last step in the biosynthesis of wall teichoic acid involves creating a phosphodiester bond between the WTA polymer and the C6 hydroxyl group of the PG MurNAc unit once the polymer is outside the cell (Kawai *et al.*, 2011).

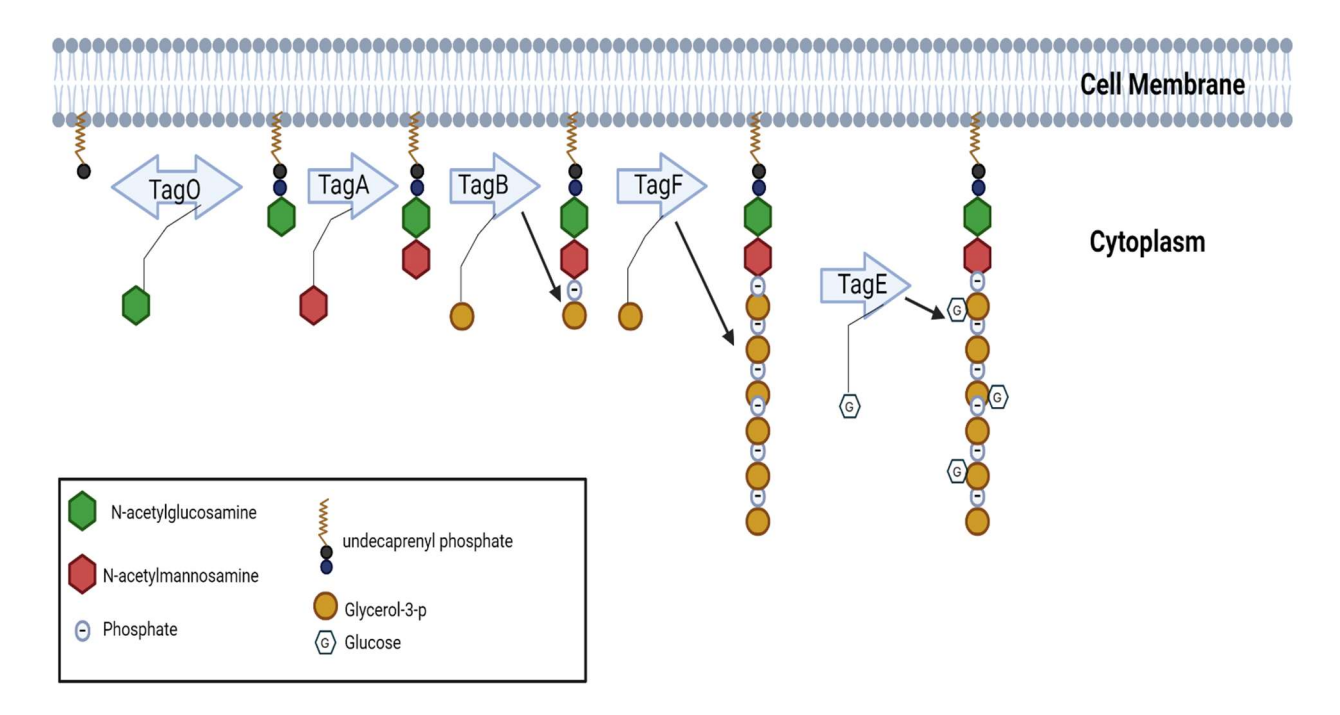


Figure 1.5: Wall teichoic acid (WTA) Biosynthesis in *B. subtilis*.

WTA biosynthesis begins in the cytoplasm with the attachment of saccharide moieties to C_55-P by the TagO and TagA enzymes. GroP is then attached by TagB and TagF to form a polyglycerol phosphate backbone. TagE then attaches glucose to the polyglycerol.

1.6 Function and Modification of Teichoic Acid

The precise role and functionality of anionic polymers in bacterial cellular processes remain somewhat elusive. However, it is clear that alterations in WTA or LTA can significantly affect bacterial growth and development in various ways. For example, alteration in WTA biosynthesis has been shown to increase the sensitivity of bacterial WTAs to certain elements in buffer solutions, temperature fluctuations and citrate (Oku *et al.*, 2009; Schirner *et al.*, 2009) and susceptibility to infection by bacteriophages. Moreover, defects in WTA synthesis in *B. subtilis* have been associated with morphological irregularities (Fedtke *et al.*, 2007). Notably, the simultaneous deletion of both WTA and LTA biosynthetic pathways has been shown to be lethal for bacterial cells, highlighting their essential role in maintaining cellular viability and integrity (Oku *et al.*, 2009; Schirner *et al.*, 2009). Interestingly for *S. aureus* loss of LTA synthesis results in a severe phenotype, whereas the loss of WTA is better tolerated, but does result in osmotic sensitivity.

1.6.1 TA involvement in Cell Elongation and Division

It is evident that LTAs and WTAs play crucial roles in cell growth, division and morphogenesis, particularly in rod-shaped bacteria like B. subtilis and Listeria monocytogenes (L. monocytogenes). D'Elia et al. (2006) observed that mutations in TagO or TagF led to a reduction in WTA production, resulting in morphological alterations towards a more spherical shape (D'Elia et al., 2006). These findings underscore the critical function of teichoic acids in bacterial morphogenesis. Atilano et al. (2010) and Qamar and Golemi-Kotra (2012) explored the associations between WTAs and PG machinery in S. aureus. The authors observed altered localisation of the putative PG cross-linking enzymes PBP4 and teichoic acid D-alanine hydrolase (FmtA) in the absence of WTAs. Additionally, disruption of LTA synthesis, achieved by inhibiting the expression of ltaS and its four paralogues responsible for LTA biosynthesis in B. subtilis, affected cell septum formation and led to the formation of unbalanced septum rings (Schirner et al., 2009). Schirner et al. (2009) also engineered a xylose-inducible promoter to control ltaS expression, followed by the strategic deletion of the remaining three *ltaS* paralogues, which allowed for the introduction of the tagO deletion under xylose-present conditions. This approach resulted in the deactivation of both WTA and LTA systems, causing lethal effects on cell structure and viability (Schirner et al., 2009). Collectively, these findings highlight the indispensable role of teichoic acids in maintaining cellular integrity and morphology in certain bacterial species. Suggesting they are likely involved in several essential processes related to cell wall synthesis and function.

1.6.2 Control of Autolytic Activity

Autolytic activity, which refers to a cell's ability to undergo programmed cell death, has been shown to be affected when WTA or LTA synthesis is impaired. Both WTAs and LTAs have been identified as potential substrates for autolysins, or cell wall hydrolases, which are essential for cell division and proliferation. Previous research has demonstrated that bacterial strains lacking WTAs exhibit increased rates of autolysis and display a distinct expression profile of endogenous autolysins (Biswas *et al.*, 2012; Maki, Yamaguchi and Murakami, 1994). This is because WTAs normally bind and sequester positively charged autolysins, and in their absence, autolysins are free to degrade the cell wall (Brown *et al*, 2013). Peschel *et al.* (2000) observed that the absence of D-Ala esters in teichoic acids increases *S. aureus*' susceptibility to

glycopeptide antibiotics by threefold. The authors also noted that the autolytic activity of the D-Ala-deficient mutant was lower and more sensitive to the staphylolytic enzyme lysostaphin compared to the wild-type variant (Peschel *et al.*, 2000). To conceal the negative charge and enable autolysins to degrade PG, positively charged D-alanyl esters should be present. This suggests that WTAs must be either absent from the septum or exhibit strong D-alanylation, as this is necessary to control autolytic activity and ensure proper separation at the cross wall during cell division (Yamamoto *et al.*, 2008).

1.6.3 Cation-Binding Activities

Teichoic acids form a dense layer of negatively charged components on the surfaces of G+ cells (Baddiley, 1970). It has been hypothesised that the repulsion between phosphate groups is mitigated by the binding of ions by WTA and LTA, effecting the structure of the polymer, and consequently, the stability of the cell wall (Kern et al., 2010; Wickham et al., 2009). A key aspect of cellular stability is the permeability and stiffness of the cell membrane, both of which are influenced by the overall architecture of these polymers (WTA & LTA), shaped by WTA-coordinated cation networks (Marquis, Mayzel and Carstensen, 1976). WTAs have also been shown to modify local pH without affecting the pH gradient across the cell wall, suggesting that WTAs may indirectly influence enzymatic activity (Biswas et al., 2012). The Dalanylation process conceals the negatively charged regions of the polymer (see later), reducing WTAs' capacity to bind cations (Heptinstall et al, 1970). This alteration not only impacts the strength and flexibility of the cell wall but may also play a role in the bacteria's capacity to withstand external pressures and avoid the immune responses of the host. D-alanylation can modify the interactions with antimicrobial peptides and potentially enhance bacterial resistance to specific antibiotics by reducing the negative charge. This alteration can have an impact on the overall survival and pathogenicity of Gram-positive bacteria.

1.7 Modifications of TA

1.7.1 Glycosylation of Teichoic Acid

The roles of glycosylation, a common modification of WTAs, is not yet fully understood. In *S. aureus*, WTA polymers are typically integrated with GlcNAc, while, in *B. subtilis*, glucose is used (Neuhaus and Baddiley, 2003). Depending on the bacterial strain, the stereochemistry of the glycosidic bond can present as either β -, α -, or a

mixture of these two anomers. In *S. aureus*, poly(ribitol-phosphate) alpha-N-acetylglucosaminyltransferase (TarM) is responsible for adding α -O-GlcNAc modifications to RboP-WTA, while poly(ribitol-phosphate) β -N-acetylglucosaminyltransferase (TarS) adds β -O-GlcNAc modifications (Xia *et al.*, 2010). Conversely, in *B. subtilis* W23, poly(ribitol-phosphate) β -glucosyltransferase (TarQ) is the enzyme responsible for attaching β -glucose units to polyRboP-WTAs (Brown *et al.*, 2012).

A substantial body of literature suggests that WTA GTs may have specific functions in glycosylation. In a study by Bae *et al.* (2004), the authors used transposon-disrupted mutant in a suspected GT from the *S. aureus* Newman strain, which resulted in reduced virulence in a nematode-killing test. The authors proposed that glycosylation may play a significant role in the pathogenicity of *S. aureus* (Bae *et al.*, 2004). The conformation of glycosidic linkages and the presence or absence of sugars can influence a polymer's structure, potentially affecting its interactions at the cell interface or within the cell envelope (Bernal *et al.*, 2009). Furthermore, the absence of these modifications in certain strains leads to noticeable changes in their phenotypes, particularly in aspects like antibiotic susceptibility and virulence (Brown *et al.*, 2012; Xia *et al.*, 2010).

1.7.2 D-alanylation of Teichoic Acid

Previous research has demonstrated that the addition of D-Ala esters to WTAs is a crucial mechanism by which bacteria can adjust their surface charge (Collins, 2002). Unlike the glycosylation of teichoic acids, which occurs within the cell, D-alanylation takes place after WTAs or LTAs are exported to the cell surface, representing the final step in this process. In the cytoplasm, D-Ala is activated by the D-alanine-D-alanyl carrier protein ligase DltA using ATP, leading to the formation of a high-energy D-alanyl-adenosine monophosphate intermediate (Percy and Gründling, 2014). This intermediate is then transferred to the phosphopantheinyl prosthetic group of the D-alanyl carrier protein Dlt, initiating the D-alanylation process. DltC, equipped with a pantothenate cofactor, facilitates the formation of a thioester bond with D-Ala via a nucleophilic attack by the sulfhydryl group on the mixed anhydride (Heaton and Neuhaus, 1994; Volkman *et al.*, 2001) (Figure 1.6).

It has been hypothesised that teichoic acid D-alanyltransferase (DltB) and DltD, whose exact functions are yet to be confirmed, assist in the transmembrane movement

of DltC and in the addition of D-Ala to LTAs and subsequently WTAs, although this process is poorly understood (May *et al.*, 2005) (Figure 1.6). DltB, a member of the membrane-bound O-acyltransferase (MBOAT) protein group, is recognised for its ability to transfer organic acids to hydroxyl groups of membrane-embedded components embedded in cell membranes (Hofmann, 2000; Shindou *et al.*, 2009). DltD is thought to be anchored in the membrane, with a short intracellular N-terminal section and larger extracellular C-terminal domain, which most likely possess esterase/thioesterase activity (Figure 1.6).

Earlier studies by Fischer and Rösel (1980) noted that an increase in sodium chloride (NaCl) reduced D-alanylation, and similarly, MacArthur and Archibald (1984) observed that a rise in pH caused a decline in D-alanylation. The addition of the positively charged amines via the attachment of D-alanyl esters to the hydroxyls on teichoic acids alters the net charge of the polymers and reduces the electrostatic repulsion between adjacent teichoic acid chains. It has also been suggested that a reduction in the electrostatic repulsion may aid in the formation of stabilising ion pairs between the cationic esters and anionic phosphate groups (Wickham *et al.*, 2009).

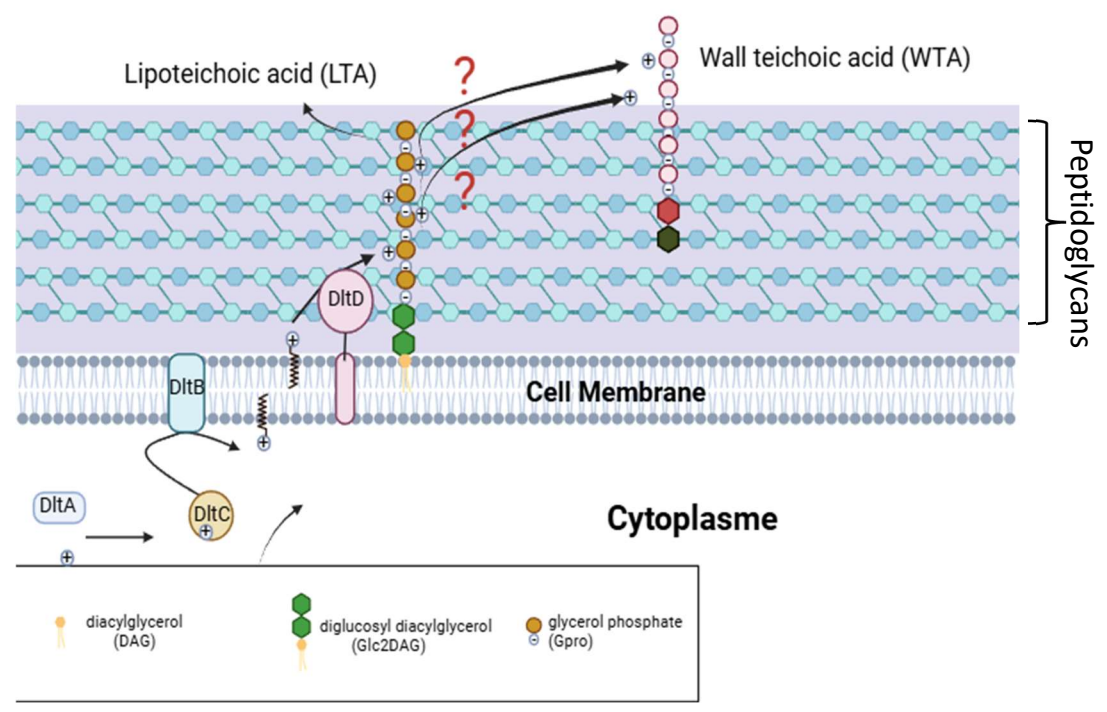


Figure 1.6: D-alanylation of Teichoic Acid in B. subtilis.

Schematic of D-Ala activation and transfer from inside the cell to the outer membrane. D-Ala is initially activated by DltA and then attached to DltC, which transfers it; by DltB activity. The D-Ala is attached to the membrane and then flipped to the outer surface. DltD assists in the D-alanylation of Lipoteichoic acid (LTA), and D-Ala is then transferred to Wall teichoic acid (WTA) by an unknown mechanism.

1.8 Specific Aims of this Project

The aims of this thesis was to investigate the redundancy of the PBPs in *B. subtilis* that are essential for bacterial survival and growth. Specifically, we aim to identify and characterise the minimal genetic set of PBPs capable of sustaining normal growth conditions and ensuring cell viability. Through this process, we hope to gain insights into the redundancy and regulation of key PBPs during cell growth and their broader implications.

This thesis has three primary objectives:

- 1. To construct and characterise a strain of *B. subtilis* with the minimal set of PBPs necessary for survival under normal growth conditions and maintaining cell viability.
- 2. To identify redundant PBPs and understand the redundancy of specific PBPs, including PBP2a and PBPH, in mediating cell growth.
- 3. To define the function of the PBP denoted PBPX.

These objectives form the foundation of this thesis. We will discuss the implications of our findings in relation to the growth of *B. subtilis* and how these insights might relate to growth in other bacterial species.

Chapter 2 Materials and methods

2.1 Bacterial Strains collection

The bacterial strains used in this thesis were created through transformation, with their characteristics presented in Table 2.1. Antibiotic resistance gene abbreviations utilised for strain selection include bla (Ampicillin), cat (Chloramphenicol), spc (Spectinomycin), kan (Kanmycin), neo (Neomycine), erm (Erythromycin), zeo (Zeocine), and ble (Phleomycin). Following the confirmation of each strain's genotype, all strains were suspended in a solution containing 20% glycerol and stored at a temperature of -80°C until further analysis.

Table 2.1. Bacterial strain characteristics and source for construction

Bacillus Subtilis Strains	Genotype	Construction / Source / Reference	
168+	Wild Type	Lab Collection	
BKE13980	∆pbpH::erm trpC 2	(Koo et al. 2017)	
BKE13980	∆pbpH::kan trpC2	(Koo et al. 2017)	
3140	trpC2 (cat Pxyl-GFPa- pbpH1-827)	Dirk Jan Scheffers' lab (Scheffers <i>et al.</i> 2004)	
YA11	168+ ∆pbpH::erm	This work: 168+ transformed with BKE13980	
YA12	168+ ∆pbpH::kan	This work: 168+ transformed with BKE13980	
YA13	$168+$ amyE Ω (spc Pxyl 1- $21pbpH$)	This work	
YA14	$\Delta pbpH::erm\ trpC2\ amyE\ \Omega$ (spc Pxyl 1-21 'pbpH)	This work: YA13 transformed with YA11	
YA15	168+ trpC2 (cat Pxyl-GFPa- pbpH1-827)	This work: 168+ transformed with 3140	
YA16	∆pbpH::kan trpC2 (cat Pxyl- GFP-pbpH1-827)	This work: YA15 transformed with YA12	
BKE25000	trpC2 ∆pbpA::erm	(Koo et al. 2017)	
BKK25000	trpC2 ∆pbpA::kan	(Koo et al. 2017)	
3103	trpC2 (cat Pxyl-GFPa- pbpA1-804)	Dirk Jan Scheffers' lab (Scheffers et al. 2004)	
YA17	168+trpC2 ΔpbpA::erm	This work: 168+ transformed with BKE25000	
YA18	168+trpC2 ∆pbpA::kan	This work: 168+ transformed with BKE25000	

YA19	168+ amyE Ω (spc Pxyl 1- 17'pbpA)	This work	
YA20	ΔpbpA:erm trpC2 amyE $Ω$ (spc Pxyl 1-17'pbpA)	This work: 168+ transformed with 3103	
YA21	168+ trpC2 (cat Pxyl-GFPa- pbpA1-804)	This work: YA20 transformed with YA17	
YA22	trpC2 ∆pbpA:kan (cat Pxyl- GFPa-pbpA1-804)	This work: YA21 transformed with YA18	
YA23	$\Delta pbpH:erm\ \Delta pbpA:kan$ $trpC2\ amyE\ \Omega\ (spc\ Pxyl\ 1 21\ 'pbpH)$	This work: YA14 transformed with YA18	
YA24	$\Delta pbpA$:erm $\Delta pbpH$:kan trpC2 amyE Ω (spc Pxyl 1- 17'pbpA)	This work: YA20 transformed with YA12	
YA25	168+ amyE Ω (spc Pxyl 1- 48'pbpA	This work	
YA26	$168+$ amyE Ω (spc Pxyl 46- 685 ʻpbpH	This work	
YA27	168+ amyE Ω (spc Pxyl 1- 45 'pbpH:pbpA'48-716)	This work	
YA28	$\Delta pbpA$:erm trpC2 amyE Ω (spc Pxyl 1-45 'pbpH :pbpA'48-716)	This work	
YA29	$168+$ amyE Ω (spc Pxyl 1- 45 'pbpH)	This work	
YA30	168+ amyE Ω (spc Pxyl 48-716'pbpA)	This work	
YA31	168+ amyE Ω (spc Pxyl 1- 48'pbpA ::pbpH'45-685)	This work	
YA32	$168 + \Delta pbpH::erm trpC2$ $amyE \Omega (spc Pxyl 1-48'pbpA$::pbpH'45-685)	This work	
YA33	$168+$ amyE Ω (spc Pxyl pbpH c.109 $_$ 111delinsGCA (p.K37A)	This work	
YA34	$168+$ amyE Ω (spc Pxyl pbpH c.124_126delinsGCA (p.Q42A)	This work	
YA35	$168+$ amyE Ω (spc Pxyl pbpH c.124_126delinsGCA (p.Q42A) c.109_111delinsGCA (p.K37A)	This work	
YA36 -YA36	168+ ΔpbpH::erm trpC2 amyE Ω (spc Pxyl pbpH) c.109_111delinsGCA (p.K37A)	This work	

YA37	168+ $\Delta pbpH$::erm trpC2 amyE Ω (spc Pxyl pbpH c.124_126delinsGCA (p.Q42A)	This work	
YA38	$168+\Delta pbpH::erm\ trpC2$ $amyE\ \Omega\ (spc\ Pxyl\ pbpH\ c.124_126delinsGCA\ (p.Q42A)$ $c.109_111delinsGCA\ (p.K37A)$	This work	
GGH	∆PbpH (markerless) trpC2	Grace Goldsmith: Unpublished	
GGA	ΔPbpH (markerless) trpC2	Grace Goldsmith: Unpublished	
GG132	ΔpbpCFDGEX::erm trpC2	Grace Goldsmith: Unpublished	
GG133	∆pbpFGX ∆dacB ∆dacF (markerless) ∆dacA ::erm trpC2	Grace Goldsmith: Unpublished	
GG136	∆pbpCFDGEX (markerless) ∆dacA ::erm trpC2	Grace Goldsmith: Unpublished	
YA39	168+ ∆PbpH (markerless) trpC2	This work	
YA40	168+ ∆PbpA (markerless) trpC2	This work	
YA41	168+ ∆pbpCFDGEX∷erm trpC2	This work	
YA42	168+ ΔpbpFGX ΔdacB ΔdacF (markerless) ΔdacA ∷erm trpC2	This work	
YA43	168+ ΔpbpCFDGEX (markerless) ΔdacA ::erm trpC2	This work	
YA-X	168+ ΔpbpCFDGEX ΔdacA (markerless) ΔponA::erm trpC2	This work	
YA-XI	168+ ΔpbpCFDGEX ΔdacA (markerless) ΔponA::erm ΔpbpH::kan trpC2	This work	
BKK16950	trpC2 ∆pbpX::kan	(Koo et al. 2017)	
AG600	trpC2 Δltas::cat Δyfnl::erm Δyqgs::spc	Aurélie Guyet: (Guyet et al. 2023)	
DLT71CA	trpC2 ∆dltAB::cat	Aurélie Guyet: (Guyet et al. 2023)	
YA44	168+trpC2 ∆pbpX∷kan	This work	
YA45	168+ trpC2 Δltas::cat Δyfnl::erm Δyqgs::spc	This work	
YA46	168 + trpC2 ∆dltAB::cat	This work	
YA47	ΔpbpH::erm trpC2 amyE Ω (spc Pxyl pbpH)	This work	

Staphylococcus Aureus	Genotype	Construction / Source / Reference	
JE2	Wild type	The Nebraska Transposon Mutant Library	
fmtA	fmtA::Tn	The Nebraska Transposon Mutant Library	
flp	flp::Tn	The Nebraska Transposon Mutant Library	
Escherichia Coli Strains	Genotype /Relevant Features		
BL21 (DE3)	fhuA2 [lon] ompT gal (λ DE3) [dcm] Δ hsdS λ DE3 = λ sBamHIo Δ EcoRI-B int::(lacI::PlacUV5::T7 gene1) i21 Δ nin5	New England BioLabs®	
YA47	BL21(DE3) pET-28a(+) + pbpA-His tag	This work	
YA48	BL21(DE3) pET-28a(+) + pbpH-His tag	This work	
DH5α	huA2 Δ(argF-lacZ)U169 phoA glnV44 Φ80 Δ(lacZ)M15 gyrA96 recA1 relA1 endA1 thi-1 hsdR17	New England BioLabs®	

2.2 Plasmids

Table 2.2 includes the name, characteristics, and the reference or source for all the plasmids used in this study. The construction used HIFI method, described in greater detail in Chapter 2, section 2.20.

Table 2.2. Plasmid characteristics and source for construction.

Name of Plasmid	Characteristics	Reference / Source	
pDR111	bla amyE' spc lacI Pspank' amyE	David Rudner, Harvard University	
pYA1	bla amyE' spc lacI Pspank pbpH' amyE	This work	
pYA2	bla amyE' spc lacI Pspank 'pbpH' amyE	This work	
pYA3	bla amyE' spc lacI Pspank pbpA' amyE	This work	
pYA4	bla amyE' spc lacI Pspank 'pbpA' amyE		
pET-28a(+)	lacI T7 promoter lac operator RBS His.tag T7.tag thrombin His.tag T7 terminator Kan	Novagen®	
pYA5	pET-28a(+) Ω pbpA-His tag (N-terminus)	This work	

pYA6	pET -28 $a(+)\Omega$ $pbpH$ -His tag (C-terminus)	This work
pYA7	pET -28 $a(+)\Omega$ $pbpH$ -His tag (N-terminus)	This work
pSHP1	oriBR322 bla amyE∷-Pxyl- mNeonGreen spec	This work
pYA8	oriBR322 bla amyE::-Pxyl- pbpH spec	This work
pYA9	oriBR322 bla amyE::-Pxyl- pbpA spec	This work
pYA10	oriBR322 bla amyE::-Pxyl- (1-135 bp) 'pbpH spec	This work
pYA11	oriBR322 bla amyE∷-Pxyl- (1- 144) 'pbpA spec	This work
pYA12	oriBR322 bla amyE::-Pxyl- (1-63 bp) 'pbpH spec	This work
pYA13	oriBR322 bla amyE::-Pxyl- (1- 51) 'pbpA spec	This work
pYA14	oriBR322 bla amyE::-Pxyl- pbpA'(144-2151) spec	This work
pYA15	oriBR322 bla amyE::-Pxyl- pbpH'(135-2058 bp) spec	This work
pYA15	oriBR322 bla amyE::-Pxyl- (1-135 bp) 'pbpH- pbpA'(144-2151) spec	This work
pYA15	oriBR322 bla amyE::-Pxyl- (1- 144) 'pbpA-pbpH'(135-2058 bp) spec	This work
pYA15	oriBR322 bla amyE::-Pxyl- pbpH'(135-2058 bp) spec	This work

2.3 Media supplements

The antibiotic, substrate, and final inducer concentrations used in liquid and solid media throughout the study are provided in Table 2.3.

Table 2.3. Antibiotics and stock solution concentration and final concentrations for *Bacillus Subtilis (B. subtilis)* and *Escherichia Coli (E. coli)*.

Antibiotics	Antibiotic Stock Solution Concentration	Final concentration of <i>B. subtilis</i>	Final concentration of E. coli
Ampicillin	50 mg/ml		100 μg/ml
Kanmycin	25 mg/ml	5 μg/ml	25µg/ml
Chloramphenicol	10 mg/ml	5 μg/ml	
Spectinomycin	100 mg/ml	50 μg/ml	
Erythromycin	20 mg/ml	1.0 μg/ml	
Zeocine	100 mg/ml	10 μg/ml	
Substrates & inducers			
5-bromo-4-chloro 3- indolyl-β-D galactopyranoside (X- Gal)		40 mg/ml	
Isopropylthio-β galactoside (IPTG)		1mM	1mM
Xylose		0.50%	0.50%

mg, milligrams; ml, millilitre; μg, microgram; mM, millimolar; %, percentage.

2.4 Plasmid DNA extraction

Plasmids were extracted using the Qiagen mini prep kit following the standard method with slight alterations. Cultures of *E. coli*, generally grown overnight at 37 degrees with appropriate antibiotic selection were used to provide the starting material. The cells (from 2 ml of culture) were pelleted by centrifugation at >8000 rpm for 3 minutes at 15-25°C. The cell pellet was then resuspended in solution P1 (200 µl) from the kit and then solution P2 (200 µl) was added and mixed gently to ensure that the majority of the cell lysed. Then solution N3 (200 µl) was added and the mixed by inversion. The resulting material was then centrifuged (max speed on microfuge for 5 min) and the cleared lysate was then applied to a QIAprep 2.0 column. Here, the plasmid DNA binds to the silica membrane, separating the plasmid DNA from other cellular components, ensuring the selective isolation of the target DNA. The QIAprep 2.0 module was then washed using buffer PE to remove any impurities, followed by

centrifugation at <8000 rpm for 1 minute at 15-25°C temperature. Finally, the purified plasmid DNA was eluted from the QIAprep 2.0 module silica membrane by adding 50 µl of elution buffer or water. The eluted plasmid DNA was then collected and used for subsequent molecular biology experiments.

2.5 Agarose gel electrophoresis

All agarose gels were prepared by dissolving an appropriate concentration of agarose into the Tris-acetate-EDTA (TAE) buffer solution, allowing the mixture to rest for 10-30 minutes to solidify and create a gel-cast in the tray with wells. The gel was then placed in an electrophoresis chamber and submerged in TAE buffer. DNA samples were mixed with loading buffer containing glycerol and a tracking dye at 50% (v/v) and 0.1% to 0.25% (w/v) concentrations, respectively, before being loaded into the appropriate wells. A DNA ladder was also loaded as a reference to facilitate fragment size estimation. The electrophoresis chamber was then connected to a power supply, and a voltage of 120 was applied for 30-60 minutes to separate the DNA fragments based on size, with smaller fragments moving through the gel faster.

2.6 Genomic DNA extraction

To purify genomic DNA (gDNA) from bacterial cultures, the Wizard Genomic DNA Purification Kit was used throughout. Bacterial cultures were initially grown in 4 ml Luria-Bertani (LB) medium and incubated at 37°C for 2–3 hours. A 2 ml aliquot of the culture was extracted and then centrifuged at >8000 rpm for 3 minutes. The bacterial supernatant was removed, and the pellet was resuspended in 50 mM (1-2ml) ethylenediaminetetraacetic acid (EDTA). The samples were then treated with lysozyme, followed by a lysis solution to disrupt cell walls. A protein precipitation solution was then added, and the sample was centrifuged again at >8000 rpm for 1-2 minutes to separate the nucleic acid-containing supernatant. The gDNA was precipitated using isopropanol and then washed with 70% ethanol. Finally, the gDNA pellet was air-dried before being resuspended in sterile water. All DNA concentrations were quantified using the Nanodrop, before being used for downstream processes.

2.7 Transformation of *B. subtilis*

The methods used to generate competent cells and subsequently transform them with exogenous DNA were adapted from Anagnostopoulos and Spizizen (1961) and further

modified by Hamoen *et al.* (2002). Briefly, bacterial cells were grown overnight in 10 ml of competence medium (detailed below) at 37°C with vigorous shaking for 12 hours. After 12 hours, 0.6–1 ml of the overnight culture was extracted, diluted in 10 ml of fresh competence medium, mixed, and allowed to grow for an additional 3 hours. Subsequently, 10 ml of starvation medium (detailed below) was added to the samples, followed by a further 2 hours of incubation with shaking.

To transform competent cells with exogenous DNA, 10–50 µl of DNA was mixed with 400 µl of the competent culture, then shaken and incubated for 1 hour at 37°C. Samples were subsequently plated on a selective medium. For smaller volumes, transformations were performed using microtiter plates. The competence and starvation media were prepared as described below:

Competence medium:

- 10 ml SMM (**Spizizen Minimal Medium**) salts
- 0.125 ml 1M MgSO4
- 0.1 ml 40% glucose
- 0.06 ml tryptophan (Trp)
- 0.01 ml ferric ammonium citrate (2.2 mg/ml)
- 0.005 ml casamino acids (CAA; 20%)

Starvation medium:

- 10 ml SMM salts
- 0.125 ml 1M MgSO4
- 0.06 ml 40% glucose

2.8 Bacterial transformation of *E. coli*

Transformation of the bacteria E. coli was conducted using chemically competent DH5 α E. coli cells. The cells were initially stored at -80° C and thawed on ice until no ice crystals were visible, ensuring that the cells were uniformly suspended. Subsequently, 50 μ l of the thawed cells were pipetted into a sterile transformation tube on ice. To minimise any potential damage to cells, all movements were minimised.

1–5 μl of the prepared plasmid DNA, ranging from 1 pg to 100 ng, was introduced to the cell mixture and then gently flicked I4–5 times to facilitate mixing.

The samples were then incubated on ice for 30 minutes to allow the DNA to penetrate the cells. The samples were then subjected to a heat shock at 42°C for exactly 90 seconds to ensure maximal transformation efficiency. The samples were then cooled on ice for 5 minutes to allow the cells to recover and express the heat-shock proteins that facilitate DNA uptake.

950 µl of room-temperature LB medium was then added to the tube to provide the necessary nutrients for the recovery and expression of the introduced genes. The cells were then incubated at 37°C for 60 minutes with vigorous shaking at 250 revolutions per minute (rpm) to promote the expression of antibiotic-resistance genes.

To identify successful transformations, several 10-fold serial dilutions of the transformed cells in the LB medium were prepared, and 50–100 µl of each dilution was applied to a pre-warmed antibiotic selection plate. The plates were then incubated overnight at 37°C. Colonies exhibiting a slower growth rate were incubated at 30°C for 24–36 hours or at 25°C for 48 hours, as appropriate. Successfully transformed colonies were identified by the presence of bacterial colonies on antibiotic selection plates. Further confirm that the insert was present in the transformants, colony PCR was used by using suitable primers. Also, where necessary restriction digestion on/or sequencing was used to confirm the correct assembly of the plasmid.

2.9 Purification of DNA bands from agarose gels

DNA fragments of interest were identified and excised from the agarose gel using sterile scalpels. The samples were then weighed in a colourless tube, and buffer QG (Qiagen) was added relative to the gel volume (100 mg gel ~100 μl). The samples were then incubated at 50°C until the gel extraction completely dissolved, with intermittent vortexing at 1,000 to 1,500 rpm to facilitate dissolution. The colour of each sample was verified to ensure it was yellow (similar to Buffer QG without dissolved agarose). Samples that were not yellow were mixed with 10 μl 3 M sodium acetate (pH 5.0), and mixed until the desired colour was achieved.

Once the correct colour was achieved, an equal volume of isopropanol was added to the sample and mixed thoroughly by vortexing at 1500-2000 rpm. A QIAquick spin column was placed in a provided 2 ml collection tube or into a vacuum manifold. The samples were then applied to the QIAquick column, followed by centrifugation

application. The flow-through tube was discarded, and the column was returned to the same tube. For samples with a volume $>800~\mu l$, this step was repeated as necessary. The purified DNA was then ready for sequencing, *in vitro*-transcription or microinjection.

If DNA was subsequently used for sequencing, prior to using the purified DNA, $500 \, \mu l$ of Buffer QG was added to the QIAquick column, and the samples were centrifuged at >8000 rpm for 1 minutes at room temperature (15-25), or a vacuum was applied. The flow-through was discarded, and the column was returned to the same tube. To wash the column, $750 \, \mu l$ of the Buffer PE (Qiagen) was added, followed by centrifugation or vacuum application. The column was then allowed to stand for 2–5 minutes if the DNA was to be used for salt-sensitive applications.

The QIAquick columns were centrifuged at >8000 rpm in the provided 2 ml collection tube for 1 minute to remove residual wash buffer and then placed into a clean 1.5 ml microcentrifuge tube. Finally, to elute the DNA, 50 µl of the Buffer EB (10 mM Tris-Cl, pH 8.5) or sterile water was added to the centre of the QIAquick membrane, and the column was centrifuged at >8000 rpm again for 1 minute. Samples with higher DNA concentrations, 30 µl of Buffer EB was added to the centre of the QIAquick membrane, and the samples were allowed to stand for 1 minute before centrifugation at >8000 rpm (all the centrifugation at room temperature). The eluted material was then stored on ice or at -20°C until use.

.

2.10 Western blotting

For the transfer of proteins from the completed sodium dodecyl sulphate (SDS) gel to the Amersham Hybond sequencing 0.4 µm polyvinylidene fluoride (PVDF) membranes, the Biorad TransBlot Turbo equipment was used. The SDS gels were removed from their cassettes, and the top and bottom portions were trimmed. The PVDF membrane was activated by immersing it in methanol for 30 seconds and then in deionised water (DH₂O) for 30 seconds to 1 minute. A sandwich assembly was prepared in the TransBlot Turbo tray, consisting of pre-soaked blue paper, the PVDF membrane, the gel, and another layer of pre-soaked blue paper. Bubbles were removed throughout.

The Turbo Bio-Rad transfer machine was set to MIDI > Standard program and run for 30 minutes. Solutions for the western blot analysis were prepared, and the transfer boxes were washed using distilled water. Following the protein transfer from the SDS gel, the PVDF membrane was washed in PBS-T (phosphate-buffered saline with 0.1% Tween 20) and subjected to three subsequent washes using PBS-T buffer for 5 minutes each on a rocking shaker set at 20 rpm. The PVDF membrane was then blocked for 1 hour at room temperature or overnight (12-20 h) in a cold room using 5% milk in PBS-T.

The primary antibody was added to the PVDF membrane and incubated for 1 hour in PBS-T with 5% milk. The PVDF membrane was then washed in PBS-T. The secondary antibody was then applied to the PVDF membrane, followed by incubation in PBS-T with 5% milk for 1 hour. Following PVDF membrane washes in PBS-T, the PVDF membranes were prepared for chemiluminescence detection using the ImageQuant LAS 400 mini system.

Prior to Western Blotting, the membrane was placed on a white tissue and treated with Pierce ECL Plus Western Blotting Substrate kit for 5 minutes. Excess substrate was removed, and the membrane was placed on a plastic cover for imaging. The ImageQuant LAS 400 mini system was set to chemiluminescence mode with manual exposure time and high-resolution sensitivity. Images were captured at incremental exposure times, and the membranes were also imaged under epi-illumination to detect the protein ladder. All images were saved and analysed for protein detection, and the final image of the membrane was scanned for documentation.

2.11 Polymerase chain reaction

All polymerase chain reaction (PCR) experiments were performed using the Q5 High-Fidelity DNA polymerase system (NEB, USA). High-quality, purified DNA templates were utilised, with gDNA concentrations ranging from 1 ng to 1 µg, and plasmid or viral gDNA concentrations ranging from 1 pg to 10 ng for a 50 µl reaction. Primers were 20–40 nucleotides in length, containing a 40–60% GC content, and designed using Primer3 software. The PCR reactions were prepared in either a 25 µl or 50 µl total reaction volume, depending on the specific requirements of the experiment. Each reaction included 5X Q5 Reaction Buffer at a concentration of 1X, 10 mM dNTPs

at a concentration of 200 μ M, 10 μ M forward and reverse primers each at a dosage of 0.5 μ M, and Q5 High-Fidelity DNA Polymerase at a concentration of 0.02 U/ μ l. The quantity of template DNA utilized was adjustable, but consistently maintained below 1,000 ng. In addition, to enhance the amplification of regions with a high GC content, a 5X Q5 High GC Enhancer was optionally added at a final concentration of 1X. The ultimate reaction volume was modified to either 25 μ l or 50 μ l using nuclease-free solution.

The Q5 Reaction Buffer contained an optimal Mg²⁺ concentration of 2.0 mM at a 1X final concentration, with the addition of 1X Q5 High GC enhancer used for difficult targets, such as those with a high GC-rich sequence. Each reaction included 200 μM of deoxynucleotide, while the Q5 High-Fidelity DNA Polymerase, which did not include dUTP, was used at a concentration of 20 units/ml (1.0 unit/50 μl reaction).

Each PCR programme included 25-35 cycles with an initial 30-second of denaturation at 98°C, followed by a 5–10 second denaturation. Annealing temperature was set 3°C above the melting temperature (Tm) of the primer with the lower Tm, and the extension temperature was 72°C. Extension times varied based on the complexity and type of experiment and are described alongside each experiment in this thesis. The extensions times used in this thesis include:

- 20–30 seconds per kilobase (kb) for complex samples
- 10 seconds per kb for short simple templates
- 40 seconds per kb for complementary DNA (cDNA) or long, complex templates.

A final extension of 2 minutes was included at 72°C. For samples where the product size was >6 kb, the extension time was increased to 40–50 seconds per kb. The resultant PCR products were blunt-ended, suitable for blunt-end cloning. Any T/A cloning required DNA purification prior to the A-addition due to Q5 High-Fidelity DNA Polymerase's propensity to degrade any overhangs.

2.12 Restriction digestion of DNA

Enzymatic digestion was conducted using a 50 μ l reaction volume for 1 μ g of substrate, with an enzyme volume \leq 10% of the total volume to avoid star activity due to excess glycerol. The incubation time was set to 1 hour. However, where required, it

was decreased using an excess of enzyme, Time-Saver Qualified enzymes, or extended up to 16 hours with fewer enzyme units. The reactions were terminated if any of the following criteria were met:

- No further DNA manipulation was needed.
- A stop solution was added.
- Further manipulation was required.
- Heat inactivation or enzyme removal using a spin column or phenol/chloroform extraction were required.

All restriction enzymes and 10X NEB buffers were stored at -20 or -80°C for longer than 30 days as per technical data sheets.

2.13 Bocillin staining

The biochemical activity of PBPs in live *B. subtilis* cultures were visualised using a fluorescently labelled penicillin derivative, Invitrogen BocillinTM FL Penicillin, Sodium Salt (Catalogue Number B13233). BocillinTM FL binds covalently to the active sites of PBPs, at the active site serine residue, which allows for the visualization of multiple PBP classes, including both high-molecular-weight and low-molecular-weight PBPs. The Bocillin FL was diluted to a final concentration of 1 mg/ml using Mili-Q water and stored at -20° C until further use. Each bacterial strain was streaked onto a plate and incubated overnight (12-17 h) at 37°C. 10 ml of the overnight culture was added to 10ml a Penassay broth and incubated for overnight at 30 °C with continuous shaking.

The overnight culture was then diluted 1:10 in lysogeny broth (LB) and grown with continuous shaking at 37°C until an optical density (OD) of 1.0 at 600 nm was achieved. 1 ml of the sample was then transferred to a sterile Eppendorf tube, and 2 μ l of the 1 mg/ml Bocillin FL stock was added to each tube with a 1-minute incubation at room temperature. The samples were then centrifuged for 3 minutes at 13,000 rpm, and the supernatant was removed. The cells in the pellet were resuspended in a volume of SDS loading buffer calculated based on the initial OD600 to normalise the cell concentration across samples as following:

SDS loading dye (μ l) = (OD600 of the lowest sample / OD600 of your sample) ×300 μ l

The cells were then lysed for 1 minute via sonication set at 20 kHz. All samples were then boiled at 85°C for 10 minutes to denature proteins. Sonication and boiling steps were repeated if any samples were difficult to pipette due to high viscosity. All samples were then prepared for SDS-polyacrylamide gel electrophoresis (PAGE) using Invitrogen NuPAGETM 4–12% Bis-Tris Protein Gels. The SDS running buffer was diluted to 1X, and the precast gels were rinsed with distilled water and assembled in a vertical gel tank. Each well was filled with 1X SDS buffer and the protein samples. The BenchMarkTM Pre-stained Protein Ladder (ThermoFisher, Catalogue Number NPO001), was also loaded to provide a reference for fragment size. The gel was run at 50 mA until a pre-determined red marker of the pre-stained protein ladder approached the bottom of the gel. This ensured that there was good resolution of the PBPs as a number of them have similar molecular weights. The progress of each gel was monitored every 30 minutes. All gels were imaged using a phosphorimager (GE Healthcare Typhoon) to visualise the fluorescently labelled PBPs.

2.14 DNA ligation

DNA ligation was performed using a chilled microcentrifuge tube with T4 DNA ligase. The reaction was set up with a 1:3 molar ratio of vector to insert DNA, calculated using the NEBioCalculator. The 20 µl reaction included 2 µl of 10X T4 DNA Ligase Buffer, 50 ng of 4 kb vector DNA, 37.5 ng of 1 kb insert DNA, nuclease-free water, and 1 µl of the T4 DNA ligase. The components were gently mixed and centrifuged at <8000 rpm for 1 minute at 15-25°C temperature. They were either incubated at 16°C overnight (12-24h) or at room temperature for 1-2h. After incubation, the ligation samples were heat-inactivated at 65°C for 10 minutes. Finally, a fraction of the ligation reaction was transformed into competent cells, and further investigation carried for transformation efficiency indicating the success of the ligation.

2.15 Beta-galactosidase activity assay

Reagents and Solutions Preparation

To measure β -galactosidase activity using the ONPG assay, the following solutions were prepared.

Z-Buffer Preparation

To prepare 1 L of Z-buffer, the following chemicals were weighed and dissolved in distilled water:

50 mM NaH₂PO₄·2H₂O: 7.8 g (M.W: 156.01)

50 mM Na₂HPO₄: 7.1 g (M.W: 141.96)

10 mM KCl: 0.75 g (M.W: 74.55)

1 mM MgSO₄·7H₂O: 0.25 g (M.W: 246.47)

The solution was then autoclaved in a 1-liter Duran bottle for sterilization. Following autoclaving, the pH of the Z-buffer was adjusted to approximately pH 7.0 using either HCl or NaOH as necessary. After pH adjustment, the buffer was filter sterilized using a 0.22 µm filter and stored at 4°C until further use.

Substrate Solution Preparation

The substrate solution consisted of 4 mg/mL ONPG (2-Nitrophenyl β -D-galactopyranoside) dissolved in sterile Z-buffer. The ONPG powder was fully dissolved to ensure complete substrate availability. As 200 μ L of substrate solution is required per sample, an excess amount of the solution was prepared and stored at -20°C for future use.

Lysis Solution Preparation

The lysis solution was prepared fresh on the day of use. To make 20 mL of lysis solution, the following components were dissolved:

Lysozyme (Sigma): 4 mg, providing a final concentration of 200 µg/mL

DNase (Sigma): 2 mg, providing a final concentration of 100 μg/mL

Triton X-100: 250 μL, providing a final concentration of 1.25%

This solution was thoroughly mixed to ensure that all components were fully dissolved. A total of 400 μL of lysis solution was used per sample.

Stop Solution Preparation

The stop solution was prepared by dissolving 10.6 g of Na_2CO_3 (M.W: 105.988) in distilled water to a final volume of 100 mL, resulting in a 1 M Na_2CO_3 solution. This solution was used to terminate the β -galactosidase reaction.

 β -galactosidase activity was assessed using a modified version of the Miller assay. Samples (200 μ l each) were stored at -20°C and defrosted in a 30°C water bath, arranged in the order of expected activity, from lowest to highest. Cell lysis was initiated by adding 400 μ l of the lysis buffer to each sample and incubating the cultures until they became transparent, indicating successful lysis. This duration varied among samples and was monitored visually.

Once transparency was achieved for all samples, the enzymatic reaction was initiated by adding 200 µl of the substrate solution to each sample at 10-second intervals, ensuring an orderly progression of reactions for accurate timekeeping. The samples were mixed and returned to the water bath. All samples were monitored until they began to turn yellow, indicating the production of o-nitrophenol (ONP) and the end of the enzymatic reaction. The reactions were stopped by adding 400 µl of 1 M Na₂CO₃, and the exact time of reaction termination was noted. The "stopped" samples were then held at room temperature until all reactions had finished. No sample exceeded 3 hours.

Following the completion of the reactions, the samples were centrifuged at full speed for 5 minutes. The supernatant was extracted and the absorbance was measured at 420 nm (A420). The absorbance of water was recorded as the blank. A negative control was also prepared by incubating sterile media and assay reagents for the maximum reaction time. The absorbance value of this blank was then subtracted from all assay readings. Beta-galactosidase activity was calculated and expressed in both nanomoles and OD (Formula 1).

A
$$A420 \times V_1 / (V_2 \times OD600 \times T_1 \times 0.00486)$$

B A420 × 6 × 1000 /
$$(T_2 \times OD600)$$

Formula 1. Beta-galactosidase activity formula. A) V^1 , final volume of the assay (ml); V_2 , volume of culture used in the assay (ml); V_1 , reaction time (minutes). The factor 0.00486 corresponds to the inverse of the molar extinction coefficient of o-nitrophenol at pH 10 and B) Beta-galactosidase activity expressed as optical density absorbance at 600 nanometres. V_2 , reaction time in minutes, and optical density (OD) 600 the OD of the culture at 600 nanometres.

2.16 DNA purification

DNA was purified using the QIAquick PCR Purification Kit. Five volumes of Buffer PB (buffer to PCR rection ratio is1:5) were mixed with each PCR reaction sample. The mixture was applied to a QIAquick column. The column was then centrifuged at 10,000 rpm for 1-2 minutes. The flow-through was discarded, and the column was washed using Buffer PE. It was then centrifuged again at 8000 rpm for 1 minutes to remove the residual wash buffer.

DNA was eluted by adding Buffer EB or sterile water to the QIAquick column, followed by centrifugation at 10,000 rpm for 1-2 minutes. When high DNA concentration was required, a smaller volume of elution buffer was added, and the sample was left to stand for 10-20 minutes at room temperature. Samples were then centrifuged at 10,000 rpm for 1-2 minutes. For gel analysis, purified DNA was mixed with a loading dye before being loading onto the gel. The success of DNA purification was evaluated using gel electrophoresis.

2.17 Labelling Bacterial Cells with Fluorescently labelled cationic compound (Poly-L-Lysine-FITC) and anionic Dextran-Rhodamine

Bacterial cells were labelled using Poly-L-lysine conjugated with fluorescein isothiocyanate (FITC) was used to facilitate fluorescence microscopy. A mid-log phase culture was grown to an OD600 of 0.5, corresponding to approximately 1×10^8 CFU/ml. To 1 ml of this culture, 5 μ l of a 10 mg/ml Poly-L-lysine-FITC stock solution was added, resulting in a final concentration of 50 μ g/ml. The mixture was gently mixed and incubated at room temperature for 30 minutes in the dark to avoid photobleaching. Post-incubation, the cells were pelleted by centrifugation at 3000 x g for 5 minutes and resuspended in 1 ml of phosphate-buffered saline (PBS) to remove excess unbound conjugate. Labelled cells were mounted on glass slides, covered with a coverslip, and visualized under a fluorescence microscope using an FITC filter set (excitation at 488 nm, emission at 520 nm). Control samples without Poly-L-lysine-FITC were prepared to assess background fluorescence, and the method was optimized by adjusting the conjugate concentration as necessary.

To label bacteria with dextran tetramethylrhodamine (10,000 MW, Thermo Fisher), bacterial cultures were grown to an OD600 of 0.5, harvested by centrifugation at 5000 g for 5-10 minutes, and washed three times with phosphate-buffered saline (PBS) to remove residual media. The bacterial pellet was then resuspended in PBS and

incubated with 1 mg/mL dextran tetramethylrhodamine for 5-10 minutes at room temperature with gentle agitation, protected from light. After incubation, the bacteria were washed three times with PBS to remove unbound dye and resuspended in a small volume of PBS. Fluorescently labelled bacteria were then observed under a fluorescence microscope using rhodamine-specific filters (excitation: 550 nm, emission: 580 nm) to determine the level of labelling.

2.18 Microscopy

Microscopic images were captured using an inverted Nikon Eclipse Ti microscope and a Sony Cool-Snap HQ2 CCD camera (Roper Scientific), operated with Metamorph 6 imaging software (Universal Imaging). Unless stated otherwise, cells were cultivated in LB medium, and images were captured during the exponential phase (OD600 of 0.5). 0.5 μl of the samples were mounted onto a 1% agarose, and brightfield illumination imaging was performed with a 250 ms (milliseconds) exposure period. For membrane labelling, 5μg/ml of the styryl dye FM 4-64 was added to bacterial samples and incubated for 10 minutes. The cells were then washed with PBS, and 0.5 μl of each sample were mounted onto a 1% agarose to fix the cells under the microscope (Fig 2.1).

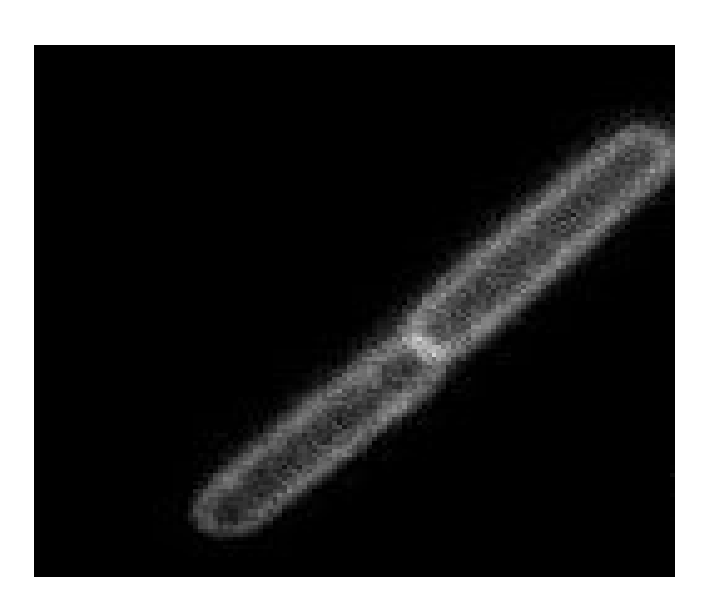


Figure 2.1: Membrane labelling. Image of 5 μ g/ml FM 4-64-labelled *B. subtilis* (168) during the exponential phase and growth in lysogeny broth.

2.19 Transmission electron microscopy

To capture images of mutant cells, a Philips CM 100 Compustage (FEI) transmission electron microscope attached to an AMT CCD camera (Deben) was used.

The cells were cultivated in LB medium at 37°C until an OD600 of 0.5 was reached. The cells were then mixed in a 1:1 ratio with Fix Buffer I, containing 2% glutaraldehyde and 0.1 M sodium cacodylate and incubated at 4°C overnight. Cells were then dehydrated and processed by the EM facility staff prior to being imaged by transmission electron microscopy (TEM).

2.20 Cloning using the NEBuilder® HiFi DNA assembly

In this thesis, we used DNA fragments of 0.2–0.5 pmol for those with 4–6 fragments, which aligns with the NEB guidelines for optimal vector assembly. To quantity the DNA required for optimal assembly, while adjusting based on DNA fragment properties, the following formula was used:

pmol = (weight in ng
$$\times$$
 1000) / (base pairs \times 650 Da)

Formula 2. Formula for calculating DAN required for optimal assembly. pmol, picomoles; ng, nanograms; Da, daltons.

A Nanodrop spectrophotometer was used to assess DNA concentrations by measuring A260 to calculate the mass of the DNA fragments, providing rapid, reliable, and valid results. Additionally, mass estimation was performed using agarose gel electrophoresis followed by ethidium bromide staining. The dye intercalates with DNA and fluoresces under ultraviolet (UV) light, facilitating the visualisation and estimation of DNA quantity compared to known standards.

In this study, a standardised protocol was employed to assemble DNA fragments into vectors, following NEB guidelines. All reactions were set up on ice, utilising different amounts and ratios of DNA depending on the number of fragments being assembled. For 2–3-fragment assemblies, 0.03–0.2 pmol of DNA fragments with a vector-to-insert molar ratio of 1:2 was used. Assemblies involving 4–6 fragments, used 0.2–0.5 pmol with a vector-to-insert ratio of 1:1. Each reaction contained the calculated volume of DNA fragments and 10 μl of NEBuilder HiFi DNA Assembly Master Mix, ensuring high fidelity of assembly, and an adjusted volume of DH₂O to achieve a total reaction volume of 20 μl. All assembled reactions were incubated in a thermocycler at 50°C for 15 or 60 minutes when assembling 2–3 or 4-6 fragments,

respectively. Following incubation, all samples were stored on ice or frozen at -20 °C for later use.

To transform samples, a 2 μ l sample of the chilled assembled product was used to transform DH5- α competent *E. coli* cells following the standard transformation protocol mentioned in section 2.8.

2.21 Zetasizer for cell surface charge

Zeta potential measurements were performed using a Malvern Zetasizer Nano ZS at Newcastle Universit. The electrokinetic potential in liquid-liquid or solid-liquid colloidal dispersions is measured by the zeta potential. Charged particles exhibit a range of electrokinetic phenomena, including electrophoresis and sedimentation potential when subjected to an electric field. In the laboratory, the zeta potential is determined using the Zetasizer Nano ZS (Malvern Panalytical), which is based on the concept of electrophoresis.

For analysis *B. subtilis* and *S. aureus* bacteria were grown to the exponential phase in LB or tryptic soy broth (TSB), respectively, at 37°C to an OD600 of approximately 1.0. A 1 ml sample of the bacteria was extracted, suspended in PBS and then transferred to a Zetasizer cuvette and inserted into the analyser. Results were obtained relatively rapidly through the application of external electric field and causing the particles (bacterial cells) to move toward the electrode with the opposite charge. This movement, referred to as electrophoretic mobility, was measured in terms of velocity under the influence of the electric field using laser Doppler velocimetry. Electrophoretic light scattering (ELS) was used to determine the electrophoretic mobility of molecules (bacteria in this test) in solution or particles in dispersion (Figure 2.2). This then permitted the comparison of the properties of cells suspended in a defined medium.

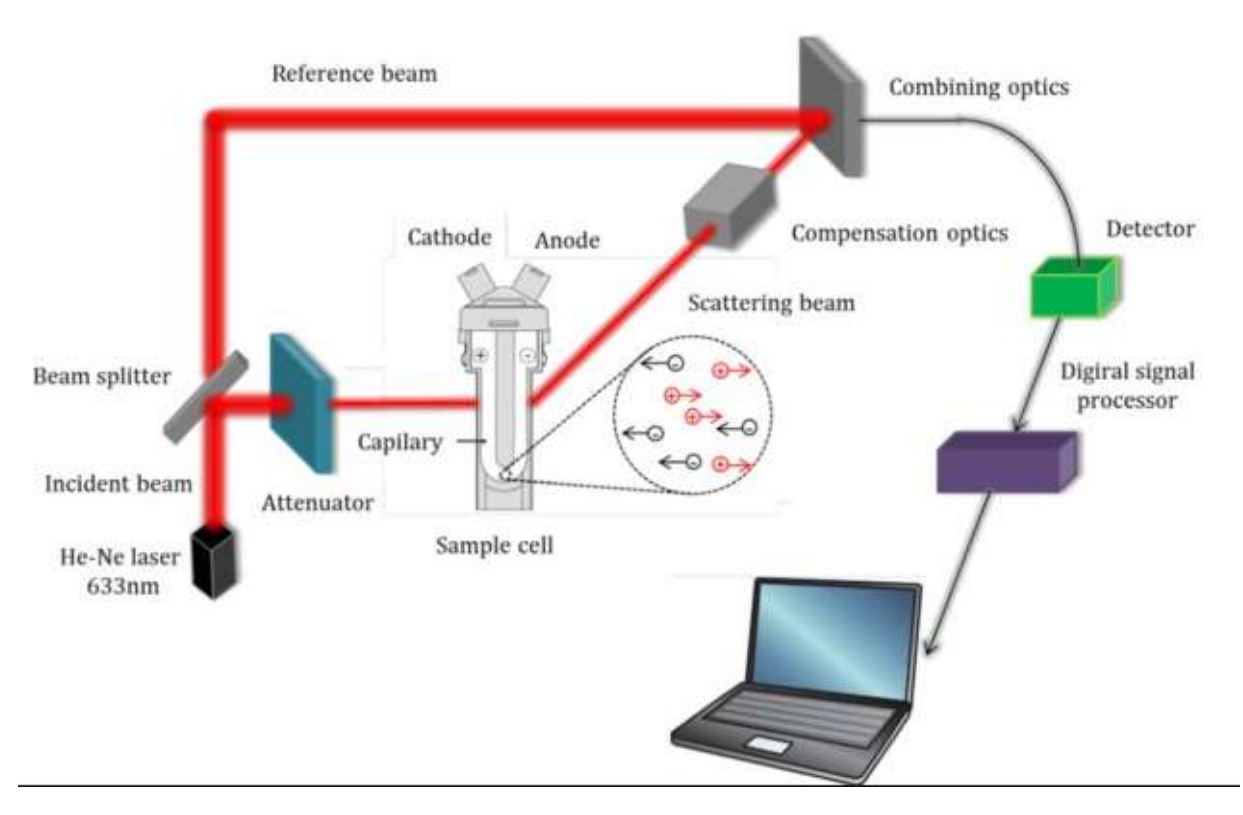


Figure 2.2: Schematic of the Zetasizer machine. The working principle of this approach is to measure bacterial surface charge by applying an electric field to the samples, causing cell migration. The schematic also shows the scattering and detection system in the Zetasizer machine. This diagram was adapted from Salado Leza (2016).

2.22 Cell-Tak application for AFM (Atomic Force Microscopy)

The Cell-Tak application was used to ensure stability of bacterial cells during microscopy (AFM). Cell-Tak was added to 0.1M NaHCO₃ buffer to create a 68 μg/ml solution, forming the Cell-Tak mixture. A sterile Petri dish, 40 mm in diameter and 11 mm in height and composed of tissue culture plastic ((TPP), Switzerland) was filled with 1 ml of the Cell-Tak mixture. The petri dish was then incubated for 45 minutes at 2–8°C with light shaking at 20 rpm. Following incubation, 1 ml of NaHCO₃ buffer was used to rinse the Petri dish, removing the solution before drying the dish for 15 minutes at 2–8°C.

Next, 1 ml of a cell-TRIS buffer solution, containing a cell concentration of 1.22 \times 10¹⁰, was added to the plate and incubated for 20 minutes at 2–8°C with light shaking at 20 rpm. The petri dish was then air dried at 2–8 °C for 15 minutes. Afterward, the remaining solution was aspirated, and the dish was air-dried again for 1-5 minutes. Finally, the Petri dish was transferred to the AFM stage and placed on ice. 3 ml of a

TRIS buffer was gradually added, acting as an imaging medium. The samples were assessed by AFM using the original Cell-Tak Application protocol, adapted from that of Dr Matthew German's lab. (Newcastle University).

2.23 Atomic force microscopy for cell rigidity

In standard atomic force microscopy (AFM) imaging, a laser is directed towards the rear of a pyramidal tip, supported by a flexible cantilever. The deflection of the light is recorded as the tip passes over the sample surface and is utilised to produce a detailed picture. AFM was used to measure bacterial cell adhesion after the cantilever pushes in, forming a linear line in the Y-axis (force). When the cantilever begins to retract, it forms a linear bacterial surface. As the cantilever leaves the bacteria, adhesive forces maintain the connection between the tip and surface, causing the tip to exert an upward pull on the surface.

Additionally, AFM was used to measure bacterial cell wall stiffness by assessing the force and distance. Initially, the AFM cantilever touches the surface of the bacteria with no force, creating a stable line. Thereafter, the cantilever begins to push, without forming a linear force line, providing a measure of bacterial cell elasticity. Once a linear line is formed, as the cantilever starts to push into the cell, this linear line was used to measure bacterial cell rigidity. Cell rigidity was measured using Cell-Tak adhesive to ensure cell stability of the bacterial cells.

2.24 Cell wall analysis methods

The original method for analysing cell walls was adapted from Atrih *et al.* (1999) and then modified from Bisicchia *et al.* (2011). The revised protocol for preparing the cell wall of the Gram-positive bacterium, *S. pneumoniae*, involved cultivating the bacteria until they reached an OD of 0.5–0.6. The cultures were then cooled in an ethanol/ice bath to 4°C and centrifuged at 10,000g at 4°C. The supernatant was discarded, and the cells remaining in the pellet were subsequently mixed with 30 ml of Tris-HCl solution at pH of 7.0, which was kept at a low temperature.

The cell suspension was then combined with 120 ml of boiling water at 100°C 5% SDS and boiled for 15 minutes before being allowed to cool at room temperature. The resulting pneumo-lysate was stored at 4°C if used immediately or stored at -20°C for later use. The lysate samples were subsequently transferred to centrifuge tubes and

centrifuged at room temperature (RT) at 12,000 g for 30 minutes, ensuring a clear supernatant. The supernatant was removed, and the pellet was resuspended in 20 ml of a 1M NaCl solution before being centrifuged again at 12,000 g for 30 minutes at RT. Following each centrifugation, the sample was washed in 1M NaCl and H₂O, and the centrifugation was repeated at 12,000 g for 30 minutes at RT. This process was repeated until the suspension no longer contained SDS.

The SDS free pellet was subsequently suspended in H₂OMBO and transferred into 2 ml screw-cap tubes containing glass beads for cell disruption. Following cell disruption facilitated by the glass beads, the suspension was filtered using a glass frit to eliminate the glass beads before being rinsed with H₂OMilli-Q and transferred to Falcon tubes. Centrifugation was repeated at 12,000 g for 30 minutes at RT to separate damaged cells. The resulting solid masses were mixed again in a solution containing 100 mM Tris-HCl at pH 7.5 and 20 mM MgSO₄.

Following the initial enzymatic treatment, DNase I and RNase were added, mixed, and then incubated at 37°C for 2 hours. CaCl_{2M} and trypsin were introduced to the sample, mixed, and then incubated for 18 hours at 37°C. The suspension was modified to contain a final concentration of 1% SDS. The sample was then incubated at 80°C for 15 minutes and centrifuged at 25,000 g for 30 minutes at RT. The supernatant was discarded, and the pellets were re-suspended in 8 M LiCl and 100 mM EDTA at pH 7.0 and then centrifuged again at 25,000 g for 30 minutes at RT. The obtained pellets were rinsed twice with high-purity water (H₂O Milli-Q) and suspended in H₂OMilli-Q before being frozen at -80°C and subjected to lyophilisation.

To extract murein from the cell walls, samples were dissolved in hydrofluoric acid and centrifuged. Finally, the liquid portion was discarded from the samples. The pellet was first washed sequentially with H₂O (Milli-Q) and then with 100 mM Tris-HCl (pH 7.0). After washing, the pellet was resuspended in 100 mM Tris-HCl (pH 7.0) before being stored. Muropeptides were acquired through the process of cellosyl digestion, which involved combining the samples, adding cellosyl buffer and enzyme, and then incubating them overnight at 37°C. The processed samples were heated, cooled, and then centrifuged at 13,000 rpm for 10 minutes at 4°C, before being stored at -20°C.

2.25 Muropeptide analysis

To analyse muropeptides, a reverse-phase (RP) column (Prontosil 120-3-C18-AQ, 3 μM, Bischoff) was attached to an Agilent Technologies Series 1200 high-performance liquid chromatography (HPLC) system. To analyse PG derived from *B. subtilis* cells using HPLC, a linear gradient from 100% of Solvent A, composed of 40 mM sodium phosphate at pH 4.5 with 0.0003% sodium azide to 100% of Solvent B, composed of 40 mM sodium phosphate and 20% methanol at pH 4.0. For analysing PG produced from an *in vitro* synthesis experiment, a linear gradient ranging from 100% Solvent A, composed of 50 mM sodium phosphate at pH 4.31 with 0.0002% sodium azide, to 100% Solvent B, 75 mM sodium phosphate with 15% methanol at pH 4.75. The linear gradients for PG from *B. subtilis* and *in vitro* synthesis were maintained at 55°C for 5 hours and 90 minutes, respectively.

A UV detector operating at 205 nm was used to detect muropeptides, while Agilent Technologies' online scintillation counter was used to track muropeptides labelled with [14C]. The HPLC data was analysed using the Laura program (v4.1.7.70) from LabLogic Systems Ltd. This then displays the peptide cross-link levels, determined using the formula x = 100 - (%TetraTetra + %TetraPenta).

2.26 Reverse transcription-quantitative PCR

The QIAGEN OneStep Ahead reverse transcription (RT)-PCR Kit was used to perform quantitative RT-PCR (RT-qPCR) in this thesis. Initially, all required reagents, including the OneStep Ahead RT-PCR Master Mix (2.5x concentration, 10 µl per reaction for a final concentration of 1x), template RNA, primer solutions, RNase-free water and the optional 5x Q-Solution (5 µl per reaction for a final concentration of 1x) were defrosted and kept on ice. A final volume of 25ul for each sample was composed of 1ul of OneStep Ahead RT-Mix, 10ul OneStep Ahead RT-PCR Master Mix, 5ul of (0.5uM each) primers forward and reverse primers, 1ul of the sample, 5ul of 5x Q-Solution and 3ul of RNase-Free Water. The reaction mixture was prepared at a volume 10% larger than necessary to account for potential pipetting errors and included a negative control lacking the template RNA to detect any contamination. Same amounts of the template RNA pool (50 µg per reaction) were added based on the abundance of the target transcript to standardise the reaction.

Following the addition of the RNA, the thermal cycler was programmed according to the manufacturer's instructions for the specified conditions. The RT-PCR cycling conditions were tailored for amplicons >1 kb. The process was as follows:

- RT was set at 45°C for 15 minutes.
- PCR activation at 95°C for 5 minutes, which inactivated OmniScript and SensiScript Reverse Transcriptases, and denatured the cDNA template.
- The cycling protocol was repeated for 40 cycles, depending on the amount of template RNA and transcript abundance, and was composed of:
 - Denaturation at 95°C for 15 seconds.
 - Annealing at 55°C for 15 seconds (approximately 5°C below the Tm of the primers).
 - Extension at 68°C for 1–4 minutes, with a recommended extension time of 1 minute per kb amplicon size.
- Final extension at 72°C for 5 minutes.

Following PCR amplification, the data were stored and analysed for expression relative to the housekeeping gene *gatP* (encoding glyceraldehyde-3-phosphate dehydrogenase).

2.27 Site-directed mutagenesis

Here the Q5[®] Site-Directed Mutagenesis Kit by NEB utilised. Here we outline the procedure used for exponential amplification of DNA, enzymatic treatment, and its subsequent transformation into $E.\ coli$, illustrated in Figure 2.3. The PCR setup utilised the following per 25 μ l reaction:

- 12.5 μl of Q5 Hot Start High-Fidelity 2X Master Mix, resulting in a final concentration of 1X.
- 1.25 μl each of the forward (YA-pbpA-Site-F) and reverse (YA-pbpA-Site-R) primers, taken from a stock solution with a concentration of 10 μM, resulting in a final concentration of 0.5 μM.
- 1 μl template DNA, ranging from 1–25 ng/μl.
- 9 µl of nuclease-free water.

The PCR cycling conditions were as follows:

- Initial denaturation step at 98°C for 30 seconds.
- 25 cycles of:
 - Denaturation at 98°C for 10 seconds
 - Annealing at a temperature optimised between 50–72 °C (specifically adjusted for mutagenic primers using NEBaseChangerTM) for 10–30 seconds
 - Extension at 72°C for 20–30 seconds per kilobase.
- Final extension at 72°C for 2 minutes, followed by a hold in the temperature at 4–10°C.

To confirm the integrity of the PCR product, a $2-5~\mu l$ sample was assessed using an agarose gel. The KLD reaction was performed by combining 1 μl of the PCR product, $5~\mu l$ of 2X KLD Reaction Buffer, $1~\mu l$ of 10X KLD Enzyme Mix and $3~\mu l$ of nuclease-free water. The mixture was then incubated at RT for 5~m l minutes.

To transform the **E. coli** cells, 5 µl of the KLD mixture was combined with 50 µl of chemically competent cells. The mixture was then incubated on ice for 30 minutes, heat-shocked at 42°C for 30 seconds and returned to ice for 5 minutes. After the heat shock, 950 µl of SOC medium was added, and the cells were gently agitated at 37°C for 1 hour to recover. A volume of 40–100 µl of this mixture was spread evenly onto selection plates and incubated overnight at 37°C. The resulting amino acid substitution was then confirmed by DNA sequencing services at Dundee University.

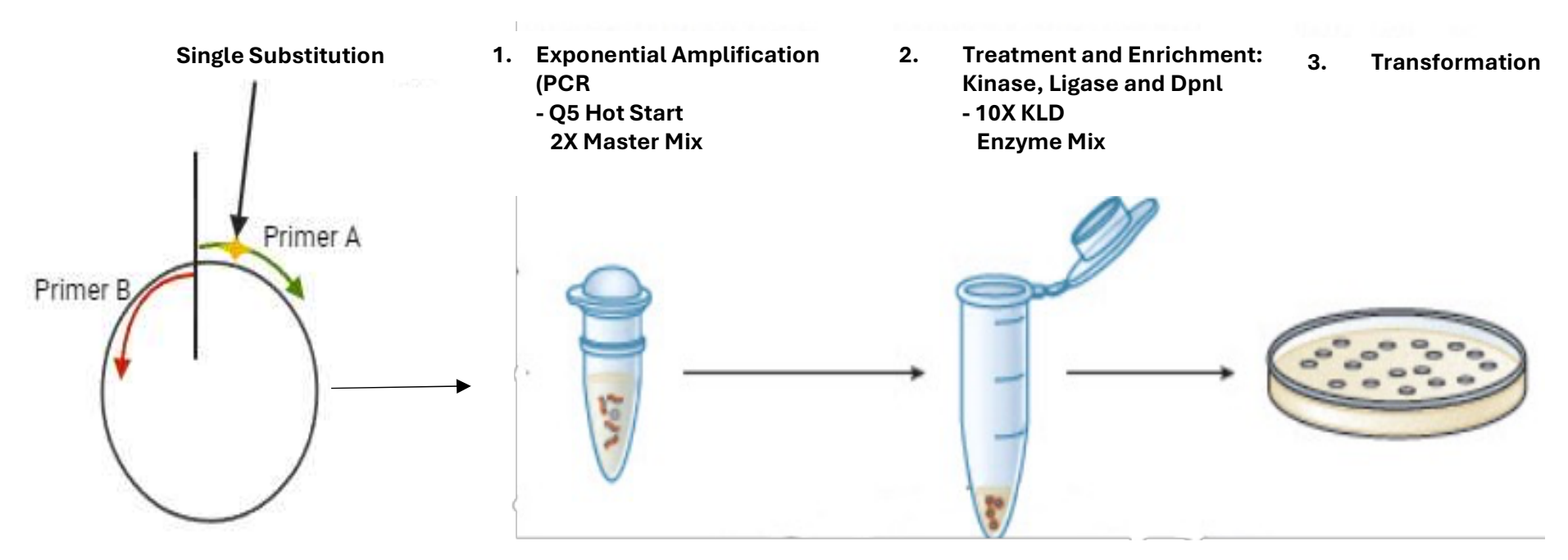


Figure 2.3: Site-directed mutagenesis.

Schematic illustrating the designed primers with amino acid substitutions and the subsequent exponential amplification followed by treatment with the KLD mixture. The final step is the transformation of the modified gene into *Escherichia coli*.

2.28 Protein band intensity by ImageJ

Protein bands from western blotting and Bocillin FL labelling were imaged and then analysed using ImageJ software. The analysis involved the following steps:

- **Image Conversion:** Each image was initially converted into an 8-bit format by selecting Image>Type > Type > 8-bit.
- Background Noise Subtraction: To subtract background noise, a rectangular
 area was drawn on the background of the image. The mean grey value of this
 background area was measured by selecting Analyse > Set Measurements and
 deselecting all options except "Mean Grey Value." This value was then
 measured.
- **Subtracting the Mean Value:** The background mean value was subtracted from the image using Process > Math > Subtract and entering the mean value.
- Band analysis: For western blot images, each band was selected by using the
 commands Analyse > Gel > Select First Lane > Plot Lanes. The line tool was
 used to draw straight lines under each bands intensity spike to mark the area of
 interest.
- Data Extraction: This procedure was repeated for each band. The quantitative
 data were for each band were then extracted and exported into Microsoft Excel
 for further analysis.

2.29 gDNA sequencing analysis

The CLC Genomics Workbench, version 7.5 was specifically designed for the analysis of gDNA. Initially, all sequencing files, primarily obtained from Illumina platforms, were imported to acquire paired-end reads. The integrity of all imported data was assessed, ensuring correct read names, before organising the data into separate folders for efficient management. After obtaining the reference genome, all data was aligned and analysed. Data was converted into tracks, consisting of both sequence and annotation tracks, to enhance the comprehensibility and utility of future analyses.

The primary focus of the analysis was to align the sequence reads with the reference genome, facilitating the detection and characterisation of genetic variations and alterations in the genome structure. The read-mapping process was performed with default settings to ensure accuracy and maintain the integrity of the analysis. Following the read mapping, a resequencing analysis was conducted to identify insertions,

deletions (InDels), structural variants (SVs), and single nucleotide polymorphisms (SNPs) within the genomic landscape. Specialised tools, including the InDels and SV analysis modules in the CLC Genomics Workbench, were employed to investigate these genomic alterations.

Any identified genomic variants were thoroughly analysed, and a comprehensive track list was developed, including crucial genomic components such as the reference genome, extracted annotations, mapped reads, identified insertions, InDels, SVs, and genetic variants. This integrated perspective enables the comparison and verification of genetic variations among various strains or experimental conditions. Particular emphasis was placed on assessing the frequency of variants and the extent of read coverage, which are essential metrics for the validity and reliability of the variants. For SNP data, an additional step involved exporting the data to Excel for a thorough comparative analysis, allowing for the identification of distinct mutations among the variants.

2.30 D-Alanine assay

2.30.1 WTA isolation for D-Alanine assay

The isolation method for *S. aureus and B. subtilis* cells used here for WTA and LTA was adapted from the work of Kho and Meredith (2018). Initially, 20 ml of LB was carefully transferred into a sterile 50 ml centrifuge tube. If needed, antibiotics were added for selection. A single colony of *S. aureus (Je2, FmtA and Flp)* or *B. subtilis* (168, PBPX, dltAB, lta3, and TagO) was then added into the LB using a sterile inoculation loop and incubated at 37°C for 2-6 hours while being continuously agitated 250 rpm to create favourable growth conditions. After incubation, the bacterial cultures were subjected to cell disruption and lysis.

Bacterial cultures were centrifuged at 5000 g for 5 minutes at 15-25°C. The supernatant was discarded, and the pellet was resuspended in 30 ml of Buffer 1 (50 mM 2-(N-morpholino) ethanesulfonic acid (MES) at pH 6.5). The sample was then centrifuged again at 5000 g for 5 minutes at 15-25°C to ensure thorough washing. The

samples were then washed again using 30 ml of Buffer 2 (4% (wt/vol) SDS, 50 mM MES, pH 6.5) to further purify the cell pellet.

The resuspended pellet was then transferred to an 800 ml water bath at boiling point (100°C) and incubated for 1 hour before being allowed to cool at RT for 30 minutes to aid in the disruption process. Following the cooling process, the suspension was centrifuged at 5000 g for 5 minutes at 15-25°C. to facilitate the separation and collection of disrupted cells, forming a pellet. The pellet obtained was then reconstituted in 1 ml of Buffer 1 and transferred to a 2 ml microcentrifuge tube, then centrifuged at 16,000 g for 1 minute at 15-25°C. The supernatant was discarded, and the pellet was mixed with 2 ml of Buffer 2, and the centrifugation was repeated. The supernatant was discarded, and the pellet was resuspended in 2 ml of Buffer 3 (2% NaCl, 50 mM MES, pH 6.5) to eliminate any remaining SDS.

The supernatant was discarded, and the remaining pellet was subjected to proteinase K digestion. Samples were mixed with 1 ml of Digestion Buffer (20 mM Tris-HCl, 0.5% SDS, pH 8.0), and 10 μ l of a 2 mg/ml proteinase K solution (equivalent to 20 μ g). The sample was subsequently placed on a heat block while continually shaking at a speed of 1400 rpm at 50°C for 4 hours to enhance enzymatic digestion. After the incubation period, the liquid mixture was centrifuged at 16,000 g for 1 minute. The supernatant was discarded, and the pellet was resuspended with 2 ml of Buffer 3, and the centrifugation step was repeated to eliminate any remaining impurities. The washing procedure with centrifugation was repeated using 2 ml of DH₂O three times to completely remove SDS from the sample.

Following the washing process, the pellet was mixed with 1 ml of 0.1 M NaOH and placed on a thermomixer for 16 hours at RT at 1400 rpm to balance the solution's acidity. Following incubation, the sample was centrifuged at 16,000 g for 1 minute at 15-25°C. The supernatant was collected in a fresh 1.7 ml microcentrifuge tube and 250 μ l of a 1 M Tris-HCl solution with a pH of 7.8 was added to neutralise the solution. The sample was then either stored at -20°C for later analysis or used for D-alanine assay.

2.30.2 LTA isolation for the D-Ala assay

To isolate crude LTA from *S. aureus (Je2, FmtA and Flp) or B. subtilis (168, PBPX, dltAB, lta3, and TagO)* cultures, 20 ml of LB was added to a 50 ml centrifuge tube with the necessary antibiotics for selection. A sterile inoculation loop was used to introduce a single colony of *S. aureus* into the 50 ml centrifuge tube containing the medium. The culture was then placed in an incubator at 37°C for overnight (16–20 hours) with continuous agitation at 250 rpm to facilitate bacterial growth. The sample was then centrifugation at 5000 g for 5 minutes at 15-25°C. The supernatant was discarded, and the cells contained within the pellet were resuspended in 2 ml of resuspension buffer. The suspension was subsequently transferred to a 2 ml screw-cap microcentrifuge tube and centrifuged at 16,000 g for 1 minute at 15-25°C, and the resulting supernatant was discarded.

The pellet was then resuspended using 2 ml of resuspension buffer, and 700 μ l of zirconia/silica beads were added to induce cell lysis. The sample was then cooled on ice for 5 minutes. To ensure cell lysis, we used the MagNA-lyser instrument, operating at 7000 rpm for 30 seconds. The sample was then cooled on ice for 5 minutes, and this process was repeated three more times.

Following cell lysis, cell membranes were collected by centrifugation at 20,000 g for 1 hour at 4°C. The supernatant was discarded and the pellet was mixed again in 350 μ l of resuspension buffer. To promote resuspension, the pellet was gently agitated using a pipette tip and thoroughly mixed. Where resuspension proved problematic, the pellet was frozen at -20°C prior to resuspension.

Extraction was completed by adding 350 μ l of 1-butanol to the resuspended pellet, which was then placed on a heat block maintained at 37°C for 45 minutes while shaking at 1400 rpm. Following the incubation period, the mixture was centrifuged at 20,000 g for 45 minutes at 4°C to separate any solid particles that could not dissolve, and the different phases of the mixture. The aqueous layer located at the bottom was transferred into a 1.7 ml microcentrifuge tube. Remaining cell debris was centrifuged again at 20,000 g for 20 minutes at 4°C, and the remaining supernatant was collected.

To initiate the lipase reaction, 50 μ l of crude LTA extract, 50 μ l of 50 mM Tris free base, and 2 μ l of 1 M NaOH were added to a PCR tube. The isolated WTA and LTA were then subjected to the D-Ala assay to measure associated alanine.

2.31 Measuring D-Ala in WTA and LTA by the D-Ala assay

2.31.1 Assay preparation and execution

All standards, controls, and samples were assayed in duplicate by using Abcam d-alanine assay kit. Initially, the DAA Probe was diluted fivefold by combining 5 μ L with 20 μ L of the DAA Assay Buffer. For each reaction, 50 μ L of both Reaction Mix and Background Mix were prepared, along with a master mix of each solution to ensure consistency. Subsequently, 50 μ L of the Reaction Mix was added to each well (96-well plate) designated for standards, samples and spikes. Similarly, 50 μ L of the Background Mix was dispensed into the sample background wells. The composition of each mix was composed of:

- DAA Assay Buffer: 42 μL.
- DAA Cofactor: 2 μL.
- DAA Enzyme Mix: 2 μL.
- DAA Developer Mix: 2 μL.
- Diluted DAA Probe: 2 μL.
- Background mix components:
 - DAA Assay Buffer: 44 μL
 - DAA Cofactor: 2 μL
 - DAA Developer Mix: 2 μL
 - Diluted DAA Probe: 2 μL

2.31.2 Incubation and measurement

Once all samples were prepared with their appropriate reagents, the assay plates were incubated at 37°C for 2 hours in a dark room. After incubation, fluorescence was measured using a microplate reader with an excitation and emission wavelengths of 535 and 587 nm, respectively. Samples containing a fluorescence value exceeding beyond

the standard curve were diluted appropriately and re-assayed. The concentration of the samples was adjusted by multiplying it by the corresponding dilution factor.

2.31.3 Data analysis

Data analysis was performed using Kit guid. The mean absorbance from each duplicate sample, control, and standard was calculated and the background fluorescence was subtracted from the respective sample and spike readings to obtain the corrected fluorescence signals, Fs and Fspike, respectively (Formula 3).

I

Formula 3. Calculation for alanine concentration. D, dilution factor; D-Ala, D-alanine; Fs,: Fspike-Fs;A pmol, picomole.

Chapter 3 Creation and characterisation of a *B. subtilis* strain with a minimal set of PBPs

3.1 Introduction

Multiple proteins are involved in the peptidoglycan biosynthetic pathway in bacteria, with PBPs playing a crucial role in the final assembly of the polymer outside the cytoplasmic membrane. PBPs facilitate key biochemical reactions, including glycosyltransferase activity, which assembles the glycan strand, and transpeptidase activity, which mediates the crosslinking of these strands. Additionally, there are peptidoglycan hydrolase PBPs with different specificities for breaking bonds in the peptidoglycan structure, such as endopeptidases and carboxypeptidases (Vollmer *et al.*, 2008). The importance of PBPs lies in their being essentially unique to bacteria, and they are inhibited by the most widely used class of antibiotics (β -lactams and cephalosporins) (Zapun *et al.*, 2008) as well as some "last resort" antibiotics (e.g., vancomycin).

The nomenclature for PBPs is rather complex, as the initial names were given based on their size, identified using labeled penicillin and SDS-PAGE. Thus, they were numerically named, e.g., PBP 1, PBP 2, etc. However, over time, more PBPs were identified in most studied bacteria, resulting in additional PBP names, e.g., PBP 2a. Then, with genome sequencing, further PBP-encoding genes were identified, and these tended to retain their gene names, e.g., *pbpH*. Consequently, when comparing different bacterial species, there are proteins with the same name that do not necessarily have the same biological function. Additionally, it is common for the gene encoding a PBP to differ from the name given to the protein itself, e.g., *ftsI* in *E. coli* encodes PBP3.

Beyond the complexities of nomenclature, the essentiality of PBPs is variable, and there seems to be a significant degree of redundancy in some bacteria, whereas others appear to have a minimal set. This has resulted in complex phenotypes when different combinations of mutations have been characterized. For example, single knockouts of the genes encoding PBP1a, PBP2a, and PBP1b can be generated in *S. pneumoniae*, but it is not feasible to create a strain with a double knockout of genes

encoding PBP1a and PBP2a (Hoskins et al., 1999; Paik et al., 1999). In contrast, in E. coli, the absence of either PBP1a or PBP1b is possible, but the absence of both is inviable, even when PBP1c is present (Denome et al., 1999; Yousif et al., 1985). In the model system used in this work, B. subtilis, deleting pbpA or pbpH as single mutations has minor effects on bacterial growth, the most significant being a slight phenotype during spore germination (Wei et al., 2003), but the loss of both PBP2a and PBPH is lethal under normal conditions. In contrast, PBP2b is an essential division protein, but abolishing the transpeptidase activity of the protein surprisingly had no effect on cell division. This serves as a prime example of redundancy in function, as in this background, the normally non-essential PBP3 was now essential for cell division (Sassine et al., 2017), somewhat similar to the mecA gene encoding PBP2a, a penicillin resistance factor in S. aureus (Fishovitz et al., 2014).

In *B. subtilis*, which has 16 distinct PBPs, removing four class A PBPs—PBP1, PBP2c, PBP2d, and PBP4—demonstrated no lethal effect, and the bacteria were able to grow, albeit with a decreased growth rate. However, these strains did exhibit a mild morphological change, as cell width decreased upon deletion of all class A PBPs (Popham & Setlow, 1996).

In this chapter, the construction, validation, and characterization of strains with multiple PBP deletions were used to understand functional redundancy and generate a strain with the minimal set of PBPs.

3.2 Results

3.2.1 Construction of a B. subtilis strain with a minimal set of PBPs

Constructing a strain with a minimal set of PBPs was a long-standing objective, and this project started with an intermediate PBP deletion strain (GG136) (G. Goldsmith, unpublished). In this strain, three out of four class A PBPs (PBP2c encoded by *pbpF*, PBP2d encoded by *pbpG*, and PBP4 encoded by *pbpD*), one out of six class B PBPs (PBP3 encoded by *pbpC*), and three out of six class C PBPs (PBP5 encoded by *dacA*, PBPX, and PBP4* encoded by *pbpE*) were deleted. Thus, this strain retained only one of the bifunctional class A PBPs, PBP1, encoded by *ponA*. Among the class B PBPs, five remained: PBP2a, PBPH, PBP2b, SpoVD, and PBP4b. Individually, these are dispensable except for PBP2b, and it was known that either PBP2a or PBPH is required for viability (Wei *et al.* 2003). In contrast, none of the class C PBPs seem to be important for vegetative growth. In this strain, the coding sequences for PBP5*, PBP4a, and PBPI were still present and potentially expressible, though most are associated with sporulation. This information was summarized in the table shown in Figure 3.1A.

This strain was constructed through the systematic deletion of PBP genes, where each deletion was marked with antibiotic resistance cassettes flanked by lox recombination sites. These resistance cassettes were subsequently removed via Cre-lox recombination, mediated by plasmid-borne Cre recombinase (pDR111). This process was iteratively repeated until the construction of strain GG136.

Whole-genome sequencing (WGS) of strain GG136 was performed to confirm the expected gene deletions and assess genome integrity. However, the sequencing data is currently unavailable for analysis. Further validation through targeted PCR and sequencing of specific loci was conducted to verify the intended deletions

. To confirm the deletions and to characterize their consequences on the expression of the remaining PBPs in strain GG136, bocillin FL labeling was employed. This method enabled the direct labeling of live bacteria in vegetative growth, detecting 8 out of 16 PBPs using SDS-PAGE and fluorescent imaging (Zhao *et al.* 1999); Figure 3.1B1) in the wild-type strain. Using the same method, the GG136 strain was analyzed.

Bocillin labeling indicated that only 4 out of 8 PBPs were detectable: PBP1 (the highest molecular weight, at the top of the gel), PBP2a, PBP2b, and PBPH (Figure 3.1B2). This gel image clearly showed that the deletions in GG136 did not result in any obvious upregulation of the remaining PBPs compared to the PBP profile of the 168 strain (Figure 3.1B1), and none of the sporulation PBPs were evident.

To further investigate the effect of the deletion of multiple PBPs (PBP2c, PBP2d, PBP4, PBP3, PBP5, PBPX, and PBPI) on the growth of the GG136 strain, a fresh single colony from an overnight culture on nutrient agar was inoculated in LB medium and incubated at 37°C with shaking. Growth was then monitored every 30 minutes for four hours. Plotting a graph of the optical density of the cultures against time (Figure 3.1C) best demonstrated this effect when the data were plotted using a linear y-axis, rather than the conventional logarithm of the optical density. Thus, for all future plots of bacterial growth, a linear scale was generally used unless otherwise stated. The plots generated indicated that the growth of the strain lacking multiple PBPs (GG136) in LB was slower compared to the 168 strain. This was numerically determined by calculating the rate at which the optical density changed between 40 to 120 minutes, where exponential growth seemed most consistent, and calculating the doubling time for the cultures. To minimize errors due to sampling, these values were calculated using four data points as follows:

Optical density of culture at 40 minutes (A) subtracted from the OD at 80 minutes (B) = $S/A \times 40 = \text{growth rate (G1)}$

Optical density at 80 minutes (A) subtracted from the OD at 120 minutes (B) = $S/A \times 40 = \text{growth rate (G2)}$

The average doubling time was calculated as (G1 + G2)/2.

This experiment was repeated several times, consistently yielding similar values (data not shown). This indicated that the loss of the PBPs had a minimal effect on the strain's ability to grow. The optical density doubled in 26.5 +/- 2 minutes for the 168 strain, while for GG136, it took 30.2 +/- 1.5 minutes. This suggests the potential to remove more of the expressed PBPs while still maintaining a viable strain.

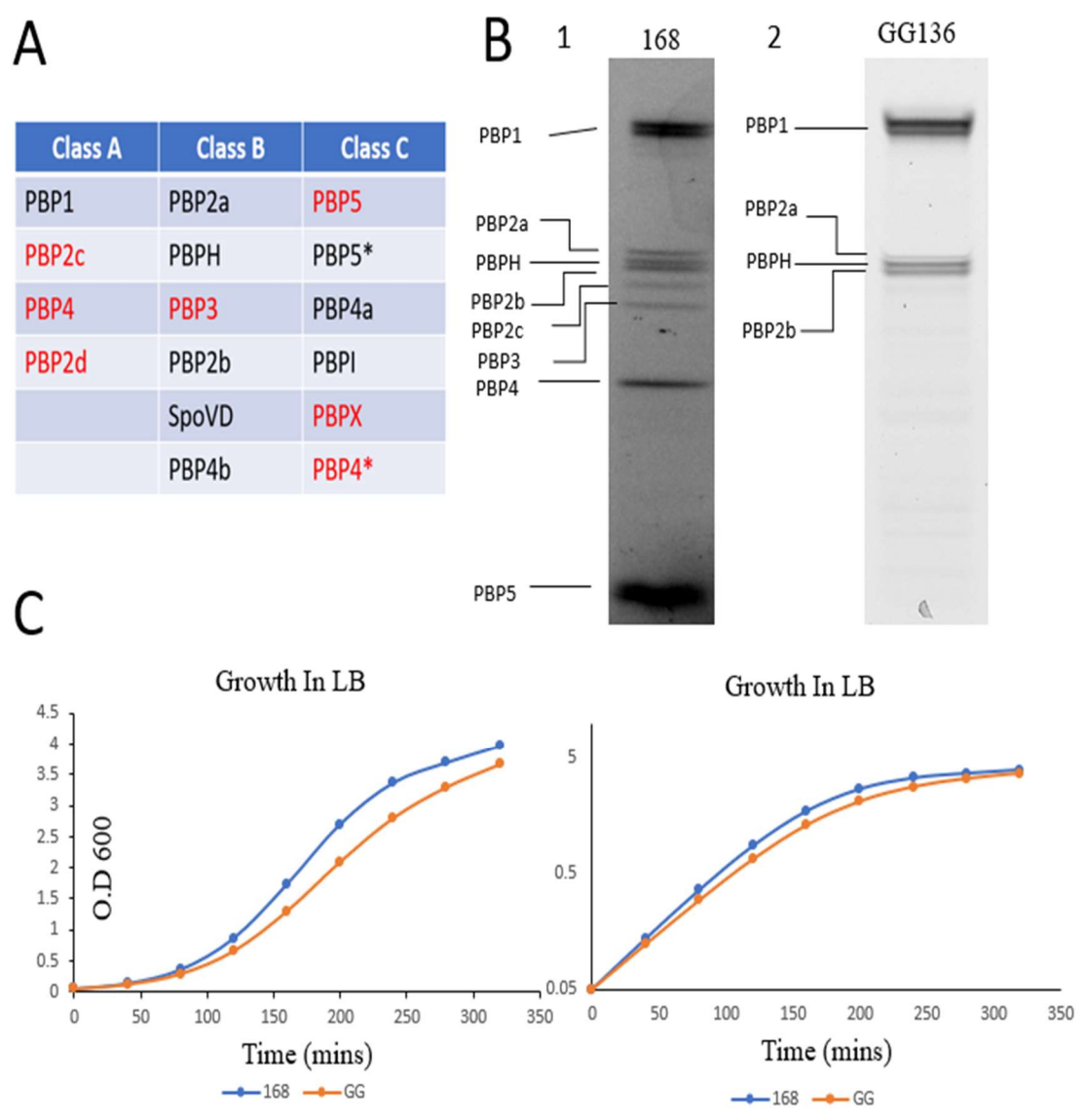


Figure 3.1: Bocillin-FL-based detection of penicillin-binding proteins in the 168 and GG136 strains.

A) All PBPs in the *B. subtilis* 168 strain; the PBPs in red are deleted in the GG136 strain, while those in black are intact. B) 1) PBPs in strain 168 detected using bocillin FL. 2) bocillin-FL labelling of the GG136 strain, the identity of the individual PBPs are shown on the left had side of the image. C) A representative growth curves of the 168 and GG136 strains in LB medium (168 in blue and GG136 in orange), left graph has a linear scale on the y-axis and on the right same data plotted using a log 10 scale on the y-axis.

3.2.2 Deletion of ponA in strain PBPs GG136

Following the confirmation that strain GG136 was deleted for the expected set of PBPs using Bocillin FL and PCR, the next logical PBP to remove was PBP1 (*ponA*), as it was the last of the Class A bifunctional PBPs present, and it had been shown that this class of PBPs can be removed in a wild-type background.

To delete *ponA* in strain GG136, a targeted knockout construct was introduced by transforming GG136 with genomic DNA from strain BKE22320, which contains a *ponA* deletion marked by an erythromycin resistance cassette flanked by lox recombinase sites (Koo *et al.*, 2017). Selection on erythromycin confirmed successful transformation, ensuring the deletion of *ponA* without restoring other PBPs. The risk with this method was that the transformation might result in the restoration of one or more of the deleted PBPs in GG136. However, this possibility was potentially advantageous, as it would ensure that transformants were obtained, indicating successful transformation and potentially revealing the required PBP complement. It was relatively easy to confirm the presence of the *pbp* gene deletions using a combination of PCR and bocillin labeling to detect the expressed PBPs.

After using the standard transformation method (section 2.7), a reasonable transformation efficiency was obtained, and several independently generated colonies were isolated. Visual inspection of the colonies, after streaking them onto fresh plates, indicated no obvious colony morphology variations, which might have been expected if the proposed strain construction was deleterious. The resulting strains were then grown exponentially, and samples were taken to confirm the genotype of the strains and their PBP profile.

To confirm gene deletions, pairs of oligonucleotide primers were designed to amplify each PBP, with each pair annealing approximately 300 bp upstream and downstream of the coding sequence of the gene of interest. This approach generated a collection of PCR oligonucleotide pairs corresponding to each PBP in the *B. subtilis* genome. These primers were then used to amplify the corresponding regions of gDNA from the parental single deletion strain (e.g., BKE22320 for *ponA*), the wild type (168), and the multiple deletion mutants isolated. The products of these PCR reactions were then

resolved by agarose gel electrophoresis, providing a way to differentiate between the presence of marker-less gene deletions, deletions where the antibiotic resistance cassette was still present, or if the wild-type gene was still present. Systematic checks of the deletion mutants using these primers confirmed that the isolates carried the expected deletions (data not shown). In parallel, analysis of bocillin-labeled cells by SDS-PAGE confirmed the absence of PBP1 from the strain (Figure 3.2B) and that only the expected PBPs were expressed. The PBP profiles also indicated that there was no significant change in the expression of the remaining PBPs (Figure 3.1B). These results suggested that viable bacterial growth was possible with the final steps of PG assembly being mediated by only three PBPs: PBP2b, PBP2a, and PBPH.

Having confirmed the genotype of the strains, one of the isolates was chosen and designated YA-X. The growth of this strain was then compared to that of the wild type in LB medium at 37 °C, as described previously (Figure 3.2C). From this, it was evident that the growth rate of strain YA-X was slower than that of previously tested strains, doubling in 37 +/- 1.1 minutes, compared to the parent strain GG136 with PBP1 (30.2 +/- 1.5 minutes) and the wild type (26.5 +/- 2 minutes). This suggests that the reduction in PBPs is affecting the bacterium's ability to grow rapidly.

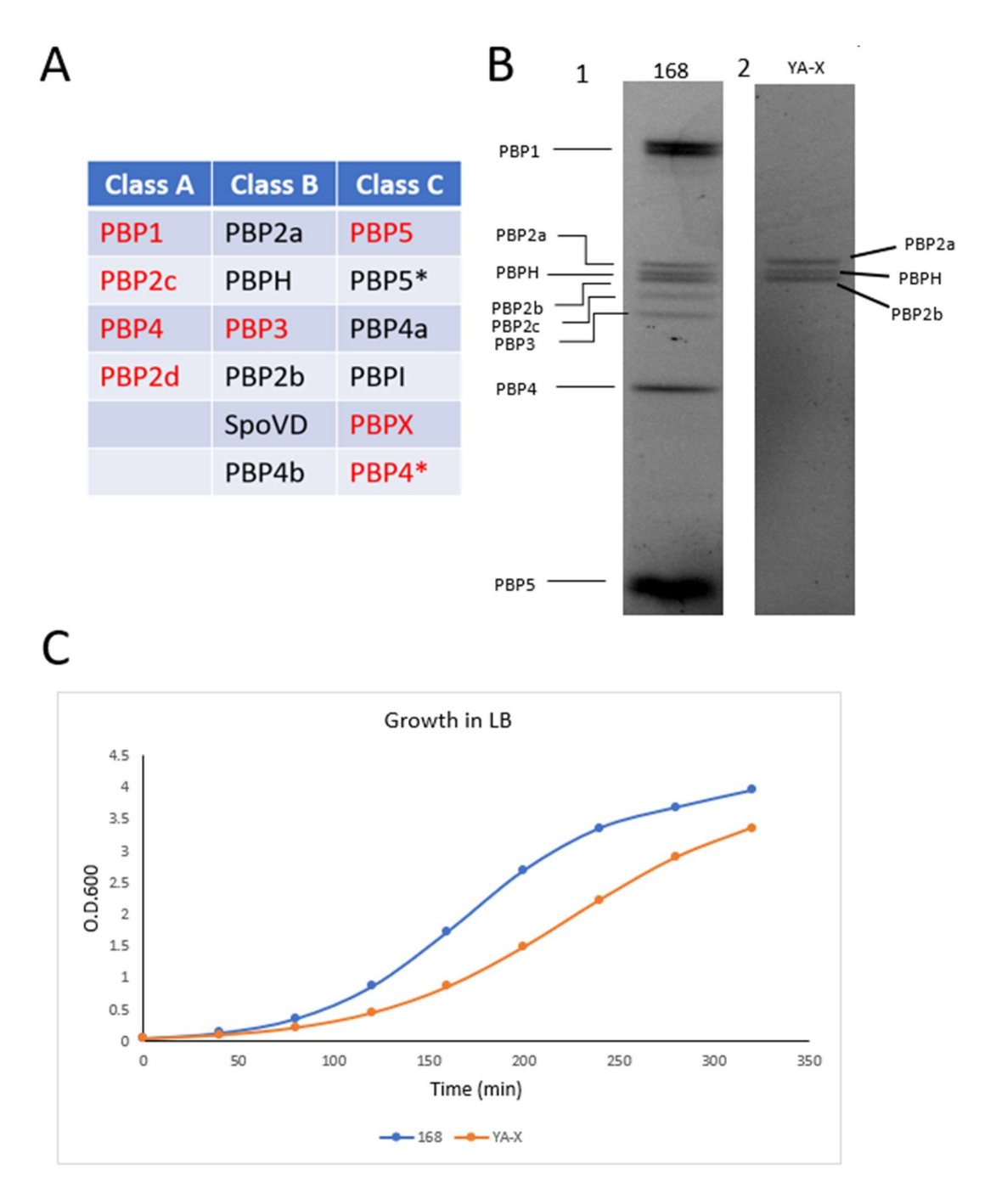


Figure 3.2: Bocillin-FL-based detection of penicillin-binding proteins in the 168 and YA-X strains. A) The table shows the full complement of PBPs in the *B. subtilis* 168 strain. The PBPs in red are deleted in the YA-X strain while those in black are intact. B) 1) Detection of PBPs in strain 168 using bocillin FL revealed eight detectable PBPs. 2) bocillin FL labelling of the YA-X strain showed only three detectable PBPs, namely PBP2a, PBP2b and PBPH. C) The growth curve of the 168 and YA-X strains in LB medium (168 in blue and YA-X in orange).

3.2.3 Deletion of *pbpH* or *pbpA* from a strain with multiple deletions (YA-X)

After deleting PBP1 and confirming its deletion and the strain's ability to maintain growth in LB, we aimed to introduce additional mutations for the remaining PBPs detectable using bocillin FL during vegetative growth. Of these, PBP2B is essential, so we targeted the deletion of either *pbpA* or *pbpH*. Using the same method described for *ponA*, null mutations for either *pbpA* or *pbpH* were attempted in YA-X. However, all attempts to introduce the *pbpA* null mutation failed, with only a few colonies being generated on selection, and upon checking, these were found to be the result of cotransformation events that did not involve a true deletion of *pbpA*.

In contrast, the *pbpH* null mutation was successfully introduced into YA-X, suggesting that PBPH is not essential for growth in the YA-X background. Analysis of the strains generated by this transformation confirmed the removal of the *pbpH* gene, initially by colony PCR and agarose gel electrophoresis (Figure 3.3A), and one isolate was designated strain YA-XI. Further verification of this strain was performed using bocillin FL labeling to identify its penicillin-binding profile (Figure 3.3B). From this, it was immediately evident that cells of strain YA-XI had only 2 (PBP2b and PBP2a) out of the normal complement of 8 PBPs.

In conclusion, strain YA-XI was generated with only two of the vegetative PBPs present (PBP2b and PBP2a), and it appeared that these were the only PBPs expressed during vegetative growth, which were sufficient to permit growth on both plates and in liquid culture. It was also indicated that the expression levels of the PBPs present remained comparable to those observed in the wild-type strain, although it seemed that PBP2a may be slightly increased relative to PBP2b. This observation is further explored in the next chapter. However, the results implied that the absence of the other PBPs was not compensated for by any significant increase in the expression of those remaining.

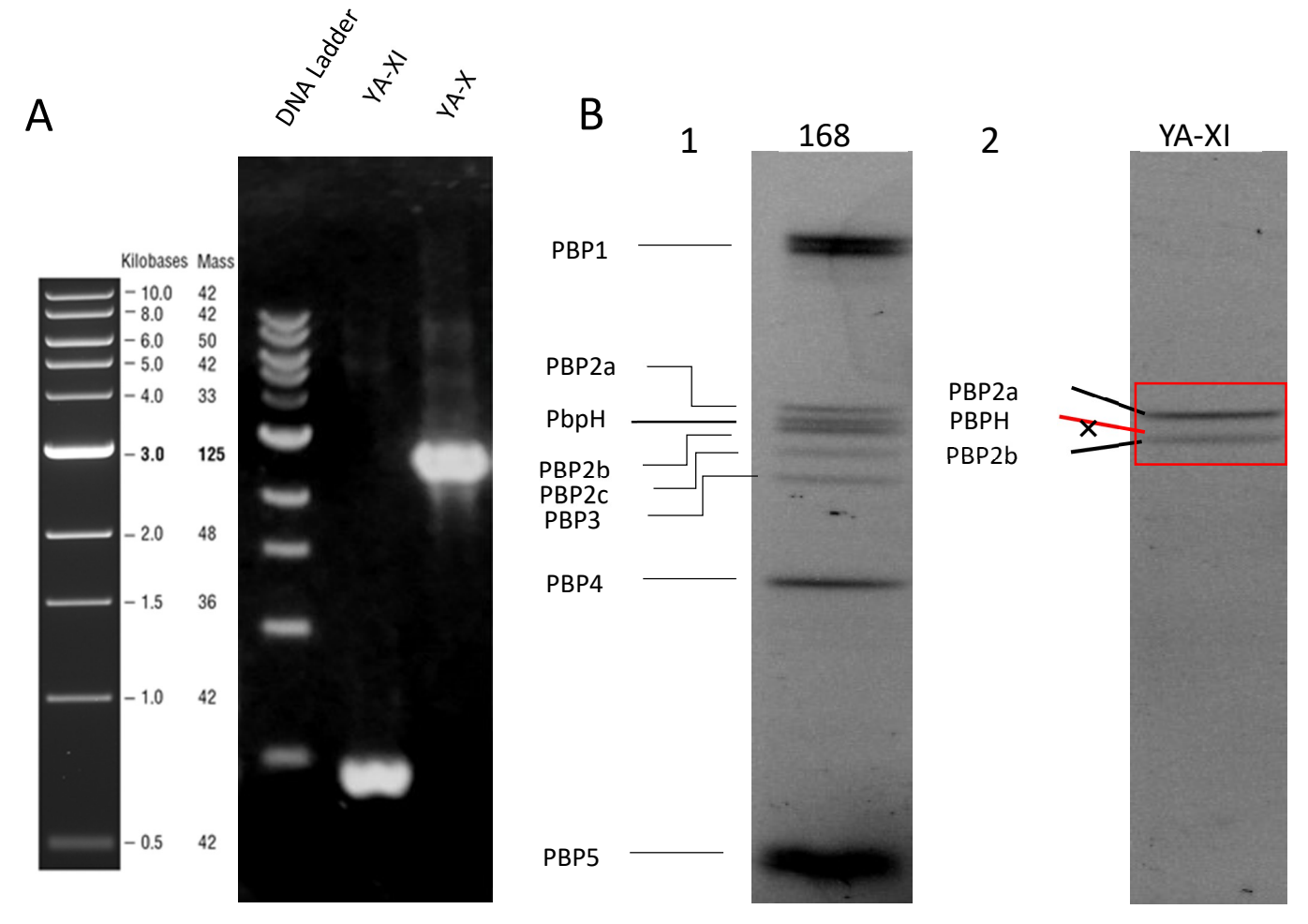


Figure 3.3: Deletion of *pbpH* from strain YA-X and detection using Bocillin FL.

A) Agarose gel image of PCR products to confirm the absence of PBPH in the YA-XI strain. The first lane shows the DNA ladder, the second lane shows the PCR product of the YA-XI strain and the third lane shows the PBPH PCR product from strain 168. B1) Bocillin FL labelling of the 168 strain demonstrating all the detectable PBPs, namely PBP1, 2a, H, 2b, 2c, 3, 4, and 5 "The identification of bands proceeded vertically, from the topmost to the bottommost on the gel." B2) Bocillin FL labelling of the YA-XI strain demonstrating only two detectable PBPs, namely PBP2a and PBP2b.

3.2.4 Growth and morphology of the strain with minimal PBPs

Detailed phenotypic analysis was conducted to determine if the deletion of multiple PBPs had resulted in any subtle morphological defects that were missed in the initial checks. The strains 168, the multiple PBP deletion strain (YA-XI), and the intermediate strain (YA-X) were grown at 37 °C in two different media: LB and NB liquid medium. The optical density (OD600) values were then plotted against time, and the resulting graphs are shown in Figure 3.4. From these plots, a clear difference in the ability of the multiply deleted strains to grow in NB compared to the wild-type parent could be seen. The strains lacking multiple PBPs (YA-XI and YA-X) seemed to reach exponential growth more slowly, resulting in an extended apparent lag phase. This was most notable in NB, where the cultures were clearly slower than the wild type. The difference between these two culture media is relatively small, as both primarily consist of peptides and yeast extract. The most significant difference is nutrient concentration, with LB containing 150% more yeast extract and approximately 60% more animal-derived peptides compared to NB. Although there may also be other more subtle differences, as the preparation of the peptides differs significantly.

The growth rate was calculated between 40 and 120 minutes. The doubling rate was 26.5 +/- 2 minutes for the 168 strain, 37 +/- 1.1 minutes for YA-X, and 45.3 +/- 1 minute for YA-XI in LB. In NB, the doubling time for the 168 strain was 48 +/- 1 minute, while the growth rate for YA-X was 65 +/- 1.1 minutes, and for YA-XI, 76 +/- 1 minute. These results indicate that *B. subtilis* cells are able to grow without *pbpE*, *pbpG*, *pbpC*, *pbpF*, *pbpX*, *pbpD*, *dacA*, *ponA*, and *pbpH*, but they exhibit slower growth rates (Figure 3.4A & B).

To investigate the effect of *pbpE*, *pbpG*, *pbpC*, *pbpF*, *pbpX*, *pbpD*, *dacA*, *ponA*, and *pbpH* mutations on the morphology of *B. subtilis*, samples were collected during exponential growth at 37 °C for the three strains: 168, YA-XI, and YA-X. Light microscopy was used to visualize the morphological changes resulting from the multiple PBP mutations. To better observe bacterial morphology, FM dye was used. FM 5-95 is a fluorescent dye frequently employed in biological processes to stain and visualize cellular membranes, particularly bacterial cell membranes. The dye integrates into the lipid bilayer of membranes and emits fluorescence upon binding.

During exponential growth, the 168 strain exhibited the characteristic rod-shaped morphology associated with *B. subtilis*, measuring approximately 2 µm long and 0.8 µm in diameter with rounded poles. In contrast, it was noticeable that YA-X cells tended to remain joined after division, resulting in chains of cells. This phenotype was even more evident in strain YA-XI, which displayed even more pronounced chaining (Figure 3.4C).

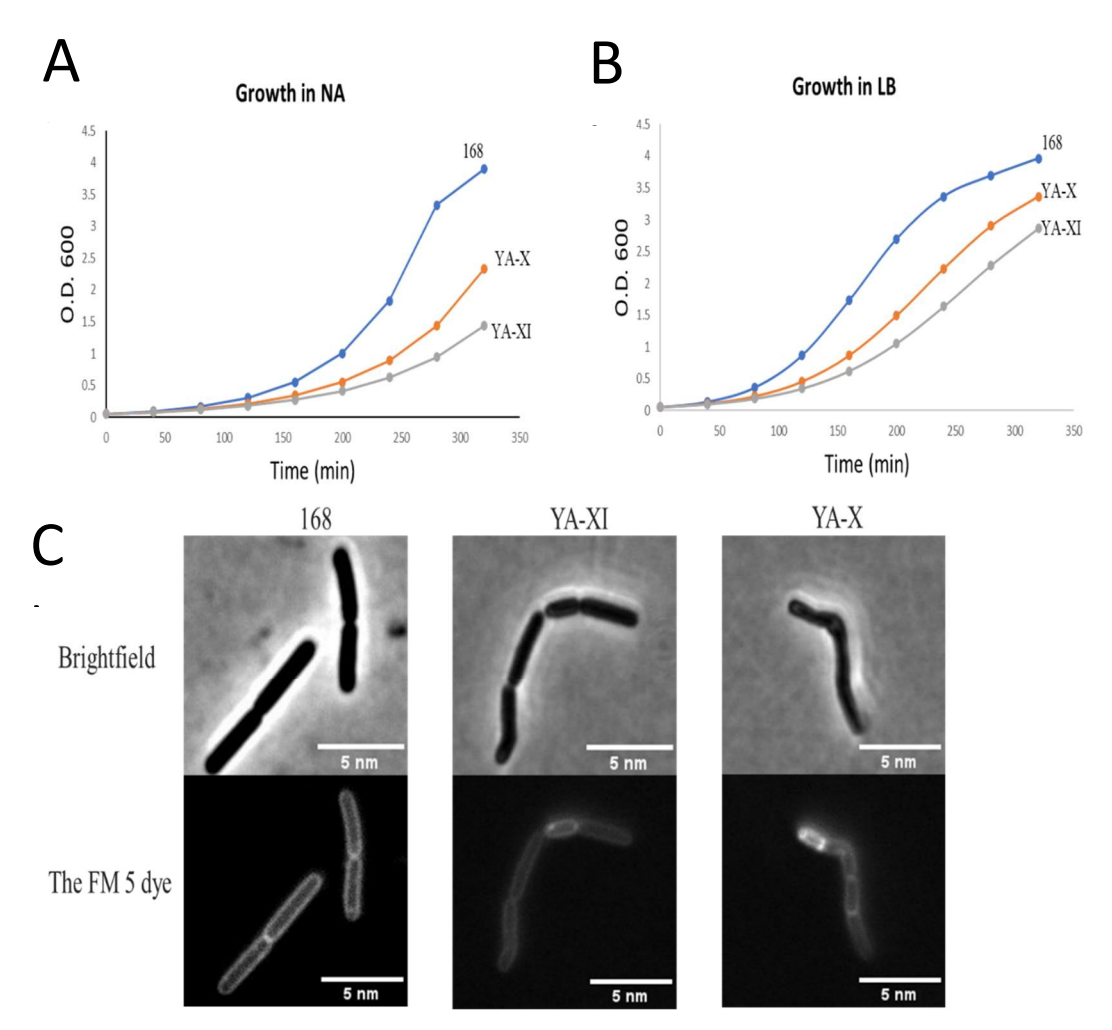


Figure 3.4: Growth and morphology of strains lacking multiple PBPs.

Plots of the growth of 168, YA-X and YA-XI in NB medium (A) or LB medium (B) at 37 °C. Panel (C) shows characteristic images of the cell morphology of the three strains 168, YA-X and YA-XI: brightfield (top) and FM 5 dye-labelled (bottom). The images were acquired after approximately 2 hours of growth and in LB medium.

3.2.5 HPLC analysis of muropeptides from 168, YA-X and YA-XI cells

Since the strains YA-X and YA-XI were apparently normal in most respects, other than exhibiting a reduced growth rate and a slight change in cell dimensions, it seems possible that the loss of multiple PBPs may simply alter the structural conformation of the PG, which still functionally provides osmotic protection. To investigate if the deleted genes had an impact on the way PG was crosslinked, samples of cell wall were prepared from exponentially growing bacteria using the method outlined in sections 2.24 and 2.25.

In brief, the strains 168, YA-X, and YA-XI were grown in LB medium and harvested upon reaching an OD of 0.5-0.6. Crude sacculi were then generated by boiling in 5% sodium dodecyl sulfate (SDS), followed by successive washes with sodium chloride (NaCl) and water (H2O) to eliminate SDS and other soluble components. Mechanical disruption was then employed using glass beads to facilitate the complete release of cellular contents trapped within the cell that could not be "dissolved out." Nucleic acids were then eliminated using deoxyribonuclease (DNase) and ribonuclease (RNase) treatments prior to the samples being washed and lyophilized. To permit analysis, the peptidoglycan (PG) of the strains was enzymatically digested into muropeptides by Cellosyl, which cuts the β-1,4-glycosidic bonds between N-acetylglucosamine and Nacetylmuramic acid. Following digestion, the samples underwent a purification process before being separated using reversed-phase high-performance liquid chromatography (RP-HPLC). The end result was an elution profile that could be correlated with that of the parent strain. This comparison was expected to determine if there was a significant alteration in the muropeptide profile, either by a change in the relative abundance of peaks or the appearance of novel peaks. Since this analytical method is well established, the identity of many of the peaks can be predicted, and where uncertainty existed, the RP-HPLC can be repeated, collecting the eluted material corresponding to the peak to permit MS analysis. Initially, the RP-HPLC muropeptide elution patterns of the two mutant strains YA-X and YA-XI were compared to that of 168, generated in parallel in this work (Figure 3.5). From this comparison, there were clear and significant differences between 168 and the two mutant strains, but the two mutant strains appeared

essentially identical. This implied that the presence or absence of PBP1a/b (ponA) had no major effect on the gross mean composition of the PG muropeptides.

Previous research has characterized the chemical identity of compounds corresponding to 38 peaks in the muropeptide profile of *B. subtilis* (Atrih, A. *et al.*, 1999, and analysis by Sassine J., unpublished). Comparison of these previous elution profiles with that obtained for 168 in this work showed very good correlation. With this correlation, it was possible to assign specific muropeptide identities to the HPLC profiles with a high degree of confidence. The molecular structures of the known muropeptides and the corresponding peak numbers are provided in Figure 3.6.

Thus, it was possible to look at the muropeptide profiles of the mutant strains in more detail and determine the identity of the molecular species that were altered in abundance. The first peak in the elution profiles that showed a considerable difference between the YA mutants and 168 was peak number 3, which was significantly lower in abundance in the YA strains. By its position in the elution time course, it was expected to represent Tri (NH₂). Thus, this Cellosyl degradation product is less abundant in the PG extracted from the two mutant strains relative to that of the wild-type strain. The second peak that demonstrated a major difference was number 11, which, in contrast to peak 3, was significantly higher in the mutant strains and corresponded to the Penta (NH₂) structure. This peak was considerably higher in YA-X and YA-XI compared to 168. Peak number 15 was next observed to be higher in 168 than in YA-X and YA-XI. Peak number 15 represents the TriTetra (NH₂) structure. Following this, peak number 21, which represents the TriTetra (NH₂)₂ structure, decreased upon deletion of multiple PBPs compared to 168. The last two peaks that were considerably increased in the multiple PBP deletion strains compared to 168 were peaks 31 and 32, which represent TriTetraTetra(NH₂)₃ and TriTetraTetra(NH₂)₃(deAc), respectively (Figure 3.5 & 3.6).

From this data, it is possible to say that the main feature that differs in the cell wall of the deletion strains relative to the wild type was a significant decrease in Cellosyl degradation products with tripeptides and an apparent increase in molecules with pentapeptides. This suggests that the most significant effect on the composition of the PG in the mutant strains is the absence of the removal of D-alanine from the peptide side chains. These changes are consistent with the deletion of *dacA*, as published previously (Atrih *et al.*, 1999). Other than this, the loss of multiple PBPs did not seem to have any other consequences for the muropeptide composition of the PG.

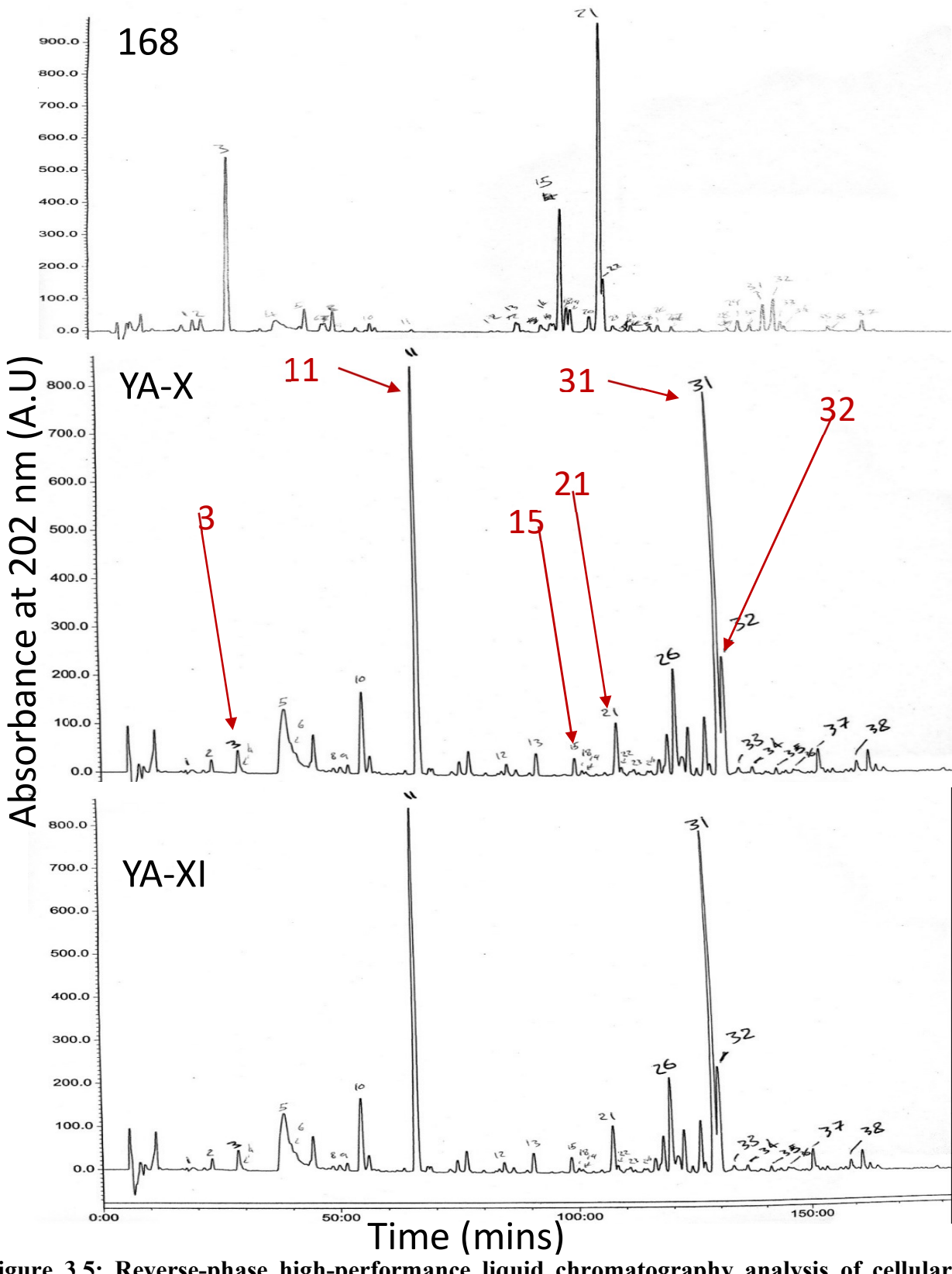


Figure 3.5: Reverse-phase high-performance liquid chromatography analysis of cellular muropeptides. Muropeptide profiles for 168, YA-X and YA-XI cells. The peaks 1–38 have been assigned according to Bisicchia *et al.* (2011) and Sassine (2017; unpublished). YA-X and YA-XI mutant cells have different muropeptide profiles with eight sharp peak differences. The peaks are 3, 11, 15, 21, 31 and 32 (red arrow), and each peak represents a specific muropeptide component.

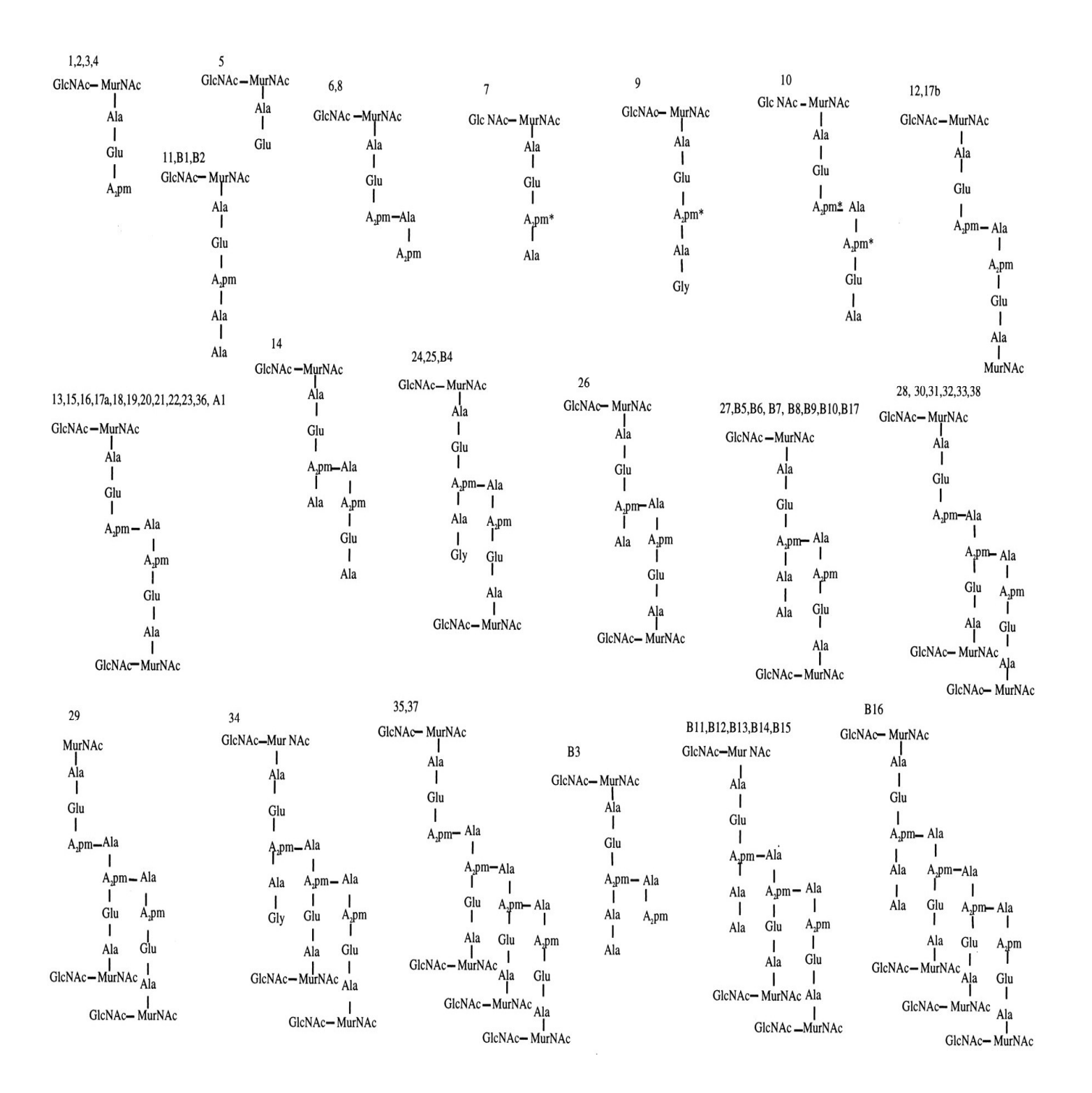


Figure 3.6: Structural composition of identified muropeptides.

The proposed fundamental arrangements for muropeptides derived from *B. subtilis* as outlined by Atrih *et al.* in 1999. Numbers correspond to the highest points.

3.2.6 Peptidoglycan composition and cross-linking of the strain with a minimal set of PBPs

Since there were some compositional alterations detected in the muropeptide analysis, it was possible that the PG in the multiple PBP deletion strains had a more subtle change that was not immediately obvious from the Cellosyl degradation. An initial prediction was that the loss of multiple PBPs would result in a significant change in the cell's ability to cross-link the glycan strands and consequently a dramatic change in the crosslinked disaccharides would be observed. Since this was not immediately obvious, a finer analysis of the cross-linkage levels was required. Thus, the HPLC data was analyzed using LabLogic Systems Ltd.'s Laura software version 4.1.7.70 with the help of Dr. J. Biboy from Newcastle University. From this, it was possible to calculate the level of peptide cross-linkage using the formula: x = 100 - (%Penta + %TetraTetra). This muropeptide analysis was applied to the 168, GG136, YA-X, and YA-XI strains.

From the values obtained, it was observed that the total amounts of monomers, trimers, tetramers, dipeptides, and pentapeptides exhibited less than a 10% variation across the strains 168, GG136, YA-X, and YA-XI (Table 3.7). The structures that showed the greatest differences among these strains were dimers, tripeptides, and tetrapeptides, as indicated in red. Specifically, the sum of dimers in strain 168 decreased by 6% compared to GG136, by approximately 12% compared to YA-X, and by around 16% compared to YA-XI. Similarly, the sum of tetrapeptides in the peptidoglycan composition of strain 168 was approximately 11% lower than in GG136, about 13% lower than in YA-X, and around 16% lower than in YA-XI.

The deletion of multiple penicillin-binding proteins (PBPs) led to an increase of more than 10% in certain structures within the peptidoglycan composition. However, other peptidoglycan structures decreased in strains GG136, YA-X, and YA-XI when compared to strain 168. Notably, the sum of tripeptides in the muropeptide composition decreased by approximately 30% in strain GG136, about 28% in strain YA-X, and around 27% in strain YA-XI, compared to strain 168. In summary, despite these differences, the degree of cross-linkage in the PBP deletion strains did not show a significant or sudden difference (Figure 3.7), but rather a modest increase, suggesting

that their peptidoglycan cross-linking was maintained despite the deletion of multiple PBPs. This is presumed to mediate the modification of the glycan strands.

	168	GG136	YA-X	YA-XI
Sum monomers	24.59	22.48	21.88	19.08
Sum dimers	60.93	66.22	71.77	75.53
Sum trimers	10.52	7.36	2.87	3.31
Sum tetramers	1.95	2.38	1.71	0.00
Sum dipeptides	2.46	13.79	11.04	7.61
Sum tripeptides	56.32	25.87	28.23	29.65
Sum tetrapeptides	40.43	50.86	53.00	56.16
Sum pentapeptides	0.79	9.47	7.74	6.57
Degree of Crosslinkage 1	38.94	39.80	39.09	39.97
% Peptides in Crosslinkage 2	75.41	77.52	78.13	80.92

Figure 3.7: High-performance liquid chromatography analysis of peptidoglycan from strains with penicillin-binding protein deletions.

The table shows the variation in peptidoglycan composition among the four strains (168, GG136, YA-X, and YA-XI). Values highlighted in red indicate statistically significant differences relative to strain 168, based on a Student's t-test with a threshold of p < 0.05. The percentage difference was calculated by the equation:

 $X = (Sum of dimers in A strain / Sum of dimers in B strain) \times 100$

The Percentage of difference = 100 - X

3.2.7 Deleting multiple PBPs reduces the cell rigidity of B. subtilis

Muropeptide analysis provided a good way to analyse a gross change in the assembly of the PG, but since it represents an average analysis of all wall material and is not able to differentiate between the cylindrical cell wall and cell poles/forming septa. It is possible that any significant local change in the PG may be averaged out and so a subtle structural change might be missed. Thus, a more direct physiological analysis of the properties of the cell wall was attempted using AFM microscopy. This idea was supported by a published study of *S. aureus* (Loskill *et al.*, 2014), where it was found that deleting PBP4 resulted in a change in the overall cell envelope rigidity. To allow this analysis, exponentially growing cells of strains 168 and YA-XI were immobilized on a surface using CorningTM Cell-Tak Adhesive (as detailed in section 2.22 of the Methods). These immobilized cells were then imaged using an Atomic Force Microscopy (AFM) tip.

The AFM data is shown in figure 3.8 as a plot for the topology of over an area where a cell was fixed to the substrate where the penetration of the AFM tip is indicated as a height on applying a defined force. The first image (left) in Figure 3.8A & B depicts a three-dimensional topographic portrayal of the bacterial cell strains 168 and YAXI respectively. The image on the right in Figure 3.8A & B is a two-dimensional viewpoint of the identical bacterial cell strain 168 and YA-XI respectively. This perspective emphasizes the arrangement of height over the length of the cell, offering intricate details about the cell's measurements and drawing attention to differences in thickness or surface structure

The resulting topographic data were further analyzed to measure specific mechanical properties of the cell envelope. In particular, the rigidity was quantified by measuring the average stiffness at different regions of the cell, including the mid-cell and the poles. This approach allowed for a comprehensive understanding of the envelope's mechanical integrity. The AFM tip was used to apply controlled forces at these specific regions, and the resulting force-distance curves were analyzed to determine the Young's modulus, which provides a measure of cell envelope stiffness.

Rigidity was calculated from force-indentation curves obtained through AFM-based nanoindentation using the Hertzian contact model, given by:

$$F = (2E / (1 - v^2)) \times tan(\alpha) \times \delta^2$$

where:

E = Young's modulus (rigidity, in kPa) •

v = Poisson's ratio (assumed ~0.5 for bacterial cell walls) •

 α = Half-angle of the AFM tip (dependent on probe geometry) •

 δ = Indentation depth (nm) •

F = Applied force (nN) •

The rigidity values were obtained by fitting the force-indentation curves using the appropriate AFM analysis software. By comparing the Young's modulus values between the wild-type 168 and the YA-XI strains, it was expected to be indicate the impact of PBP loss on the structural integrity of the cell wall, considering any variations in rigidity between the mid-cell and the poles.

The results indicated that the rigidity of the wild type 168 was around 2 kPa (Kilopascal; Fig 3.8C), whereas the multiple PBPs deletion strain YA-XI was estimated to be approximately 1 kPa. Thus, although the cross-linkage level of YA-X Peptidoglycan was not significantly different from the 168, the overall cell wall rigidity was apparently decreased.

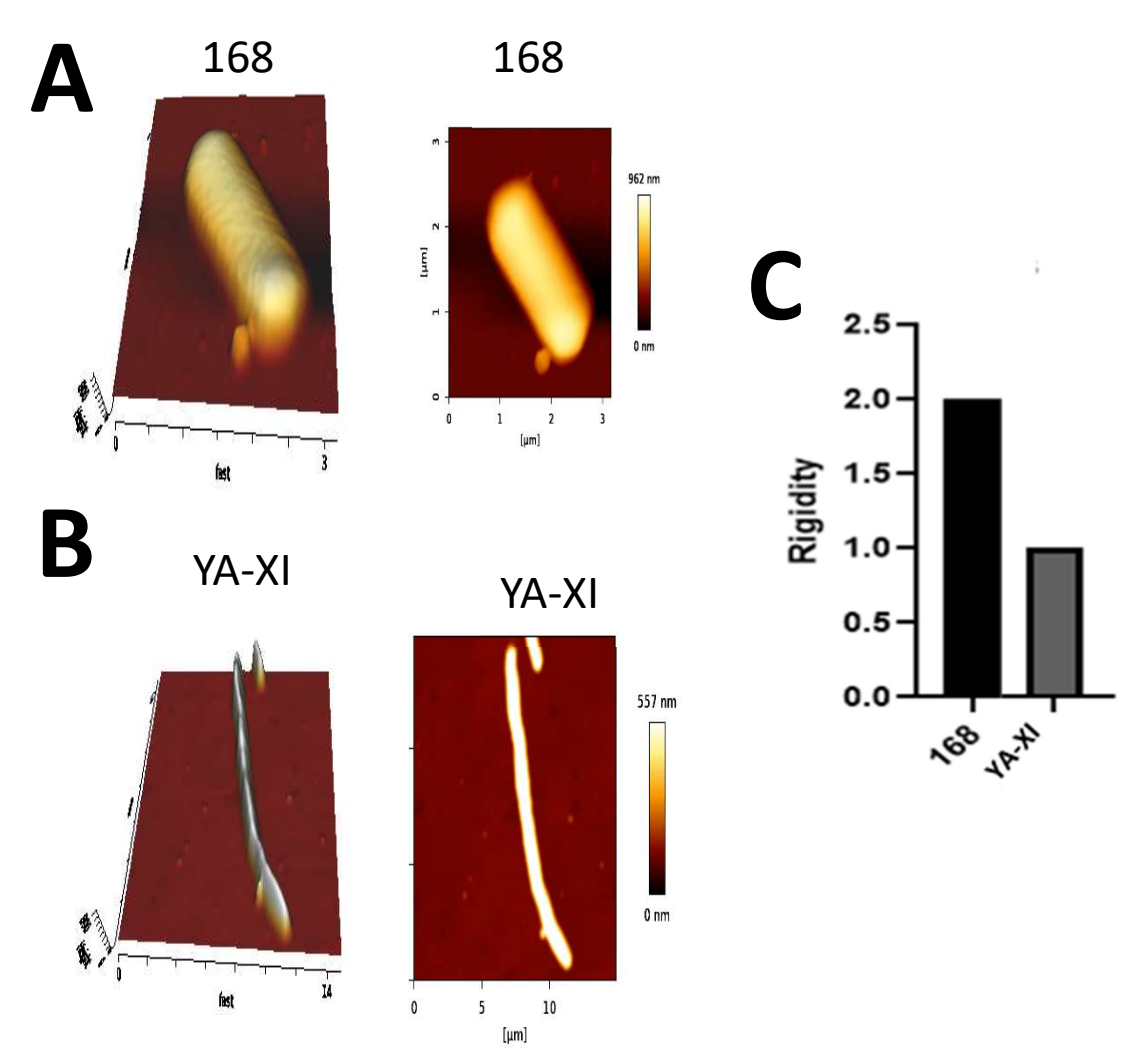


Figure 3.8: Cell envelope rigidity of 168 and YA-XI strains by AFM.

A) Left: 3D AFM image of strain 168, rotated upward. Right: Topography image of strain 168 showing surface height distribution (scale bar max: 962 nm). (B) Left: 3D AFM image of strain YA-XI, rotated upward. Right: Topography image of strain YA-XI (scale bar max: 557 nm). The AFM scale differs between panels A and B, likely reflecting differences in cell morphology, surface structure, and rigidity between the strains. (C) Rigidity (Young's modulus in kPa) of strains 168 and YA-XI, measured from at least three individual cells per strain. YA-XI displays significantly reduced rigidity compared to strain 168, which may explain the observed differences in AFM height measurements.

3.2.8 Deletion of multiple PBPs impacts the *motI*, *spo0F* and *spo0B* genes

At the outset of this project, a concern was that over the course of constructing the gene deletion strains, which involved multiple transformations and selection steps, the strains might have acquired mutations that suppressed the need for PBPs or otherwise interfered with the experimental questions being asked. To ensure that this was not an issue, the genome of the multiple deletion strain YA-XI was sequenced using the Illumina technique. The resulting short reads were then assembled onto the reference sequence of 168 (AL009126.3) and analyzed for any unexpected sequence differences using CLS software (Chapter 2, section 2.29). To confirm these insertions and deletions, PCR amplification across the affected regions was performed, followed by Sanger sequencing. This approach ensured accurate detection of sequence changes and ruled out potential misalignments from short-read sequencing.

From this sequence assembly, three sequence indels were identified that were not expected. The first was a 65-nucleotide deletion in the coding sequence of spo0F. The second was a 58-nucleotide deletion in the spo0B gene, and finally, there were two 20nucleotide insertions in the *motI* gene (Figure 3.9). The mutations in *spo0F* and *spo0B* would cause both loss of amino acids and a frameshift, essentially resulting in null mutations for these genes. This would be expected to impact on the strain's ability to sporulate but not affect vegetative growth. Similarly, the MotI protein, a cyclic-di-GMP receptor protein that regulates flagellar rotation (Chen 2012), would affect cell motility but should not directly impact vegetative growth or cell wall synthesis. Therefore, it can be concluded that the deletion of multiple PBPs and achieving minimal sets of PBPs may have caused the bacteria to acquire mutations in the motI, spo0F, and spo0B genes at some stage in the process. These mutations were probably randomly acquired because of strain propagation and transformation and are not related to our study. This latter possibility is supported by some preliminary sequencing data obtained by G. Goldsmith (unpublished), which suggests that all three mutations were spontaneously acquired in intermediate PBP deletion strains used to generate GG136.

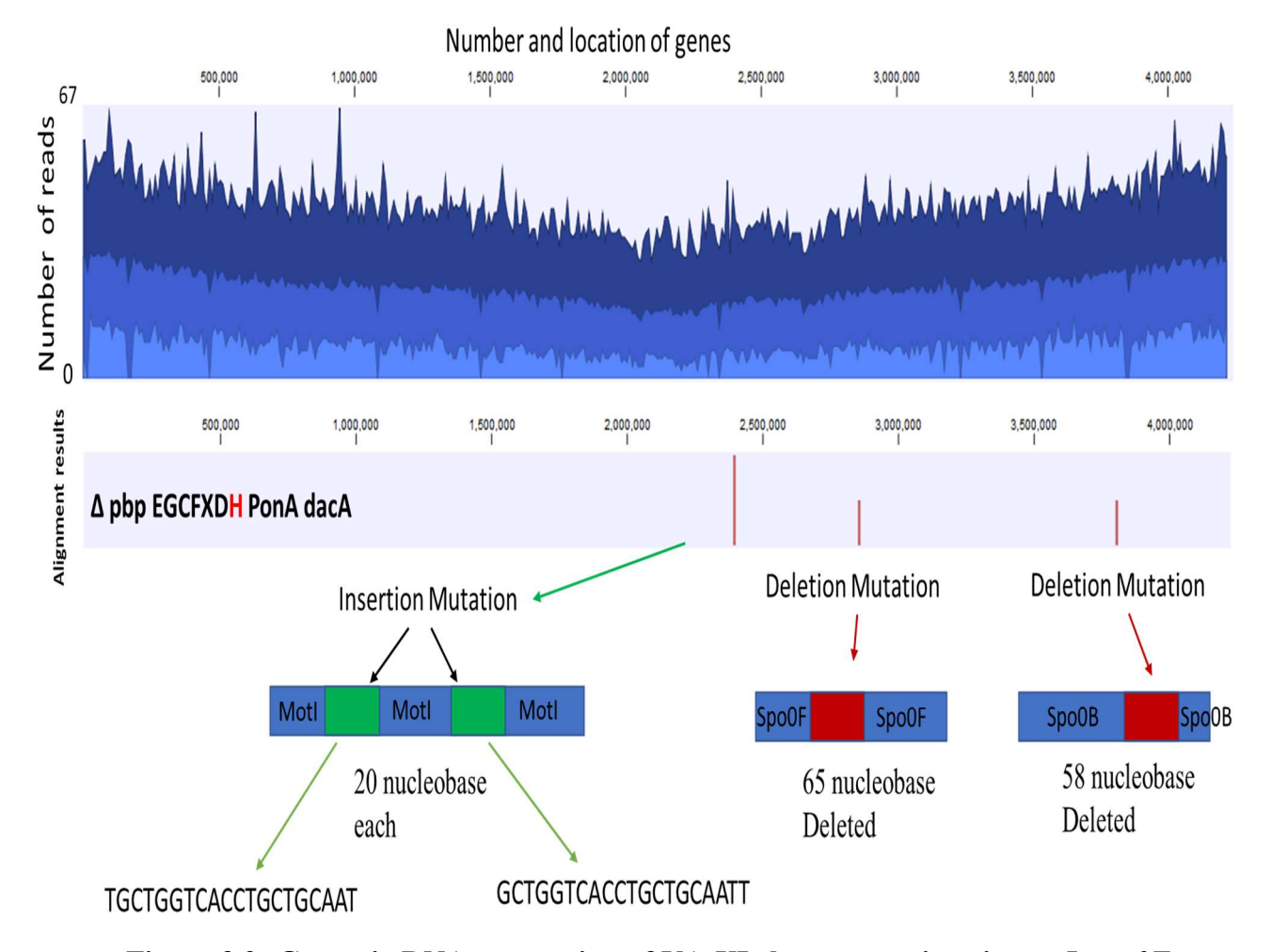


Figure 3.9: Genomic DNA sequencing of YA-XI shows mutations in *motI*, *spo0F* and *spo0B*.

The sequencing results were analysed using CLS software. The top spike chart shows the number of reads for YA-XI gDNA starting from zero to 67 reads. The middle figure represents the location of genes (the large numbers from 500.00 to 4000.000) and the long and short red lines represent the mutations found upon comparing the sequence to the reference gene via alignment. The bottom figure shows the mutated genes, the type of mutation (insertions in green and deletions in red) and the number of mutated nucleobases.

3.2.9 Analyses of the *B. subtilis* YA-XI ultrastructure by TEM

Since light microscopy indicated a subtle difference in the cell morphology of the multiple PBP deletion strains, as well as an apparent propensity for the cells to remain attached after division, a more detailed examination of the cell structure was carried out using transmission electron microscopy (TEM). This offered an enhanced perspective on the ultrastructural alterations and potential modifications to the cell envelope caused by the absence of multiple PBPs in the strain designated YA-XI, in comparison to the wild-type strain 168.

For this purpose, both the 168 and YA-XI strains were cultivated until they reached the mid-exponential growth phase in a nutrient-rich medium, specifically Luria-Bertani (LB) broth, at a temperature of 37 °C. The cells were then fixed and processed for visualization under the TEM as thin sections, a process carried out by the staff of the electron microscopy facility at Newcastle University.

Observations of the 168 strain through the microscope showcased cells with a regular morphology and characteristic cell dimensions. The positioning of the septum at the midpoint of each cell was indicative of normal septum formation and cellular division processes. However, examination of the YA-XI strain revealed a stark contrast. The YA-XI cells were noticeably elongated compared to the wild type, suggesting that the absence of multiple PBPs had a pronounced impact on cell wall integrity. This was evidenced by the appearance of a rougher cell wall surface in the YA-XI strain, as opposed to the smoother cell wall observed in the 168 strain, possibly signaling compromised cell wall integrity (Figure 3.10A). Moreover, the ultrastructural examination of the YA-XI strain indicated a damaged cell wall exhibiting a mesh-like appearance (Figure 3.10B). However, these observations were specific to certain cells in the EM samples; within the same sample, some cells appeared normal, while others displayed an asymmetrically positioned cell division site (Figure 3.10B), suggesting that the deficiency in multiple PBPs adversely affected cell septum formation. These observations suggest that normal cellular processes are impacted in the deletion mutant, but the findings are limited by the small number of cells that could be visualized as good sections, and time constraints did not permit further investigation in this direction.

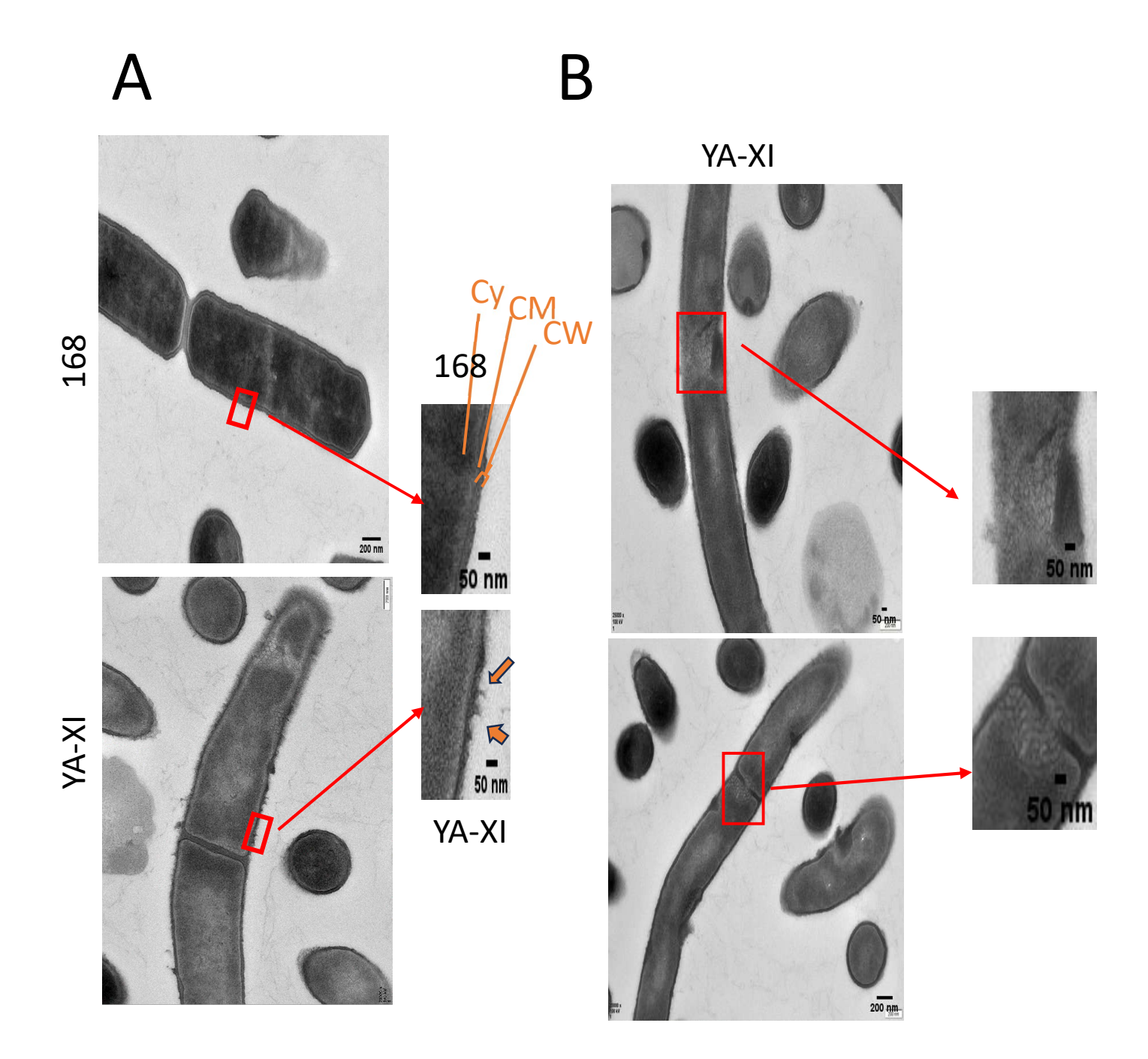


Figure 3.10: Transmission electron microscopy images for strain 168 and a strain with multiple penicillin-binding protein deletions (YA-XI).

A) Characteristic TEM images showing the cell surface structure of the wild type strain (A) and YA-XI (B). Cyt = cytoplasm, CM = cytoplasmic membrane, CW = cell wall. Arrows indicate the rough cell surface. Areas of the cell envelope are enlarged (red box) to show significant differences.

3.3 Discussion

Most previous studies on cell wall synthesis have focused on the deletion of a single or two PBPs or, as an exception in the case of B. subtilis, the removal of all class A (bifunctional) PBPs, to determine the impact of such deletions on cell growth and morphology. In this work, we aimed to define the minimal set of PBPs required for normal growth in B. subtilis and having defined this, characterized the resulting phenotype. The results presented in this study offer insights into the functional roles, redundancy, and essentiality of PBPs in bacterial cell wall synthesis and maintenance. The use of bocillin FL, a fluorescent penicillin derivative, facilitated the direct detection of active PBPs in living bacterial cells, circumventing the limitations associated with cell membrane preparation. This approach confirmed the presence of eight detectable PBPs (PBP1, PBP2c, PBP4, PBP2a, PBPH, PBP3, PBP2b, and PBP5) out of the 16 PBPs encoded in the B. subtilis genome. bocillin FL in vivo labeling and SDS gel analysis also confirmed its reliability in detecting PBPs, indicating that it seems to react with all surface-exposed PBPs rather than specifically binding to only active PBPs. This resolved a concern about this labeling technique and suggests that PBPs are always capable of binding to the substrate and remaining active. Thus, the resulting fluorescence intensity of PBPs on SDS-PAGE directly reflects the abundance of the PBPs in the membrane upon treatment. Exploiting this direct labeling method provided a quick and simple way to validate the genetic manipulations expected to remove specific PBPs. It also offered a way to determine if the loss of specific PBPs altered the abundance of the others.

Starting with a strain carrying seven PBP deletions (GG136), which had no phenotype, it was confirmed that only three vegetatively expressed PBPs were present. This had been considered to be almost the minimal set of PBPs, as those that remained (PBP1, PBP2B, and PBP2A or PBPH) were thought to have critical roles. The importance of PBP1 was initially indicated by the phenotype of the null mutant (Popham and Setlow, 1996), which exhibited a conditional phenotype. Later, PBP1's role in the divisome and elongasome was highlighted by its localization, alternating depending on the cell's state, growing or dividing (Scheffers and Errington, 2004; Claessen *et al.*, 2008). In contrast, the role of PBP2B has been well established as a key component of the division

complex (Daniel *et al.*, 2000). PBP2a and PBPH are more complex to understand; both have been implicated in the formation of cylindrical cell walls and hence cell elongation. This is primarily based on the fact that the double mutant lacking both PBP2a and PBPH resulted in coccoid cells. This result also implied that they were functionally interchangeable, which explains why the single mutants exhibited only very mild phenotypes (Wei *et al.*, 2003). However, it has also been determined that these proteins are localized to division sites (Sauvage *et al.*, 2008), suggesting they may have dual roles.

On deleting further PBPs in strain GG136, the options were rather limited, and the expectation was that the resulting strains would either exhibit severe phenotypes or would simply be inviable. Thus, it was surprising that the null mutation for *ponA* (PBP1) could be introduced into this background (Section 3.2.2). This result aligns with previous studies conducted by Popham and Setlow (1996) and Errington and Emami (2016), where the viability of a strain lacking all Class A PBPs was shown to be maintained through the transglycosylase activity of RodA and FtsW. However, in this work, there was no requirement for elevated levels of magnesium in the culture medium for the viability of the mutant strain. Interestingly, in the multiple deletion strain (YAX, with just PBP2b, PBP2a, and PBPH present), this requirement was not evident, and the strain was able to propagate well under the conditions we tested.

Knowing that either PBP2a or PBPH could be removed was the next step toward generating a strain with the minimal set of PBPs. Attempts to introduce the deletion of PBP2a were challenging and generally resulted in very few viable colonies after transformation, and these could be rapidly shown to be incorrect. In contrast, the introduction of the *pbpH* deletion was easily accomplished. This seems to indicate that PBPH is functionally redundant to PBP2a, but either its biochemical activity or its expression is not a complete replacement for PBP2a. Consequently, this project progressed by focusing on the *pbpH* deletion in the multiple-PBP-knockout strain YA-X (Section 3.2.3). These results confirmed subtle differences between the two purported functionally redundant proteins, similar to those observed by Wei *et al.* (2003), and this aspect formed the basis of Chapter 4.

Thus, at the genetic level the minimal essential PBPs complement seemed to be defined by strain YA-XI where only PBP2b and PBP2a are present during vegetative growth. The remaining HMWT PBPs in the YA-XI strain were SpoVD and PBP4b, which belong to class B and are involved in peptidoglycan synthesis during sporulation and are not expressed in vegetative growth. The analysis presented here finds no evidence that these PBP play a role in the viability of strain YA-XI as they were not detected by bocillin labelling, but technically this possibility has to be considered and if time had permitted these genes would have been deleted to eliminate this possibility

Analysis of the growth and morphology of B. subtilis strains with varying numbers of PBP deletions provides an insight into the functional redundancy of these proteins. The fact that strains YA-XI and YA-X, which lacked several PBPs, exhibited notably slower growth rates compared to the wild-type strain 168, potentially underscores the importance of having multiple PBPs in bacterial growth rates. This reduced growth rate is consistent with the suggestions of the review by Straume et al. (2021), who indicated that the deletion of PBPs leads to a decrease in bacterial growth. The difference in the growth rates of the mutant strains, compared to the wild type, in LB and NA suggests a potential medium-specific effect on cells with compromised cell wall synthesis machinery. One difficulty in the analysis that was observed related to the culture medium used to make comparisons and how to interpret any differences observed, in the work LB was used as a standard medium for liquid culture and NB with agar for solid media. On looking at strain growth in these two media in liquid form (without agar) the general trends were the same, but the observed growth rates were different. This on consideration could probably be a reflection of the difference in the availability of nutrients and ions, there is also a possibility that osmotic differences may be a factor combined with the effect of growing in an air water interface when strains are grown on plates as opposed to being in suspension. These represent a complex analytical challenge and could only be indirectly addressed in the later experimental work.

The morphological changes observed due to PBP deletions, specifically the increased cell length and decreased cell diameter related to the deletion of PBP1, suggest an impact on the balance between new wall synthesis and its controlled degradation, as reported by McPherson and Popham (2003). This aligns with findings by Dion *et al.*

(2019) that show deleting PBP1 leads to cell elongation, consistent with observations in the YA-X strain, which lacked PBP1 and exhibited longer, thinner cells compared to strain 168. However, in the YA-XI strain, where PBP1 was intact but the cells were still elongated, this suggests that mutations in several PBPs, rather than just PBP1, contribute to this morphological change.

The other notable difference that was observed was the fact that the deletion strains grew as chains of cells rather than becoming detached after division. This phenotype was rather unexpected as this sort of effect is more commonly associated with defects in cell wall degradation. Alternatively, this chaining of the cells could be caused by a defect or delay in the cell division process. It is well established that in many rod-shaped bacteria like B. subtilis that cell enlargement, generally through elongation, is independent of cell division. This is best demonstrated by strains depleted for essential cell division proteins, e.g. FtsZ, which result in long filamentous cells, or PBP2B depletion where the division process is only partially defective and essentially slow. Here the filaments have gradual divisions occurring, but not at the frequency necessary for normal cell length and result in cells remaining attached together longer. Thus it seems reasonable to the most probable cause of the chaining phenotype is related to slow maturation of the division septum, due to the collective absence of PBP that would normally function to "mature" the forming cell poles. These ideas from the initial light microscopy were to some degree confirmed by TEM imaging of cell sections. The fact that the YA-X strain demonstrated a rough cell wall compared to the wild-type presented interesting possibilities. This roughness was also observed in a study by Sassine et al. (2021), who found that disruption of the UgtP protein, which serves as a glucolipid anchor of LTA in B. subtilis, contributed to imbalanced PG synthase and hydrolase activity, causing the roughness of the bacterial cell wall. These findings fit with the ideas indicated above, in that multiple peptidoglycan crosslinking enzymes are missing, while the hydrolases remained intact, especially the critical two LytE and CwlO, which could cause imbalanced peptidoglycan synthesis/hydrolysis activity. It is worth mentioning here that deleting peptidoglycan hydrolases can also cause roughness of the cell membrane (Wilson et al., 2023). Thus, supporting the idea of imbalanced

peptidoglycan synthesis and hydrolysis would lead to cell wall roughness, but not necessarily lead to an obvious phenotype or growth defect.

With this concept in mind isolation of the peptidoglycan and muropeptides analysis was carried out to determine if there was a significant change in the confirmation of the structure of PG. The comprehensive analysis of peptidoglycan composition and crosslinking in B. subtilis strains168, YA-XI and YA-X, surprisingly revealed no notable difference in the degree of cross-linkage among the strains. This implies that there could be a complex compensatory mechanism within the cell wall biosynthetic machinery enabling the maintenance of cross-linking integrity despite the absence of specific PBPs. A study by Sassine et al. (2021) proposed a role for a regulatory protein, UgtP, claiming that combining mutations in ugtP and lytE leads to a decreased PG synthase/hydrolase ratio and, subsequently, cell impairment and lysis. On the other hand, deleting ugtP with ponA, encoding PBP1, contributes to an increase in the PG synthase/hydrolase ratio. A concept that is also supported by other publications in the field (Sassine et al. 2021). However, it is difficult to determine if HPLC analysis can provide support for this idea. It is possible that the observation that the sum of dimers increased in YA-XI and YA-X compared to the wild-type 168 strain, accompanied by a decrease in tripeptides and tetrapeptides could support the concept. The increase in dimers and decrease in trimers and tetramers may be caused by the conversion of the trimers and tetramers by hydrolase activity since the major hydrolases LytE and CwlO in strains YA-XI and YA-X and conversion of trimers and tetramers to dimers is facilitated by endopeptidase activity (Atrih et al., 1999).

After investigating the morphological features of *B. subtilis* strains lacking multiple critical PBPs, we analyzed the potential genomic changes due to these deletions in the gDNA of the YA-X strain and compared it to the gDNA of the wild type. gDNA sequencing of the YA-XI strain confirmed the deletion of the nine targeted PBPs and revealed two deletion mutations in genes involved in sporulation onset, specifically *spo0F* and *spo0B*. Additionally, a mutation was identified in the *MotI* gene, which is associated with bacterial motility. These mutations in *spo0F*, *spo0B*, and *MotI* are not expected to impact bacterial growth, as the study focuses on vegetative growth. Although these mutations could potentially be repaired, time constraints and the need

to focus on other aspects of the research precluded such efforts. Thus, although these mutations are probably a technical issue, they represent possible future work.

The results of this study provide significant insights into the structural and functional consequences of deleting multiple PBPs in *B. subtilis*. Specifically, the findings reveal that the removal of several non-essential PBPs leads to a reduction in cell wall rigidity, despite negligible changes in peptidoglycan cross-linking. This observation aligns with previous research conducted by Loskill and Pereira (2014), who demonstrated a similar effect in *S. aureus* following the deletion of PBP4, highlighting the role of PBPs in determining cell wall architecture and mechanical properties. The use of AFM to assess cell wall rigidity in *B. subtilis* strains 168 and YA-XI further underscored the importance of PBPs in maintaining the structural integrity of the bacterial cell envelope (Loskill and Pereira, 2014). The minimal set of PBPs in the YA-XI strain, despite not significantly altering the cross-linking of peptidoglycan, evidently led to a less rigid cell wall. This suggests that the presence or absence of specific PBPs can have profound effects on the physical properties of the cell wall beyond the biochemical composition of peptidoglycan but despite that the bacteria was able to adapt and survived with minimal sets of PBPs.

The primary finding of this chapter is that PBP2a and PBP2b are the essential penicillin-binding proteins (PBPs) required for functional cell wall assembly in *B. subtilis*, allowing for viable growth without significant phenotypic alterations. The redundant partner of PBP2a, PBPH, was unable to substitute for PBP2a and sustain bacterial growth when only the minimal PBP set was present. Consequently, Chapter 4 will further investigate the roles of the redundant partners PBP2a and PBPH.

Furthermore, PBPX, which is proposed to be regulated by σ^X to modulate surface charge and resist cationic antimicrobial peptides (Cao and Helmann, 2004), was not detectable as a penicillin-binding protein using the bocilin FL method. Its deletion did not result in notable differences in growth or morphology under normal conditions. The biological role of this proposed PBP is further investigated in, Chapter 5.

Chapter 4 Analysis of the functional redundancy of PBP2a and PBPH

4.1 Introduction

PBPs are characterised by redundancy, in that most of bacterial species seem to have multiple genomically encoded PBP genes, with *B. subtilis* harbouring 16 distinct PBPs (Sauvage *et al*, 2008). This redundancy shows that overlapping functionalities may have benefits regarding evolutionary pressures (McPherson *et al*, 2001). With the compensatory activity of its counterparts, disruptions in one PBP's function may frequently go undetected (Popham and Setlow, 1996). While much research has focused on the relationship between PBPs and β-lactam antibiotics, the functional overlaps among PBPs, especially in natural environments, are less well understood. Among the various PBPs, PBP2a and PBPH in *B. subtilis* have garnered attention due to their essential and overlapping roles in cell wall synthesis and maintenance.

PBP2a and PBPH, both belonging to the Class B PBPs, share significant similarities in their apparent roles within the cell elongation complex of *B. subtilis*. Both PBP2a and PBPH are presumed to serve as transpeptidases, crucial for the formation of cross-links between peptidoglycan strands (Wei *et al.*, 2003). Furthermore, both proteins are vital components of the Rod system, which is responsible for cell elongation and ensures the bacterium maintains its unique rod shape (Garner *et al.*, 2011). Their involvement in this system is highlighted by their uniform distribution throughout the cylindrical portion of the cell, consistent with their role in cell elongation (Scheffers *et al.*, 2004). Furthermore, these two penicillin-binding proteins (PBPs) exhibit overlapping functions in the formation of the bacterial cell wall. The indispensability of both *pbpA* (encoding PBP2a) and *pbpH* in maintaining essential cell wall synthesis and structure is evident from the fact that the of a double mutant was not viable under normal conditions (Wei *et al.* in 2003).

Although PBP2a and PBPH share certain similarities, they display distinct differences in terms of their expression patterns, stability, and essentiality. The *pbpA-lacZ* fusion construct demonstrated that *pbpA* is predominantly expressed during the vegetative growth stage, while the expression of the *pbpH-lacZ* fusion gene is minimal in the early

logarithmic growth phase but substantially increases in the late phase (Wei et al., 2003). PBP2a exhibits instability in the absence of the PrsA protein, which is essential for its correct folding and stability. This interaction has not been observed in PBPH (Hyyryläinen et al, 2010). Also, in contrast to pbpH mutants, when pbpA is deleted, there is a difficulty with the cells growing into cylindrical shapes and a delay in the growth of spores. The mutant spores initially grow in an oval shape before returning to their normal rod shape (Murray et al, 1998; Wei et al, 2003). In addition, the previous chapter (Chapter 3) demonstrated that in a strain with essentially the minimal set of penicillin-binding proteins (PBPs) called YA-XI, PBPH could be deleted, whereas PBP2a could not. This suggests a greater importance for PBP2a in comparison to PBPH, although it could also simply reflect differences in expression level and regulation.

The observed differences have prompted this study, and this chapter examines the redundancy of *pbpA* and *pbpH*, with a focus on how the deletion or alteration of one gene influences the function and properties of the other. Given the redundancy between PBP2a and PBPH, it is hypothesized that the deletion or overexpression of one may significantly impact the behavior of the other, providing deeper insights into their roles in bacterial cell wall synthesis and maintenance.

4.2 Results.

4.2.1 Deletion of pbpH changes the abundance of PBP2a

Previous analyses had indicated the redundancy of pbpA and pbpH, but not how cells adapted to the loss of either one of them. To determine how the loss of PBP2a or PBPH impacted on the overall abundance of PBPs two strains were constructed: one with a deletion of the gene encoding PBP2a ($\Delta pbpA$ (YA17)) and another with a deletion of PBPH ($\Delta pbpH$ (YA11)). These strains, along with the wild-type strain 168, were grown in parallel at 37°C in LB medium. Samples were collected during the exponential growth phase, at an OD600 range of 0.05 to 0.5. The optical density was recorded for each culture and to minimize variations in sample loading.

The samples were labelled with bocillin-FL dye for 2 minutes, a timeframe determined to be sufficient for bocillin to bind to the PBPs. NuPAGE Bis-Tris Gels at 4–12% concentrations were used for separating these PBPs. Distinguishing between the bands for PBP2a, PBP2b, and PBPH was challenging because of their similar molecular weights of 79.96 kDa, 79.21 kDa, and 76.98 kDa, respectively. To enhance resolution, MOPS buffer (Invitrogen) was used, and electrophoresis was conducted over 10 hours at low voltage to achieve optimal protein separation. The results were visualized using a fluorescent imager (Figure 4.1A).

In strain 168, the bands corresponding to the expected set of expressed PBPs were clearly visible. By comparing the two deletion strains, we identified PBP2a as the upper band of a triplet slightly above the middle of the image. PBPH migrated slightly lower than PBP2a but was still identifiable. Interestingly, in the strain lacking PBPH, the intensity of the PBP2a signal was markedly higher compared to that in strain 168, even though the intensity of other PBP bands remained comparable. This effect was reproducible across independent cultures, suggesting that the absence of PBPH leads to an increase in the abundance of penicillin-labelled PBP2a.

The increased level of PBP2a observed in the $\Delta pbpH$ strain suggests several possible mechanisms. First, it is possible that PBP2a and PBPH require incorporation into a proposed elongation complex to become active and bind penicillin, thus in the absence of one of the PBPs the other is in the active complex. Second, PBPH might

displace PBP2a from its position in the elongation complex, leading to degradation of PBP2a. Third, transcriptional regulation might alter the relative expression of these two PBPs in response to "low" cell wall synthesis, with PBPH expression leading to reduced PBP2a expression.

To differentiate between these possibilities, a strain was constructed in which the PBPH promoter was swapped for a conditionally repressed promoter (P_{xyl}), and the coding sequence of GFP was fused to the inducible PBPH copy (strain 3140). The native pbpH gene was then deleted in strain 3140 to give strain YA16 ($\Delta pbpH::kan trpC2(cat P_{xyl}-GFP-pbpH^{1-827})$), allowing PBPH expression to be independent of normal regulatory systems and modulated by the addition of xylose to the culture medium.

Using the same methods as previously described, the PBP profiles of the P_{xyl} *GFP-pbpH* cat strain, grown with and without xylose, were analysed alongside the wild-type strain and a $\Delta pbpA$ strain (Figure 4.1B). Overexpression of PBPH was clearly evident on comparing the signals obtained in the presence and absence of xylose since the protein was now shifted to a significantly higher molecular weight by the fusion with *GFP*. Additionally, the alteration in the relative abundance of PBP2a observed in the $\Delta pbpH$ strain was not present when PBPH was artificially expressed, indicating that PBPH abundance seems to modulate PBP2a levels.

However, variations in sample loading and electrophoresis conditions between the experiments could influence result interpretation. To address potential errors, several biological and technical repeats were conducted. Independent cultures were grown, and samples were analysed using gel electrophoresis and fluorescence imaging. The resulting images were quantitatively analysed, and the abundance of PBP2a was determined relative to the abundance of the other PBPs (excluding *GFP*-PBPH). Representative images and quantifications are shown in Figure 4.2. The relative abundance of PBP2a in strain 168 was 2.43% of the total bocillin-FL labelled protein signal. In contrast, deletion of *pbpH* increased PBP2a abundance from 2.43% to 7.38% (Figure 4.2C), despite the fact that PBPH was a relatively small proportion of the total bocillin signal. In the experiment involving inducible PBPH expression, PBP2a

abundance in strain 168 was approximately 2.5%. Deleting *pbpH* without adding xylose, thereby preventing PBPH production, increased PBP2a abundance to 7.29%. When xylose was added, and *GFP*-PBPH was overproduced, PBP2a levels decreased to 1.5%, which is lower than in strain 168 (Figure 4.2D). Thus, it appeared that increasing the abundance of PBPH to higher than normal levels reduced the level of PBP2a even further.

In summary these results indicate that the absence of PBPH leads to a 2- to 4-fold increase in detectable PBP2a levels. This observation suggests that a direct transcriptional regulation mechanism is unlikely, given that PBPH expression was artificially regulated. Instead, it implies that PBPH could be altering PBP2a stability or activity. To further differentiate between these possibilities, the true abundance of PBP2a needs to be determined independently of its ability to bind bocillin-FL, as this assay may only detect biochemically "active" PBPs.

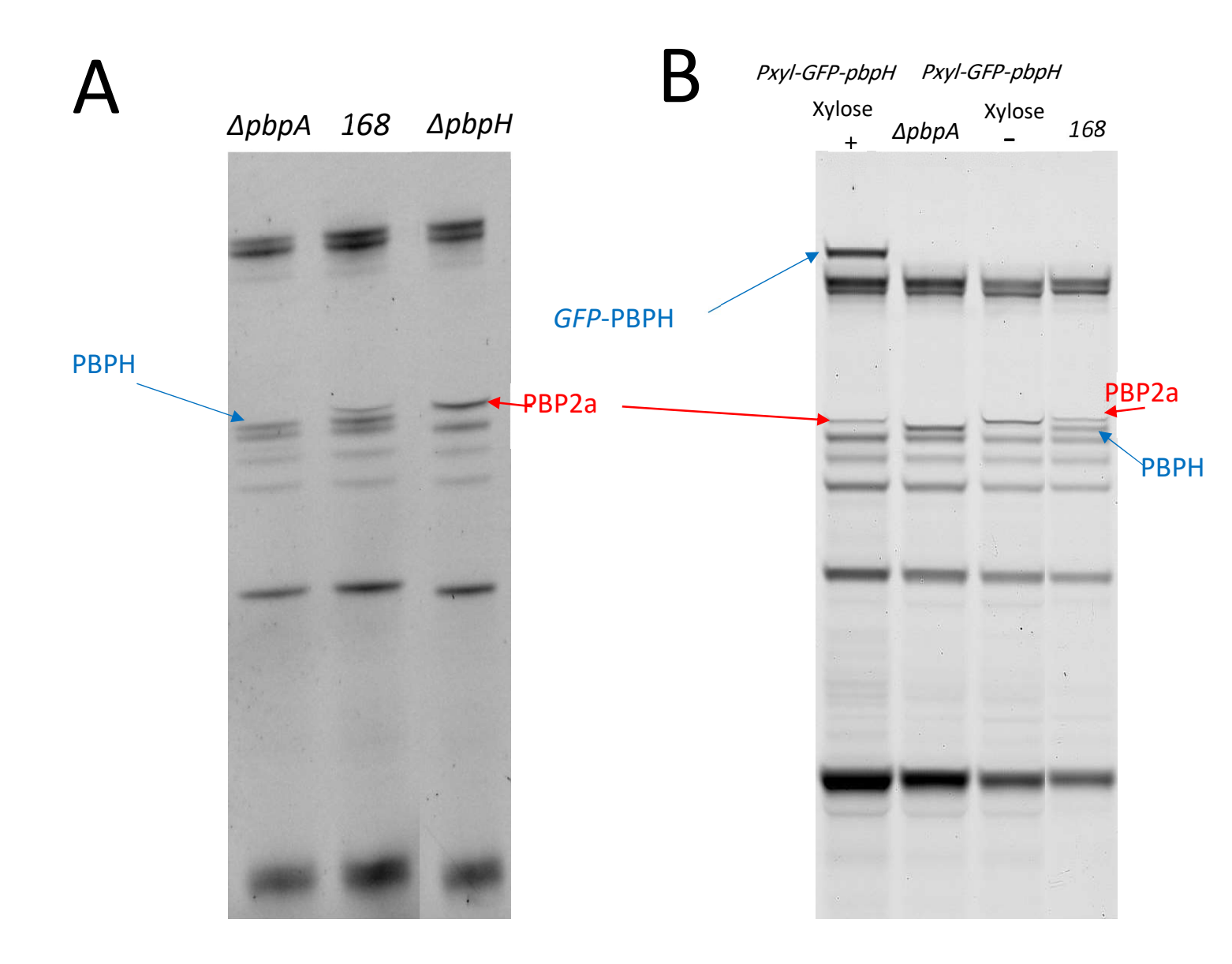
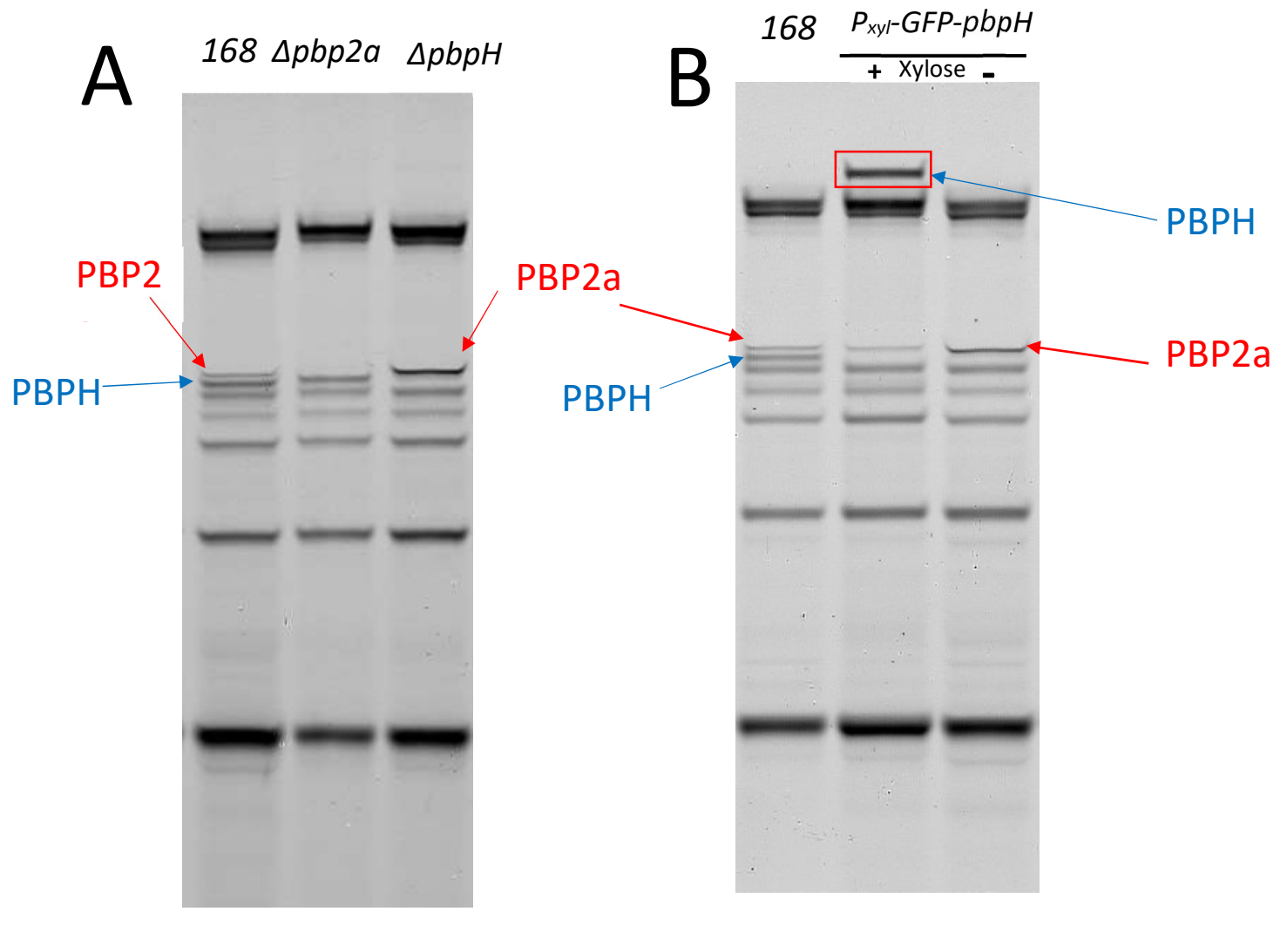


Figure 4.1: Deleting *pbpH* increases the abundance of PBP2a.

A) Bocillin FL labelling was performed on the $\triangle pbpH$ strain lacking PBPH, strain 168 (wild type) and the $\triangle pbp2a$ strain lacking PBP2a. PBP2a (red arrow) and PBPH (blue arrow) are indicated. B) Bocillin FL labelling was performed on the 168 and P_{xyl} -GFP-pbpH strains with 1% xylose (expressing GFP-PBPH) and without 1% xylose (no GFP-PBPH expression)



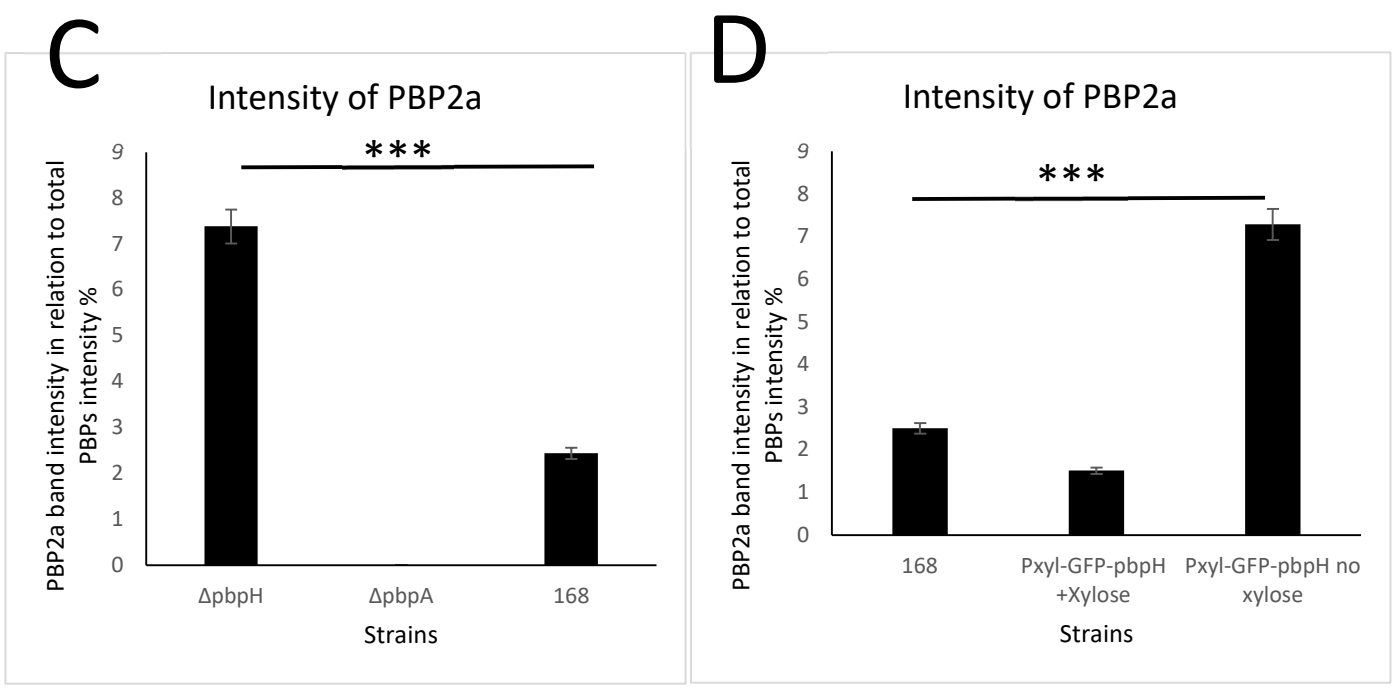


Figure 4.2: Deleting *pbpH* increases PBP2a detection.

A) Bocillin FL labelling was performed on strains 168 (wild type), $\Delta pbpA$, and $\Delta pbpH$, which lacks the PBPH protein. PBP2a (red arrow) and PBPH (blue arrow) are indicated. B) Bocillin FL labelling was performed on the 168 and P_{xyl} -GFP-pbpH strains with (expressing GFP-PBPH) and without 5% xylose (silencing GFP-PBPH expression). The GFP-PBPH band is in the red box. C) PBP2a band intensity in relation to total PBP intensity (%) from image (A) for the $\Delta pbpH$, $\Delta pbpA$ and 168 strains. This experiment was repeated three times independently, with a P-value > 0.005. D) PBP2a band intensity in relation to the total PBP intensity (%) from image (B) for strains 168 and P_{xyl} -GFP-pbpH with or without xylose. ***This experiment was repeated three times independently, with a P-value > 0.005.

4.2.2 Overexpression and purification of PBP2A and PBPH

Having demonstrated the effect of *pbpH* deletion on the detectable level of PBP2a, a logical step was to determine the true abundance of PBP2a by another means. The logical solution for this was to generate antibodies against the PBP. For this the *pbp2a* coding sequence was cloned into a pET28(a)+ plasmid such that a N-terminal hexahistidine tag (His-PBP2a) was introduced and expression would be under T7 promoter control. This plasmid (pYA5) was then transformed into *E. coli* BL21 (DE3) cells, to allow expression and production (4.3A)

E. coli BL21 with the plasmid pYA5 was grown in 200 ml of LB medium for 1 hour with IPTG addition to determine if there was expression of the PBP2a protein. The cells were harvested and suspended in buffer (Tris-HCL 10 mM, 300 mM NaCl), and sonicated for 30 seconds to lyse the cells. In addition, a protease inhibitor (EDTA) was added to prevent PBP2A degradation during extraction and purification. Then through trial and error a purification protocol was devised. Through this process it was found that the detergent Triton X100 (0.5%) was found to aid in protein extraction, presumably because PBP2a has a transmembrane domain, and this detergent extracted it out of membrane vesicles generated by sonication. The lysate was then passed through an Ni column (Thermo Fisher) to affinity purify PBP2a by virtue of his tag that had been added to the protein. The total cell lysate was first added to the column, followed by washing with a low concentration of imidazole (20 mM) to clear nonspecific protein binding, and then His-PBP2a was eluted with a high concentration of imidazole (100 mM) Loading samples taken over the duration of the extraction and purification process (Figure 4.3B) showed that a protein corresponding to the overexpressed PBP2a was obtained in a relatively pure state.

The eluted material was then concentrated by dialysis and found to be sufficient to use to generate a polyclonal antiserum (using the 28-day protocol of Eurogentec). The resulting polyclonal antisera generated using the purified PBP2a was then tested for specificity by Western blot. Here total protein samples from the wild type strain (168) and $\Delta pbpA$ were resolved on SDS-PAGE and blotted to PVDF membranes. The using a standard detection method (methods 2.10) it was found that a single clear band was

detected in the sample from 168 at a molecular weight corresponding to that expected for PBP2a, whereas no signal was evident for the PBP2a deletion mutant (Figure 4.3C).

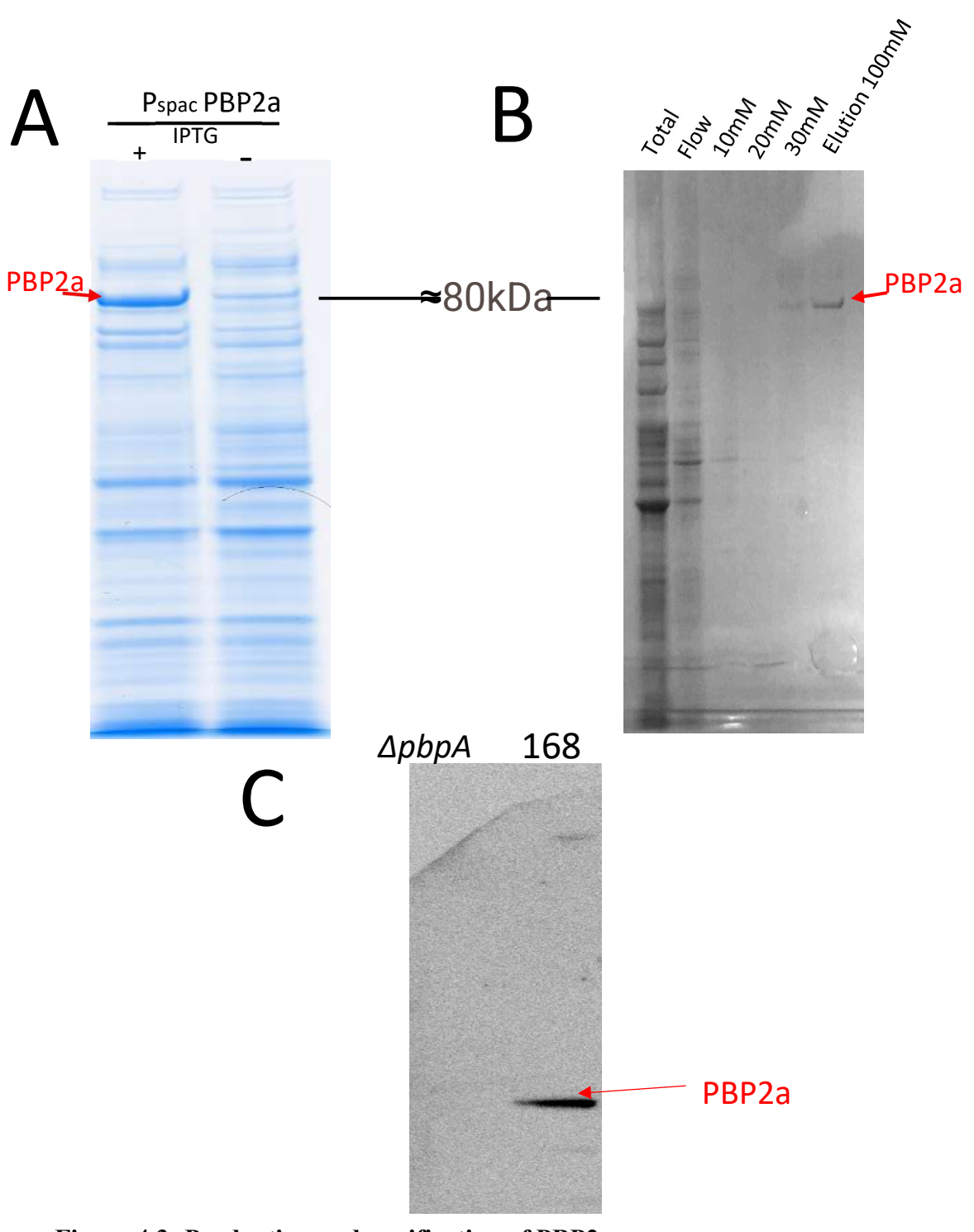


Figure 4.3: Production and purification of PBP2a.

A) Protein extraction from *E. coli* BL21 containing an inducible copy of PBP2a under the control of the T7 promoter. IPTG addition revealed the high quality of PBP2a tagged with the His tag. The PBP2a-His induction time was 60 minutes, and the protein extract was stained with the Coomassie stain. B) PBP2a purification using a nickel column. The first lane shows the total lysate before passage through the column, and the second lane shows the lysate after passage through the column, where PBP2a binds to the column. Lanes 3–5 were washed with a low imidazole concentration (20 mM) and eluted with a high imidazole concentration (100 mM). C) testing of anti-PBP2a antisera using Wester blotting against total protein from 168 and Δ*pbpA* using a 1/2000 dilution of antisera.

Although PBP2a and PBPH have some sequence similarities, the purification of PBPH was problematic. Like the pbp2a, the coding sequence of pbpH was cloned into a pET28(a)+ plasmid with an N-terminal hexahistidine tag (His-PBPH) under the control of the T7 promoter. The resulting plasmid (pYA6) was then transformed into E. coli BL21 (DE3) cells and used for His-PBPH production. Adding IPTG to a growing culture of the strain showed a reasonable production of His-PBPH (Figure 4.4A). However, unlike PBP2a, using Tris-HCL 10 mM buffer with 300 mM NaCl and sonication for 30 seconds did not solubilise PBPH, and the protein was detected in pellet 1 and pellet 2 after centrifugation at different speeds. Use of range of triton-X100 concentrations was used to aid PBPH solubilisation, however, this showed no indication of solubilising the PBPH protein as it which was detected in pellet 1 and pellet 2 after centrifugation (Figure 4.4C). Next, 6 M urea was used under these conditions PBPH was detected in the supernatant after centrifugation (Figure 4.4D). Being able to get the protein in solution then permitted the solution containing PBPH to be applied to a nickel column to purify PBPH. However, PBPH-His did not bind to the column, making purification not possible by this method. It was also found that using variations in both expression time and extraction methodology the same issues existed, in that the protein was not soluble and the His tag, although present, (detected by use of a His-tag specific antibody, data not shown) it did not show any affinity to the resins used. Consequently, due to time constraints it was impossible to continue this aspect of the work.

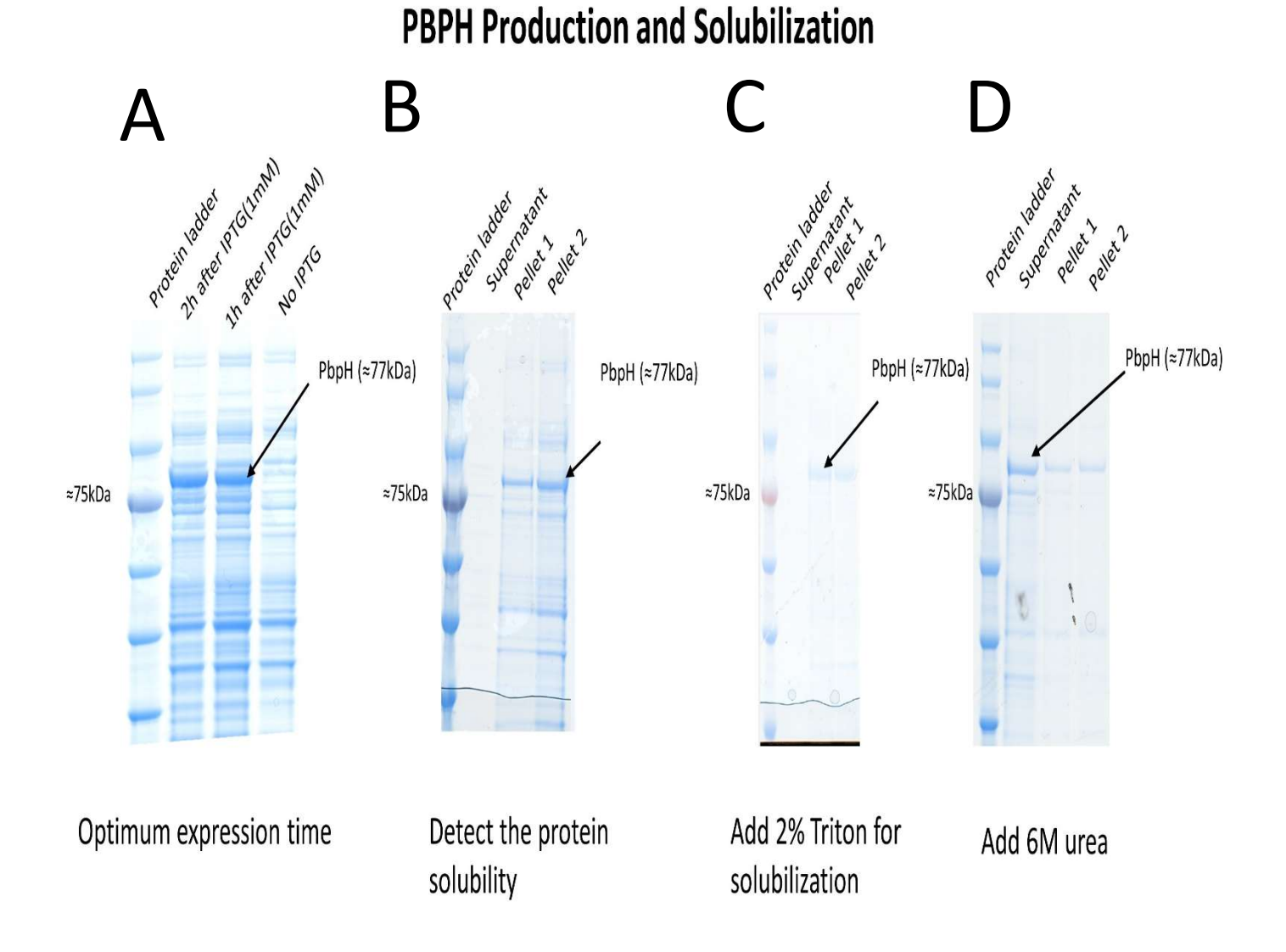


Figure 4.4: Production and purification of PBPH.

A) PBPH production 1 and 2 hours after induction and without IPTG, with the Coomassie stain. B) Solubility of PBPH: PBPH must be detected in the supernatant to confirm its solubility before purification. C) Addition of 2% Triton detergent to solubilise PBPH. D) Addition of 6M urea to solubilise PBPH and Coomassie staining.

4.2.3 Effect of PBPH deletion on PBP2A quantity

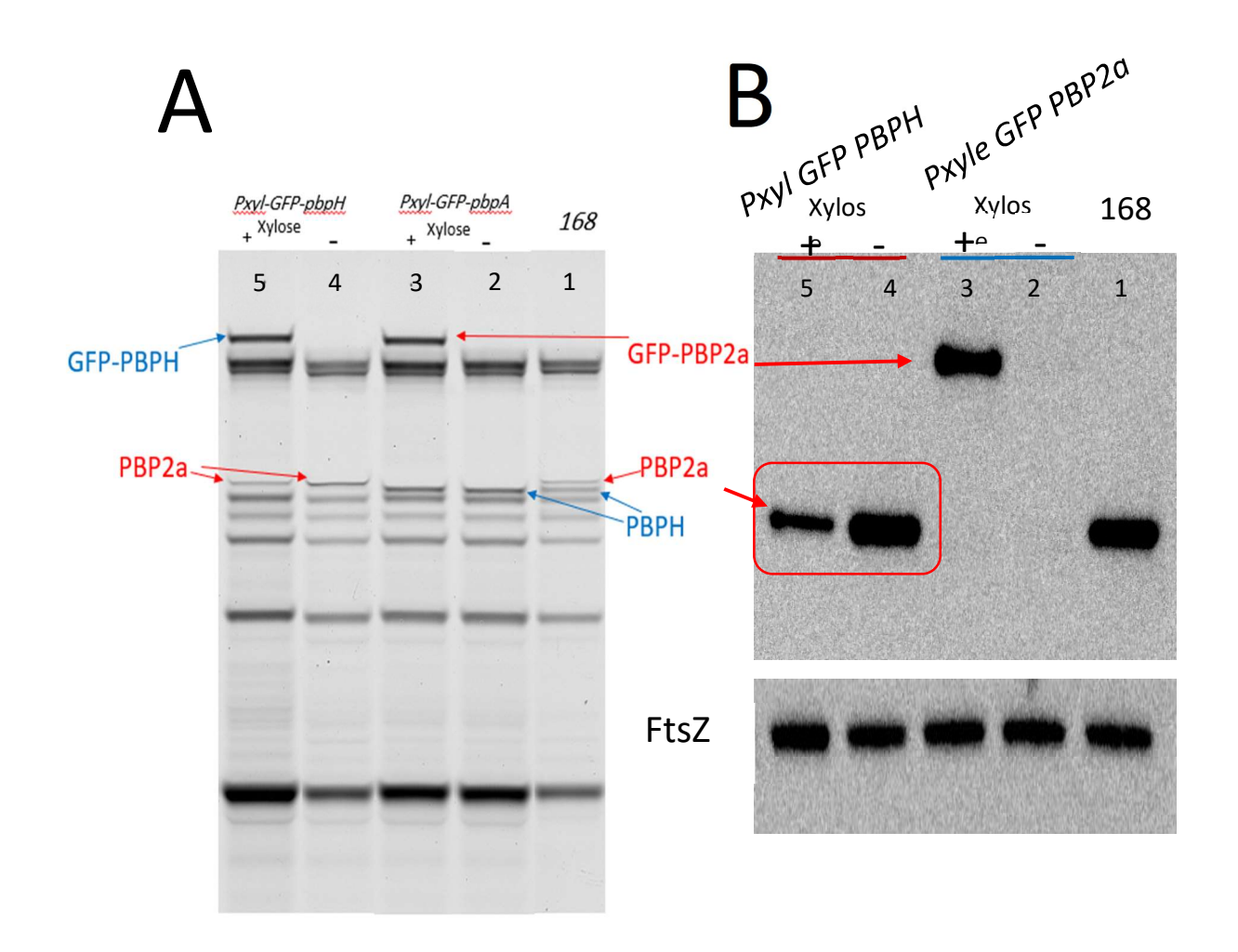
As the PBP2a antisera were confirmed to be specific to the protein and did not cross-react with other proteins in *B. subtilis* (Fig. 4.3C). This allowed for the accurate determination of PBP2a abundance, as opposed to merely detecting the proportion of PBP2a that bound bocillin. By Western blotting. To assess the impact of *pbpH* deletion on the abundance of PBP2a, Western blotting was performed on samples obtained from strains 168, P_{xyl}-GFP-pbp2a (YA22) with and without xylose, and P_{xyl}-GFP-pbpH (YA16) with and without xylose. The strains were cultivated under optimal conditions, and proteins were extracted, separated using SDS-PAGE, and subsequently transferred onto PVDF membranes. Subsequently, the membranes were then probed with the anti-PBP2a antibody to identify the levels of PBP2a (method 2.10). To ensure precise comparison, the blots were additionally tested with antisera that specifically target the cell division protein FtsZ. This protein was used as a loading control to standardize the PBP2a signals across all samples.

In strain 168, the PBP2a antibody successfully detected PBP2a, as expected (Fig. 4.5B, lane 1). In the P_{xyl} -GFP-pbpA strain, GFP-PBP2a was detected at a higher molecular weight when grown in the presence of xylose, due to the GFP fusion (Fig. 4.5B, lane 3). Lanes 2 and 3 in the Western blot confirmed the specificity of the anti-PBP2a antibody for P_{xyl} -GFP-pbp2a without and with xylose, respectively. Lanes 4 and 5 included the P_{xyl} -GFP-pbpH strain to assess the effect of pbpH deletion on PBP2a quantity, with lane 4 representing the strain without xylose and lane 5 with xylose. In the absence of xylose, there was no significant effect on PBP2a levels compared to strain 168. However, upon xylose induction, GFP-PBPH expression resulted in a notable reduction in PBP2a quantity (Fig. 4.5B, lane 5).

To correct for differences in total protein loading, the blot was also probed with antisera specific to the cell division protein FtsZ. The FtsZ signal served as a loading control, indicating consistent protein levels across samples regardless of genetic manipulation. Band intensities for PBP2a were quantified relative to FtsZ using ImageJ software. The relative intensities of PBP2a, normalized to FtsZ, were as follows: strain 168, 29.48%; P_{xyl} -GFP-pbp2a without xylose, 0%; P_{xyl} -GFP-pbp2a with xylose, 28.25%; P_{xyl} -GFP-pbpH without xylose, 33.2%; P_{xyl} -GFP-pbpH with xylose, 5.6% (Fig. 4.5C).

Further analysis comparing the relative intensity of PBP2a in all strains and conditions to that of strain 168 revealed that P_{xyl} -GFP-pbp2a without xylose showed no PBP2a expression, as expected. Upon xylose induction, PBP2a expression increased, though it remained less than a one-fold difference compared to strain 168. In the P_{xyl} -GFP-pbpH strain without xylose, PBP2a levels were comparable to strain 168, with a less than one-fold difference. However, upon xylose induction and high pbpH expression, the relative intensity of PBP2a decreased six-fold compared to strain 168 (Fig. 4.5C).

The Western blot results consistent with the findings from bocillin-FL staining, confirming that the observed decrease in PBP2a levels upon PBPH induction was not solely due to a decrease in activity, but also a decrease in the actual amount of PBP2a protein. The significant reduction of PBP2a intensity by a factor of six upon PBPH induction indicates that PBPH has a negative regulatory effect on the abundance of PBP2a, most likely by reducing its synthesis or stability through a specific mechanism. The consistency observed between the two methods strengthens the conclusion that the induction of PBPH has a significant impact on the abundance of PBP2a.



(

Strains	Fold of PBP2a relative intensity compared to the 168
168	
P _{xyl} - <i>GFP</i> -PBP2a No xylose	
P _{xyl} - <i>GFP</i> -PBP2a + xylose	<1
P _{xyl} - <i>GFP</i> -PBPH No xylose	<1
P _{xyl} - <i>GFP</i> -PBPH + xylose	6 Folds decreased

Figure 4.5: Effect of *pbpH* deletion on PBP2A abundance

- **A)** Bocillin-stained SDS-PAGE gel showing the expression of PBP2a and PBPH in *B. subtilis* strains. Lane 1 corresponds to the wild-type strain 168. Lanes 2 and 3 represent P_{xyl}-GFP-pbp2a (YA22) without and with xylose, respectively. Lanes 4 and 5 represent P_{xyl}-GFP-pbpH (YA16) without and with xylose, respectively. PBP2a and PBPH are indicated by arrows, with *GFP*-tagged versions of the proteins visible at higher molecular weights due to the *GFP* fusion.
- **B)** Western blot analysis of PBP2a expression in the same strains. Lane 1 corresponds to the wild-type strain 168, lanes 2 and 3 correspond to P_{xyl} -GFP-pbp2a (YA22) without and with xylose, respectively, and lanes 4 and 5 correspond to P_{xyl} -GFP-pbpH (YA16) without and with xylose, respectively. GFP-PBP2a band is detected at higher molecular weights, and the presence of xylose induces their expression. The expression of FtsZ is shown as a loading control in the lower panel.
- C) Quantitative analysis of PBP2a expression relative to FtsZ in the different strains and conditions. The table shows the fold change in PBP2a intensity compared to strain 168, with or without xylose induction. Induction of *GFP*-PBPH with xylose results in a six-fold decrease in PBP2a levels, indicating that PBPH negatively affects PBP2a expression.

4.2.4 Determining if *pbpH* expression results in reduced *pbp2a* transcription

As *pbpH* deletion affects the amount of PBP2a by analysing its abundance using bocillin FL labelling and Western blotting. Thus, it seemed that transcriptional regulation was most likely to be occurring, although protein stability was still an option. To study the impact of *pbpH* deletion on the regulation of *pbp2a* expression, we examined transcriptional regulation in *B. subtilis*.

To investigate the effect of pbpH deletion on pbpA expression, we initially used a lacZ gene transcriptional fusion with the pbpA gene, derived from strain MGNA-C461. This fusion, previously constructed as part of a gene function study (Murray $et\ al.$, 1997), was used to report on pbpA expression levels through the production of β -galactosidase, which can be measured using ortho-nitrophenyl-galactoside (ONPG) as a substrate (Figure 4.6A).

The pbpA'-lacZ fusion was transformed into strain YA47, where the native copy of pbpH was deleted, and an inducible copy of pbpH under the control of the P_{xyl} promoter was integrated at the amy E locus to result in strain YA36 ($\Delta pbpH \ amy E \Omega P_{xyl} - pbpH$). This strain was then grown in the presence and absence of xylose and samples were collected at 40, 80, 120, and 160 minutes, and the specific activity of β-galactosidase was determined at each time point to indirectly indicate the level of pbpA expression. These values were then used to generate a bar graph to permit comparison of the expression of pbpA in the same strain when pbpH was not expressed (grown in the absence of xylose) or when it was expressed (xylose added to the culture medium) (Fig. 4.6B). As can be seen from this graph in the absence of PBPH (no xylose), the expression of pbpA was increased at all time points compared to when PBPH was present (with xylose). This suggests that PBPH may play a regulatory role in suppressing pbpA expression and hence when PBPH is absent, this suppressive effect is lifted, leading to increased pbpA transcription. However, although the difference in expression levels consistent between experimental repeats and the different time points, it was relatively small (~12%). Thus, although this experiment indicated the potential regulatory role of PBPH in modulating pbpA expression. Further experiments were needed to support this conclusion and provide an indication of how PBPH influences

pbpA expression, whether directly through transcriptional control or indirectly through other regulatory pathways.

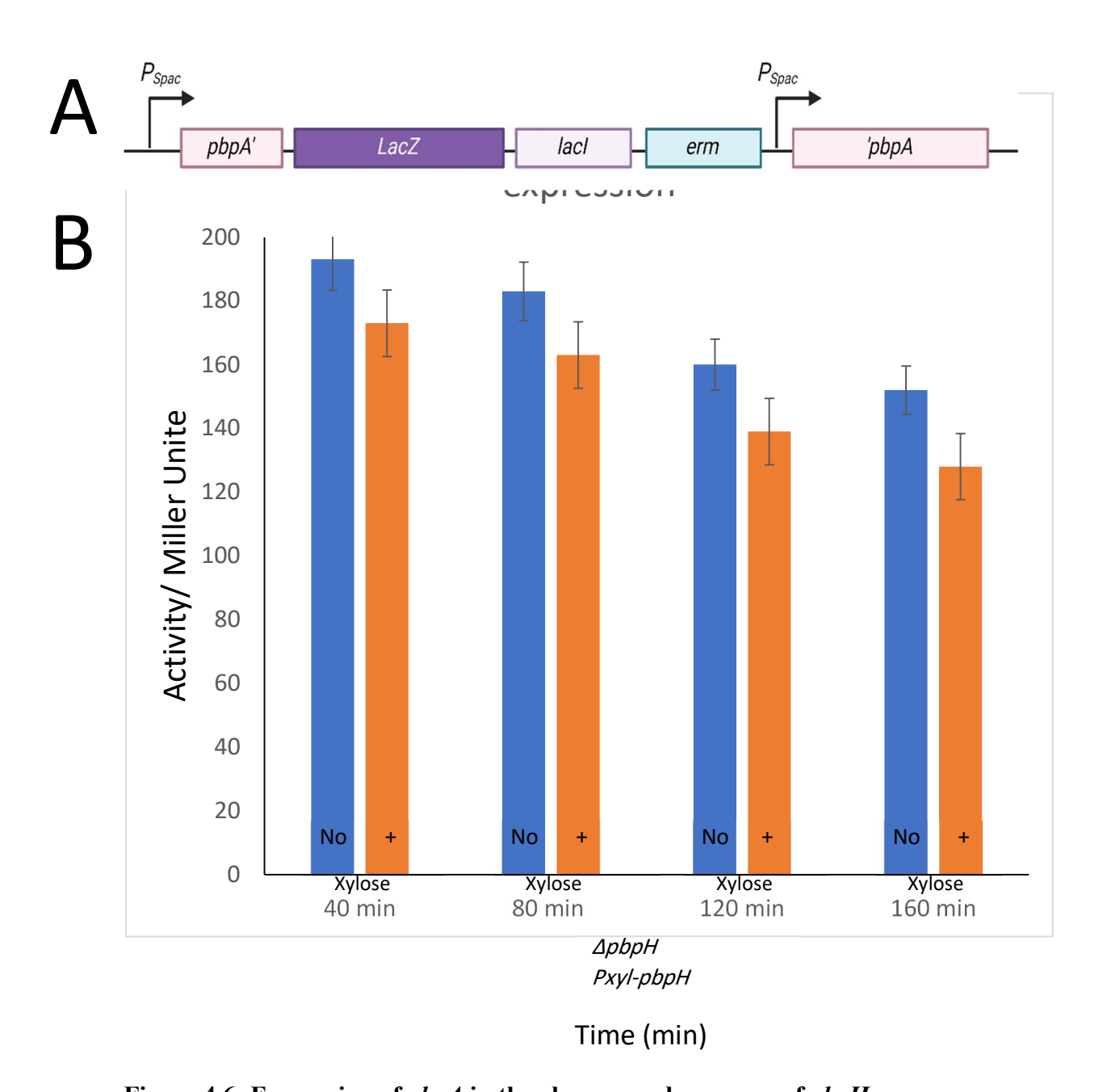


Figure 4.6: Expression of *pbpA* in the absence and presence of *pbpH*.

A) The schematic shows the genetic construct of the modified pbpA, where the lacZ gene was integrated into pbpA under pbpA's promoter control. To provide β -galactosidaseas a report for pbpA expression. B) pbpA expression after 40, 80, 120 and 160 minutes of growth in $\Delta pbpH$ -P_{xyl}-pbpH with (blue bar) and without xylose (orange bar). The values represent the average specific activities for three independent repeats of the experiment with erro bars indicating SD.

4.2.5 Effect of *pbpH* deletion on *pbpA* expression measured by RT-qPCR

Since there was only a subtle difference in the levels of pbpA expression on inducing the expression of pbpH in the previous experiment, it was unclear if the observed effect was significant or if the stability of LacZ was masking a significant change in transcription. To resolve this question and directly look at the mRNA levels RT-qPCR technique was employed. Here the analysis focused on the level of expression for the genes of interest specifically in exponential phase as it had previously been indicated that this was when both were most significant (Sauvage et al. 2008). Bacterial cultures were grown in a nutrient-rich medium (LB), and on reaching a early to mid-exponential phase, as shown in (Figure 4.7A) total RNA from each bacterial strain was extracted. This total RNA was subsequently subjected to reverse transcription and then sequencespecific primers were deployed to amplify the target genes, which included pbp2a and pbpH, using gatB as a control (see methods 2.25). The rationale behind employing gatB as a reference gene is rooted in its consistent expression pattern throughout bacterial exponential growth (corroborated by Nicolas et al., 2012); data showing the expression profile of gatB gene under a range of growth conditions is shown in supplementary figure 4.1 extracted from Subtiwiki.

The cycle threshold Ct values obtained from RT-qPCR for pbpA and pbpH were normalized against gatB to compensate for any variations in RNA quantity or quality among the samples. The $\Delta\Delta$ Ct method was employed to determine the relative expression levels of pbpA and pbpH. This method enables the comparison of gene expression across various experimental conditions.

The expression levels of pbpA were normalized and represented on a graph (Figure 4.7B) to visually depict the impact of pbpH deletion and subsequent reintroduction (through xylose induction) on pbpA expression. The graph shows the levels of pbp2a expression in three different strains: the wild-type strain (168), the YA36 (P_{xyl} pbpH::Sp $\Delta pbpH$::Cm) strain without xylose (which suppresses pbpH expression), and the same strain with xylose (which induces pbpH expression).

Notably, the expression profiles of pbp2a and pbpH in the 168 strain were similar. Whereas, in the YA36 strain where pbpH expression was repressed, as indicated by the fact that no RNA transcript of phpH was detected, pbp2a transcript detection was significantly higher compared to that of the wild type strain. Interestingly, adding xylose, which restores pbpH to essentially the same level as determined for 168. In parallel with this there was a significant decrease in pbp2a expression (compared to condition where no xylose was added), bringing it to a level comparable to that of the 168 strain, but significantly lower than determine for samples where pbpH expression was repressed (in the absence of xylose; Figure 4.7B). These findings are consistent with the β -galactosidase results (section 4.2.5) and support the idea that pbpH expression plays a regulatory role in pbpA expression. The results are also much more consistent with the observations made at the protein level, in that the transcriptional change is significantly more dramatic (approx. 2-fold change) that that see for the β -galactosidase data (where it was a fractional increase).

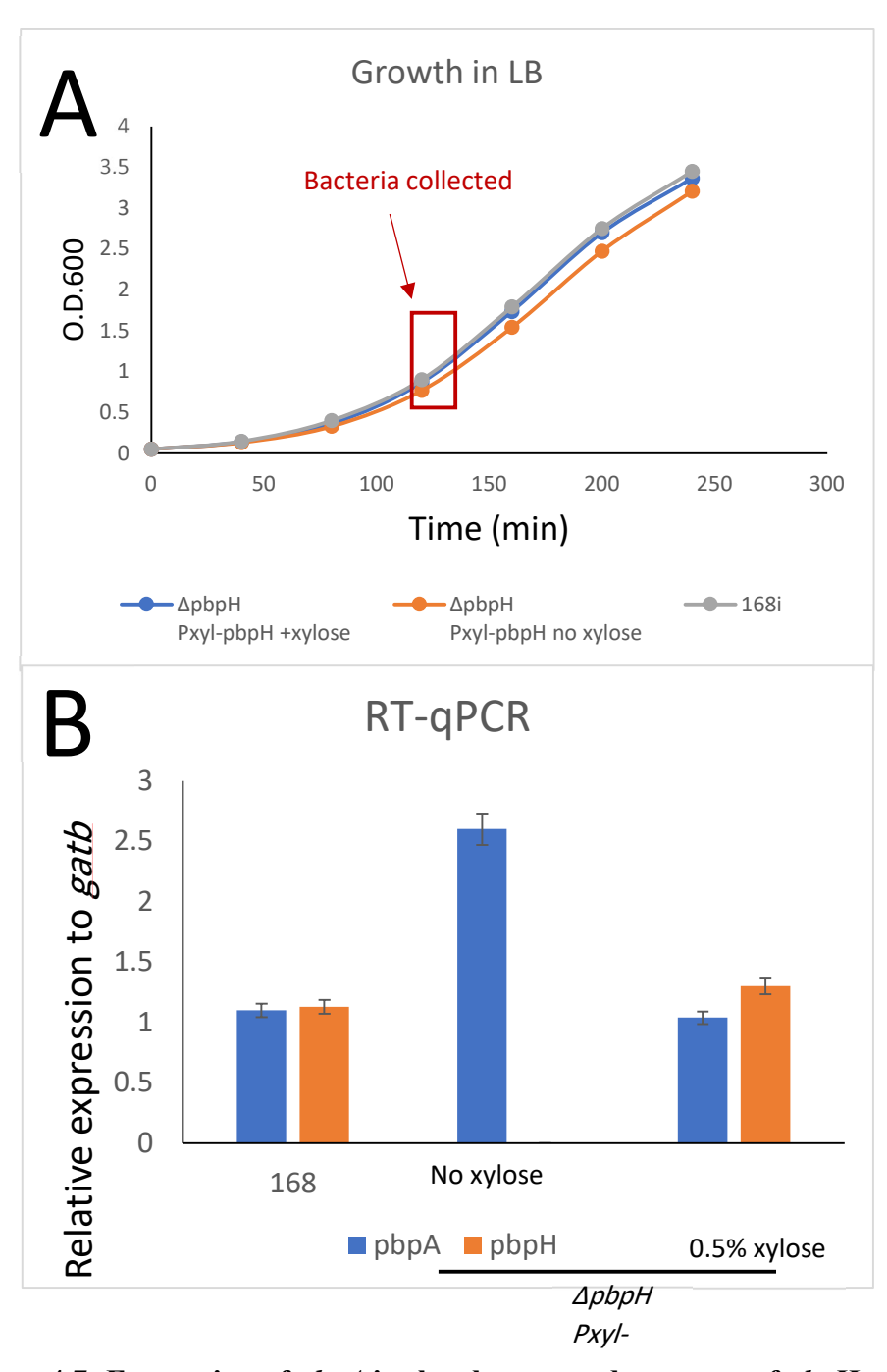


Figure 4.7: Expression of *pbpA* in the absence and presence of *pbpH*.

A) Growth of strain 168, $\Delta pbpH$ - P_{xyl} -pbpH without xylose and $\Delta pbpH$ - P_{xyl} -pbpH with xylose. The samples were collected after approximately 120 minutes of growth (red box). B) RT-qPCR to assess the relative expression of pbp2a (blue bar) and pbpH (orange bar) to gtpA in strain 168 and $\Delta pbpH$ - P_{xyl} -pbpH with and without 0.5% xylose. ERROR bars show standard deviation SD.

4.2.6 Effects of PBP2a or PBPH cytosolic tail deletions on bacterial growth Identifying the cytosolic tail *of PBP2a* and *PBPH*

Since it was apparent that artificially expressing pbpH resulted in a change in pbpA expression, it seemed possible that the abundance of PBPH was in some way influencing transcription. For this to function the cell must be able to detect PBPH in some way. A possible candidate for detection is the N-terminal amino acids of PBPH, as this small domain is cytosolic, whereas the rest of the protein has to be extracellular for it to function. Thus, it was proposed that the cytosolic domains of both PBP2a and PBPH might be crucial components in the regulation mechanism. To determine if these domains play significant roles in the function of the proteins, we investigated the effects of their removal. Specifically, we aimed to delete these cytosolic domains from either PBP2a or PBPH in a strain where the truncated form was the only expressed copy. This strategy was designed to force the bacteria to rely on either a truncated version of PBP2a or PBPH for survival and growth. Thus, the first step was to define the cytosolic domains of both proteins. For this an alignment of the amino acid sequences for a number of PBPH-like and PBP2a-like proteins was generated (Figure 4.12). In so doing this seemed to clearly define the cytosolic domain as its rich of charged (negative in blue and positive in red) and hydrophilic amino acids before the hydrophobic amino acids started to appear which predicted to be the transmembrane domain.

To test if these short sequences had any significant role in the biological function of the PBPs, the coding sequence for start of the gene for PBP2a and PBPH was altered to remove the cytosolic domain and place the start codon of the gene being immediately in front of the sequence predicted to encode the transmembrane spanning amino acids. To achieve this, the coding sequences of the PBP2a and PBPH genes were first amplified by PCR from the genomic DNA of *B. subtilis*, using primers designed to exclude the cytosolic domain (YA-TRUNCATED *pbpH*-FF and YA-TRUNCATED *pbpH*-FR). These PCR products were then cloned into the plasmids pYA12 (for PBPH) and pYA13 (for PBP2a) using NEBuilder® HiFi DNA assembly techniques (section 2.19). The modified genes were inserted downstream of the P_{xyl} promoter within the plasmids, ensuring that their expression would be under the control of xylose induction.

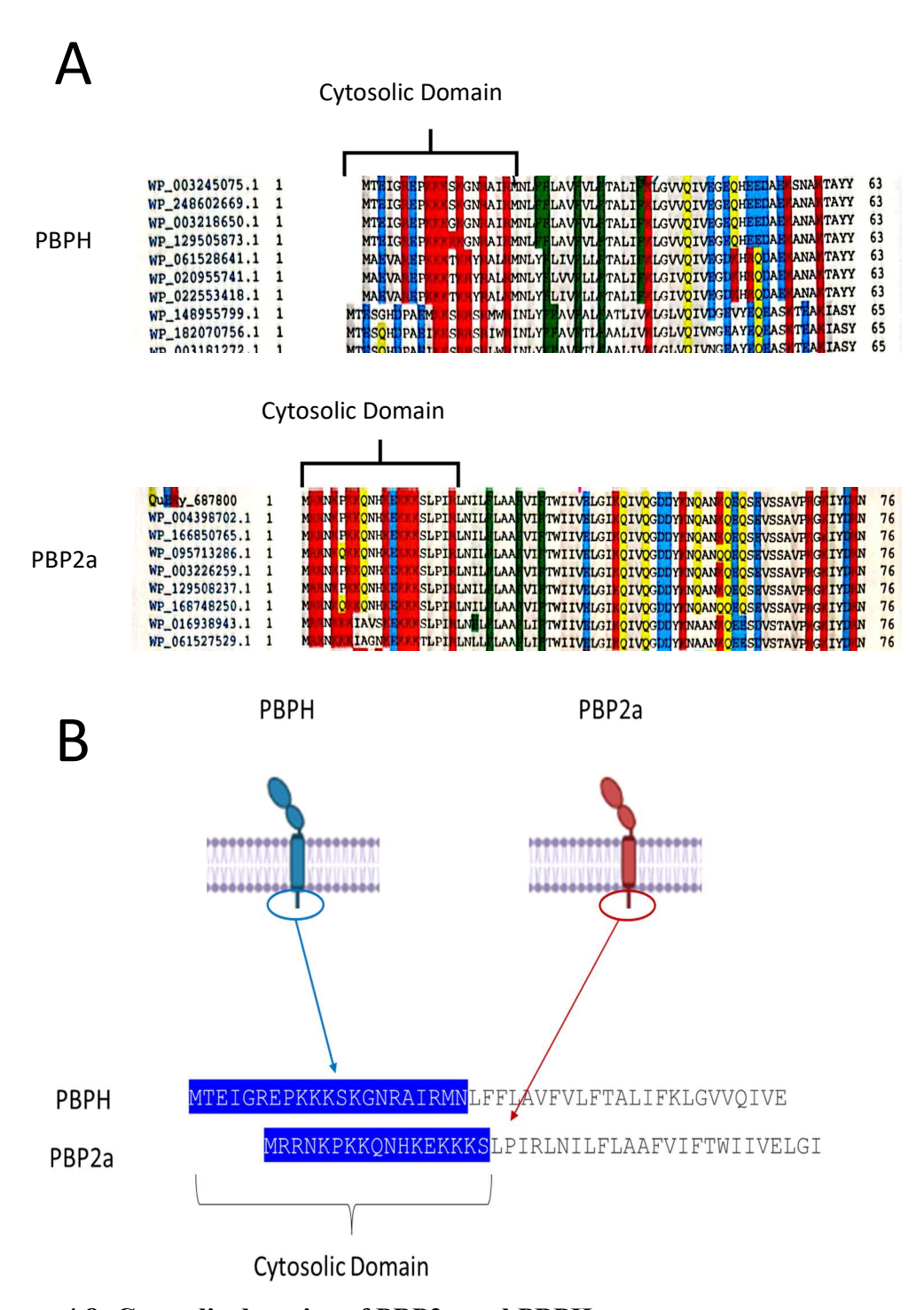


Figure 4.8: Cytosolic domains of PBP2a and PBPH.

A) PBPH-like and PBP2a-like proteins alignment and Cytosolic domines are predicted. B) The schematic shows PBPH in blue and PBP2a in red where they are anchored in the cell membrane, while the cytosolic domains of both proteins are inside the bacterial cell (indicated inside the circle). The amino acid sequences of PBPH and PBP2a and the cytosolic domain are highlighted in blue for both.

Removal of the cytosolic domain of PBP2a and bacterial growth with truncated PBP2a

Following the construction of plasmid pYS13, we introduced it into the 168 then the native pbpA gene was deleted to give strain YA20. This strain only encodes the truncated version of PBP2a under P_{xyl} control. Then a deletion of pbpH was introduced into strain YA20 selecting for the null mutation presence of xylose. This resulted in the isolation of strain YA24 where it was expected that growth was dependent on the truncated version of PBP2a (denoted 'PBP2a) and as the expression of this gene would be dependent on xylose. To verify the successful removal of both native genes encoding PBP2a and PBPH from the strain and to confirm the presence of the inducible, truncated version of PBP2a, PCR was initially used. Using oligonucleotides either side of the gene deletions generated products consistent with the expected sizes for the deletions. These and other PCR generated products were also used to permit sequencing, particularly of the inducible constructions, to confirm that the DNA sequence for subtle changes were as expected. Finally, to confirm expression of the modified PBP genes, samples of the cultured cells were bocillin-FL labelled, resolved on a 4-12% protein gel and imaged as previously described. (Figure 4.9A). From this image it was clear that the native PBP2a and PBPH proteins were absent and a faster migrating PBP was present, corresponding to the truncated PBP2a, the gel.

Since these tests confirmed that the strain construction was as expected, we compared the growth of our modified strain, 'PBP2a (YA24), with the wild-type strain (168). This comparison was conducted in LB medium with the addition of xylose at 37 °C and shaking at 250 rpm to permit the growth profile of the strains to be plotted against time (Fig 4.9A). A test in the presence of xylose therefore dependant on truncated PBP2a resulted in no difference in growth of strain 'PBP2a (YA24) compared to the wild type 168. The results indicate that the removal of the cytosolic tail of PBP2a did not have any impact on the growth of strain.

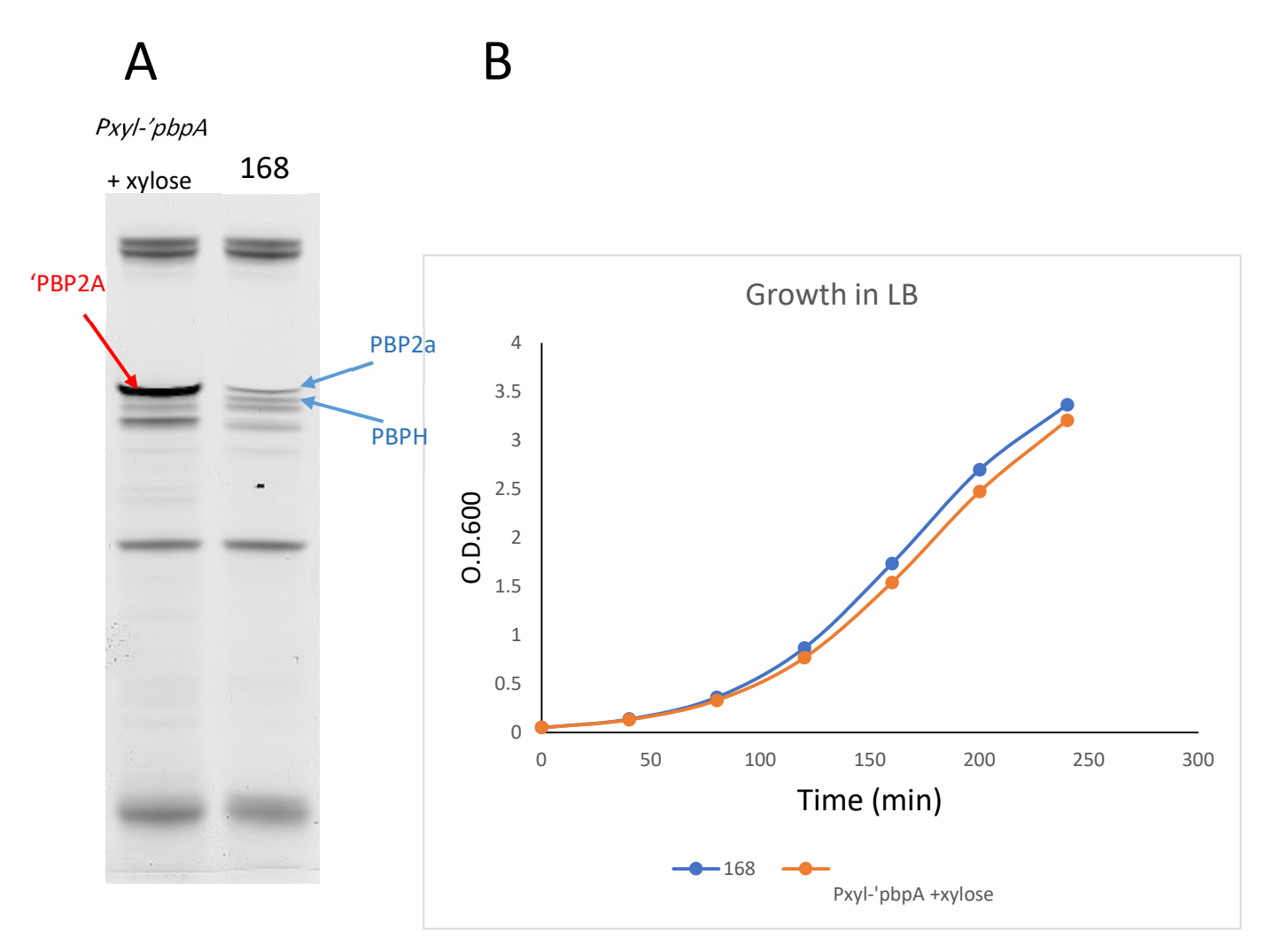


Figure 4.9: Effect of the deletion of the PBP2a cytosolic domain on *B. subtilis* growth.

A) A Bocillin FL image that shows PBP bands in P_{xyl} -'pbpA + xylose and 168. The truncated 'PBP2a band is indicated by the red arrow in P_{xyl} -'pbpA, while normal PBP2a and PBPH are indicated by the blue arrow in strain 168. B) Growth of strain 168 and the strain lacking the original PBP2a and PBPH and containing an inducible copy of truncated 'PBP2A.

Removal of the cytosolic domain of PBPH and bacterial growth with truncated PBPH

Since the cytosolic tail of PBP2b did not seem to have any role in PBP2a function we set out to construct a bacterial strain where a modified version of PBPH where the cytosolic tail was removed.

The initial step involved the construction of a truncated PBPH variant lacking its cytosolic domain. This was generated by PCR using oligonucleotides YA-TRUNCATED pbpH-FF and YA-TRUNCATED pbpH-FR to result in a truncated pbpH gene fragment lacking the cytosolic domain and this DNA fragment was then cloned into pSHP1 such that expression was mediated by the P_{xyl} promoter, which allowed for the inducible expression of the truncated gene. This specific gene construct was incorporated into the pSHP1 plasmid, The resulting plasmid (pYA10) was then transformed into 168 and correct insertion of the P_{xyl} 'pbpH construct confirmed by PCR, to give strain YA13. Then this strain was transformed with the knockout of the native pbpH gene using genomic DNA from YA11, to give strain YA14, resulting in a strain where the only copy of pbpH is deleted for the cytosolic tail and conditionally expressed (in the presence of xylose. To determine if this modified version of PBPH was functional, strain YA14 was transformed with DNA from YA18 to introduce a pbpA null mutation and the transformants selected for in the presence of xylose, to allow pbpH expression, and kanamycin to select for the pbpA null mutation. The resulting colonies were then checked for the presence of the appropriate antibiotic resistance markers and dependence for xylose and one of the strains designated YA23.

To confirm the successful removal of PBPH and PBP2a and verify the presence of the inducible truncated version of PBPH, we initially used sequencing of PCR generated product corresponding to the P_{xyl} 'pbpH construction. Then bocillin-FL labelling was used to permit detection the 'PBPH. These labelled samples were then subjected to separation using a 4–12% protein gel and a fluorescent imager for detection of the PBPs in strains 'PBPH and 168. The results (fig. 4.10) of this analysis revealed that with the addition of xylose, the modified 'PBPH strain lacked the full-length versions of both

PBP2a and PBPH. It contained only the inducible, truncated version of PBPH, which was detectably smaller than the full-length variant on the gel.

Following these molecular characterisations, we assessed the growth dynamics of the modified strain ('PBPH) in comparison with the wild-type 168 strain. This comparison was conducted using LB medium with xylose at 37 °C with agitation at 250 rpm. Despite the modified strain's dependency on truncated PBPH, following the removal of the full-length PBP2a and PBPH, its growth rate was comparable to that of the wild-type 168 strain. The results indicate that the cytosolic tail of PBPH is not affecting the growth of bacteria (Figure 4.10B).

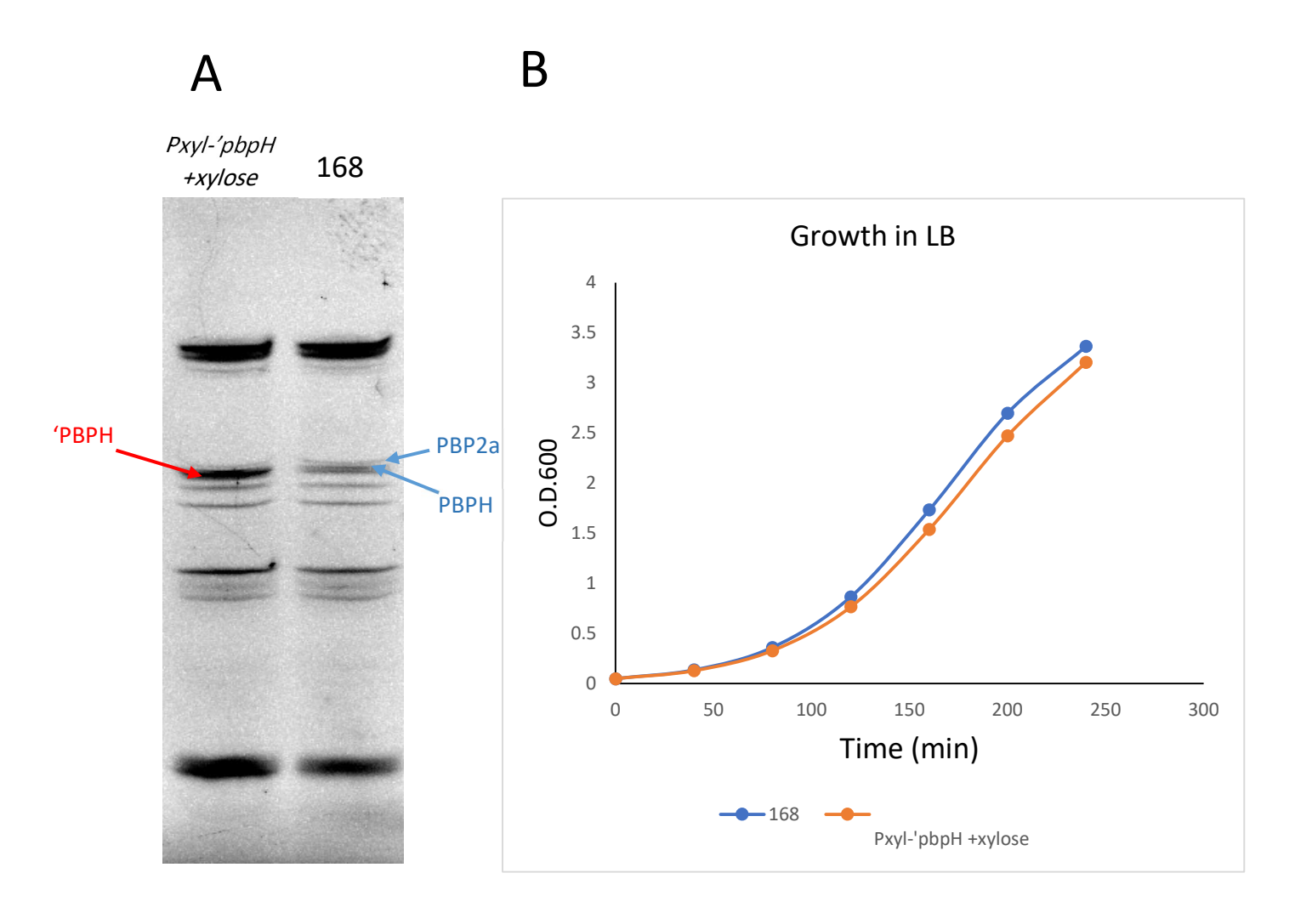


Figure 4.10: Effect of deletion of the PBPH cytosolic domain on B. subtilis growth.

A) A Bocillin FL image that shows PBP bands in P_{xyl} -'pbpH + xylose and strain 168. The truncated 'PBPH band is indicated by the red arrow in P_{xyl} -'pbpH, while normal PBP2a and PBPH are indicated by the blue arrow in strain 168. B) Growth of strain 168 and the strain lacking the original PBP2a and PBPH and containing an inducible copy of truncated 'PBPH.

4.2.7 A chimeric PBPH with the transmembrane domain of PBP2a

As N-terminal portion of both PBPs did not seem to have a functional role in the ability of PBP2a and PBPH to act in the elongosome (Chapter 1 section 1.6.4), it seemed possible that this region had a role in how they compete with each other to associate with the elongation apparatus. Previous results potentially indicating that PBPH pushes PBP2a out of the complex, causing it to degrade and so lowers its abundance. To test if PBPH transmembrane domain was responsible for the change in PBP2a quantity. The PBP2a and PBPH transmembrane domains were predicted, the PBPH cytosolic tail is short and stops at the point where nonpolar amino acids start to appear (leucine, followed by a pair of phenylalanines and then alanine), which is predicted to form the start of the transmembrane domain. The domain ends at the point where polar and charged amino acids start to appear, including glutamic acid, glutamine and histidine (Figure 4.11D). In PBP2a, the transmembrane domain started where leucine, proline and isoleucine began to appear after three positively charged lysines and a polar serine. The end-of-pipe transmembrane domain of PBP2a appeared where a positively charged lysine was followed by a polar glutamine (Figure 4.11D). Transmembrane domains of PBP2a and PBPH were swapped with each other to assess if this altered the observation that PBPH displaced PBP2a (Figure 4.11).

Initially, full-length PBP2a and PBPH were cloned individually in the pSHP1 plasmid under the control of the P_{xyl} promotor to provide control constructs. Then similar constructs were made using PCR amplified sections of the genes. The PBP transmembrane domains were amplified in such a way that they could then be fused to to the other PBP coding sequence that had been amplified without the TM sequence. The two DNA fragment (*pbpH* with TM domine of *pbpA*) being linked together using NEBuilder HiFi (cloning as described in Chapter 2, Section 2.20) and cloned into pSHP1. The resulting plasmids were then transformed into strain 168, selecting for the appropriate antibiotic and screening the resulting transformant for amylase activity. Clones lacking amylase activity being the result of a recombination exchange of the cloned genes for a section of the chromosomally encoded amylase gene (*amyE*). This resulted in the creation of strain YA31, where a chimeric version of *pbpH* was present at the *amyE* locus encoding the N-terminal segment of PBP2a. The original copy of

PBPH was deleted to prevent interference with the induced copy of PBPH-TM This resulted in the creation of strain YA32. Using an anti-PBP2a antibody in western blotting, PBP2a signals were found to be similar in 168 with and without xylose. Unlike the strain with the full PBPH protein, the strain containing PBPH with the transmembrane domain of PBP2a, in the presence of xylose and overexpression of PBPH with the transmembrane domain of PBP2a, rescued the PBP2a protein from the decrease (Figure 4.11B and C). The FtsZ protein (a cell-division initiation protein involved in septum formation) was utilised as a loading reference, and after electrophoresing the samples, the gel was separated before antibody treatment to avoid unwanted interactions and background, and the loading reference protein FtsZ and the PBP2a protein were treated with the corresponding antibodies separately. Although the bands showed no clear differences visually, the band intensity of PBP2a in each of the three strains and under each of the different conditions was quantified using the ImageJ software to corroborate the visual findings. The band intensity percentage was calculated relative to the loading reference FtsZ for each strain. The intensities of PBP2a were close to the intensities of FtsZ in all the strains, and a value of 100% indicates no difference in intensity between PBP2a and FtsZ. In the 168 strain, the relative intensity percentage of PBP2a was 106% without xylose and 100% with xylose. However, in P_{xyl}-PBPH (TM of PBP2a) strain, the relative intensity percentage of PBP2a, thePBP2a without xylose was 86% and increased to 122% with xylose instead of going down (Figure 4.11).

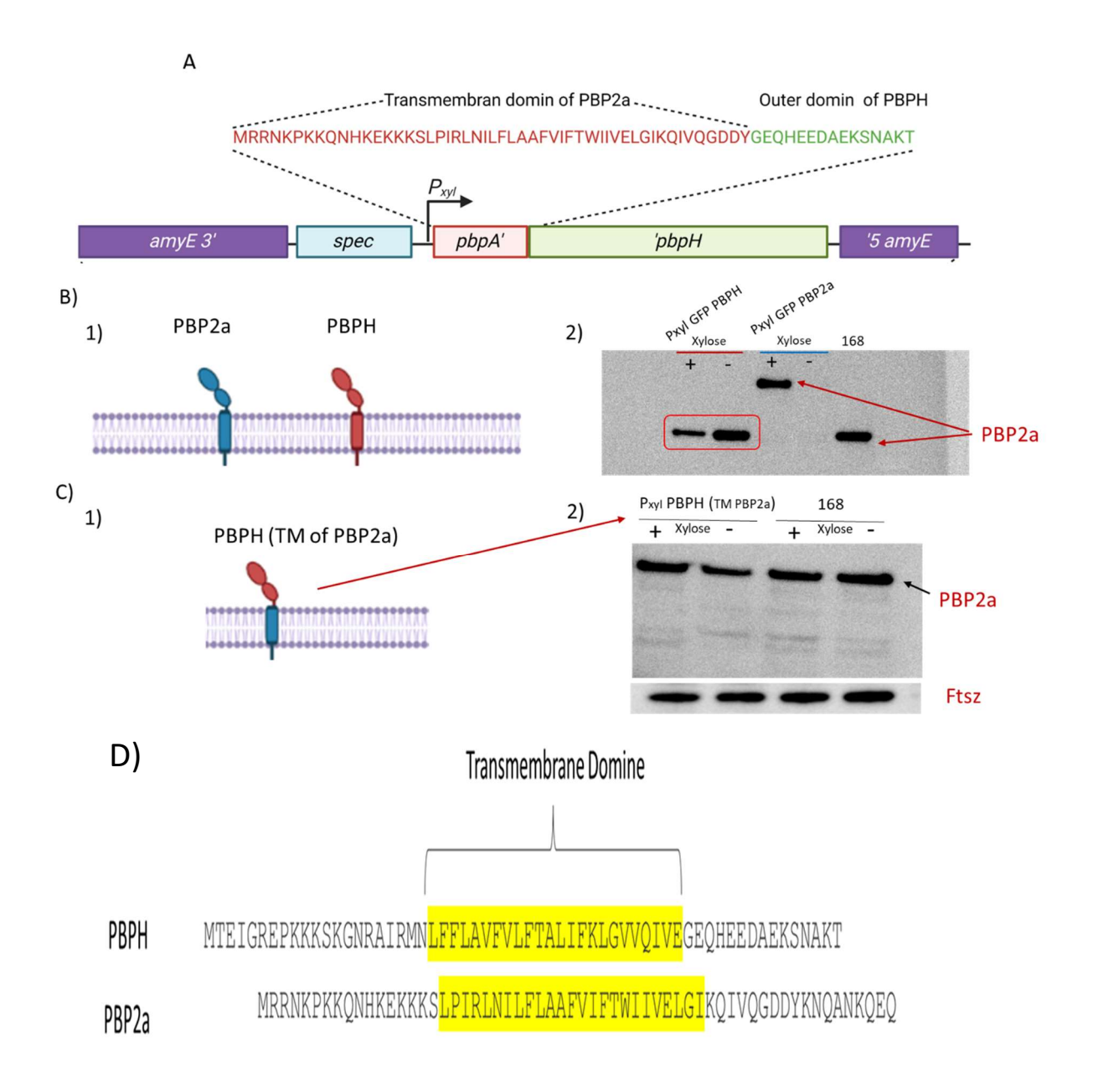


Figure 4.11: Creation of a chimeric PBPH and evaluation of its effect on PBP2a abundance by western blotting.

A) The schematic shows the constructed strain, that is, PBPH (green) with the transmembrane domain of PBP2a (red). It was inserted into the Pshp1 plasmid and cloned into the 168 strain under the control of the P_{xyl} promoter. B) (1) Normal PBP2a and PBPH, located at the cell membrane. (2) Western blot of PBP2a when the normal PBPH protein is overexpressed. C) (1) The schematic illustrates the constructed protein located at the cell membrane with the transmembrane domain of PBP2a and the outer membrane of PBPH. (2) Western blot of PBP2a in the absence and presence of the chimeric protein (PBPH with the transmembrane domain of PBP2a) and FtsZ

as a loading reference. D) TM domine of PBP2a and PBPH indicated in yellow colour.

4.2.8 Site-directed mutagenesis of the PBPH transmembrane domain

As previously shown, the transmembrane domain of PBPH is involved in causing the decrease the PBP2a quantity upon overexpression of PBPH. To determine if this is mediated by a specific feature in the transmembrane spanning domain, the N-terminal amino acid sequence of a number of Bacillus genes encoding a gene corresponding to PbpH based on the National Centre for Biotechnology Information (NCBI) database. The PbpH protein sequence of B. subtilis was blasted against bacilli organisms and all proteins with high similarity were aligned to the PBPH from B. subtilis. and the amino acid residues with similar characteristics colour coded. Non-polar amino acids were highlighted in grey and green, positively charged amino acids in red, negatively charged amino acids (blue) and polar amino acids (yellow) were marked, as shown in Figure 4.12A From this comparison there were some features that seemed to be strongly conserved within the segment that is presumed to span the membrane, being indicated by the fact it was composed predominantly of non-polar, uncharged amino acids, with polar amino acids on its edges. However, two amino acids were distinguishable and constant in most of the assessed B. subtilis potentially PbpH encoding genes, namely glutamine at position 42, along with lysine in some strains and arginine in others. Interestingly the glutamine is polar but located in the middle of the transmembrane domain of PBPH, while lysine or arginine are positively charged amino acids also located in the middle of the bioinformatically predicted transmembrane domain at position 36.

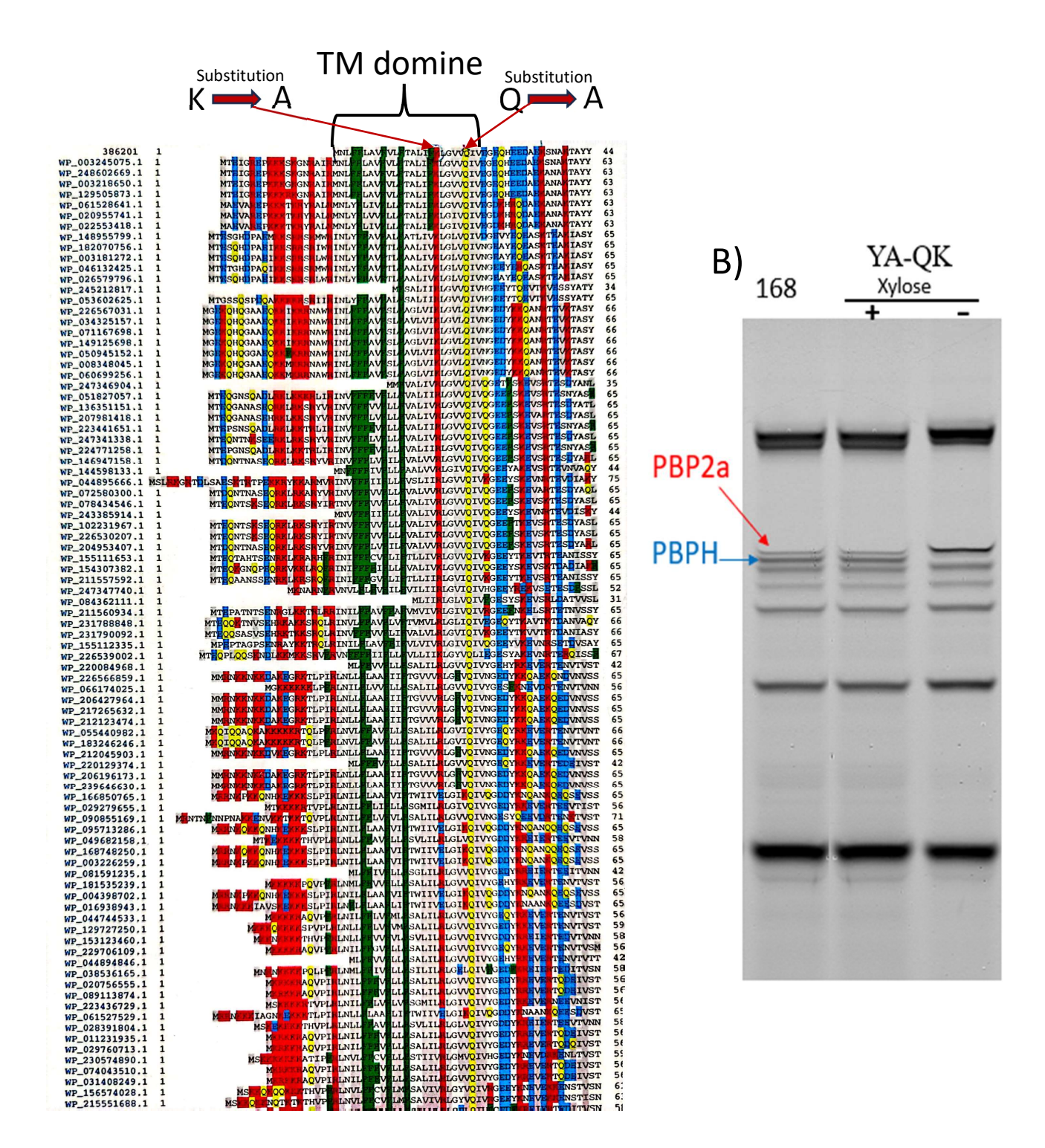
Similarly, the (NCBI) database was also used to blast the PBP2a sequence against bacilli strains. Similar alignment and analysis to PBPH was conducted to PBP2a and the PBP2a also has conserved glutamine (Q) as polar amino acid in the middle of predicted transmembrane domain but unlike PBPH the charged amino acid in the transmembrane of PBP2a was Arginine or Glutamic acid (E) instead of lysine which found in PBPH (supplementary Fig 4.3)

Thus, it was possible that these amino acids were acting to promote PBPH to interact with the elongation apparatus and displace PBP2a. To test this hypothesis site-direct

mutagenesis was used to change both of these amino acids in the coding sequence of a full length pbpH gene cloned in plasmid pYA16 (oriBR322 bla

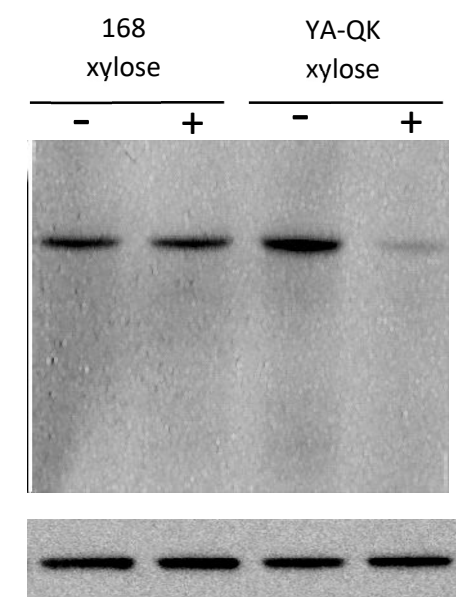
amyE::- P_{xyl} pbpH (p.Q42A) (p.K37A)spec). This plasmid was then used to introduce the modified version of *pbpH* into strain YA11 (168 Δ*pbpH*::*erm*) to give strain YA-QK (Figure 4.12A). The functionality of mutated PBPH was tested by bocillin Fl since the bocillin is bind to the bioactive PBPs (Fig 4.12B)

Western blotting was carried out on strains 168 and YA-QK with and without xylose addition to evaluate the change in PBP2a quantity following mutations in lysine and glutamine. Their substitution with alanine in the PBPH transmembrane domain did not change the effect of deletion and overexpression of *pbpH* on the quantity of PBP2a (Figure 4.12B). By calculating the relative intensity of the PBP2a band using FtsZ as a loading control and comparing it to that in strain 168, the deletion and expression of the transmembrane domain-modified PBPH (strain YA-QK) was found to have an effect on the abundance of PBP2a on expression of the modified PBPH or decreasing it fivefold upon overproduction of the modified PBPH (Figure 4.12C).



C) D)

Western Blot of Anti-PBP2a antibodies



Strains	Fold of PBP2a relative intensity compared to the 168
168 No xylose	
168 + xylose	<1
YA-QK No xylose	≈ 2 Folds increased
YA-QK + xylose	≈5 Folds decreased

FtsZ

Figure 4.12:

Expression of a mutated pbpH gene where the transmembrane domain was altered and the impact on PBP2a abundance.

A) Bioinformatics analysis shows several PBPH in Bacilli strains sequences aligned by colour based on the amino acid property. The data was obtained from NCBI. The transmembrane and the substituted amino acids (Q and K to A) are indicated. B) Bocillin-FL labelling of 168 and YA-QK strain with and without xylose. C) Western blot using anti-PBP2a antibodies for strains 168 and YA-QK with and without xylose. The FtsZ antibody was utilised as a loading reference. D) The table shows the PBP2a band intensity in relation to that of FtsZ, compared to the PBP2a band in strain 168 (without xylose as the wild type). Data are presented as fold change in 168 + xylose, YA-QK - xylose and YA-QK + xylose. The data are based on three independent experiments, and the P-value is > 0.05.

4.3 Discussion

To evaluate the activity of PBP2a and PBPH in B. subtilis, an activity-based probe that covalently binds to the active site of PBPs, bocillin-FL, was used. PBPs are the binding target of β-lactam antibiotics such as penicillin, which inhibits their enzyme activity and stops the manufacture of new cell walls, leading to cell death. The catalytic serine present in all PBPs in B. subtilis interacts with the component that β -lactams mimic, the terminal D-Ala-D-Ala of the peptidoglycan pentapeptide. Bocillin-FL, a fluorescent derivative of penicillin V, exhibits a strong attraction to all active PBPs. As a result, it can be employed as an activity-based probe to accurately measure the enzymatic activity of all PBPs (Chowdhury et al., 2010; Sharifzadeh et al., 2020; Zhao et al., 1999). Additionally, inactivated PBP2b could not bind the bocillin-FL probe, which indicates that bocillin-FL only binds to active PBPs (Sassine et al., 2017). Therefore, bocillin-FL labelling showed that upon deletion of pbpH, the detected amount of PBP2a increased; this was confirmed by overexpressing pbpH, which returned the level of PBP2a to the normal level or even slightly less compared to the wild type. The increase in PBP2a abundance upon the deletion of pbpH could potentially be caused by the functional redundancy of PBP2a and PBPH in cell elongation (Dion et al., 2019; Sauvage et al., 2008) and the cell recognising a "need" and upregulating expression of PBP2a to compensate. Our data supports the functional redundancy of PBP2a and PBPH established by Wei et al. (2003). Additionally, the increase in PBP2a following pbpH deletion suggests that their TP activity is cooperative, and both work simultaneously, rather than PBPH not functioning until PBP2a is stopped. This raises a question as to why would B. subtilis have two such proteins? This question may have been addressed by study by Mitchell et al. (2023) evaluated the activity of PBPs in B. subtilis at different pH values and revealed that in an alkaline medium (pH 9), PBPH activity was halted, while at an acidic pH, both PBP2a and PBPH activities were stopped. These data suggest that PBP2a carries out TP activity in alkaline conditions, helping the bacteria to grow when PBPH activity is lost.

However, another interpretation of the results obtained could be that bocillin-FL labelling represent the active PBPs and there was a "pool" of dormant PBP2a present,

rather than the cell mediating a transcriptional response to reduced PBPH activity, and specifically up regulating *pbpA* expression. Although several studies have used the fluorescent penicillin method (bocillin-FL) to investigate the quantity of PBP (Pucci *et al.*, 2002; Zhao *et al.*, 1999), the labelling method differs and often the PBPs are labelled after extraction form the cell. In this work the labelling was always done on live cells, exploiting the fact that the covalent binding of the fluorescent penicillin is very rapid, but probably only bale to interact with "exposed" and active proteins. Therefore, the results of the penicillin labelling had to be treated with caution as to what was happening. To try and resolve this question another way to determine the relative abundance of PBP2a and PBPH was required that was not activity related. The solution opted for in this work was to generate polyclonal antisera specific to the protein in question. This was then expected to permit detection by Western blotting and could be used in conjunction with bocillin-FL labelling to detect total levels of the protein and what proportion was biochemically binding penicillin, and hence active.

To generate polyclonal antisera overexpression and purification of the two PBP was attempted using E. coli as the producing organism. This was successful in both cases, however only PBP2a could be purified in sufficient quantity to permit the generation of an antiserum. PBPH could not be over expressed significantly, and the material produced, although confirmed as having the His-tag, both through sequencing of the clones and by antisera did not bind to the nickel column and so enrichment was not possible in the time available. However, an anti-PBP2a antisera was obtained, and this was then tested to validate the specificity of this antibodies. The western blot analysis was conducted to evaluate the presence of PBP2a. When PBP2a was present, the antibodies effectively linked to it and were identified using western blot analysis (Fig 4.5A). Nevertheless, in the absence of PBP2a, the antibodies failed to attach, thereby demonstrating their exclusive affinity for PBP2a. Furthermore, the impact of elevated PBPH production on the levels of PBP2a was investigated. The Western blot analysis revealed that an excess production of PBPH resulted in a decrease in the amount of PBP2a. Therefore, the deletion of PBPH may increase the quantity of PBP2a, while overproduction of PBPH may reduce the quantity of PBP2a. As a result, bocillin FL binds to more PBP2a in the absence of PBPH and to less PBP2a when PBPH is

overproduced. This variation in PBP2a levels affects the capacity of bocillin FL to label it. The observed changes in PBP2a levels caused by *pbpH* deletion or overexpression suggest that the relationship between PBP2a and PBPH is regulated by the bacteria. This raises the question of whether this regulation occurs through transcriptional mechanisms or protein degradation pathway.

To further explore this regulatory relationship, β-galactosidase results showed that the expression of pbpA increased upon the deletion of pbpH; this increase was consistent over time (40, 80, 120 and 160 minutes) and significant based on three independent experiments. However, since the β-galactosidase method indirectly measured the expression of pbpA, RT-qPCR was utilised to confirm the increase in pbpA expression at the level of the amount of mRNA present in the culture. The results of both techniques were compatible, indicating that the redundant partners PBP2a and PBPH undergo transcriptional regulation. PBP expression regulation has been studied in two independent studies, promoter and transcription analysis of PBP genes was performed for S. pneumoniae R6 and Streptococcus gordonii. The studies found that the PBP promoters in these bacteria had an extended -10 region (Pribnow-Schaller box) that was highly conserved, while the -35 region was poorly conserved among the PBPs in both. The variation in the -35 sequence suggests that different PBPs may be regulated and that probably either by different sigma factors or by altering the efficiency of the same sigma factor to bind to the promoter. This aligns with our findings, which indicate that pbpA is also transcriptionally regulated, and that expression of pbpH results in reduced pbpA expression suggesting that sigma factor interactions may play a role in the regulation of these genes.

An essential inquiry in comprehending the regulation of PBP2a synthesis is how the bacterial cell perceives the lack or decrease of this protein and subsequently determines to increase its production. A possible mechanism involves the regulation of gene expression by a cascade of downstream signalling events. For instance, the synthesis of PBP2a can be triggered by a signal transduction mechanism controlled by the genes on the staphylococcal cassette chromosome mec (SCCmec) genetic element. This process involves a sensor protein called MecR1, which is located in the cell membrane. MecR1

transmits signals through conformational changes and proteolysis of its cytoplasmic domain (García-Castellanos *et al.*, 2004; Sharma *et al.*, 1998; Zhang *et al.*, 2001)

Given this context, we explored whether the cytosolic domains or transmembrane segments of PBPH and PBP2a play a similar role in their regulation and stability. To test this, we removed the cytosolic domains of PBPH or PBP2a and deleted the redundant partner, ensuring that bacterial growth now depended on the truncated PBPH or PBP2a. This showed that the truncated PBP was functional and was not required for interaction with the elongation complex. It was also evident from this that the loss of the cytosolic domain of PBPH cytosolic domain did not have a role in regulating the expression level of PBP2a. Thus, it appeared that the regulation of *pbpA* expression by abundance of PBPH was not mediated by detection of the cytosolic domain of PBP. However, this finding does not rule out the importance of cytosolic domains in all PBPs. For example, in *S. pneumoniae*, substituting the PBP2x cytosolic domain (12 amino acids) with the PBP2b cytosolic domain (27 amino acids) significantly impacted PBP2x function and negatively influenced bacterial viability (Berg *et al.*, 2014). This observation suggests that while the cytosolic domains are not critical for PBPH and PBP2a, they may play a role for other PBPs.

Given that the cytosolic tail did not affect PBP2a regulation, we turned our attention to the transmembrane (TM) segment. The TM domain of PBPs is crucial role in anchoring the protein to the cell membrane and deleting it would result in the protein is not translocated across the membrane. To try and gain a further insight into the mechanism, we substituted the TM domain of PBPH with that of PBP2a to construct a chimeric protein. Our data demonstrated that upon substitution of the PBPH TM domain, the overproduction of PBPH (with TM of PBP2a) altered the early observed decrease in PBP2a quantity upon deletion of the original PBPH. This indicates that the TM domains of the redundant pair play a role in regulating PBP2a levels. In our study, PBPH and PBP2a were located in the elongasome complex; therefore, it is possible that PBPH with the transmembrane domain displaces PBP2a out of the elongasome complex upon overproduction (Figure 1.3) perhaps facilitating faster "growth" at the expense of robustness. This concept is weakly supported by the fact that it has been determined

that PBPH is more sensitive to β -lactams, inferring that it may have a more open catalytic domain compared to PBP2a (Emmins and Daniel, unpublished; Sharifzadeh *et al.*, 2020) perhaps facilitating faster growth.

To further understand the regulatory role of TM domains, we performed a sequence alignment of PBPH and PBP2a with PBPs from other *Bacillus* species to identify conserved amino acids potentially responsible for the observed expression changes in PBP2a (section 4.2.7). Or by changing these residues the PBP would no longer interact correctly with the elongation system, and so would be dysfunctional. However, of the candidates identified not significant effect was observed when expressed in Bacillus. In a way these results were similar to that described by Berg *et al.* (2014) characterising the cytoplasmic tails and transmembrane region of PBPX in *S. pneumoniae*. This implies that there may be multiple features that act collectively in mediating the observed effect, the loss of anyone having minimal effect. Or that there is a component missing from our understanding that still needs to be characterised.

Chapter 5 D-Ala transfer from LTA to WTA is mediated by PBPX

5.1 Introduction

A physiochemical property of the cell envelope is its surface charge and is proposed to have diverse roles in how bacterial cells interact with ions, particles and surfaces. *B. subtilis* has a negative surface charge stemming from anionic polymers (WTA and LTA), as described in the details chapter (1.7). The phosphate group in teichoic acids providing the negativity of the surface charge (Dickson and Koohmaraie, 1989). Dalanylation of teichoic acid modulates the cell's surface charge and reduces its overall negativity. In this respect it is well known that the charge on the cell surface influences pathogenic bacterial interactions with the host immune system, for example changing the susceptibility to antimicrobial peptides (AMPs) and the entrance of metabolites into cells (Bar-Even *et al.*, 2011; Goulter, Gentle and Dykes, 2009; Yeung and Grinstein, 2007).

The mechanisms of action underlying the antimicrobial activities of AMPs are varied, but a topic that has received considerable interest is their intracellular inhibitory activities and/or their membrane-lytic action. Furthermore, the modulation of bacterial surface charge in B. subtilis through the addition or removal of D-Ala from teichoic acid components has been shown to significantly influence bacterial susceptibility to AMPs (Assoni et al., 2020). The dltABCD operon encodes a set of proteins known to mediate lipoteichoic acid D-alanylation of LTA in both S. aureus and B. subtilis as described in Section 1.9. The D-alanylation of LTA is required for the WTA Dalanylation (Reichmann, Cassona and Gründling, 2013). As pointed out in the introduction (section 1.9), it's unclear how the D-alanine transferred from LTA to WTA. Interestingly, FmtA protein in S. aureus has been implicated in teichoic acid Dalanylation but it hydrolyses off the D-alanine from the teichoic acids (Qamar and Golemi-Kotra, 2012) (Fig 5.1). Given FmtA's role in teichoic acid D-alanine hydrolyses and its influence on cell surface charge (Collins et al., 2002; Rahman et al., 2016)., it is intriguing to note the structural similarities between FmtA and another protein of interest, PBPX in B. subtilis. As a homologous protein, PBPX could potentially

contribute to similar processes, thus warranting a deeper investigation into its function and its relationship with proteins like FmtA.

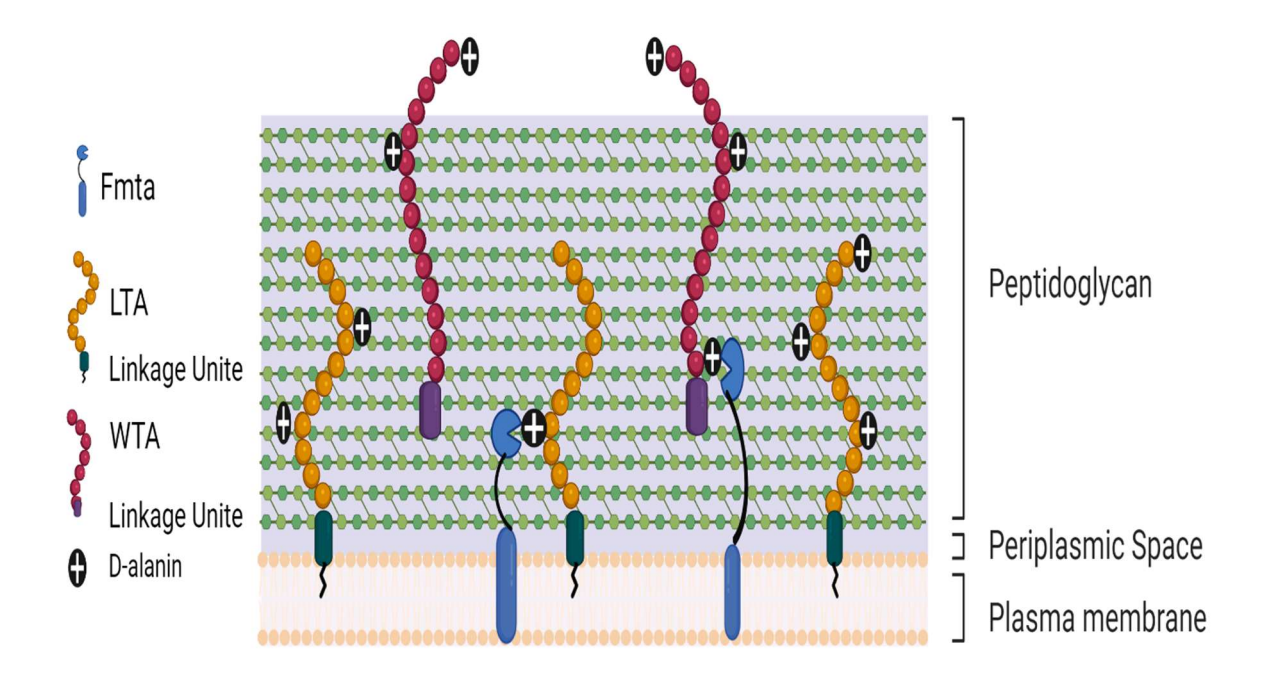


Figure 5.1: The function of the FmtA protein.

The schematic shows the FmtA protein anchored to the cell membrane and the catalytic domain extending to the outer side, where it functions. The FmtA protein (blue) hydrolyses the phosphodiester bond and cleaves D-Ala from LTA (yellow) and WTA (red).

5.2 Results

5.2.1 Comparative Analysis of PBPX and Related Proteins Across Multiple Bacterial Species

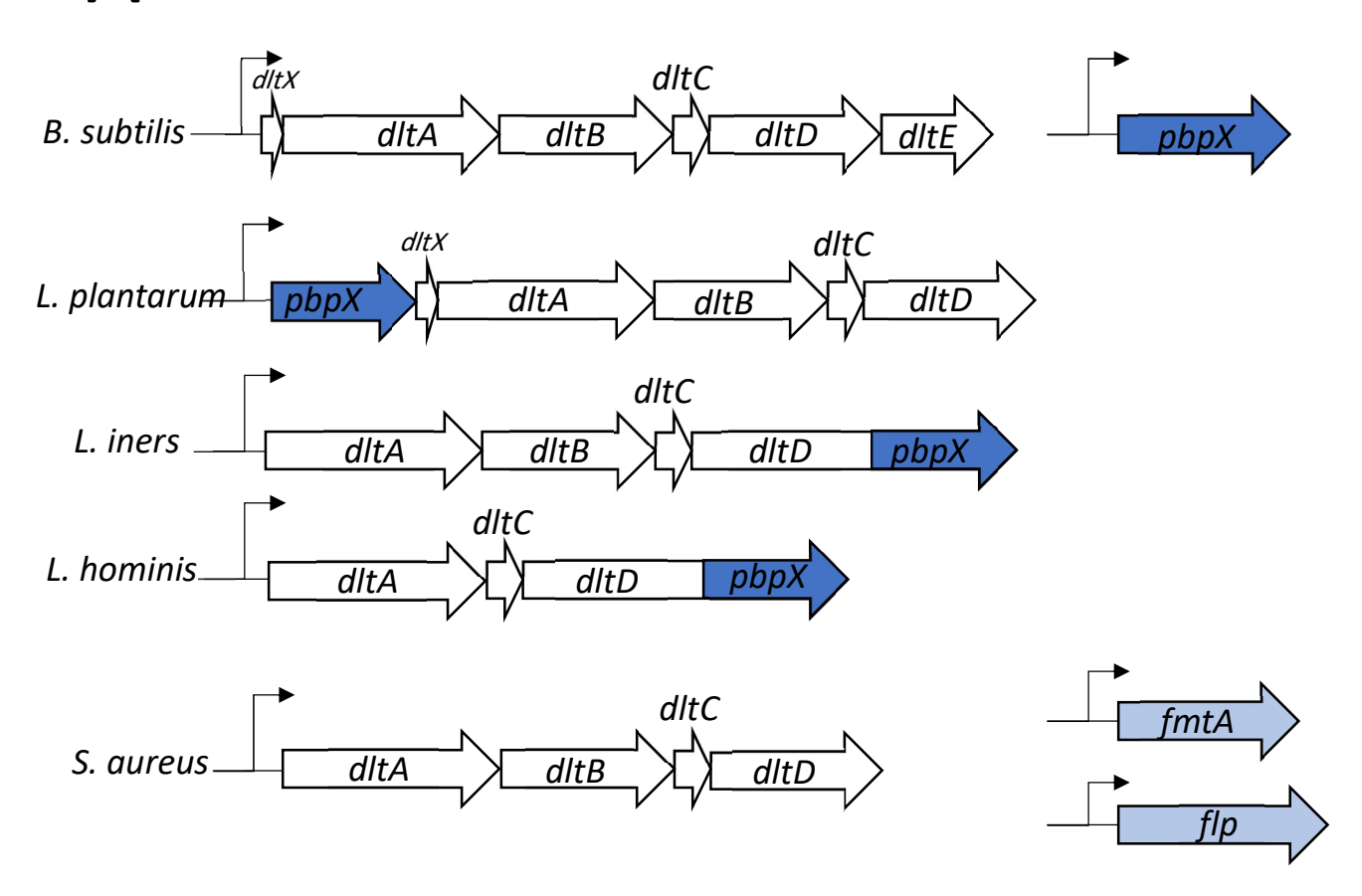
From the described in chapter 3 (3.2.1) it was notable that although *pbpX* had been annotated as encoding a PBP and transcriptional data suggested that it was expressed under most growth conditions. However, no corresponding penicillin binding protein could be identified by bocillin-FL labelling combined with SDS-PAGE. Thus, it seemed that PBPX may have been misannotated. To address this the amino acid sequence of PBPX was used to search the National Centre for Biotechnology Information (NCBI) database using the BLAST tool and STRING database (https://string-db.org/) to identify proteins with similarity to PBPX from *B. subtilis* and provide an indication of genetic context. Through these methods, several bacterial species containing PBPX-like proteins were identified, of these most similar proteins that were from model bacteria were chosen for further analysis, specifically those identified in *Lactobacilli* and *S. aureus*. Interestingly, in some bacterial species, the PBPX-like protein was named PBPX, while others had β-lactamase-like protein names or completely different names, presumably reflecting differences in the bioinformation annotation pipelines used on submission (Fig 5.2A).

Looking in more detail at the gene with similarity to PBPX in *B. subtilis*, and their genetic context in other bacterial species, the potential homologues in Lactobacilli became particularly interesting. One such protein also named PBPX2, was identified in *Lactobacillus plantarum*, with a similarity score of 136 (Fig 5.2B); based on the STRING database, where a bit score above 60 is considered to indicate that there is a lower probability of the similarity occurring by chance. In *L. plantarum*, *pbpX2* was found to be located in the same operon as *dlt* genes, specifically, upstream of the *dlt* genes and right before *dltX*, as shown in Figure 5.2A. Another protein showing high similarity was found in *Lactobacillus iners*. Its similarity score to PBPX was 108 (Fig 5.2B), and this PBPX-like protein was named β-lactamase. Interestingly, the coding sequence for this gene was located at the end of the *dlt* operon and the protein was found to be fused to the downstream of that had significant similarity to DltD (Figure 5.2A). Similarly, in *Lactobacillus hominis*, the PBPX-like protein was found to be fused

with the dltD coding sequence. Its similarity score to PBPX from B. subtilis was (106) (Fig 5.2A&B). Finally, two proteins from S. aureus, FmtA and Flp, were found to share significant similarity (over 60%, with a 120-bit score) with PBPX from B. subtilis (Figure 5.2B). The primary structure of both FmtA and PBPX resembles that of serine-active-site PBPs and β-lactamases, particularly hydrolase class C β-lactamases (Rahman et al., 2016; Straume et al., 2021), suggesting a similar function for these proteins. In contrast, less is known about the Flp protein. Studies indicate that it is non-essential and does not bind penicillin (Komatsuzawa et al., 2000). However, its inferred amino acid sequence is similar to that of PBPs and S. aureus FmtA, with notable conservation in three motifs found in PBPs and β-lactamases.

In the rest of this chapter, the function of PBPX is explored on the basis that it exhibits significant similarity to *S. aureus* FmtA (Rahman *et al.*, 2016; Zhao *et al.*, 2012), which has been extensively characterised and Flp where characterisation has only been partially explored, with no definite conclusion as to its function.





B

S. aureus flp L. plantarum L. iners L. hominis B. subtilis S. aureus fmtA

Figure 5.2: Proteins homologous to PBPX from *B. subtilis* in various bacterial species and their sequence alignments.

A) Location of *B. subtilis pbpX*-like genes in *L. plantarum*, *L. iners*, *L. hominis* and *S. aureus*. The *pbpX*-like genes are in blue boxes, with similar proteins having different known names, like FmtA and Flp, in light blue. B) Sequence alignments of PBPX-like proteins. Amino acids shaded in dark purple are identical, while those in light purple are similar. Structural models of PBPX homologs were predicted using AlphaFold to assess conservation of active site architecture. The *L. hominis* alignment represents the C-terminal half of the protein.

5.2.2 Minimal inhibitory concentration of the AMP CAMA against *B. subtilis* 168 and *S. aureus* Je2

Given the significant similarity between PBPX of B. subtilis and FmtA and Flp of S. aureus, we examined the phenotypic consequences of the null mutants in both bacterial species. To characterize the sensitivity to the cationic AMP CAMA, we first determined the minimal inhibitory concentration (MIC) of CAMA for the wild-type strains of B. subtilis (strain 168) and S. aureus (strain Je2). Strain 168 was grown in LB medium with different concentrations of CAMA (1–10 µM) in 10 wells of a 96-well plate and incubated at 37 °C for about 5 hours, while strain Je2 was grown in TSB medium with 5–20 µM CAMA under the same conditions. The utilization of distinct media, namely LB for B. subtilis and TSB for S. aureus, was necessary in order to optimize the growth conditions for each species, taking into account their unique physiological and nutritional needs. LB medium is highly suitable for the growth of B. subtilis due to its abundance of nutrients, which promotes its rapid proliferation. On the other hand, TSB medium, with its well-balanced composition, facilitates vigorous growth of S. aureus. This method ensured consistent patterns of growth, enabling precise evaluation of CAMA's inhibitory effects. Growth was measured every 5 minutes, and the optical density readings were plotted against time to generate growth profiles under the different conditions (Fig. 5.3).

For *B. subtilis* there was a clear retardation of the strains ability to grow as the concentration of CAMA increased from 1 μ M to 4 μ M, but at 5 μ M and above all

growth seemed to be inhibited over the period of the assay. This indicated that 5 μ M was the minimum concentration necessary to block growth of the initial inoculum of *B. subtilis*. At lower concentrations it must be assumed that it is either sufficient to prohibit the growth of a proportion of the cells, but not all. Thus, over time the cells still alive are able to grow and eventually result in an increase in the optical density. Thus, in the presence of 4 μ M of CAMA, the culture to 220 min before there was an observable increase in optical density. Whereas, in the presence of 3 μ M, 2 μ M and 1 μ M CAMA, a shorter period of time was required before growth was detected (165, 110 and 55 minutes respectively; Figure 5.3A).

A similar effect was seen to *S. aureus* strain Je2, although the effective concentration of CAMA was different. Here, strain Je2 was killed by 12.5 μ M and above; however, at lower concentrations, it showed growth after a delay that was proportional to the concentration of CAMA. A 10 μ M CAMA concentration delayed Je2 growth to approximately 233 minutes and 7.5 μ M delayed Je2 growth to approximately 180 minutes. Je2 required around 116 minutes to develop detectable growth in the lowest concentration used (5 μ M); see Figure 5.3B).

The results determine the minimum inhibitory concentration (MIC) of CAMA for wild-type *B. subtilis* and *S. aureus*, which serves as a fundamental measure of sensitivity for comparing the impact of mutations on bacterial resistance. This data will enable further examination of how particular genetic mutation influences the susceptibility of these bacteria to CAMA in coming results in this chapter.

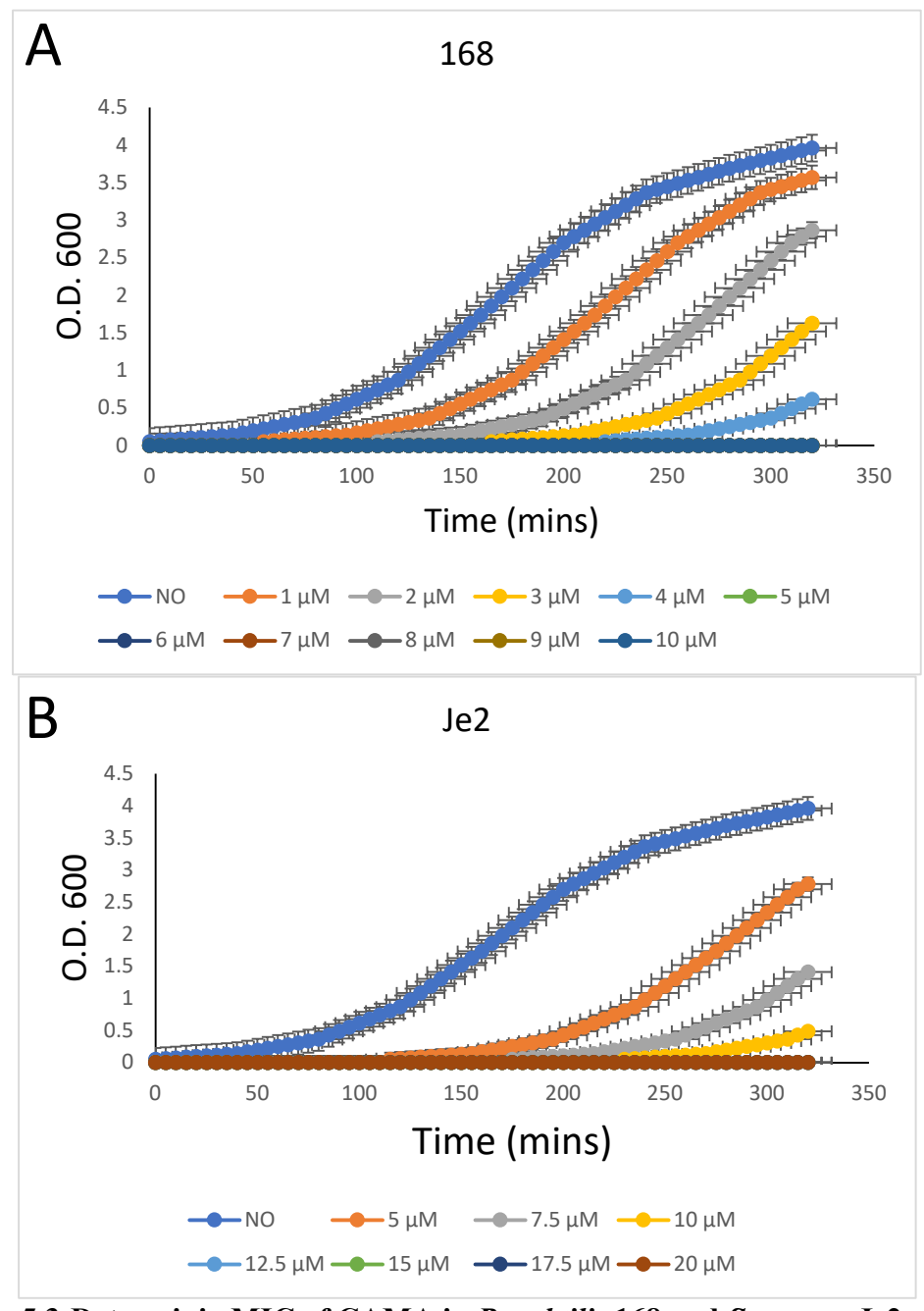


Figure 5.3: Determinig MIC of CAMA in B. subtilis 168 and S. aureus Je2

A) The charts above show the growth of 168 in LB with different concentration of CAMA (0- 10 $\mu M)$ to determine the MIC of CAMA. B) The growth of Je2 with different concentration of CAMA (0 - 20 $\mu M)$. The experiment was repeated 3 independent times and the error bar represent the SD.

5.2.3 Deletion of *pbpX* or *dltAB* increases *B. subtilis* sensitivity to the cationic AMP CAMA.

After determining the minimum inhibitory concentration (MIC) of CAMA at 5 µM for the wild-type B. subtilis strain 168, the investigation was extended to assess the effects of deleting the pbpX or dltAB genes on bacterial sensitivity to CAMA. Using the same method as described in the earlier (section 5.2.2) but with different starting concentrations of CAMA (0, 2.5, 5, and 10 µM). Experiments were conducted to compare the selectivity of the wild-type strain 168, $\triangle dltAB$ (YA46), and $\triangle pbpX$ (YA44) to CAMA. The strains were cultured in LB medium with an OD600 of 0.1 after the MIC of 5 μ M was established. These strains were then diluted in 0, 2.5, 5 and 10 μ M of CAMA. At CAMA concentrations of 0, bacterial growth in all three strains was observed; however, at concentrations of 2.5 µM the only strain was able to grow was the 168 but the Δdlt and $\Delta pbpX$ were not able to grow at that concentration. Strain 168 showed delay in bacterial proliferation and bacterial growth at 2.5 µM, for approximately 150 minutes (Figure 5.4). However, at 5 and 10 μM, no strain showed growth. These data were reproducible, and the plot show the average of three independent experiments. These findings imply that, in comparison to strain 168, strains $\triangle dltAB$ and $\triangle pbpX$ were significantly more sensitive to CAMA. The apparent regrowth seen on prolonged incubation of the cultures probably suggests that there are some surviving cells on initial treatment or that the AMP gets degraded with time and perturbed cells can grow once the inhibitory compound is removed. This in a way emphasises the increase sensitivity of the deletion mutants and hints a subtle difference between pbpX, where limited regrowth was observed, and dltAB where this did not seem to occur under the conditions used.

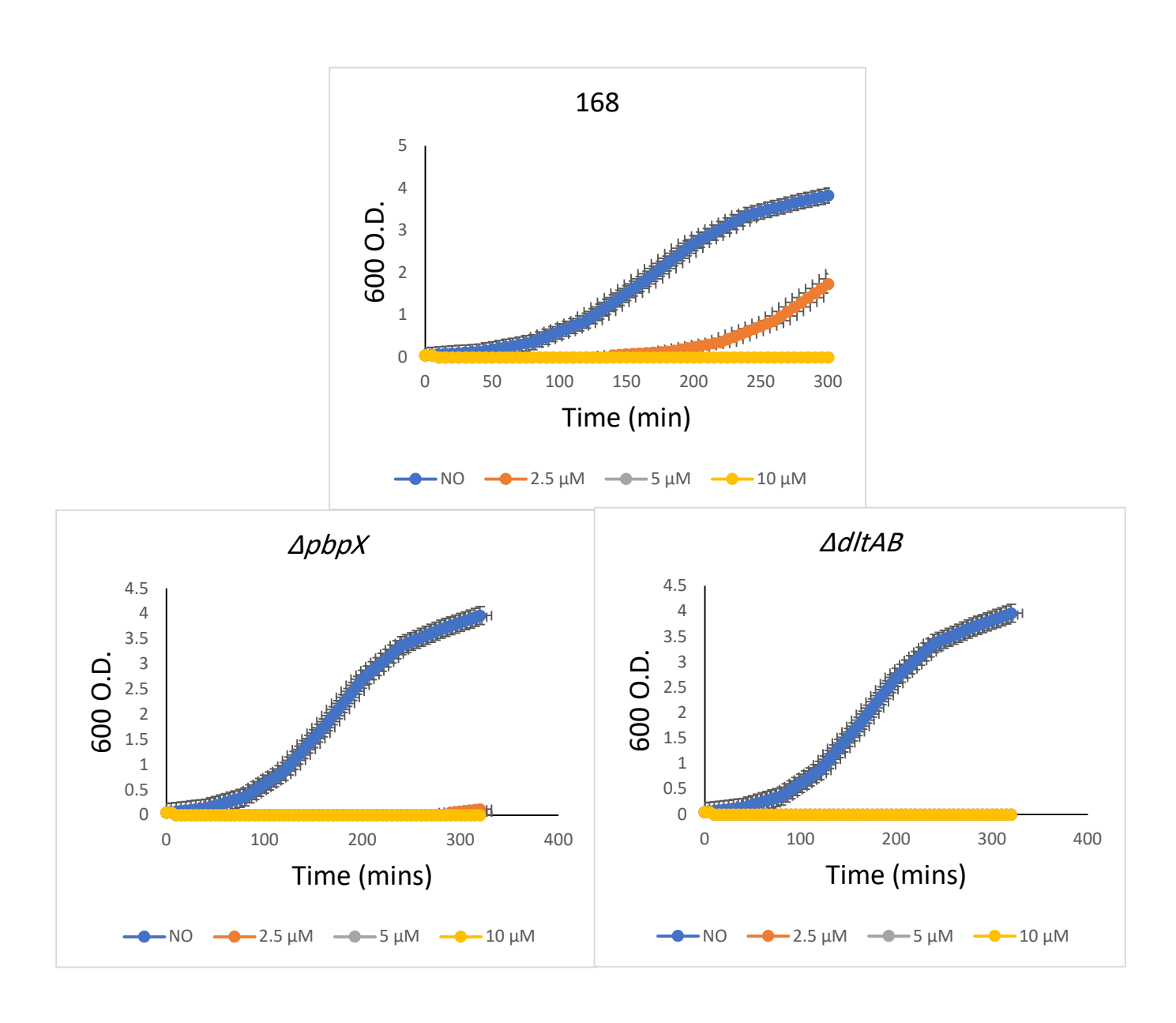


Figure 5.4: Sensitivity of 168, Δ pbpX and Δ dltAB to the cationic antimicrobial peptide CAMA.

Cell growth with the addition of different concentrations of CAMA: none (blue), 2.5 μ M (orange), 5 μ M (grey) and 10 μ M (yellow). Strain 168 is at the top, $\Delta pbpX$ is in the middle and $\Delta dltAB$ is at the bottom. The y-axis represents the time in minutes, while the x-axis represents the absorbance at OD600.

5.2.4 Deletion of *fmtA* and *flp, in S. aureus*, have opposite effects in relation to sensitivity to cationic AMPs

As previously shown, at 12.5 μ M, CAMA could inhibit the bacterial growth of S. aureuss (section 5.2.2). The MIC was both assessed visually and quantified using a turbidity analysis on the plate reader. All samples were tested in duplicate/triplicate (n = 2 or 3) to assess the reliability of the results. Following the determination of the MIC using the CAMA AMP on S. aureus, the growth of three strains of S. aureus, namely Je2 (wild type), fmtA and flp was assessed with different concentrations of CAMA (0, 6.25, 12.5, 25 and 50 μ M). The Je2 strain at 6.25 μ M was able to grow after delaying in growth for approximately 150 minutes but at high concentration of CAMA (12.5, 25 and 50 μM), no cells grew in the Je2 strain. On the other hand, fmtA strain at 6.25 μM was able to grow earlier than Je2 after about 100 minutes and in 12.5 and 25 µM CAMA, it was also able to grow after approximately 150 and 250 minutes respectively. It was only when the ΔfmtA strain was exposed to 50 μM CAMA that it showed no growth. This implies that the loss of FmtA results in the bacteria being able to tolerate the presence of the AMP at significantly higher concentrations. In contrast, the Δflp strain was unable to grow even at lower concentration of CAMA 6.25 µM (Figure 5.5). Consistent with previously published data, deleting *fmtA* results in increased resistance to the AMP (CAMA), whereas the flp mutation results in significantly increased sensitivity to the AMP (Figure 5.5). A phenotype that is rather similar to that seen for the pbpX mutation in B. subtilis.

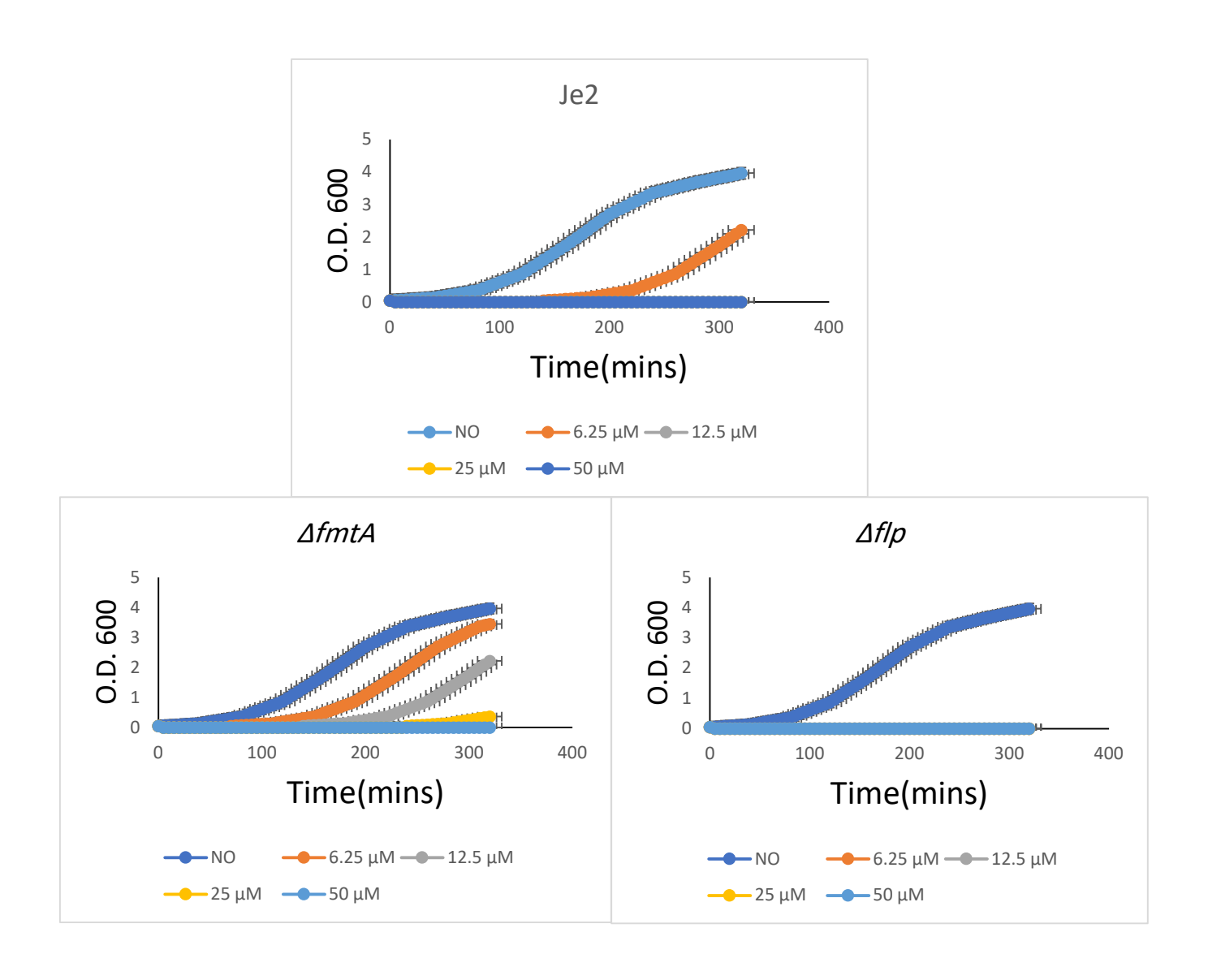


Figure 5.5: Sensitivity of Je2, Δ FmtA and Δ Flp to the cationic antimicrobial peptide CAMA.

Cell growth with the addition of different concentrations of CAMA: none (dark blue), 6.25 μ M (orange), 12.5 μ M (grey), 25 μ M (yellow) and 50 μ M (light blue). Je2 is at the top, Δfmt A is in the middle and Δflp is at the bottom. The y-axis represents the time in minutes, while the x-axis represents the absorbance at OD600.

5.2.5 Deleting *pbpX* or *dltAB* increases the cell capacity to bind a cationic fluorescent label but decreases binding to an anionic fluorescent label

To further investigate the potential reasons behind the CAMA sensitivity results (5.2.3), a crude test to determine the surface charge was used. Here the binding of a fluorescently charged polymer to the cells was determined (method section 2.17). Briefly, exponentially growing cells of the strains 168, Δ*pbpX* and Δ*dlABt* were exposed to dilute solutions of poly-L-lysine–fluorescein isothiocyanate (poly-L-lysine–FITC; cationic) or dextran tetramethylrhodamine (anionic) in PBS for a short period. The cells were then washed with PBS to remove any unbound dye and, the bacterial cells were prepared for microscopy examined for fluorescence. Characteristic images of cells of each strain are shown in Figure 5.8. Where Poly-L-lysine was used, a fluorescence signal for all strains was clearly detectable. In contrast, the dextran did not result in any significant cell labelling (Figure 5.8B). This seemed to be consistent with the idea that the bacterial cell surface has a net negative charge and hence only a positively charge polymer is bound.

Notably, the $\triangle dltAB$ mutant displayed higher fluorescence per unit area than the $\triangle pbpX$ mutant, indicating a more pronounced alteration in surface charge or polymer-binding properties. Since DltAB is responsible for incorporating D-alanine into teichoic acids, its deletion results in a more negatively charged cell surface, which is known to enhance electrostatic interactions with cationic antimicrobial peptides (AMPs), potentially increasing susceptibility to AMP-mediated killing. Similarly, the $\triangle pbpX$ mutant also exhibited altered surface charge, though its precise contribution to AMP sensitivity requires further investigation.

These findings support the initial idea that *pbpX*, like *dltAB*, plays a role in regulating bacterial surface charge, which may influence interactions with host immune defenses and antimicrobial compounds.

.

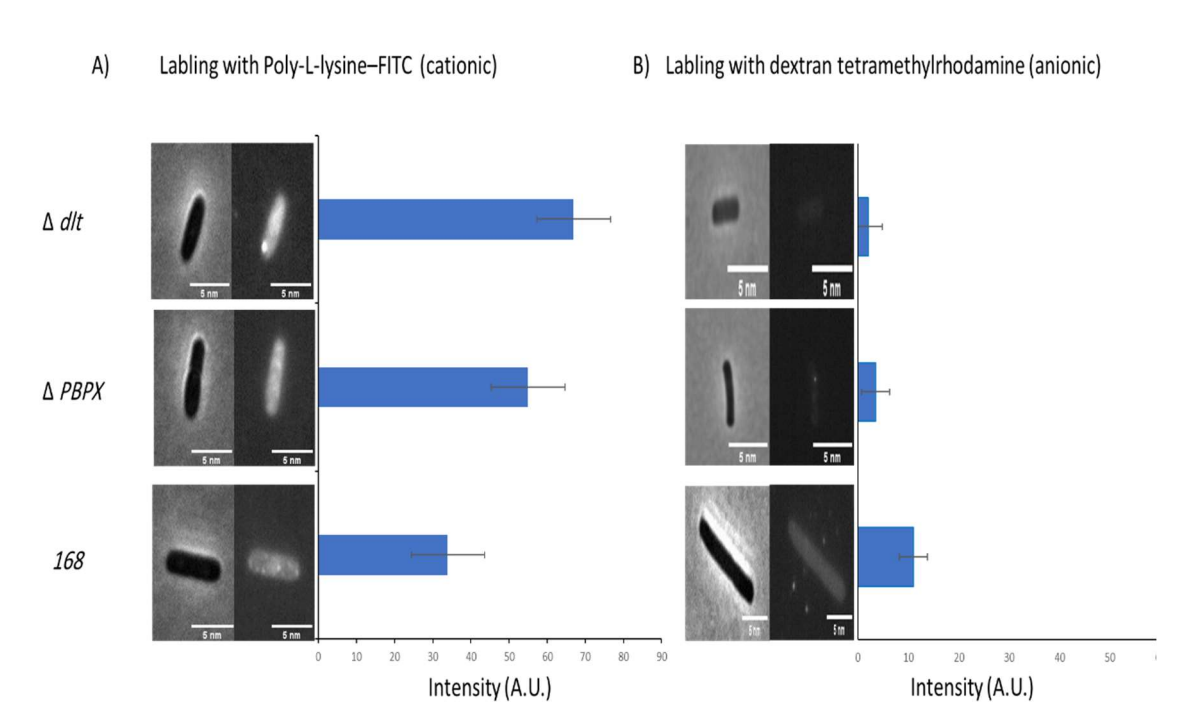


Figure 5.6: Labelling of 168, $\Delta pbpX$ and Δdlt with cationic and anionic fluorescent-tagged chemicals.

Labelling of 168, $\triangle pbpX$ and $\triangle dlt$ with poly-L-lysine-FITC (cationic) or dextran tetramethylrhodamine (anionic). A) Labelling of 168, $\triangle pbpX$ and $\triangle dlt$ with poly-L-lysine-FITC (cationic). The brightfield image is on the left, the fluorescent image is on the right and the bar chart represents the fluorescence intensity for 50 cells of each strain. B) Labelling of 168, $\triangle pbpX$ and $\triangle dlt$ with dextran tetramethylrhodamine (anionic). The brightfield image is on the left, the fluorescent image is on the right and the bar chart represents the fluorescence intensity for 50 cells of each strain.

5.2.6 Deleting *pbpX* or *dltAB* shifts the cell surface charge towards negative in *B. subtilis*

As the charged polymer labelling was a relatively crude assay for cell surface charge, a more direct measurement was used by measuring the how an electric field influenced the motion of bacterial cells in suspension using a Zetasizer (Malvern Instruments). This provided a precise measurement of the charge on the cells under the conditions used (deletion of genes of interest). Here a set of strains were analysed where the mutations introduced were known to result in specific changes in the cell wall composition and should have specific effects. The first of these was a strain deleted for tagO and so unable to produce of WTA and would be expected to have a reduced surface charge due to the absence of the wall bound phosphate-based polymers (Brown, Santa Maria and Walker, 2013; D'Elia et al., 2006). To contrast with this strain, a strain selective in LTA synthesis was also analysed, YA45 (\(\Delta 1 ta 3 \)), this would be expected to result in an increased surface charge as the absence of LTA would prevent D-ala modification of the WTA (Reichmann, Cassona and Gründling, 2013). Finally, strain YA46 was deleted for *dltAB* and hence unable modify the TA by adding D-alanine resulting in a similar effect to that of the strain lacking LTA (Kovács et al., 2006). Although, in this case, it was possible that presence of both LTA and WTA combined with the absence of the D-ala modification might result in a higher net negative charge. The idea being that these strains would provide reference points to relate values obtained for a strain with the *pbpX* mutation.

For the charge determination, exponentially growing cells were analyzed as 1 ml samples of culture in Zetasizer cuvettes. Since the bacteria grew in LB medium to the exponential phase, the composition of the medium, particularly the NaCl concentration, could influence the cell surface charge by masking negative charges and reducing cell repulsion. To mitigate these effects and ensure that the intrinsic cell surface charge was accurately measured, samples were washed and resuspended in Milli-Q water before analysis.

After these preparations, the study revealed that the cell surface charge of bacterial strain 168 was slightly negative, at -12.3 mV. However, following the deletion of pbpX, a significant shift toward a more negative charge, at -35.5 mV, was observed.

Additionally, deletion of *dltAB* in strain YA46 resulted in an even greater increase in negativity, with a charge of –42.4 mV. Similar trends were observed in the *lta* and *tagO* strains, which also showed a greater negative charge compared to the 168 strain.

The results suggested that deleting *pbpX*, *dltAB*, *Lta* (the triple mutant (YA45)), *and tagO*, genes lead to a significant increase in the negativity of the cell surface charge. The most pronounced shifts were observed with deletions of *dltAB* and *pbpX*, suggesting that PBPX, in particular, plays a crucial role in modulating cell surface charge, likely through its interaction with D-alanine modifications on teichoic acids (WTA and LTA). This shift in cell surface charge is significant as it may influence various physiological processes, especially resistance to antimicrobial agents. These align with the CAMA sensitivity results in section 5.2.3.

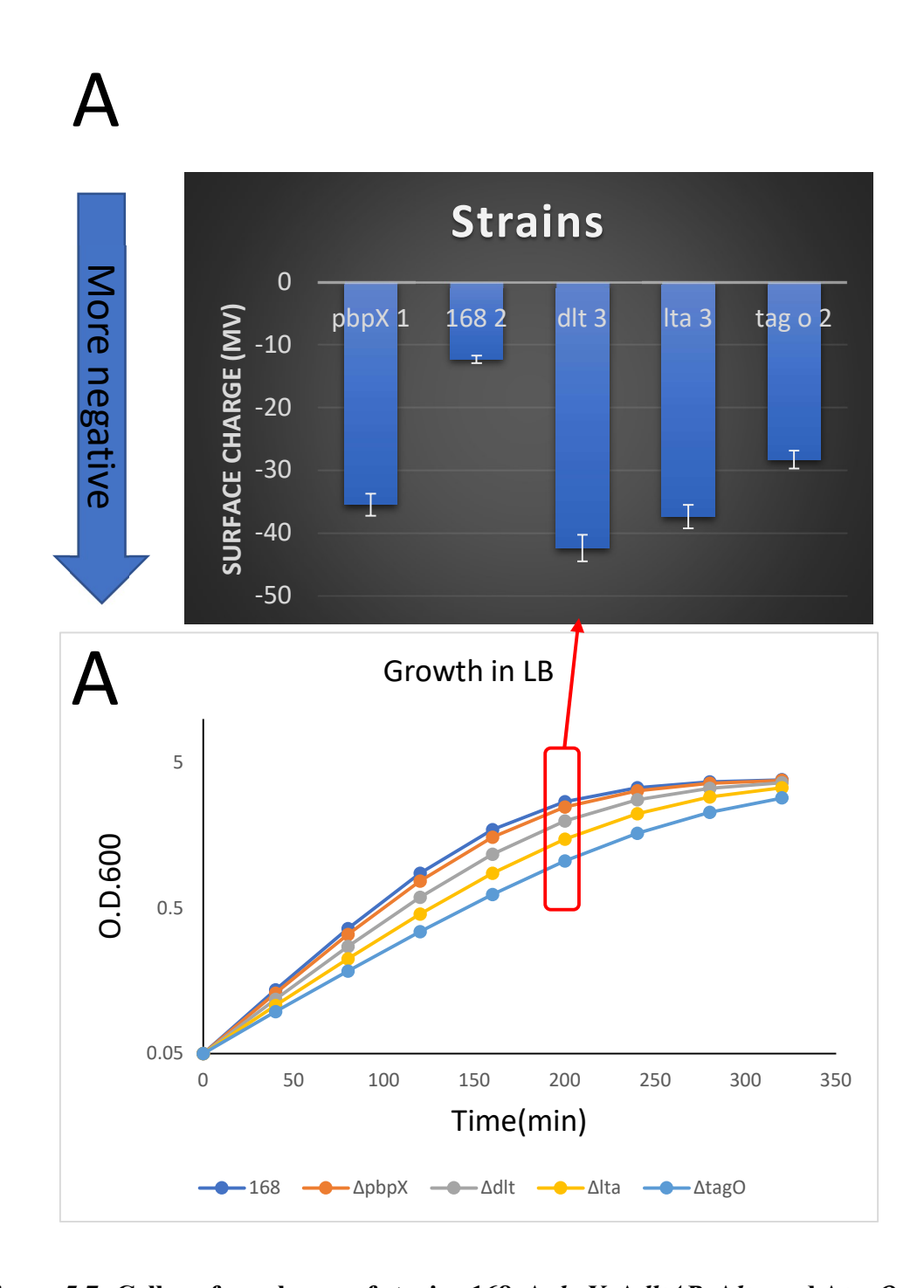


Figure 5.7: Cell surface charge of strains 168, $\Delta pbpX$, $\Delta dltAB$, Δlta and $\Delta tagO$.

The Zetasizer machine was used to assess the cell surface charge of 168, $\Delta pbpX$, $\Delta dltAB$, Δlta and $\Delta tagO$. A) The cell surface charge is measured in mV and any negative values go below 0 on the scale. From left to right, the cell surface charge is shown for strains $\Delta pbpX$, 168, $\Delta dltAB$, Δlta and $\Delta tagO$. B) The growth curve for $\Delta pbpX$, 168, $\Delta dltAB$, Δlta and $\Delta tagO$. The point at which the samples were collected to measure the cell surface charge is shown (red box).

5.2.7 Deleting *fmtA* decreases cell surface charge negativity but deleting *flp* increases it in *S. aureus*

To determine if deletion of fmtA and flp in S. aureus had any effect on cell the surface properties the Zetasizer method used above was used for the strains $\Delta fmtA::kan$ and $\Delta flp::kan$, along with the wild-type strain Je2. In this case, the culture medium was changed to tryptic soy broth, and mid-exponential and stationary phase cells were analyzed. Each bacterial strain was grown at 37 °C and the cells were washed and suspended in Mili-Q water immediately before measurement.

The Je2 strain had a negative cell surface charge in both the mid-exponential and stationary growth phases at -18 and -21 mV respectively. In the deleted *fmtA* strain, the cell surface charge was comparable to the Je2 with slightly less negative in the mid-exponential phase at -17 mV and stationary phase at -19 mV. This was expected as the FmtA hydrolyses the D-alanine, which has the positive charge, from the teichoic acid. Surprisingly, the strain with deleted *flp* showed significant increase negativity of the cell surface charge in both mid-exponential at -22 mV and stationary phase at -27 mV compared to the wild type Je2 (Figure 5.7).

while the *fmtA* deletion showed predictable effects on cell surface charge, the deletion of *flp* revealed a more pronounced impact, indicating a possible new role for this protein in the regulation of cell surface charge in the Je2 strain and probably through the Dalanine on the teichoic acids which will be investigated in the next results section 5.2.9.

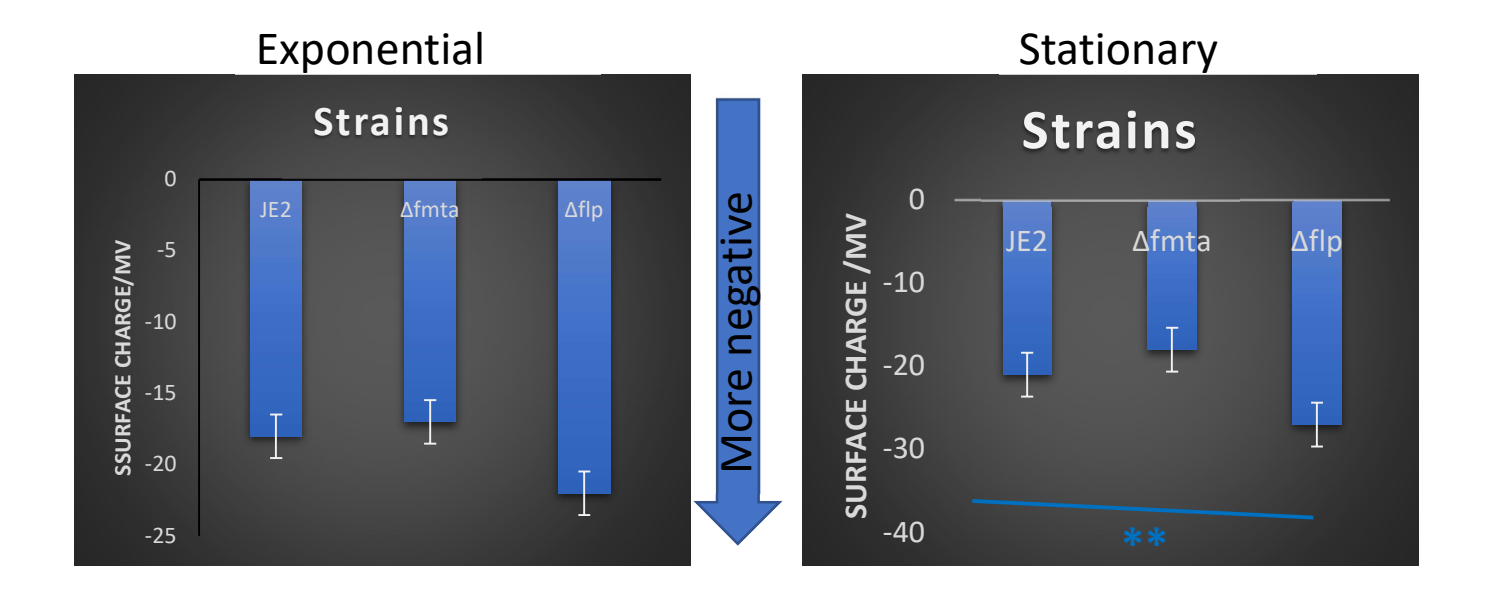


Figure 5.8: Cell surface charge of Je2, $\Delta fmtA$ and Δflp analysed using the Zetasizer machine.

A) Cell surface charge is measured in mV and any negative values go below 0 on the scale. Cell surface charge during the exponential phase (left) and stationary phase (right). From the left to the right, the cell surface charge for strains Je2, $\Delta fmtA$ and Δflp is shown. ** The data represent three independent experiments, and the P value was < 0.005.

5.2.8 Determination of the distribution of D-ala on the teichoic acids in the cell envelope

The impact of pbpX deletion on the D-alanylation of LTA and WTA was investigated by isolating WTA and LTA through distinct extraction methods, followed by hydroxide release of D-alanine and subsequent quantification via an enzymatic assay. Detailed methods are provided in Chapter 2, Section 2.30. Initially, LB medium was inoculated with fresh colonies of strains 168, $\Delta pbpX$, Δdlt , Δlta , and $\Delta tagO$, all of which are known to exhibit specific changes in cell wall composition.

The $\triangle dlt$ mutant served as a negative control, as it lacks D-alanine attachment on teichoic acids. Similarly, the $\triangle lta$ strain, which is blocked in LTA synthesis, should also show no D-alanine in the extracts. In contrast, the tagO null strain, lacking WTA, was expected to show D-Ala attached only to LTA, potentially at higher levels due to the absence of WTA. Comparing these results to those of the $\triangle pbpX$ strain allowed us to assess the role of PBPX in D-alanylation.

Cultures were grown to mid-exponential phase, and samples were standardized by dry weight to ensure valid comparisons. However, variations in wall composition due to mutations introduced some expected errors.

For WTA analysis, bacterial strains were boiled in SDS to remove soluble material, leaving peptidoglycan with attached WTA. This was treated with NH₄OH to detach D-Ala. For LTA analysis, total cellular material was extracted with 1-butanol, followed by NH₄OH treatment to remove D-Ala. The D-Ala content was quantified using an Abcam kit (ab239721) in a 96-well plate reader, and concentrations were expressed as μ M per mg of sample (Chapter 2, Section 2.31).

In strain 168, D-Ala levels associated with LTA were marginally higher than those linked to WTA. Both Δdlt and Δlta strains exhibited negligible D-Ala amounts in both LTA and WTA samples, as expected. The tagO samples posed a complex issue due to the absence of a significant cell wall component, potentially leading to an overestimation of D-alanine. However, the measured values aligned with predictions.

In contrast, the $\Delta pbpX$ strain showed a significant increase in LTA-related D-Ala compared to WTA, suggesting that the loss of PBPX impairs the transfer of D-Ala from LTA to WTA.

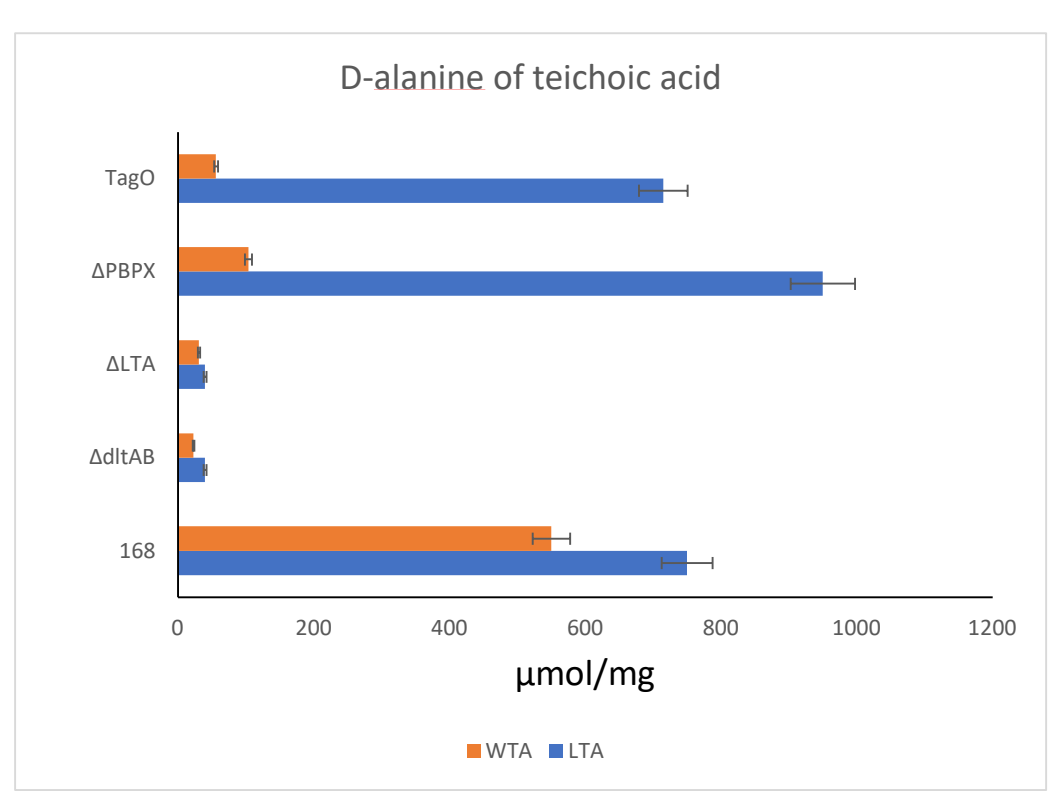


Figure 5.9: D-alanine assay for Wall or membrane bound samples

The bar chart shows the D-Ala associated (μ mol per mg of dry cell wall material) with WTA (orange bar) and LTA (blue bar) in 168, $\Delta pbpX$, Δdlt , Δlta and $\Delta tagO$. The data represent three independent experiments, and the error bars represent the standard deviation of each dataset relative to the mean.

5.2.9 The effect of *fmtA* or *flp* deletion on D-Ala associated with LTA and WTA in *S. aureus*

As Using the same methodology as applied to *B. subtilis* samples, we were able to crudely fractionate *S. aureus* cells and determine D-alanylation of the teichoic acids. However, a more limited set of mutant strains was available due to the lethality of certain gene deletions (specifically the LTA null strain) or the unavailability of isogenic strains, such as the *tagO* and *dlt* null mutants, which are suggested to be essential in some *S. aureus* strains. As a compromise, the work focused on the Je2 background and the two mutants *fmtA* and *flp*, both of which were transposon insertion mutations in Je2 from the Nebraska collection (Table 2.1). For these three strains, samples representing WTA and LTA were generated as previously described, and the amount of D-Ala released under alkaline conditions was determined for each sample (Figure 5.11).

The data in Figure 5.11 indicate that in the Je2 strain, the concentration of D-Ala in the LTA extracts was approximately 600 μ mol/mg, while in the WTA extracts, it was around 400 μ mol/mg. The $\Delta fmtA$ strain exhibited a similar pattern but with elevated levels of D-Ala in both LTA (~750 μ mol/mg) and WTA (~500 μ mol/mg). This suggests that the absence of FmtA leads to increased D-alanylation of both LTA and WTA.

A notable disparity was observed when comparing the *fmtA* and *flp* mutants. The *fmtA* mutant displayed D-alanine levels comparable to the wild-type strain, measuring approximately 750 μmol/mg in LTA and 500 μmol/mg in WTA. On the other hand, the *flp* mutant exhibited a notable decrease in D-Ala linked to WTA, with levels dropping below 100 μmol/mg. However, the D-Ala levels in the LTA extracts (~800 μmol/mg) were comparable to or slightly higher than those in the other strains.

The noticeable decrease in WTA-bound D-Ala in the Δflp strain, along with the consistently or slightly increased levels of D-Ala in LTA, indicates that Flp has a distinct function in the D-alanylation of WTA. The Δflp strain displayed the least amount of D-Ala content in WTA in comparison to the other two strains, indicating that Flp plays a vital role in the appropriate modification of WTA through D-alanine (Figure 5.11).

These findings indicate a clear similarity between the *flp* null mutant of *S. aureus* and the *pbpX* null mutant of *B. subtilis*, particularly in how the deletion of these genes affects the D-alanylation of teichoic acids. Both mutants show a disrupted D-Ala distribution, which may indicate a shared role of these proteins in the regulation or localization of D-Ala attachment to WTA.

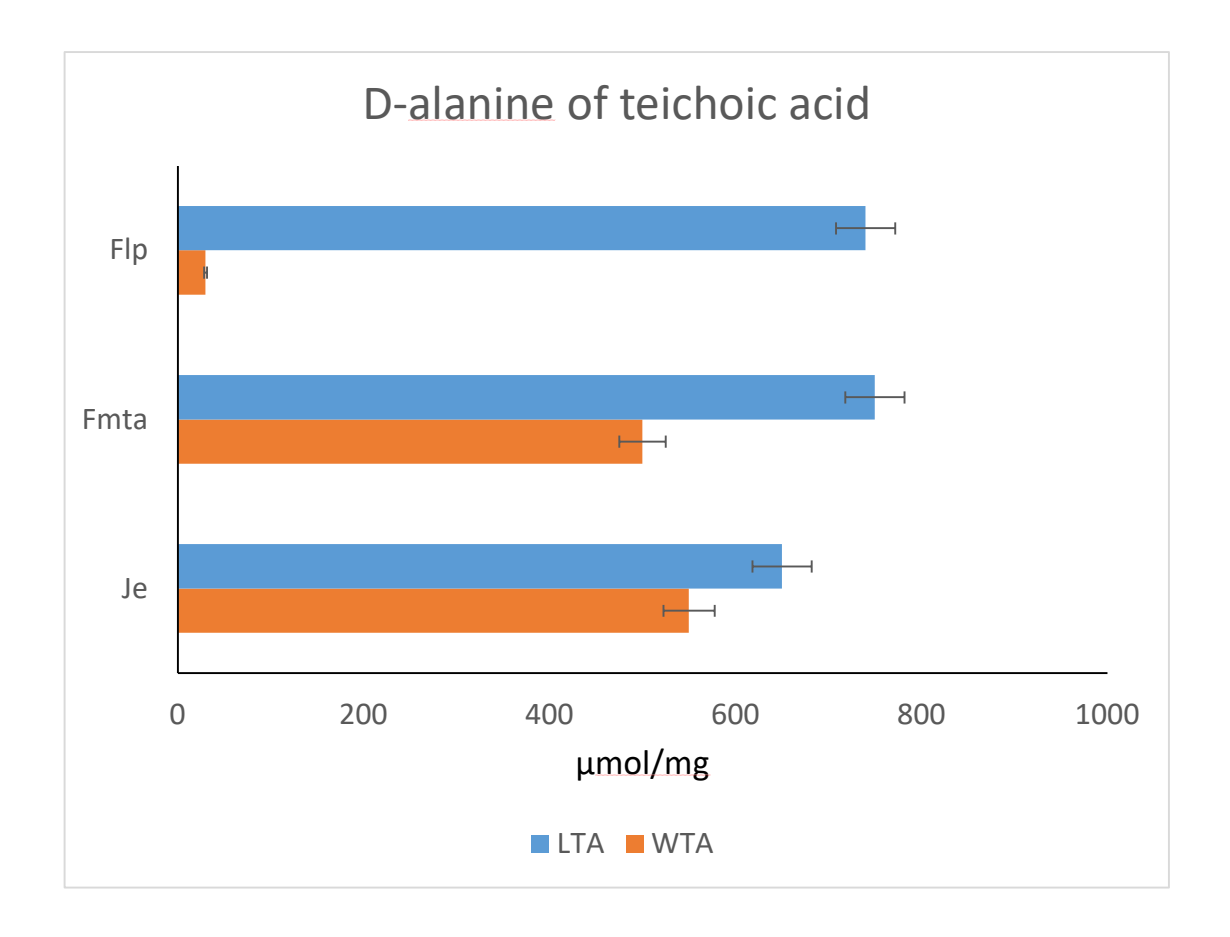


Figure 5.10: D-alanine assay for Je2, $\triangle fmtA$ and $\triangle flp$.

The bar chart shows the D-Ala associated (μ mol per mg of dry cell wall material) with WTA (orange bar) and LTA (blue bar) in Je2, $\Delta fmtA$ and Δflp . The data represents three independent experiments, and the error bars represent the standard deviation of each dataset relative to the mean.

5.2.10 Deleting *pbpX*, *dltAB* or *LTA* decreases cell envelope rigidity compared to the wild type

Saar-Dover and colleagues (2012) found that blocking LTA D-alanylation reduced the rigidity of the Streptococcal cell wall as measured by AFM analysis, and unblocking it restored bacterial envelope stiffness. To determine whether this effect was specific to this bacterial species or potentially a general feature of Gram-positive bacteria, a similar set of experiments was carried out on *B. subtilis* strains. It was also particularly interesting to determine whether this change in the properties of the cell wall was mediated by LTA or WTA. In this respect, the deletion of *pbpX* potentially provided the genetic means to answer this question. As a starting point, it was important to confirm that the AFM analysis was performed on cells mounted in a way that preserved viability. The original method described in Chapter 2, Section 2.18, was used to prepare the samples for AFM, with some minor modifications adapted from Edmondson (2018). The main modifications (see Methods 2.22) involved avoiding the Cell-Tak adhesive from drying out on the imaging surface before the cell suspension could be added. This meant that the drying time for the Cell-Tak was reduced to 15 minutes after washing with the Cell-Tak-NaHCO3 buffer solution, and the incubation temperatures were reduced to 4°C. Additionally, the Cell-Tak concentration was determined empirically.

Having determined the best conditions for stable cell attachment, it was possible to reproducibly image cells of the wild-type strain 168 and strains mutated for *dltAB*, LTA- (the triple mutant (YA45)), and *pbpX* mounted from cultures in mid-exponential growth (as determined by the growth curve plotted in Fig. 5.11B, with data acquired from cultures at different times). However, due to the incubation times involved in mounting the cells and the imaging time, the cells were unlikely to still be in this growth phase.

Images were taken of five well-isolated cells for each strain mounted in a standard way (characteristic images shown in Fig. 5.11A). From these, it was clear that the results obtained exhibited very little variation within samples (i.e., for a specific strain), but there were clear differences depending on the genotype of the strain. These differences are summarized as the calculated average wall stiffness for the cylindrical portion of the cell for each strain (Fig. 5.11C)

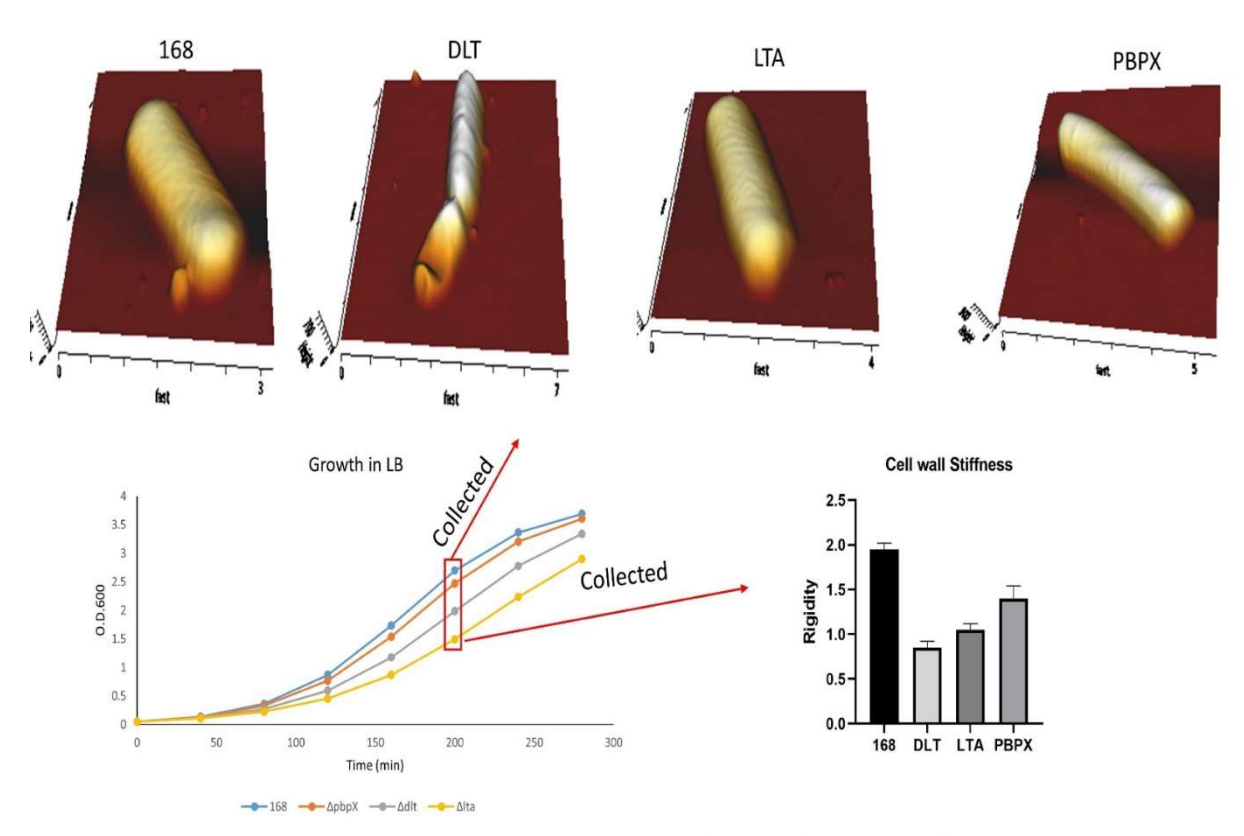


Figure 5.11: Cell wall rigidity of 168, $\Delta pbpX$, Δlta and Δdlt measured by atomic force microscopy.

A) Rotated 3D images for 168, Δdlt , Δlta and $\Delta pbpX$ (from left to right). B) The growth curve in LB medium of 168, Δdlt , Δlta and $\Delta pbpX$ and the sample collection point (red box) for AFM (Data from cultures grown on different days and plotted on the same graph). C) The cell rigidity of 168, Δdlt , Δlta and $\Delta pbpX$ for 5 cells of each strain. The rigidity of of all the strains are measured by kPa (Kilopascal) for at least 3 cells each

5.3 Discussion

Determination of a proteins potential function often relies on comparison of the amino acid sequence with other proteins of known function. This has resulted in a bioinformatics annotation that is based on the conservation of specific domains but relies on the idea that the known domains are a comprehensive representation of all variants and that the biochemically active residues are coordinated appropriately by the surrounding amino acids, resulting in a defined active site. However, the concept is rather open to miss-interpretations. This work highlights this limitation of bioinformatics and indicates that gene function annotation needs to be continuously updated, taking into account newly characterised genes and the continuously updated catalogue of sequenced genomes.

PBPX has been annotated as a penicillin binding protein for a significant period of time and only through a fortuitous similarity search that its biological role was indicated by through inferred similarity and the identification of gene fusions in a small number of bacterial species in the data bases. The bioinformatic similarity results indicate that PBPX of *B. subtilis* is a member of a conserved set of proteins that function in the modification of wall teichoic acids in Gram positive bacteria. Also, the results point to *S. aureus* encoding two PBPX like genes, *fmtA* and *flp*. Interestingly, previous characterisation of FmtA fairly conclusively indicated that acting to remove D-alanine from teichoic acid (Rahman *et al*, 2016), whereas *flp* has not been well studied in this respect (Komatsuzawa *et al*, 2000). Looking at other species of bacteria where PBPX like proteins were identified, the Lactobacilli seemed a conserved gene arrangement of a PBPX like gene with the Dlt operon. And in two cases a fusion protein was identified between DltD and PBPX that seemed to reinforce the link between PBPX and D-alanylation of TA.

These observations directed experimental work toward trying to gain supporting evidence using the rational that if D-alanylation of TA was altered the net surface charge of the cell would be altered and this would have consequence for the sensitivity of the bacterial strain for cationic antimicrobial peptides as well as alter the binding of charged molecules. In vivo analysis of both of these properties generated data that

implied that in *B. subtilis* loss of PBP X activity resulted in a phenotype similar to that resulting from the inactivation of the Dlt operon.

Poly-L-lysine–FITC labelling was utilized as a crude starting point to evaluate the cell surface charge of various strains. We found that deleting pbpX or dltAB made the cell surface bind the positively charged polymer, which was evident from the increased fluorescence intensity of the cationic label (Section 5.2.5), inferring increased negative charge. Among the strains, dltAB and $\Delta pbpX$ displayed the highest fluorescence respectively, suggesting the greatest increase in negative surface charge, likely because the disruption of the LTA D-alanylation pathway plays a significant role (Kingston et al, 2013). These findings were further supported by Zetasizer measurements, which confirmed the increased surface negativity in the $\Delta pbpX$ strain. Altogether, these results suggest that removing pbpX or dltAB interferes with normal cell wall modifications, leading to an increase in negative surface charge, with the loss of dltAB having a particularly strong effect. Although the Zetasizer method has some limitations, like sensitivity to the experimental conditions, it seems that it could be valuable tool when paired with fluorescence labeling for understanding cell surface charge dynamics for future work.

Using the Zetasizer for *S. aureus* strains showed that the mean cell surface's negative charge slightly reduced upon removing *fmtA* in *S. aureus* compared to Je2, with a more noticeable decrease during the stationary phase. This is consistent with the idea that the absence of FmtA leads to the accumulation of D-Ala in the teichoic acids (Rahman *et al.*, 2016). In contrast, an increase in surface negativity was observed upon deleting of *flp*, especially as the cells entered the stationary phase, suggesting less D-Alanylation of the TA might be occurring. Comparison of these findings with that seen for *pbpX* in *B. subtilis*, implied that Flp might be functionally analogous to PBPX and FmtA was, as previously published, having the opposite function. Thus, from the results presented in this chapter, PBPX acts to attach D-alanine to the wall teichoic acid and as such provides a missing step in TA D-alanylation modification pathway that has been inferred for a significant period of time (Figure 1.6; Rahman *et al.*, 2016; Reichmann *et al.*, 2013).

A potential pathway involved in regulating surface charge in *S. aureus* is through the FmtA protein. When FmtA is present at high concentrations, it removes D-alanine from

LTA and therefore suppresses biofilm formation. However, at low concentrations of FmtA, where the LTA becomes heavily D-alanylated, it requires the presence of WTA (Qamar and Golemi-Kotra, 2012), probably to accept the transferred D-alanine from LTA, potentially by Flp, as our results suggest. In *B. subtilis*, the cell surface charge modulation seems slightly different because *B. subtilis* does not contain a protein like FmtA. Instead, our data showed the PBPX protein transferring the D-alanine from LTA to WTA to modulate the cell surface charge.

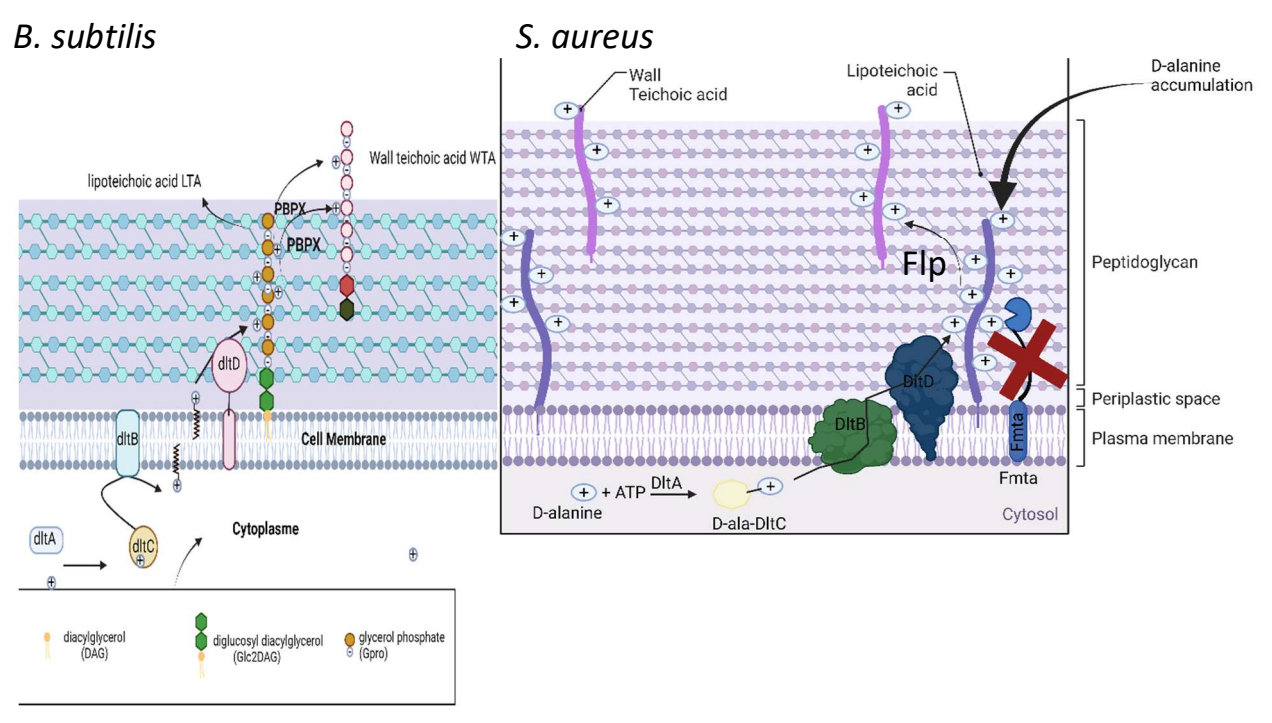


Figure 5.12 Surface charge modulation in B. subtilis and S. aureus

In *B. subtilis*, PBPX is the only recognized protein that modulates cell wall charge by transferring D-alanine from LTA to WTA. In *S. aureus*, FmtA removes D-alanine from LTA, while Flp facilitates D-alanine transfer to WTA. The role of FmtA in D-alanine removal is supported by Rahman *et al.*, 2016, whereas the function of Flp was determined in this study through fluorescence-based charge assays and statistical analysis (p < 0.05, Student's *t*-test, n = X), showing a similar phenotype to *pbpX* mutants in *B. subtilis*. Deletion of *fmtA* resulted in D-alanine accumulation, as indicated in the model. This suggests that Flp plays a role in regulating surface charge, similar to PBPX, and its absence disrupts D-alanine distribution in the cell envelope.

.

This understanding of cell surface charge is further supported by experiments measuring the D-Ala associated with WTA and LTA, particularly in strains where *pbpX* were deleted, the *pbpX*-deleted strain showed a slight increase in LTA-associated D-

Ala but a significant decrease in WTA-associated D-Ala (Section 5.2.8). Since LTA is required for WTA D-alanylation, this indicates that D-Ala is transferred from LTA to WTA, which requires a transferring protein. Based on the D-Ala data, PBPX is the candidate protein that transfers D-Ala from LTA to WTA, and deleting *pbpX* stops this process and drastically decreases WTA D-alanylation. Additionally, this explains the increase in cell surface negative charge upon *pbpX* deletion.

In *S. aureus*, deleting FmtA, which is the candidate orthologue of PBPX, did not have a similar effect on WTA-associated D-Ala, but the D-Ala bound to WTA slightly decreased and LTA-associated D-Ala increased compared to that in Je2 (Section 5.2.9). The increase in LTA-bound D-Ala is consistent with the lack of the hydrolytic activity of FmtA toward the ester bond between D-Ala on WTA. However, deleting Flp led to an increase in LTA-bound D-Ala and a significant decrease in D-Ala attached to WTA. This effect on D-Ala attachment is similar to that seen in the *pbpX* deletion of Bacillus and suggests that Flp in *S. aureus* is a potential orthologue of PBPX in *B. subtilis*.

To try and put these results into a biologically meaningful context it seems that *S. aureus* has two proteins (FmtA and Flp) to modulate TA charge. Whereas. *B. subtilis* seems to require only PBPX for this function. This could be because *S. aureus* is pathogenic and has developed a more sophisticated approach to modulate surface charge to resist the challenges of the host immune system. In contrast, *B. subtilis* is more of an environmental bacterium does not need to adapt to sudden environmental changes or combat the immune system. Future research could further investigate how these proteins behave under the stress of immune system components, but the use of a broadly active antimicrobial peptide CAMA (Geitani *et al.*, 2022) as a way to assess sensitivity and the effect of potential cell surface changes seems to support this idea (Section 5.2.3 & 5.2.4)

Here, regarding *S. aureus*, CAMA could completely inhibit the growth of Je2 at a 12.5 μM concentration; however, deleting FmtA decreased bacterial sensitivity to CAMA and at 12.5 μM, the bacteria could survive and grow. In contrast, deleting Flp increased sensitivity to CAMA and at a low concentration of 6.25 μM, the strain was unable to survive. The inhibition of wild-type Je2 growth at 12.5 μM indicates that CAMA has a bactericidal effect on *S. aureus*, and the decrease in sensitivity upon FmtA deletion potentially occurs because of the accumulation of D-Ala in teichoic acid, which

increases the cell surface charge positivity and leads to the repulsion of cationic AMPs. On the other hand, the increase in sensitivity to CAMA upon deletion of Flp possibly occurred due to a decrease in the cell surface charge positivity, especially that contributed by D-Ala on the surface of the bacterial cell membrane.

In *B. subtilis*, CAMA inhibited the growth of wild-type strain 168 at 5 μ M, but deleting *pbpX* increased sensitivity to CAMA, as did deleting *dltAB*, to an even greater degree. The increase in sensitivity to CAMA following the deletion of *dltAB* can be explained by the deletion stopping teichoic acid D-alanylation by stopping D-Ala activation as an AMP ester; this occurred through the deletion of DltA preventing DltB, which has several membrane-spanning regions, from transferring D-Ala molecules from DltC to C55-P, as proposed by Fischer (1994) and Reichmann, Cassona and Gründling (2013). The increase in sensitivity to CAMA following *pbpX* deletion was caused by the increase in cell surface negative charge, likely related to the D-Ala in teichoic acid. PBPX expression is regulated by the sigma X factor σ^X , and loss of this sigma factor increases sensitivity to cationic AMPs, specifically nisin. Although the increase in sensitivity has been attributed previously to two genes, *dltA* and *pssA*, regulated by the σ x factor (Cao and Helmann, 2004), our data suggest that PBPX is also involved in changing cell surface charge and therefore increasing sensitivity to cationic AMPs.

The general functional role of TA D-alaylation is unclear, there is a clear indication that it is altering cell surface charge, and this could have a number of potential effects. Currently, the most significant that is easy to assay is the resistance to CAMPS and this has tended to be the main focus of most of the research due to its clinical importance. However, since this system is also present in non-pathogenic bacteria, there is a suggestion that it may play a more intrinsic role in cell physiology. Biofilm formation is one that is potentially interesting and a simple aspect to consider, here it may be an advantage to reduce surface charge as a way to permit cells to remain in close proximity. In considering this aspect a potential role for FmtA is suggested, as its apparent activity may promote cell dissociation from a biofilm, by charge repulsion, and this may be advantageous in a host-pathogen situation to permit dissemination. In this respect it is interesting to consider the fact that FmtA's activity would result in the cells potentially becoming more sensitive to the action of CAMPS. From a different perspective, the possible role of TA and their modification in regulating the autolytic enzymes within

the cell envelope, through retention or repulsion perhaps, is supported by a number of studies (Biswas *et al.*, 2012; Maki, Yamaguchi and Murakami, 1994; Yamamoto *et al.*, 2008). But at this time, it is difficult to directly test as the tools to look at this sort of *in vivo* biochemical regulation are not well developed. However, a possible indirect consequence of dysregulated cell wall function is offered by AFM imaging as it potentially provides an understanding of the physical properties of the cell wall at the single cell level. Several studies have used AFM for this purpose (Goss and Volle, 2020; Tuson *et al.*, 2012). Deleting *dltAB* decreased cell wall rigidity presumably because of the absence of teichoic acid D-alanylation. Thus, strain with blocked LTA synthesis would be expected to have the same effect as the D-alanine pathway is also blocked. Finally, the *pbpX* mutant represents an intermediate state, here the LTA can be D-alanylated but the WTA remains un modified. Interestingly here the end result is an intermediate level of rigidity (less than the WT, but more than *dltAB* or LTA) also decreased bacterial cell wall rigidity compared to that of strain 168, but not as much as the *dltAB*- and *LTA*-deleted strains.

A possible model to explain these effects could be built on the concept that the rigidity of the wall is mediated by the fact that the cell envelope is a complex matrix of polymers that are all, to some degree, negatively charged. Consequently, there is a level of repulsion between the constituent polymers that at the extreme, where all are highly negative, results in an open matrix that is compressible (Nikaido, 2003). This state could be considered to be that where there is no D-alanylation and both LTA and WTA are present in the wall (the dltAB mutant). The absence of LTA removes a certain level of negativity in the wall matrix and hence reduces the level of repulsion to some degree and so the matrix is less expanded, but there will be no WTA modification and so it is softer than when the teichoic acid polymer charge is moderated by the attachment of D-alanine. This concept of the state of the cell envelope is difficult to experimentally test in vivo, but analysis of intact sacculi of B. subtilis (cell envelopes extracted for all soluble components) seem to imply that the WTA has a role in opening up the wall matrix and allowing the diffusion of large molecules (M. Chow, unpublished), and is also supported by other work looking at the density of the cell wall matrix (Gutberlet et al, 1997).

At a different scale the cell surface charge could also have an impact on how individual cells are able to associate to form a biofilm. Here the concept would be that formation of a dense biofilm would require moderation of the surface charge that could be mediated by D-alanylation of the TA, or through some other mechanism and then to permit dissemination of cells out of the biofilm a potential "physical" mechanism could be to increase cell to cell repulsion, by increased surface "negativity". This concept is potentially interesting but complicated by the existence of extracellular polymers that enhance biofilm formation and of course by the relative abundance of salt ions in the environment. However, for this perspective it is tempting to infer that for *S. aureus*, FmtA may have a role in this process, possibly explaining the observation that it has a role in pathogenesis, which seems contradictory to the functions discussed earlier in this section.

Chapter 6 General discussion and future directions

PBPs have been of research interest for decades as they are the main targets of antibiotics. Most bacteria have several sets of PBPs with overlapping functions. The redundancy of PBPs allows researchers to delete several PBPs without fatality. When class A bifunctional PBPs were deleted in B. subtilis, the bacteria could adapt and survive. However, no research on further PBP deletions has been performed. In this work, we aimed to delete PBPs additional to class A PBPs and identify minimal sets of PBPs required for bacterial survival and strain characterisation. Based on our findings, it can be concluded that bacteria can survive with as low as two essential PBPs, which, in the case of B. subtilis, are PBP2a (or PBPH) and PBP2b. Although the bacteria could survive with the minimal sets of PBPs, their growth, muropeptide composition and cell wall rigidity differed from those of the wild-type variants, probably because the bacteria needed to adapt to losing several PBPs. This research clearly illustrates that B. subtilis requires only two PBPs during exponential growth but also raises the question 'Do all other bacteria also require only two PBPs to survive?' For Bacillus the apparent separation of cell division and growth into distinct processes but seeming to share common proteins presents the possibility that the minimal PBP necessary for growth are indicative of this and is supported by past analyses. PBP2b is well established as a key component of the cell division apparatus and does not seem to have any role in elongation. By contrast PBP2a, and PBPH (which will be discussed later) appear to have a distinct role in elongation and there is no clear suggestion that they have an essential function in division. Thus, it seems likely that S. aureus, which technically has not elongation system, should be capable of functioning with only one active PBP, a concept that is supported by the fact that MRSA strains are able to tolerate high levels of b-lactam mediated inhibition of PBP by virtue of the presence of MecA, a PBP that has very low affinity of penicillin. Building on this concept, an interesting question is raised about how universal PBP redundancy is in other bacteria, such as Actinobacteria where cell growth occurs at the cell poles/division sites (Brown et al.g, 2011). Interestingly in Gram negative bacteria the question has not been fully addressed, but here there is the potential for PG assembly through the activation of L,Dtranspeptidases which are not penicillin sensitive (Magnet et al, 2008). However, it is unclear if the PBP proteins are dispensable, even if not active. This is also suggested for

S. aureus MRSA where at least FtsI is still required, even though inactivated by penicillin.

To better understand the implication of our results, future studies could address the needs of other bacterial species for PBPs and whether they need only two PBPs or even fewer. Particularly since our understanding is limited to a few specific bacterial species and under rather artificial conditions This study contributes to narrowing down the essential PBPs required for bacterial survival and the concept of defining the minimal function gene complement for a synthetic bacterium. It also provides a different perspective to the evolution of bacteria resistant to β -lactams and provides a focus on the need to design novel antibiotics that specifically target the essential processes where functional redundancy is less prevalent, and hence evolution of resistance is more complicated.

When deleting several PBPs in B. subtilis, pbp2A could not be deleted in the absence of PBPH due to the functional overlap between these two proteins. PBP2a and PBPH are both TPs that are part of the bacterial elongasome complex. The redundancy of PBP2a and PBPH was first discovered by Wei and colleagues in 2003; since then, no published studies have focused on these critical, redundant partners. In this research, we aimed to investigate the redundancy of PBP2a and PBPH by monitoring the effects of deleting one on the activity, quantity and expression of its partner and identifying domains involved in the regulation of these two proteins. Based on Bocillin FL activity assays, western blotting and RT-qPCR, it can be concluded that the deletion of pbpH increases the activity, quantity and expression of PBP2a. The results indicate that PBP2a and PBPH are tightly regulated, with the RT-qPCR results suggesting that the regulation occurs at the transcriptional level. It is clear that the B. subtilis regulate PBP2a and PBPH to maintain a certain level of activity. Additionally, the results showed that the transmembrane domain of PBPH is involved in regulating quantity and activity of PBP2a to meet requirements. This work clearly illustrates that the redundant pair, PBP2a and PBPH are transcriptionally regulated and the transmembrane domain of PBPH is involved in this regulation but also raises the question of how exactly they are regulated and what other proteins, if any, are involved. To better understand the implications of these results, future studies could address the mechanism of regulation and the involvement of the PBPH transmembrane domain. This study contributes to

better understanding PBP2a and PBPH redundancy in terms of activity/quantity and expression. In addition, the domain responsible for regulation was identified.

During the PBP deletion studies, PBPX did not bind bocillin-FL (an artificial penicillin labelled with a fluorescent marker) and, therefore, was not detectable, although it is known to contain a β-lactamase-like domain. PBPX is classified as an LMW (class C) PBP in B. subtilis. There are few studies on PBPX, and its function is still unknown. Therefore, we aimed to identify the potential function of PBPX. Based on the observed Zetasizer cell surface charge, cationic antimicrobial peptide sensitivity, and D-Ala assay results, it can be concluded that PBPX deletion shifted the cell surface charge to negative, the cell became more sensitive to a cationic antimicrobial peptide (CAMA), and WTA D-alanylation was decreased. Previous research identified the steps of teichoic acid D-alanylation, but the process of transfer of D-Ala from LTA to WTA is still elusive. Our results indicate that PBPX functions as a D-Ala transferase that transfers D-Ala from LTA to WTA and that this influenced the overall cell surface charge, assisting the bacteria in becoming more resistant to cationic antimicrobial peptides. This research clearly illustrates that PBPX plays a role in cell surface charge modulation through WTA D-alanylation, and therefore, contributes to cationic antimicrobial peptide resistance. It also raises the question 'Do other bacteria contain proteins with the same function as PBPX?' In this research, we also investigated PBPXlike proteins in S. aureus. Although both FmtA and Flp proteins showed high structural similarity to PBPX, only Flp showed similar changes in cell surface charge and cationic antimicrobial peptide sensitivity. This study contributes to a better understanding of bacterial surface charge modulation via D-alanylation that leads to bacterial resistance to antimicrobial peptides and perhaps also key aspects of bacterial colonisation, by clinically and environmentally, in the form of biofilms.

Chapter 7 References

Adam, M., Fraipont, C., Rhazi, N., Nguyen-Distèche, M., Lakaye, B., Frère, J.M., *et al.* (1997) 'The bimodular G57-V577 polypeptide chain of the class B penicillin-binding protein 3 of *Escherichia coli* catalyzes peptide bond formation from thiolesters and does not catalyze glycan chain polymerization from the lipid II intermediate', *J Bacteriol*, 179(19), pp. 6005-6009.

Aguilera Rossi, C.G., Gómez-Puertas, P. and Ayala Serrano, J.A. (2016) 'In vivo functional and molecular characterization of the Penicillin-Binding Protein 4 (DacB) of *P. aeruginosa*', *BMC Microbiol*, 16(1), p. 234.

Amiri, E.O., Farmani, J., Amiri, Z.R., Dehestani, A. and Mohseni, M. (2021) 'Antimicrobial activity, environmental sensitivity, mechanism of action, and food application of αs165-181 peptide', *Int J Food Microbiol*, 358, p. 109403.

Anderson, J.S., Matsuhashi, M., Haskin, M.A. and Strominger, J.L. (1967) 'Biosynthesis of the peptidoglycan of bacterial cell walls. II. Phospholipid carriers in the reaction sequence', *J Biol Chem*, 242(13), pp. 3180-3190.

Araki, Y. and Ito, E. (1989) 'Linkage units in cell walls of gram-positive bacteria', *Crit Rev Microbiol*, 17(2), pp. 121-135.

Assoni, L., Milani, B., Carvalho, M.R., Nepomuceno, L.N., Waz, N.T., Guerra, M.E.S., *et al.* (2020) 'Resistance mechanisms to antimicrobial peptides in grampositive bacteria', *Front Microbiol*, 11, p. 593215.

Atilano, M.L., Pereira, P.M., Yates, J., Reed, P., Veiga, H., Pinho, M.G. and Filipe, S.R. (2010) 'Teichoic acids are temporal and spatial regulators of peptidoglycan cross-linking in *Staphylococcus aureus*', *Proc Natl Acad Sci USA*, 107(44), pp. 18991-18996.

Atrih, A., Bacher, G., Allmaier, G., Williamson, M.P. and Foster, S.J. (1999) 'Analysis of peptidoglycan structure from vegetative cells of *Bacillus subtilis* 168 and role of PBP 5 in peptidoglycan maturation', *J Bacteriol*, 181(13), pp. 3956-3966.

Baddiley, J. (1970) 'Structure, biosynthesis, and function of teichoic acids', *Acc Chem Res*, 3(3), pp. 98-105.

Bae, T., Banger, A.K., Wallace, A., Glass, E.M., Aslund, F., Schneewind, O. and Missiakas, D.M. (2004) 'Staphylococcus aureus virulence genes identified by bursa aurealis mutagenesis and nematode killing', *Proc Natl Acad Sci USA*, 101(33), pp. 12312-12317.

Barbour, A.G. (1981) 'Properties of penicillin-binding proteins in *Neisseria* gonorrhoeae', *Antimicrob Agents Chemother*, 19(2), pp. 316-322.

Bar-Even, A., Noor, E., Flamholz, A., Buescher, J.M. and Milo, R. (2011) 'Hydrophobicity and charge shape cellular metabolite concentrations', *PLoS Comput Biol*, 7(10), p. e1002166.

Bartholomew, J.W. and Mittwer, T. (1952) 'The Gram stain', *Bacteriol Rev*, 16(1), pp. 1-29.

Bernal, P., Zloh, M. and Taylor, P.W. (2009) 'Disruption of D-alanyl esterification of *Staphylococcus aureus* cell wall teichoic acid by the β-lactam resistance modifier (-)-epicatechin gallate', *J Antimicrob Chemother*, 63(6), pp. 1156-1162.

Bertonha, A.F., Silva, C.C.L., Shirakawa, K.T., Trindade, D.M. and Dessen, A. (2023) 'Penicillin-binding protein (PBP) inhibitor development: A 10-year chemical perspective', *Exp Biol Med*, 248(19), pp. 1657-1670.

Bhat, S.V., Sultana, T., Körnig, A., McGrath, S., Shahina, Z. and Dahms, T.E.S. (2018) 'Correlative atomic force microscopy quantitative imaging-laser scanning confocal microscopy quantifies the impact of stressors on live cells in real-time', *Sci Rep*, 8(1), p. 8305.

Bhavsar, A.P., Erdman, L.K., Schertzer, J.W. and Brown, E.D. (2004) 'Teichoic acid is an essential polymer in *Bacillus subtilis* that is functionally distinct from teichuronic acid', *J Bacteriol*, 186(23), pp. 7865-7873.

Billings, G., Ouzounov, N., Ursell, T., Desmarais, S.M., Shaevitz, J., Gitai, Z. and Huang, K.C. (2014) 'De novo morphogenesis in L-forms via geometric control of cell growth', *Mol Microbiol*, 93(5), pp. 883-896.

Bisicchia, P., Noone, D., Lioliou, E., Howell, A., Quigley, S., Jensen, T., Jarmer, H. and Devine, K.M. (2007) 'The essential YycFG two-component system controls cell wall metabolism in *Bacillus subtilis*', *Mol Microbiol*, 65(1), pp. 180-200.

Bisson-Filho, A.W., Hsu, Y.P., Squyres, G.R., Kuru, E., Wu, F., Jukes, C., *et al.* (2017) 'Treadmilling by FtsZ filaments drives peptidoglycan synthesis and bacterial cell division', *Science*, 355(6326), pp. 739-743.

Biswas, R., Martinez, R.E., Göhring, N., Schlag, M., Josten, M., Xia, G., *et al.* (2012) 'Proton-binding capacity of *Staphylococcus aureus* wall teichoic acid and its role in controlling autolysin activity', *PLoS One*, 7(7), p. e41415.

Blair, K.M., Turner, L., Winkelman, J.T., Berg, H.C. and Kearns, D.B. (2008) 'A molecular clutch disables flagella in the *Bacillus subtilis* biofilm', *Science*, 320(5883), pp. 1636-1638.

Boehm, A., Kaiser, M., Li, H., Spangler, C., Kasper, C.A., Ackermann, M., *et al.* (2010) 'Second messenger-mediated adjustment of bacterial swimming velocity', *Cell*, 141(1), pp. 107-116.

Boonstra, M., de Jong, I.G., Scholefield, G., Murray, H., Kuipers, O.P. and Veening, J.W. (2013) 'Spo0A regulates chromosome copy number during sporulation by directly binding to the origin of replication in *Bacillus subtilis*', *Mol Microbiol*, 87(4), pp. 925-938.

Bouhss, A., Crouvoisier, M., Blanot, D. and Mengin-Lecreulx, D. (2004) 'Purification and characterization of the bacterial MraY translocase catalyzing the first membrane step of peptidoglycan biosynthesis', *J Biol Chem*, 279(29), pp. 29974-29980.

Bouhss, A., Dementin, S., van Heijenoort, J., Parquet, C. and Blanot, D. (2002) 'MurC and MurD synthetases of peptidoglycan biosynthesis: borohydride trapping of acylphosphate intermediates', *Methods Enzymol*, 354, pp. 189-196.

Brott, A.S. and Clarke, A.J. (2019) 'Peptidoglycan O-Acetylation as a Virulence Factor: Its Effect on Lysozyme in the Innate Immune System', *Antibiotics (Basel)*, 8(3), p. 94.

Brown, P.J., Kysela, D.T., Brun, Y.V. (2011) 'Polarity and the diversity of growth mechanisms in bacteria', *Semin Cell Dev Biol*, 22(8), pp. 790–798.

Brown, S., Meredith, T., Swoboda, J. and Walker, S. (2010) 'Staphylococcus aureus and Bacillus subtilis W23 make polyribitol wall teichoic acids using different enzymatic pathways', *Chem Biol*, 17(10), pp. 1101-1110.

Brown, S., Santa Maria, J.P., Jr and Walker, S. (2013) 'Wall teichoic acids of grampositive bacteria', *Annu Rev Microbiol*, 67, pp. 313-336.

Brown, S., Xia, G., Luhachack, L.G., Campbell, J., Meredith, T.C., Chen, C., *et al.* (2012) 'Methicillin resistance in *Staphylococcus aureus* requires glycosylated wall teichoic acids', *Proc Natl Acad Sci USA*, 109(46), pp. 18909-18914.

Burbulys, D., Trach, K.A. and Hoch, J.A. (1991) 'Initiation of sporulation in *B. subtilis* is controlled by a multicomponent phosphorelay', *Cell*, 64(3), pp. 545-552.

Cao, M. and Helmann, J.D. (2004) 'The *Bacillus subtilis* extracytoplasmic-function sigmaX factor regulates modification of the cell envelope and resistance to cationic antimicrobial peptides', *J Bacteriol*, 186(4), pp. 1136-1146.

Carballido-López, R., Formstone, A., Li, Y., Ehrlich, S.D., Noirot, P. and Errington, J. (2006) 'Actin homolog MreBH governs cell morphogenesis by localization of the cell wall hydrolase LytE', *Dev Cell*, 11(3), pp. 399-409.

Chen, Y., Chai, Y., Guo, J.H. and Losick, R. (2012) 'Evidence for cyclic Di-GMP-mediated signaling in *Bacillus subtilis*', *J Bacteriol*, 194(18), pp. 5080-5090.

Chen, Z., Srivastava, P., Zarazúa-Osorio, B., Marathe, A., Fujita, M. and Igoshin, O.A. (2022) '*Bacillus subtilis* histidine kinase KinC activates biofilm formation by controlling heterogeneity of single-cell responses', *mBio*, 13(1), p. e0169421.

Cho, H., Wivagg, C.N., Kapoor, M., Barry, Z., Rohs, P.D., Suh, H., *et al.* (2016) 'Bacterial cell wall biogenesis is mediated by SEDS and PBP polymerase families functioning semi-autonomously', *Nat Microbiol*, 19, p. 16172.

Claessen, D., Emmins, R., Hamoen, L.W., Daniel, R.A., Errington, J. and Edwards, D.H. (2008) 'Control of the cell elongation-division cycle by shuttling of PBP1 protein in *Bacillus subtilis*', *Mol Microbiol*, 68(4), pp. 1029-1046.

Collins, L.V., Kristian, S.A., Weidenmaier, C., Faigle, M., Van Kessel, K.P., Van Strijp, J.A., *et al.* (2002) '*Staphylococcus aureus* strains lacking D-alanine

modifications of teichoic acids are highly susceptible to human neutrophil killing and are virulence attenuated in mice', *J Infect Dis*, 186(2), pp. 214-219.

Daniel, R.A. and Errington, J. (2003) 'Control of cell morphogenesis in bacteria: two distinct ways to make a rod-shaped cell', *Cell*, 113(6), pp. 767-776.

Daniel, R.A., Harry, E.J. and Errington, J. (2000) 'Role of penicillin-binding protein PBP 2B in assembly and functioning of the division machinery of *Bacillus subtilis*', *Mol Microbiol*, 35(2), pp. 299-311.

Davidson, P., Eutsey, R., Redler, B., Hiller, N.L., Laub, M.T. and Durand, D. (2018) 'Flexibility and constraint: evolutionary remodeling of the sporulation initiation pathway in Firmicutes', *PLoS Genet*, 14(9), p. e1007470.

Defeu Soufo, H.J. and Graumann, P.L. (2006) 'Dynamic localization and interaction with other *Bacillus subtilis* actin-like proteins are important for the function of MreB', *Mol Microbiol*, 62(5), pp. 1340-1356.

D'Elia, M.A., Millar, K.E., Beveridge, T.J. and Brown, E.D. (2006) 'Wall teichoic acid polymers are dispensable for cell viability in *Bacillus subtilis*', *J Bacteriol*, 188(23), pp. 8313-8316.

Delisle, J., Cordier, B., Audebert, S., Pophillat, M., Cluzel, C., Espinosa, L., *et al.* (2021) 'Characterization of TseB: A new actor in cell wall elongation in *Bacillus subtilis*', *Mol Microbiol*, 116(4), pp. 1099-1112.

Denome, S.A., Elf, P.K., Henderson, T.A., Nelson, D.E. and Young, K.D. (1999) 'Escherichia coli mutants lacking all possible combinations of eight penicillin-binding proteins: viability, characteristics, and implications for peptidoglycan synthesis', *J Bacteriol*, 181(13), pp. 3981-3993.

Devine, K.M. (2012) 'Bacterial L-forms on tap: an improved methodology to generate *Bacillus subtilis* L-forms heralds a new era of research', *Mol Microbiol*, 83(1), pp. 10-13.

Dhand, A., Bayer, A.S., Pogliano, J., Yang, S.J., Bolaris, M., Nizet, V., *et al.* (2011) 'Use of antistaphylococcal beta-lactams to increase daptomycin activity in eradicating

persistent bacteremia due to methicillin-resistant *Staphylococcus aureus*: role of enhanced daptomycin binding', *Clin Infect Dis*, 53(2), pp. 158-163.

Dickson, J.S. and Koohmaraie, M. (1989) 'Cell surface charge characteristics and their relationship to bacterial attachment to meat surfaces', *Appl Environ Microbiol*, 55(4), pp. 832-836.

Dion, M.F., Kapoor, M., Sun, Y., Wilson, S., Ryan, J., Vigouroux, A., *et al.* (2019) '*Bacillus subtilis* cell diameter is determined by the opposing actions of two distinct cell wall synthetic systems', *Nat Microbiol*, 4(8), pp. 1294-1305.

Domínguez-Cuevas, P., Mercier, R., Leaver, M., Kawai, Y. and Errington, J. (2011) 'The rod to L-form transition of *Bacillus subtilis* is limited by a requirement for the protoplast to escape from the cell wall sacculus', *Mol Microbiol*, 83(1), pp. 52-66.

Dramsi, S., Davison, S., Magnet, S. and Arthur, M. (2008) 'Surface proteins covalently attached to peptidoglycan: examples from both gram-positive and gram-negative bacteria', *FEMS Microbiol Rev*, 32(2), pp. 307-320.

Edmondson, M. (2018) Can real-time nanoscale microscopy help design improved antibiotics? Masters thesis. Newcastle University.

Egan, A.J.F. and Vollmer, W. (2013) 'The physiology of bacterial cell division', *Ann N Y Acad Sci*, 1277, pp. 8-28.

Egan, A.J.F., Errington, J. and Vollmer, W. (2020) 'Regulation of peptidoglycan synthesis and remodeling', *Nat Rev Microbiol*, 18(8), pp. 446-460.

Emami, K., Guyet, A., Kawai, Y., Devi, J., Wu, L.J., Allenby, N., Daniel, R.A. and Errington, J. (2017) 'RodA as the missing glycosyltransferase in Bacillus subtilis and antibiotic discovery for the peptidoglycan polymerase pathway', *Nat Microbiol*, 2, p. 16253.

Errington, J. and Wu, L.J. (2017) 'Cell cycle machinery in *Bacillus subtilis*', *Subcell Biochem*, 84, pp. 67-101.

Eswaramoorthy, P., Erb, M.L., Gregory, J.A., Silverman, J., Pogliano, K., Pogliano, J. and Ramamurthi, K.S. (2011) 'Cellular architecture mediates DivIVA ultrastructure and regulates min activity in *Bacillus subtilis*', *mBio*, 2(6), p. e00257-11.

Fabret, C. and Hoch, J.A. (1998) 'A two-component signal transduction system essential for growth of *Bacillus subtilis*: implications for anti-infective therapy', *J Bacteriol*, 180(23), pp. 6375-6383.

Fedtke, I., Mader, D., Kohler, T., Moll, H., Nicholson, G., Biswas, R., *et al.* (2007) 'A *Staphylococcus aureus* ypfP mutant with strongly reduced lipoteichoic acid (LTA) content: LTA governs bacterial surface properties and autolysin activity', *Mol Microbiol*, 65(4), pp. 1078-1091.

Figge, R.M., Divakaruni, A.V. and Gober, J.W. (2004) 'MreB, the cell shape-determining bacterial actin homologue, co-ordinates cell wall morphogenesis in *Caulobacter crescentus*', *Mol Microbiol*, 51(5), pp. 1321-1332.

Fischer, W. (1994) 'Lipoteichoic acid and lipids in the membrane of *Staphylococcus aureus*', *Med Microbiol Immunol*, 183(2), pp. 61-76.

Fischer, W. and Rösel, P. (1980) 'The alanine ester substitution of lipoteichoic acid (LTA) in *Staphylococcus aureus*', *FEBS Lett*, 119(2), pp. 224-226.

Fishovitz, J., Hermoso, J.A., Chang, M. and Mobashery, S. (2014) 'Penicillin-binding protein 2a of methicillin-resistant *Staphylococcus aureus*', *IUBMB Life*, 66(8), pp. 572-577.

Formstone, A. and Errington, J. (2005) 'A magnesium-dependent *mreB* null mutant: implications for the role of *mreB* in *Bacillus subtilis*', *Mol Microbiol*, 55(6), pp. 1646-1657.

Foster, S.J. and Popham, D.L. (2002) 'Structure and synthesis of cell wall, spore cortex, teichoic acids, S-layers, and capsules', in A.L. Sonenshein, R. Losick and J.A. Hoch (eds.) *Bacillus subtilis and its closest relatives: from genes to cells*. Washington, DC: American Society for Microbiology Press, pp. 21-41.

Galinier, A., Delan-Forino, C., Foulquier, E., Lakhal, H. and Pompeo, F. (2023) 'Recent Advances in Peptidoglycan Synthesis and Regulation in Bacteria', *Biomolecules*, 13(5), p. 720.

Gan, L., Chen, S., and Jensen, G.J. (2008) 'Molecular organization of Gram-negative peptidoglycan', *Proc Natl Acad Sci USA*, 105(48), pp. 18953-18957.

Garner, E.C., Bernard, R., Wang, W., Zhuang, X., Rudner, D.Z., and Mitchison, T. (2011) 'Coupled, circumferential motions of the cell wall synthesis machinery and MreB filaments in *Bacillus subtilis*', *Science*, 333(6039), pp. 222-225.

Geitani, R., Moubareck, C.A., Costes, F., Marti, L., Dupuis, G., Sarkis, D.K., and Touqui, L. (2022) 'Bactericidal effects and stability of LL-37 and CAMA in the presence of human lung epithelial cells', *Microbes Infect*, 24(3), p. 104928.

Geitani, R., Moubareck, C.A., Xu, Z., Karam Sarkis, D., and Touqui, L. (2020) 'Expression and roles of antimicrobial peptides in innate defense of airway mucosa: potential implication in cystic fibrosis', *Front Immunol*, 11, p. 1198.

Ghuysen, J.M., Charlier, P., Coyette, J., Duez, C., Fonzé, E., Fraipont, C., *et al.* (1996) 'Penicillin and beyond: evolution, protein fold, multimodular polypeptides, and multiprotein complexes', *Microb Drug Resist*, 2(2), pp. 163-175.

Goffin, C. and Ghuysen, J.M. (1998) 'Multimodular penicillin-binding proteins: an enigmatic family of orthologs and paralogs', *Microbiol Mol Biol Rev*, 62(4), pp. 1079-1093.

Goffin, C., Fraipont, C., Ayala, J., Terrak, M., Nguyen-Distèche, M., and Ghuysen, J.M. (1996) 'The non-penicillin-binding module of the tripartite penicillin-binding protein 3 of *Escherichia coli* is required for folding and/or stability of the penicillin-binding module and the membrane-anchoring module confers cell septation activity on the folded structure', *J Bacteriol*, 178(18), pp. 5402-5409.

Goss, J.W. and Volle, C.B. (2020) 'Using atomic force microscopy to illuminate the biophysical properties of microbes', *ACS Appl Biomater*, 3(1), pp. 143-155.

Goulter, R.M., Gentle, I.R., and Dykes, G.A. (2009) 'Issues in determining factors influencing bacterial attachment: a review using the attachment of *Escherichia coli* to abiotic surfaces as an example', *Lett Appl Microbiol*, 49(1), pp. 1-7.

Gray, A.N., Egan, A.J., Van't Veer, I.L., Verheul, J., Colavin, A., Koumoutsi, A., *et al.* (2015) 'Coordination of peptidoglycan synthesis and outer membrane constriction during *Escherichia coli* cell division', *eLife*, 4, p. e07118.

Guinane, C.M., Cotter, P.D., Ross, R.P., and Hill, C. (2006) 'Contribution of penicillin-binding protein homologs to antibiotic resistance, cell morphology, and virulence of *Listeria monocytogenes* EGDe', *Antimicrob Agents Chemother*, 50(8), pp. 2824-2828.

Gutberlet, T., Frank, J., Bradaczek, H., and Fischer, W. (1997) 'Effect of lipoteichoic acid on thermotropic membrane properties', *J Bacteriol*, 179(9), pp. 2879-2883.

Guyet, A., Alofi, A., and Daniel, R.A. (2023) 'Insights into the Roles of Lipoteichoic Acids and MprF in *Bacillus subtilis*', *mBio*, 14(1), p. e0266722.

Harry, E., Monahan, L., and Thompson, L. (2006) 'Bacterial cell division: the mechanism and its precision', *Int Rev Cytol*, 253, pp. 27-94.

Haydon, D.J., Stokes, N.R., Ure, R., Galbraith, G., Bennett, J.M., Brown, D.R., *et al.* (2008) 'An inhibitor of FtsZ with potent and selective anti-staphylococcal activity', *Science*, 321(5896), pp. 1673-1675.

Heaton, M.P. and Neuhaus, F.C. (1992) 'Biosynthesis of D-alanyl-lipoteichoic acid: cloning, nucleotide sequence, and expression of the *Lactobacillus casei* gene for the D-alanine-activating enzyme', *J Bacteriol*, 174(14), pp. 4707-4717.

Heaton, M.P. and Neuhaus, F.C. (1994) 'Role of the D-alanyl carrier protein in the biosynthesis of D-alanyl-lipoteichoic acid', *J Bacteriol*, 176(3), pp. 681-690.

Heptinstall, S., Archibald, A.R., and Baddiley, J. (1970) 'Teichoic acids and membrane function in bacteria', *Nature*, 225(5232), pp. 519-521.

Hofmann, K. (2000) 'A superfamily of membrane-bound O-acyltransferases with implications for wnt signaling', *Trends Biochem Sci*, 25(3), pp. 111-112.

Hoskins, J., Matsushima, P., Mullen, D.L., Tang, J., Zhao, G., Meier, T.I., *et al.* (1999) 'Gene disruption studies of penicillin-binding proteins 1a, 1b, and 2a in *Streptococcus pneumoniae*', *J Bacteriol*, 181(20), pp. 6552-6555.

Hwang, D.S., Gim, Y., and Cha, H.J. (2005) 'Expression of functional recombinant mussel adhesive protein type 3A in *Escherichia coli*', *Biotechnol Prog*, 21(3), pp. 965-970.

Hwang, D.S., Sim, S.B., and Cha, H.J. (2007) 'Cell adhesion biomaterial based on mussel adhesive protein fused with RGD peptide', *Biomaterials*, 28(28), pp. 4039-4046.

Hyldgaard, M., Mygind, T., Vad, B.S., Stenvang, M., Otzen, D.E., and Meyer, R.L. (2014) 'The antimicrobial mechanism of action of epsilon-poly-l-lysine', *Appl Environ Microbiol*, 80(24), pp. 7758-7770.

Hyyryläinen, H.L., Marciniak, B.C., Dahncke, K., Pietiäinen, M., Courtin, P., Vitikainen, M., *et al.* (2010) 'Penicillin-binding protein folding is dependent on the PrsA peptidyl-prolyl cis-trans isomerase in *Bacillus subtilis*', *Mol Microbiol*, 77(1), pp. 108-127.

Ishihama, A. (2012) 'Prokaryotic genome regulation: a revolutionary paradigm', *Proc Jpn Acad Ser B Phys Biol Sci*, 88(9), pp. 485-508.

Jones, L.J., Carballido-López, R., and Errington, J. (2001) 'Control of cell shape in bacteria: helical, actin-like filaments in *Bacillus subtilis*', *Cell*, 104(6), pp. 913-922.

Jorasch, P., Wolter, F.P., Zähringer, U., and Heinz, E. (1998) 'A UDP glucosyltransferase from *Bacillus subtilis* successively transfers up to four glucose residues to 1,2-diacylglycerol: expression of *ypfP* in *Escherichia coli* and structural analysis of its reaction products', *Mol Microbiol*, 29(2), pp. 419-430.

Kawai, Y., Marles-Wright, J., Cleverley, R. M., Emmins, R., Ishikawa, S., Kuwano, M., Heinz, N., Bui, N. K., Hoyland, C. N., Ogasawara, N., Lewis, R. J., Vollmer, W., Daniel, R. A., and Errington, J. (2011) 'A widespread family of bacterial cell wall assembly proteins', *EMBO J*, 30(24), pp. 4931–4941

Kern, T., Giffard, M., Hediger, S., Amoroso, A., Giustini, C., Bui, N.K., *et al.* (2010) 'Dynamics characterization of fully hydrated bacterial cell walls by solid-state NMR: evidence for cooperative binding of metal ions', *J Am Chem Soc*, 132(31), pp. 10911-10919.

Kho, K. and Meredith, T.C. (2018) 'Extraction and analysis of bacterial teichoic acids', *Bio-protocol*, 8(21), p. e3078.

Kingston, A.W., Liao, X., and Helmann, J.D. (2013) 'Contributions of the $\sigma(W)$, $\sigma(M)$, and $\sigma(X)$ regulons to the lantibiotic resistome of *Bacillus subtilis*', *Mol Microbiol*, 90(3), pp. 502-518.

Kiriukhin, M.Y., Debabov, D.V., Shinabarger, D.L., and Neuhaus, F.C. (2001) 'Biosynthesis of the glycolipid anchor in lipoteichoic acid of *Staphylococcus aureus* RN4220: role of YpfP, the diglucosyldiacylglycerol synthase', *J Bacteriol*, 183(11), pp. 3506-3514.

Kock, H., Gerth, U., and Hecker, M. (2004) 'MurAA, catalysing the first committed step in peptidoglycan biosynthesis, is a target of Clp-dependent proteolysis in *Bacillus subtilis*', *Mol Microbiol*, 51(4), pp. 1087-1102.

Kojima, N., Araki, Y., and Ito, E. (1985) 'Structure of the linkage units between ribitol teichoic acids and peptidoglycan', *J Bacteriol*, 161(1), pp. 299-306.

Koksharova, O., Safronova, N., and Dunina-Barkovskaya, A. (2022) 'New antimicrobial peptide with two CRAC motifs: activity against *Escherichia coli* and *Bacillus subtilis*', *Microorganisms*, 10(8), p. 1538.

Komatsuzawa, H., Choi, G.H., Fujiwara, T., Huang, Y., Ohta, K., Sugai, M., and Suginaka, H. (2000) 'Identification of a *fmtA*-like gene that has similarity to other PBPs and beta-lactamases in *Staphylococcus aureus*', *FEMS Microbiol Lett*, 188(1), pp. 35-39.

Koo, B.M., Kritikos, G., Farelli, J.D., Todor, H., Tong, K., Kimsey, H., *et al.* (2017) 'Construction and analysis of two genome-scale deletion libraries for *Bacillus subtilis*', *Cell Syst*, 4(3), pp. 291-305.e7.

Kovács, M., Halfmann, A., Fedtke, I., Heintz, M., Peschel, A., Vollmer, W., et al. (2006) 'A functional dlt operon, encoding proteins required for incorporation of Dalanine in teichoic acids in gram-positive bacteria, confers resistance to cationic antimicrobial peptides in *Streptococcus pneumoniae*', *J Bacteriol*, 188(16), pp. 5797-5805.

Lages, M.C., Beilharz, K., Morales Angeles, D., Veening, J.W., and Scheffers, D.J. (2013) 'The localization of key *Bacillus subtilis* penicillin-binding proteins during cell growth is determined by substrate availability', *Environ Microbiol*, 15(12), pp. 3272-3281.

Lazarevic, V. and Karamata, D. (1995) 'The *tagGH* operon of *Bacillus subtilis* 168 encodes a two-component ABC transporter involved in the metabolism of two wall teichoic acids', *Mol Microbiol*, 16(2), pp. 345–355.

Leaver, M. and Errington, J. (2005) 'Roles for MreC and MreD proteins in helical growth of the cylindrical cell wall in *Bacillus subtilis*', *Mol Microbiol*, 57(5), pp. 1196-1209.

Liao, X. and Hancock, R.E. (1997) 'Identification of a penicillin-binding protein 3 homolog, PBP3x, in *Pseudomonas aeruginosa*: gene cloning and growth phase-dependent expression', *J Bacteriol*, 179(5), pp. 1490-1496.

Lim, J.S., Lee, K.M., Kim, S.H., Nam, S.W., Oh, Y.J., Yun, H.S., *et al.* (2008) 'Nanoscale characterization of *Escherichia coli* biofilm formed under laminar flow using atomic force microscopy (AFM) and scanning electron microscopy (SEM)', *Bull Korean Chem Soc*, 29(11), pp. 2114-2118.

Loose, M. and Mitchison, T.J. (2014) 'The bacterial cell division proteins FtsA and FtsZ self-organize into dynamic cytoskeletal patterns', *Nat Cell Biol*, 16(1), pp. 38-46.

Loskill, P., Pereira, P.M., Jung, P., Bischoff, M., Herrmann, M., Pinho, M.G., and Jacobs, K. (2014) 'Reduction of the peptidoglycan crosslinking causes a decrease in stiffness of the *Staphylococcus aureus* cell envelope', *Biophys J*, 107(5), pp. 1082-1089.

Louise Meyer, R., Zhou, X., Tang, L., Arpanaei, A., Kingshott, P., and Besenbacher, F. (2010) 'Immobilization of living bacteria for AFM imaging under physiological conditions', *Ultramicroscopy*, 110(11), pp. 1349-1357.

Lovering, A.L., Lin, L.Y., Sewell, E.W., Spreter, T., Brown, E.D., and Strynadka, N.C. (2010) 'Structure of the bacterial teichoic acid polymerase TagF provides insights into membrane association and catalysis', *Nat Struct Mol Biol*, 17(5), pp. 582-589.

Löwe, J. and Amos, L.A. (1998) 'Crystal structure of the bacterial cell-division protein FtsZ', *Nature*, 391(6663), pp. 203-206.

MacArthur, A.E. and Archibald, A.R. (1984) 'Effect of culture pH on the D-alanine ester content of lipoteichoic acid in *Staphylococcus aureus*', *J Bacteriol*, 160(2), pp. 792-793.

Macheboeuf, P., Contreras-Martel, C., Job, V., Dideberg, O., and Dessen, A. (2006) 'Penicillin binding proteins: key players in bacterial cell cycle and drug resistance processes', *FEMS Microbiol Rev*, 30(5), pp. 673-691.

Magnet, S., Dubost, L., Marie, A., Arthur, M., and Gutmann, L. (2008) 'Identification of the L,D-transpeptidases for peptidoglycan cross-linking in *Escherichia coli*', *J Bacteriol*, 190(13), pp. 4782–4785.

Maki, H., Yamaguchi, T., and Murakami, K. (1994) 'Cloning and characterization of a gene affecting the methicillin resistance level and the autolysis rate in *Staphylococcus aureus*', *J Bacteriol*, 176(16), pp. 4993-5000.

Marquis, R.E., Mayzel, K., and Carstensen, E.L. (1976) 'Cation exchange in cell walls of gram-positive bacteria', *Can J Microbiol*, 22(7), pp. 975-982.

Mataraci, E. and Dosler, S. (2012) 'In vitro activities of antibiotics and antimicrobial cationic peptides alone and in combination against methicillin-resistant Staphylococcus aureus biofilms', Antimicrob Agents Chemother, 56(12), pp. 6366-6371.

May, J.J., Finking, R., Wiegeshoff, F., Weber, T.T., Bandur, N., Koert, U., and Marahiel, M.A. (2005) 'Inhibition of the D-alaninecarrier protein ligase from *Bacillus subtilis* increases the bacterium's susceptibility to antibiotics that target the cell wall', *FEBS J*, 272(12), pp. 2993-3003.

McPherson, D.C. and Popham, D.L. (2003) 'Peptidoglycan synthesis in the absence of class A penicillin-binding proteins in *Bacillus subtilis*', *J Bacteriol*, 185(4), pp. 1423-1431.

McPherson, D.C., Driks, A., and Popham, D.L. (2001) 'Two class A high-molecular-weight penicillin-binding proteins of *Bacillus subtilis* play redundant roles in sporulation', *J Bacteriol*, 183(20), pp. 6046-6053.

Meeske, A.J., Riley, E.P., Robins, W.P., Uehara, T., Mekalanos, J.J., Kahne, D., *et al.* (2016) 'SEDS proteins are a widespread family of bacterial cell wall polymerases', *Nature*, 537(7622), pp. 634-638.

Meeske, A.J., Sham, L.T., Kimsey, H., Koo, B.M., Gross, C.A., Bernhardt, T.G., and Rudner, D.Z. (2015) 'MurJ and a novel lipid II flippase are required for cell wall biogenesis in *Bacillus subtilis*', *Proc Natl Acad Sci USA*, 112(20), pp. 6437-6442.

Megrian, D., Taib, N., Jaffe, A.L., Banfield, J.F., and Gribaldo, S. (2022) 'Ancient origin and constrained evolution of the division and cell wall gene cluster in bacteria', *Nat Microbiol*, 7(12), pp. 2114-2127.

Mengin-Lecreulx, D. and van Heijenoort, J. (1993) 'Identification of the glmU gene encoding N-acetylglucosamine-1-phosphate uridyltransferase in *Escherichia coli*', *J Bacteriol*, 175(19), pp. 6150-6157.

Meredith, T.C., Swoboda, J.G., and Walker, S. (2008) 'Late-stage polyribitol phosphate wall teichoic acid biosynthesis in *Staphylococcus aureus*', *J Bacteriol*, 190(8), pp. 3046-3056.

Michie, K.A. and Löwe, J. (2006) 'Dynamic filaments of the bacterial cytoskeleton', *Annu Rev Biochem*, 75, pp. 467-492.

Mitchell, S.L., Kearns, D.B., and Carlson, E.E. (2023) 'Penicillin-binding protein redundancy in *Bacillus subtilis* enables growth during alkaline shock', *bioRxiv*, p. 2023.03.20.533529.

Morales Angeles, D., Macia-Valero, A., Bohorquez, L.C., and Scheffers, D.J. (2020) 'The PASTA domains of *Bacillus subtilis* PBP2B strengthen the interaction of PBP2B with DivIB', *Microbiology*, 166(9), pp. 826-836.

Morgenstein, R.M., Bratton, B.P., Nguyen, J.P., Ouzounov, N., Shaevitz, J.W., and Gitai, Z. (2015) 'RodZ links MreB to cell wall synthesis to mediate MreB rotation and robust morphogenesis', *Proc Natl Acad Sci USA*, 112(40), pp. 12510-12515.

Müller, P., Ewers, C., Bertsche, U., Anstett, M., Kallis, T., Breukink, E., *et al.* (2007) 'The essential cell division protein FtsN interacts with the murein (peptidoglycan) synthase PBP1B in *Escherichia coli*', *J Biol Chem*, 282(50), pp. 36394-36402.

Murray, T., Popham, D.L., and Setlow, P. (1997) 'Identification and characterization of pbpA encoding *Bacillus subtilis* penicillin-binding protein 2A', *J Bacteriol*, 179(9), pp. 3021-3029.

Murray, T., Popham, D.L., and Setlow, P. (1998) 'Bacillus subtilis cells lacking penicillin-binding protein 1 require increased levels of divalent cations for growth', J Bacteriol, 180(17), pp. 4555-4563.

Neuhaus, F.C. and Baddiley, J. (2003) 'A continuum of anionic charge: structures and functions of D-alanyl-teichoic acids in gram-positive bacteria', *Microbiol Mol Biol Rev*, 67(4), pp. 686-723.

Nicolas, P., Mäder, U., Dervyn, E., Rochat, T., Leduc, A., Pigeonneau, N., *et al.* (2012) 'Condition-dependent transcriptome reveals high-level regulatory architecture in *Bacillus subtilis*', *Science*, 335(6072), pp. 1103-1106.

Nikaido, H. (2003) 'Molecular basis of bacterial outer membrane permeability revisited', *Microbiol Mol Biol Rev*, 67(4), pp. 593-656.

Oggioni, M.R., Pozzi, G., Valensin, P.E., Galieni, P., and Bigazzi, C. (1998) 'Recurrent septicemia in an immunocompromised patient due to probiotic strains of *Bacillus subtilis*', *J Clin Microbiol*, 36(1), pp. 325-326.

Oku, Y., Kurokawa, K., Matsuo, M., Yamada, S., Lee, B.L., and Sekimizu, K. (2009) 'Pleiotropic roles of polyglycerolphosphate synthase of lipoteichoic acid in growth of *Staphylococcus aureus* cells', *J Bacteriol*, 191(1), pp. 141-151.

Paik, J., Kern, I., Lurz, R., and Hakenbeck, R. (1999) 'Mutational analysis of the *Streptococcus pneumoniae* bimodular class A penicillin-binding proteins', *J Bacteriol*, 181(12), pp. 3852-3856.

Patel, Y., Zhao, H., and Helmann, J.D. (2020) 'A regulatory pathway that selectively up-regulates elongasome function in the absence of class A PBPs', *eLife*, 9, p. e57902.

Pazos, M., Peters, K., Casanova, M., Palacios, P., Van Nieuwenhze, M., Breukink, E., *et al.* (2018) 'Z-ring membrane anchors associate with cell wall synthases to initiate bacterial cell division', *Nat Commun*, 9(1), p. 5090.

Pedersen, L.B., Angert, E.R., and Setlow, P. (1999) 'Septal localization of penicillin-binding protein 1 in *Bacillus subtilis*', *J Bacteriol*, 181(10), pp. 3201-3211.

Percy, M.G. and Gründling, A. (2014) 'Lipoteichoic acid synthesis and function in gram-positive bacteria', *Annu Rev Microbiol*, 68, pp. 81-100.

Perego, M., Glaser, P., Minutello, A., Strauch, M.A., Leopold, K., and Fischer, W. (1995) 'Incorporation of D-alanine into lipoteichoic acid and wall teichoic acid in *Bacillus subtilis*. Identification of genes and regulation', *J Biol Chem*, 270(26), pp. 15598-15606.

Pereira, M.P., Schertzer, J.W., D'Elia, M.A., Koteva, K.P., Hughes, D.W., Wright, G.D., and Brown, E.D. (2008) 'The wall teichoic acid polymerase TagF efficiently synthesizes poly(glycerol phosphate) on the TagB product lipid III', *Chembiochem*, 9(9), pp. 1385-1390.

Peschel, A., Vuong, C., Otto, M., and Götz, F. (2000) 'The D-alanine residues of *Staphylococcus aureus* teichoic acids alter the susceptibility to vancomycin and the activity of autolytic enzymes', *Antimicrob Agents Chemother*, 44(10), pp. 2845-2847.

Popham, D.L. and Setlow, P. (1996) 'Phenotypes of *Bacillus subtilis* mutants lacking multiple class A high-molecular-weight penicillin-binding proteins', *J Bacteriol*, 178(7), pp. 2079-2085.

Popham, D.L. and Setlow, P. (1994) 'Cloning, nucleotide sequence, mutagenesis, and mapping of the *Bacillus subtilis* pbpD gene, which codes for penicillin-binding protein 4', *J Bacteriol*, 176(23), pp. 7197-7205.

Popham, D.L. and Setlow, P. (1995) 'Cloning, nucleotide sequence, and mutagenesis of the *Bacillus subtilis ponA* operon, which codes for penicillin-binding protein (PBP) 1 and a PBP-related factor', *J Bacteriol*, 177(2), pp. 326-335.

Price, K.D., Roels, S., and Losick, R. (1997) 'A *Bacillus subtilis* gene encoding a protein similar to nucleotide sugar transferases influences cell shape and viability', *J Bacteriol*, 179(15), pp. 4959-4961.

Qamar, A. and Golemi-Kotra, D. (2012) 'Dual roles of FmtA in *Staphylococcus aureus* cell wall biosynthesis and autolysis', *Antimicrob Agents Chemother*, 56(7), pp. 3797-3805.

Rahman, M.M., Hunter, H.N., Prova, S., Verma, V., Qamar, A., and Golemi-Kotra, D. (2016) 'The *Staphylococcus aureus* methicillin resistance factor FmtA is a D-amino esterase that acts on teichoic acids', *Nat Commun*, 7, p. 10572.

Rajagopal, M., Walker, S., and Kahne, D. (2017) 'An unexpected new function for the conserved YycFG two-component regulatory system in the synthesis of teichoic acid in *Bacillus subtilis*', *J Am Chem Soc*, 139(44), pp. 15761-15766.

Ranjit, D.K., Endres, J.L., Bayles, K.W., and Ji, Y. (2011) 'Staphylococcal LytSR two-component regulatory system: a novel regulator of autolysis and cell death', *J Bacteriol*, 193(9), pp. 1714-1724.

Reid, S.D., Hong, W., Dewar, S.J., and El Khamisy, S.F. (2017) 'Human cytosolic DNA exonuclease TREX1 and the control of DNA damage and autoimmunity', *Front Immunol*, 8, p. 894.

Rice, K.C., and Bayles, K.W. (2008) 'Molecular control of bacterial death and lysis', *Microbiol Mol Biol Rev*, 72(1), pp. 85-109.

Rice, K.C., and Bayles, K.W. (2003) 'Death's toolbox: examining the molecular components of bacterial programmed cell death', *Mol Microbiol*, 50(3), pp. 729-738.

Rohrer, S., and Berger-Bächi, B. (2003) 'Application of a bacterial two-hybrid system for the analysis of protein-protein interactions between FemABX family members: the mechanism of methicillin resistance in *Staphylococcus aureus*', *J Microbiol Methods*, 55(1), pp. 87-94.

Rowan, R.M., Rowe, A.J., Henderson, P.J.F., and Middleton, D.A. (2013) 'Probing membrane protein assembly and structure using pulsed EPR spectroscopy', *Biochem Soc Trans*, 41(2), pp. 412-418.

Rudner, D.Z., and Losick, R. (2002) 'A sporulation membrane protein tethers the prosigmaK processing enzyme to its inhibitor and dictates its subcellular localization', *Genes Dev*, 16(8), pp. 1007-1018.

Ruggiero, A., Marasco, D., Squeglia, F., Soldini, S., Pedone, E., Berisio, R., and Vitagliano, L. (2010) 'Structure and function relationships in the bacterial cell wall biosynthesis', *Protein Pept Lett*, 17(1), pp. 128-139.

Saddler, G.S., and Bradbury, J.F. (2005) 'Potato scab caused by *Streptomyces* species', in Schumann, G.L. (ed.) *Plant Health Instructor*. St. Paul, MN: APS Press, pp. 114-116.

Santos-Beneit, F., Roberts, D.M., Cantlay, S., McCormick, J.R., and Ellis, R.J. (2020) 'The role of MreB cytoskeleton in cell envelope synthesis during growth and sporulation in *Streptomyces coelicolor*', *PLoS Genet*, 16(1), p. e1008630.

Sauvage, E., Kerff, F., Terrak, M., Ayala, J.A., and Charlier, P. (2008) 'The penicillin-binding proteins: structure and role in peptidoglycan biosynthesis', *FEMS Microbiol Rev*, 32(2), pp. 234-258.

Schneider, T., and Sahl, H.G. (2010) 'An oldie but a goodie – cell wall biosynthesis as antibiotic target pathway', *Int J Med Microbiol*, 300(3), pp. 161-169.

Schumacher, M.A., Balani, P., Min, J., Chinnam, N., Hansen, S., Vulic, M., *et al.* (2021) 'Mechanism of ATP hydrolysis by the MinD cell division protein from *Bacillus subtilis*', *Biochem J*, 478(12), pp. 2235-2251.

Sewell, E.W., and Brown, E.D. (2014) 'Taking aim at wall teichoic acid synthesis: new biology and new leads for antibiotics', *J Antibiot (Tokyo)*, 67(1), pp. 43-51.

Sham, L.T., Butler, E.K., Lebar, M.D., Kahne, D., Bernhardt, T.G., and Ruiz, N. (2014) 'Bacterial cell wall', *J Am Chem Soc*, 136(5), pp. 1802-1805.

Sieradzki, K., Tomasz, A., and Wondrack, L. (1999) 'Increased cell wall turnover is associated with vancomycin resistance in *Staphylococcus aureus*', *J Bacteriol*, 181(8), pp. 2351-2358.

Soldo, B., Lazarevic, V., Pooley, H.M., and Karamata, D. (2002) 'Characterization of a *Bacillus subtilis* thermosensitive teichoic acid-deficient mutant: gene *mnaA* (*yvyH*) encodes the UDP-N-acetylglucosamine 2-epimerase', *J Bacteriol*, 184(15), pp. 4316-4320.

Son, H., Fujioka, M., and Aso, T. (2014) 'Molecular dissection of antibiotic resistance in Gram-positive bacteria', *Chem Soc Rev*, 43(13), pp. 4537-4552.

Spratt, B.G. (1975) 'Distinct penicillin-binding proteins involved in the division, elongation, and shape of *Escherichia coli* K12', *Proc Natl Acad Sci USA*, 72(8), pp. 2999-3003.

Steen, A., Buist, G., Leenhouts, K.J., El Khattabi, M., Grijpstra, F., Zomer, A.L., *et al.* (2005) 'Cell wall attachment of a widely distributed peptidoglycan binding domain is hindered by cell wall constituents', *J Biol Chem*, 280(13), pp. 12100-12107.

Stohl, E.A., and Seifert, H.S. (2006) 'Neisseria gonorrhoeae RecX inhibits RecA recombinase activity through a direct, monomer-monomer interaction', *J Biol Chem*, 281(21), pp. 16111-16123.

Strahl, H., Bürmann, F., and Hamoen, L.W. (2014) 'The actin homologue MreB organizes the bacterial cell membrane', *Nat Commun*, 5, p. 3442.

Sullivan, M., Popham, D.L., and Setlow, P. (1997) 'The products of the spoVD operon are essential for dipicolinic acid uptake into developing spores of *Bacillus subtilis*', *J Bacteriol*, 179(2), pp. 590-593.

Szurmant, H., and Ordal, G.W. (2004) 'Diversity in chemotaxis mechanisms among the bacteria and archaea', *Microbiol Mol Biol Rev*, 68(2), pp. 301-319.

Tiyanont, K., Doan, T., Lazarus, M.B., Fang, X., Rudner, D.Z., and Walker, S. (2006) 'Imaging peptidoglycan biosynthesis in *Bacillus subtilis* with fluorescent antibiotics', *Proc Natl Acad Sci USA*, 103(29), pp. 11033-11038.

Tsui, H.C., Zheng, J.J., Magallon, A.N., Ryan, J.D., Carr, P.D., Barendt, S.M., and Winkler, M.E. (2016) 'Suppression of a deletion of the SRP GTPase FlhF, involved in htrA (DegP) regulation, by mutations in the penicillin-binding protein PBP1A in *Streptococcus pneumoniae*', *J Bacteriol*, 198(5), pp. 749-765.

Turner, R.D., Ratcliffe, E.C., Wheeler, R., Golestanian, R., Hobbs, J.K., and Foster, S.J. (2010) 'Peptidoglycan architecture can specify division planes in *Staphylococcus aureus*', *Nat Commun*, 1, p. 26.

Typas, A., and Sourjik, V. (2015) 'Bacterial protein networks: properties and functions', *Nat Rev Microbiol*, 13(9), pp. 559-572.

van Heijenoort, J. (2001) 'Recent advances in the formation of the bacterial peptidoglycan monomer unit', *Nat Prod Rep*, 18(5), pp. 503-519.

Veening, J.W., Smits, W.K., and Kuipers, O.P. (2008) 'Bistability in bacterial virulence gene expression', *Annu Rev Microbiol*, 62, pp. 193-210.

Vollmer, W., Blanot, D., and de Pedro, M.A. (2008) 'Peptidoglycan structure and architecture', *FEMS Microbiol Rev*, 32(2), pp. 149-167.

Vollmer, W., and Holtje, J.V. (2004) 'The architecture of the murein (peptidoglycan) in gram-negative bacteria: vertical scaffold or horizontal layer(s)?', *J Bacteriol*, 186(19), pp. 5978-5987.

Weidenmaier, C., Kokai-Kun, J.F., Kristian, S.A., Chanturiya, T., Kalbacher, H., Gross, M., *et al.* (2004) 'Role of teichoic acids in *Staphylococcus aureus* nasal colonization, a major risk factor in nosocomial infections', *Nat Med*, 10(3), pp. 243-245.

Weidenmaier, C., Peschel, A., Kempf, V.A., Lucindo, N., Yeaman, M.R., Bayer, A.S., *et al.* (2005) 'D-alanine incorporation into teichoic acids protects *Staphylococcus aureus* against toll-like receptor 2-dependent host defense in a mouse tissue cage infection model', *J Infect Dis*, 191(1), pp. 89-96.

Wheeler, R., Turner, R.D., Bailey, R.G., Salamaga, B., Mesnage, S., Mohamad, S.A., *et al.* (2015) 'Bacterial cell enlargement requires control of cell wall stiffness mediated by peptidoglycan hydrolases', *mBio*, 6(4), p. e00660-15.

Wilson, J.R., Lin, L., and Grinstaff, M.W. (2007) 'Bacterial adhesion and cell attachment to metal oxide nanoparticles', *Langmuir*, 23(11), pp. 5675-5680.

Winkler, M.E., Gellert, M., and Smith, H.O. (2002) 'Molecular biology of bacterial transformation', *Annu Rev Microbiol*, 56, pp. 75-100.

Wong, J.L., Akerley, B.J., and Gitai, Z. (2019) 'The role of peptidoglycan in bacterial shape', in Cossart, P., Maloy, S., and Schachter, M. (eds.) *Mechanisms of bacterial pathogenesis*. Cold Spring Harbor, NY: Cold Spring Harbor Laboratory Press, pp. 37-52.

Wu, L.J., and Errington, J. (2004) 'Bacillus subtilis SpoIIIE protein required for DNA segregation during asymmetric cell division', Science, 306(5697), pp. 1756-1759.

Wu, Y., Simmons, C.R., and Mobashery, S. (2014) 'Mechanistic characterization of the resistance of methicillin-resistant *Staphylococcus aureus* to beta-lactam antibiotics', *Proc Natl Acad Sci USA*, 111(10), pp. 3749-3754.

Yao, X., Jericho, M., Pink, D., and Beveridge, T. (1999) 'Thickness and elasticity of gram-negative murein sacculi measured by atomic force microscopy', *J Bacteriol*, 181(22), pp. 6865-6875.

Zapun, A., Contreras-Martel, C., and Vernet, T. (2008) 'Penicillin-binding proteins and beta-lactam resistance', *FEMS Microbiol Rev*, 32(2), pp. 361-385.

Zhao, H., Patel, Y., and Helmann, J.D. (2016) 'A regulatory circuit links cell wall homeostasis and envelope stress response in *Bacillus subtilis*', *Mol Microbiol*, 102(3), pp. 438-452.

Zheng, X., and Quinn, T.P. (2020) 'Bacterial cell wall structure and interactions with proteins', in Zhang, Y. and Schmidt, M.A. (eds.) *Bacterial cell wall research in the post-genomic era*. New York, NY: Springer, pp. 25-46.

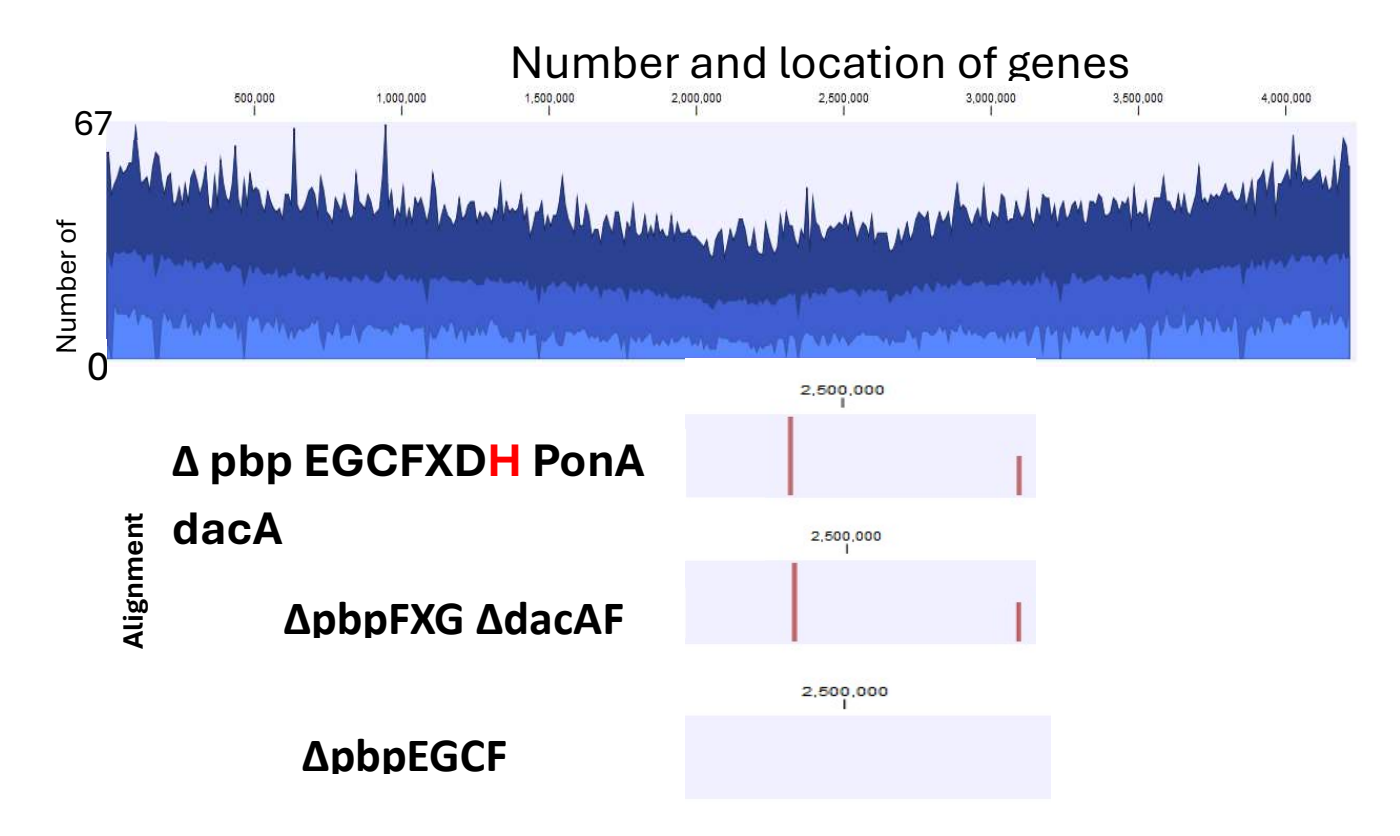
Zhou, X., and Merghoub, T. (2018) 'A review of recent progress on the role of bacterial cell wall in antibiotic resistance', *Chem Commun (Camb)*, 54(43), pp. 5554-5562.

Appendices

Appendix A. Oligonucleotides

Name	Sequence	Purpose
YA-FULL	GATTCCTAGGATGACTGAAATAGGACGTGAACCAAAG	Cloning of Full pbpH in 168
pbpH-FF		
YA-FULL	GGGGCCCGTTTATTTTTTACTGTGTTTTTTTTCGAGCTCTGCG	
pbpH-FR		
YA-FULL	AAAAATAAACGGGCCCCCCC	
pbpH-VF		
YA-FULL	CTATTTCAGTCATCCTAGGAATCTCCTTTCTAGATGCATT	
pbpH-VR		
YA-	GATTCCTAGGATGAACCTTTTTTTCCTAGCTGTCTTTGTTCT	Cloning of
TRUNCATE		truncated
D pbpH-FF		<i>pbpH</i> in
YA-	GGGGCCCGTTTATTTTTTACTGTGTTTTTTTTCGAGCTCTGCG	168
TRUNCATE		
D pbpH-FR		_
YA-	AAAAATAAACGGGCCCCCC	
TRUNCATE		
D pbpH-VF		
YA-	CTATTTCAGTCATCCTAGGAATCTCCTTTCTAGATGCATT	
TRUNCATE		
D pbpH-VR		
YA-FULL	GATTCCTAGGATGAGGAGAAATAAACCAAAAAAGCAAAATCA	Cloning of Full <i>pbpA</i> in 168
pbpA-FF	TAAAG	
YA-FULL	GGGGCCCGTTTAGTTATCAGAAGACGTTGTGTTTTCTGCAT	
pbpA-FR		
YA-FULL	ATAACTAAACGGGCCCCCCC	
pbpA-VF		
YA-FULL	TTCTCCTCATCCTAGGAATCTCCTTTCTAGATGCATTTTATGTC	
pbpA-VR	A	
YA-pbpA-	CGGCAGCCATATGAGGAGAAATAAACCAAAAAAGC	PBP2a
PET-FF		purificatio n
YA-pbpA-	GGTGGTGGTGCTATTAGTTATCAGAAGACGTTGTG	
PET-FR		
YA-pbpA-	TTCTCCTCATATGGCTGCCGCG	
PET-VF		
YA-pbpA-	TGATAACTAATAGCACCACCACCACCACCACTGAGATC	
PET-VR		
YA-pbpH-	ACTGGGCATCGTTGAAGGCGAACAGCATGAAGAAGAC	Chimeric protein
TM2a-VF		
YA-pbpH-	TACTCCTCATCCTAGGAATCTCCTTTCTAGATGCATTTTATGTC	(PBPH
TM2a-VR	A	with TM of PBP2a)
YA-pbpH-	GATTCCTAGGATGAGGAGAAATAAACCAAAAAAGCAAAATCA	
TM2a-FF	TAAAG	

CGCCTTCAACGATGCCCAGTTCCACAATAATCCAGGT	
TGTTCAAATTAAGCAGATCGTGCAAGGTGATGATTAC	Chimeric protein (PBPH with TM of PBP2a)
CTATTTCAGTCATCCTTAGGAATCTCCTTTCTAGATGCATT	
GATTCCTAGGATGACTGAAATAGGACGTGAACCAAAG	
TGACCCGTAGAATTTGAACAACCCCGAGCTTAAAAAT	
GCATTAATTTTTGCACTCGGGGTTGTTGCAATTGTTGAAGG	Site direct mutagenes
AGTGAATAGAACAAGACAGC	is
GGCAACAACTAATGTGCAACTTAC	Checking Psph1
GATAATTCGCGGCCGCTCTAGAACTAG	plasmid
	TGTTCAAATTAAGCAGATCGTGCAAGGTGATGATTAC CTATTTCAGTCATCCTTAGGAATCTCCTTTCTAGATGCATT GATTCCTAGGATGACTGAAATAGGACGTGAACCAAAG TGACCCGTAGAATTTGAACAACCCCGAGCTTAAAAAT GCATTAATTTTTGCACTCGGGGTTGTTGCAATTGTTGAAGG AGTGAATAGAACAAAGACAGC GGCAACAAACTAATGTGCAACTTAC

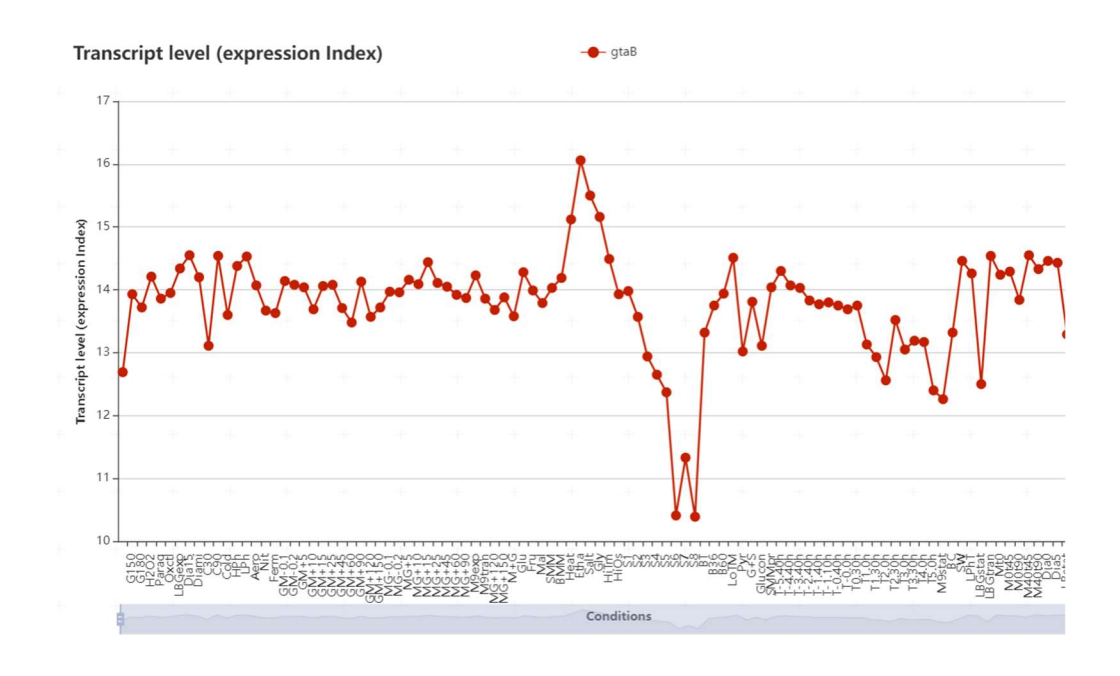


Supplementary Figure 3.1 gDNA sequencing for diffrenent strains that lack of number of PBPs

The top image shows the number of reads from the gDNA sequencing from 0 to 67 reads. Strain Δpbp EGCFXDH PonA dacA has two mutations compared to the referencing gDNA 168 and the mutation show in red lines (one is long and the other is short). The long one is the mutation in motI genes while the short one is mutation in Spo0F gene. The $\Delta pbpFXG \Delta dacAF$ strain also show exact same mutation in motI and Spo0F genes. However, the $\Delta pbpEGCF$ did not show any mutation in motI nor Spo0F.

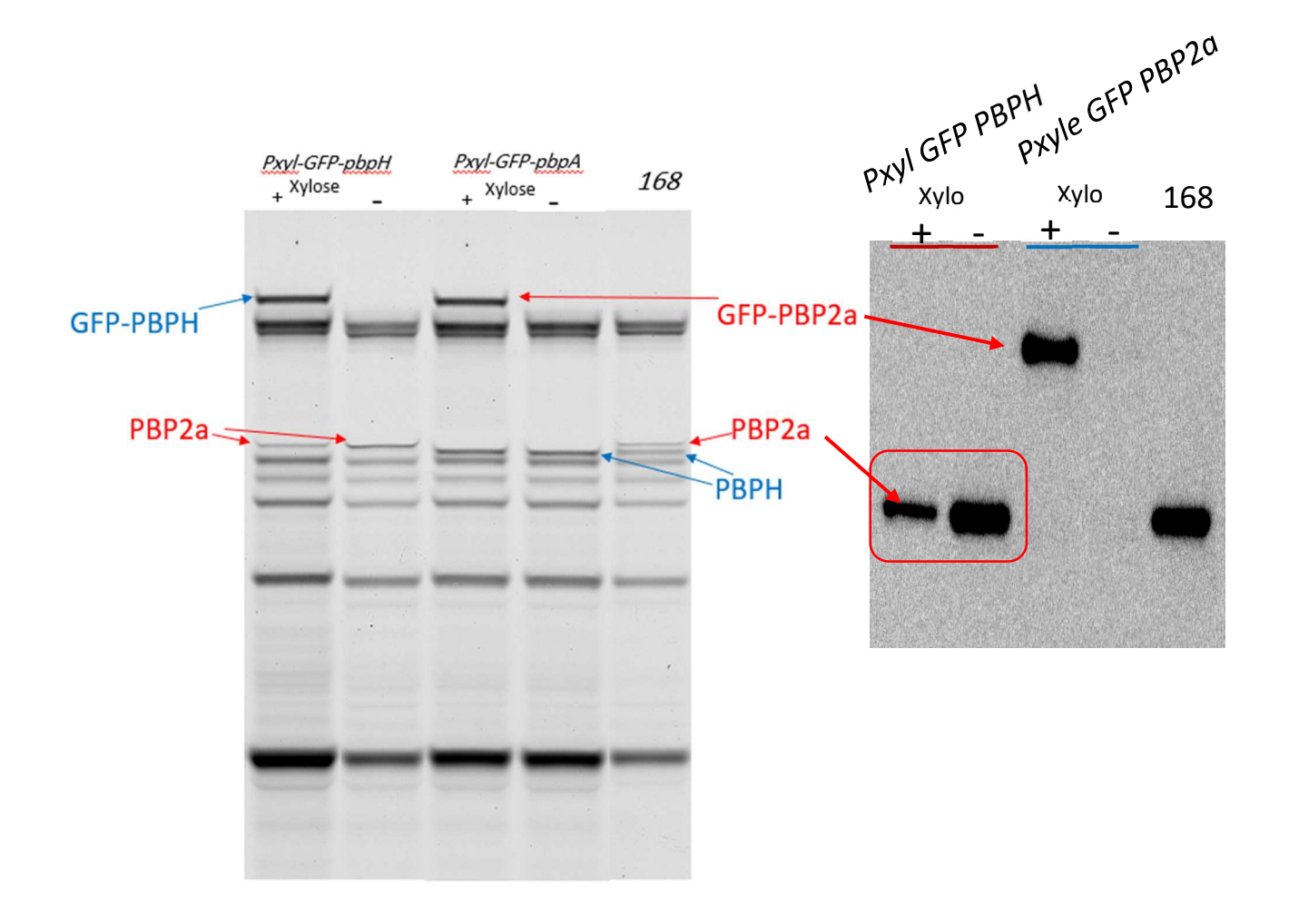
Appendix 4

gtaB expression profile



Supplementary figure 4.1. The expression profile of gtaB gene.

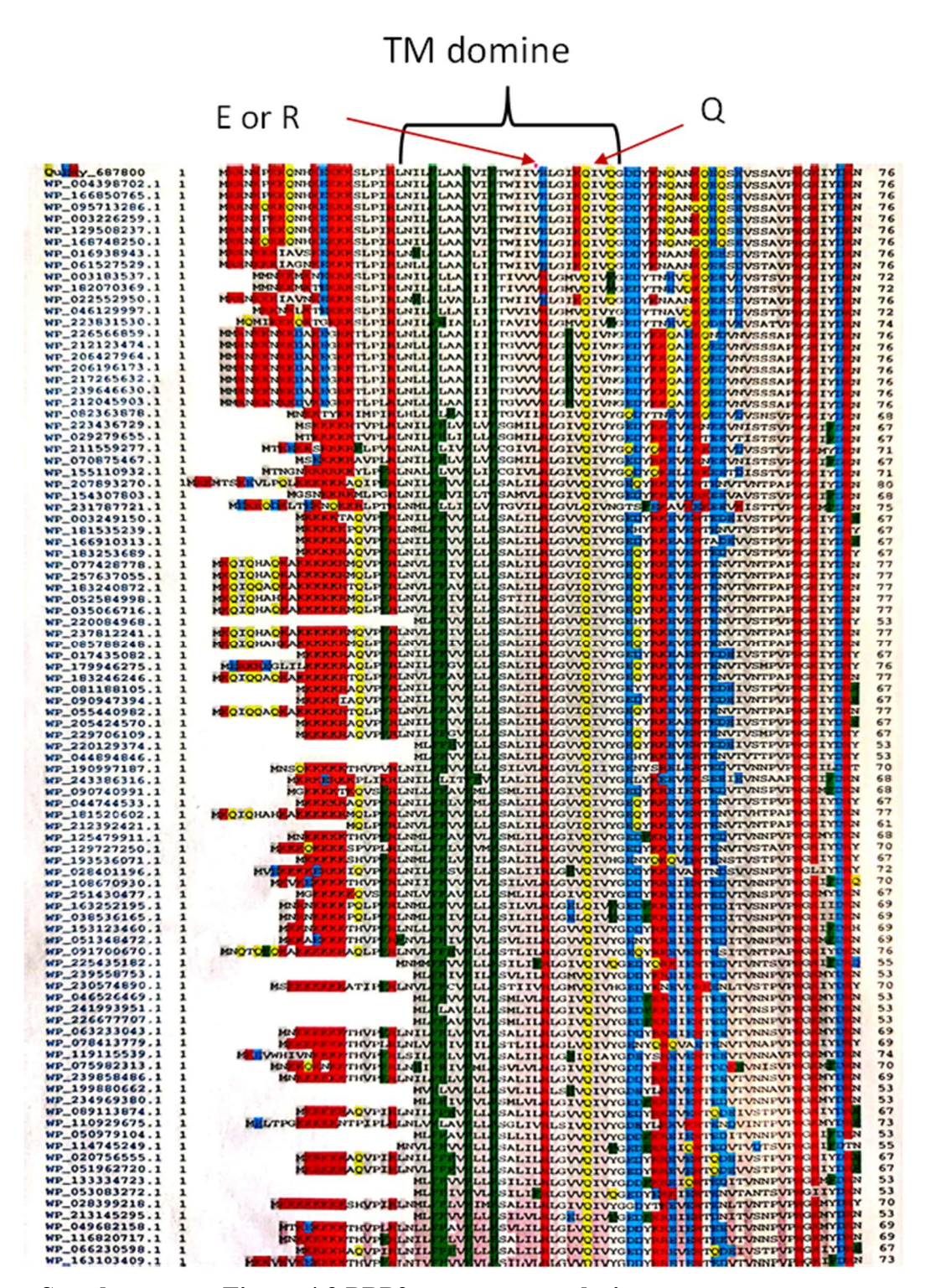
The expression profile of *gatB* gene across different growth conditions. The figures are adapted from SubtiWiki database 2.0/ Expression Data Browser.



Supplementary figure 4.2 Bocillin FL labling aligen with western blot results.

A) Bocillin FL labelling was performed on the 168, Pxyl-*GFP*-pbpA strains with 1% xylose (expressing *GFP*-PBPH) and without 1% xylose (no *GFP*-PBP2a expression) and Pxyl-*GFP*-pbpH strains with 1% xylose (expressing *GFP*-PBPH) and without 1% xylose (no *GFP*-PBPH expression). PBP2a (red arrow) and PBPH (blue arrow) are indicated.

B) PBP2a quantity in strains 168, Pxyl-*GFP*-pbp2a and *Pxyl-GFP*-pbpH with and without xylose was measured. The strains were grown in LB medium, and samples were collected in the exponential growth phase



Supplementary Figure 4.3 PBP2a sequence analysis

Bioinformatics analysis shows several PBP2a in Bacilli*B. subtilis* strains sequences aligned by colour based on the amino acid property. The data was obtainted from NCBI. The two distinct amino acids in transmembrane domin were Arganine or Glutamic acid and Glutamine. Non-polar amino acids were highlite in grey and green, positively charged amino acids in red, negatively charged amino acids (blue) and polar amino acids (yellow) were marked, as shown in Figure